U.PORTO

FEUP FACULDADE DE ENGENHARIA
UNIVERSIDADE DO PORTO

NUMERICAL AND EXPERIMENTAL STUDY OF A SOLAR HYBRID COLLECTOR FOR COMBINED PRODUCTION OF ELECTRICITY AND HEAT

Ana Maria Raposo João

Thesis submitted to the Faculty of Engineering of University of Porto in accordance with the requirements for the degree of Doctor in Mechanical Engineering

Department of Mechanical Engineering

Supervisor: Professor Armando Carlos Oliveira

Co-supervisor: Doutor Szabolcs Varga

Agosto 2015

To my mother

Acknowledgements

Undertaking this PhD has been a truly life-changing experience for me and it would not have been possible to do without the support and guidance that I received from many people.

This thesis was supervised by Professor Armando Oliveira, Associate Professor at the Faculty of Engineering of University of Porto (FEUP) to who I am grateful for accepting this supervision, as well as all the conditions that put at my disposal to ensure its accomplishment. His guidance was objective, effective, and especially tenacious through this long journey. I would like also to address special thanks to Doutor Szabolcs Varga, who co-supervised this work, by his dedication and constant monitoring. His advisement through key moments of experimental work was essential. They were much more than supervisors, they were true professors. Their guidance and advices allowed me to improve my scientific and personal competences, which ultimately changed my viewpoints in different subjects.

I am also very grateful to all the colleagues that work with me in the laboratory L402, Mario Guindeira that helped with experimental and maintenance support, Karla Gonçalves that provided valuable instructions concerning the use of TRNSYS, and colleagues from laboratory L001 that helped with technical problems of some equipment. I want also to address my appreciation to Doutora Ana Palmero, specifically for the support with TRNSYS but generally for the gentle encouragement, and for being always willing to help.

I want to also express my thanks to my friend, Benilde Pinto, that made valuable contributions to this thesis by providing verification on the manuscript.

I am indebted to my colleagues at ISEP, that voluntarily acceded to a working overload, to relief myself from some of my assignments: José Lopes da Costa, Marina Duarte, Rui Rego, Vera Ribeiro and Aristides Ferreira de Castro. To all of them, my true gratitude: it meant more than just the hours spent.

The emotional support of colleagues, friends and family played an important role on keeping the will and balance. For all of them, from the closest to the more distant, that helped through so many ways and situations, my deepest thank you.

Abstract

In this thesis the efficiency of a hybrid photovoltaic/thermal (PV/T) solar collector is assessed, based on results from the simultaneous production of heat and electricity, obtained by numerical methods and experimental tests. The structural configuration of the studied collector includes glass cover, sheet and tube geometry and application of the photovoltaic cells on the top surface of the absorber plate.

The interest on the research on this type of collectors has been growing since the 1990s, evolving from a starting point of thematic innovation, to the current state, where different configurations and heat transfer fluids have been already studied and several units are commercially available. The main and innovative aim of this thesis is the constructive optimization of the hybrid solar collector, considering two factors:

i. the location of the photovoltaic cells, comparing their application near the water inlet side with the opposite side;

ii. the ratio between the area with photovoltaic cells and the total area of the absorber plate, named as *packing factor* (*Pf*).

This analysis is first approached from the perspective of the overall efficiency of the PV/T collector, and then by analysing the economic savings and environmental impact achieved when included in a domestic hot water (DHW) system.

A small dimension prototype was built. The photovoltaic modules were applied over the absorber plate, especially adapted to the small dimensions of the prototype (0.5 m width and 1 m length). The prototype was instrumented in order to measure ambient temperature, incident radiation, increase in water temperature, and generated electricity. Three different configurations of the prototype were tested: with one, two and three photovoltaic modules applied, corresponding to different values of the packing factor.

A mathematical model of the PV/T collector was developed, based on the energy balances existing in its different components. The heat and electricity outputs can be obtained using the model, upon different environmental and operating conditions. The

existence of temperature gradients along the three dimensions led to a three-dimensional discretization of the domain, in the area where PV cells are applied in the absorber plate. The other areas only require a 2D scheme discretization. A generic equation solver software was used, Engineering Equation Solver (EES), for the application of the mathematical model. EES can numerically solve thousands of coupled non-linear algebraic and differential equations. A high accuracy thermodynamic and transport property database is provided for hundreds of substances in a manner that allows it to be used with the equation solving capability. It is adaptable for any parametric study, since it is basically a numerical tool, allowing the user to define all the constraints. The model was validated with the experimental results.

A parametric study was also developed, to exhaustively and systematically evaluate the effect of key factors in collector efficiency: inlet water temperature, incident radiation and ambient temperature. The influence of the location of the PV cells and the packing factor, parameters especially focused in this thesis, were particularly studied. This parametric analysis is based on results obtained from the developed mathematical model, which allows versatility for considering different simulation conditions. It was found that collector efficiency increases with the ambient temperature and the incident radiation, and is hindered by increasing the water inlet temperature and the application of photovoltaic cells. It was concluded that the positive effect of placing the cells in the fluid inlet area is favoured when the ratio between the areas with and without cells is balanced, *i.e*, for a *Pf* of about 50%. The increase in *Pf* causes a reduction in overall efficiency, effect that is amplified by an increase in the water inlet temperature. The degree of detail of this study is a differentiating factor, among other works of the same nature.

The assessment of the economic impact of PV/T configurations with different *Pf* values is accomplished, based on the results of the annual thermal and electrical energy converted for a typical household application. The results are obtained using a dynamic simulation program (TRNSYS). TRNSYS includes an extensive library of components and climatic data. The pre-defined components, termed “types”, follow mathematical and physical considerations, so that the user must adapt the input data to the specific formulations underlying that component. Different versions of the “type” chosen for the PV/T collector were needed, corresponding to different *Pf* values. The mathematical model developed in EES was used to provide the TRNSYS inputs related to collector performance for the different layouts. For the Portuguese temperate continental climate,

two different locations were considered: Porto, near the Atlantic Ocean, with a mild and dry summer, and Faro, near the Mediterranean, with a dry and hot summer. They belong to two different climatic zones, characterized as “Csb”, for Porto, and “Csa”, for Faro, according to the Köppen-Geiger classification (IPMA, 2015). The energy-saving values obtained are then converted into economic savings through the prices of natural gas and electricity. It was concluded that the total coverage of the absorber area with photovoltaic cells is advantageous. The dependence of the results from the national economic context, with electricity substantially more expensive than natural gas, is complemented by a similar analysis for a country, within the EU, where this proportion is minimal: Bulgaria. Even so, it was confirmed that to privilege the electrical component brings economic advantages. The *Pf* effect was also analysed from the point of view of environmental impacts, through the CO_2 emission savings resulting from energy conversion with natural gas and electricity. Taking this into account, the use of cells in the entire area of the absorber also proved to be advantageous. These results may have a significant value for the industry, since they provide the ground information for the optimum design of a PV/T collector. They also represent support information to the collector users or certification entities, through the quantification of economic and environmental results.

Resumo

Nesta tese é avaliada a eficiência de um coletor solar híbrido, com base em resultados da produção simultânea de calor e eletricidade, obtidos através de métodos numéricos e de ensaios experimentais. A configuração estrutural do coletor estudado inclui cobertura de vidro, geometria de placa e tubos, e aplicação das células fotovoltaicas sobre a placa absorvedora.

O interesse da investigação neste tipo de coletores tem vindo a crescer desde a década de 1990, evoluindo de um ponto inicial de inovação no tema, até ao estado atual, em que diferentes configurações e fluidos de transferência térmica foram já estudados, e diversas unidades se encontram disponíveis no mercado. O objetivo principal e inovador desta tese é a análise e otimização construtiva do coletor solar híbrido, atendendo a dois fatores:

i. a localização das células fotovoltaicas, comparando a sua aplicação junto da zona de entrada da água, com a zona de saída;
ii. a razão entre a área em que são aplicadas as células fotovoltaicas e a área total da placa absorvedora, designada como "fator de enchimento" (*Pf*).

Este estudo assenta inicialmente na avaliação da eficiência global do coletor, e posteriormente na perspetiva de maximização da poupança económica e impacto ambiental conseguidos pela utilização de um coletor híbrido incluído num sistema doméstico de Águas Quentes Sanitárias.

Um protótipo de pequenas dimensões (0,5 m de largura e 1 m de comprimento) foi construído. Módulos fotovoltaicos adaptados especialmente às dimensões do coletor foram aplicados sobre a placa absorsora. O protótipo foi instrumentado, por forma a medir o aumento de temperatura atingido na água, a potência elétrica gerada, temperatura ambiente e radiação incidente. Três configurações diferentes do protótipo foram testadas: com um, dois e três módulos fotovoltaicos aplicados, correspondendo a diferentes valores de *Pf*..

Foi desenvolvido um modelo matemático do coletor, baseado nos balanços energéticos nos seus diferentes componentes. O modelo permite calcular a produção de calor e eletricidade, mediante diferentes condições ambientais e operacionais. A existência de gradientes de temperatura ao longo das três dimensões levou à discretização tridimensional do domínio na zona de aplicação dos módulos fotovoltaicos na placa absorvedora. Para a aplicação do modelo matemático foi utilizado um *software* genérico de resolução de equações, Engineering Equation Solver (EES). Este *software* permite resolver numericamente sistemas de milhares de equações algébricas não lineares e diferenciais. Uma base de dados de propriedades termodinâmicas e de transporte é fornecida para centenas de substâncias, por forma a ser usada conjuntamente com a resolução das equações. O seu uso é facilmente adaptável para qualquer estudo paramétrico, uma vez que consiste basicamente numa ferramenta numérica, permitindo ao utilizador definir todas as condições de utilização. O modelo foi validado experimentalmente.

Neste trabalho é também desenvolvido um estudo paramétrico, para avaliar de forma exaustiva e sistemática o efeito de fatores chave para a eficiência do coletor: a temperatura de entrada da água, a radiação incidente e a temperatura ambiente. A influência da localização das células e do *Pf*, parâmetros em especial análise nesta tese, foi particularmente estudada. Esta análise é feita com base em resultados obtidos através do modelo matemático desenvolvido, que permite versatilidade para a consideração das diferentes condições da simulação. Verificou-se que a eficiência do coletor aumenta com a temperatura ambiente e a radiação incidente, e é prejudicada pelo aumento da temperatura de entrada da água e pela aplicação das células fotovoltaicas. Concluiu-se que o efeito positivo da colocação das células na zona da entrada do fluido, se bem que reduzido, é favorecido quando a razão entre a área com e sem células é equilibrada. O aumento de *Pf* provoca uma redução na eficiência, efeito que é amplificado por um aumento da temperatura de entrada da água. O grau de detalhe com que este estudo é desenvolvido é um fator diferenciador, quando comparado com outros já existentes.

A avaliação do impacto económico de *Pf* é feita com base nos resultados da energia térmica e elétrica conseguidos anualmente com a utilização de um coletor híbrido, para uma aplicação doméstica típica. Os resultados são obtidos com recurso a um programa de simulação dinâmica (TRNSYS) que inclui uma extensa biblioteca de componentes e dados climáticos. Os componentes pré-definidos, designados “tipos”,

obedecem a considerações matemáticas e físicas, pelo que o utilizador é obrigado a adaptar as características de cada componente à formulação específica subjacente. Foi necessária a utilização de diferentes versões do "tipo" escolhido para o coletor PV/T, correspondendo a diferentes valores de *Pf*. O modelo matemático desenvolvido em EES foi usado para determinar os *inputs* específicos para as diferentes versões do componente do colector, relacionados com os parâmetros de performance. Para o clima temperado continental de Portugal, dois diferentes locais foram considerados: Porto, banhado pelo oceano atlântico, com um verão temperado e seco, e Faro, próximo do mar Mediterrâneo, com um verão quente e seco. Estes dois locais pertencem a duas zonas climáticas distintas, caracterizadas como "Csb", para o Porto, e "Csa", para Faro, de acordo com a classificação climática de Köppen-Geiger (IPMA, 2015). Os valores da poupança energética são convertidos em poupança económica, através da aplicação do preço do gás natural e da eletricidade. Foi concluído que o preenchimento completo da área da placa absorvedora com células fotovoltaicas é vantajoso. A dependência dos resultados do contexto nacional, em que a eletricidade é substancialmente mais cara do que o gás natural, é complementada através de uma análise semelhante realizada para um país da UE em que essa proporção é mínima: Bulgária. Mesmo assim, confirmou-se que privilegiar a componente elétrica traz vantagens económicas. O efeito de *Pf* foi também analisado sob o ponto de vista do impacto ambiental, através da conversão da poupança energética de gás natural e eletricidade nas respetivas emissões de CO_2. Também, de acordo com este aspeto, a aplicação de células em toda a área da placa absorvedora se revelou vantajosa. Estes resultados podem ter grande interesse para a indústria, uma vez que fornecem informação para fundamentar o melhor *layout* do coletor híbrido. Além disso, a quantificação dos benefícios ambientais e monetários representa também informação relevante para os utilizadores e entidades certificadoras.

Contents

List of Figures

List of tables

Nomenclature

List of abbreviations

APA	Agência Portuguesa do Ambiente
APREN	Associação Portuguesa das Energias Renováveis
a-Si	Amorphous silicon
ASTM	American Society for Testing and Materials
BIPV	Building Integrated Photovoltaic
BIPVT	Building Integrated Photovoltaic/Thermal
BRIC	Brazil, Russia, India, China, and South Africa
CIS	$CuInSe_2$
CPC	Compound Parabolic Collector
c-Si	Monocrystalline silicon
DHW	Domestic Hot Water
EC	European Commission
EES	Engineering Equation Solver
EPIA	European Photovoltaic Industry Association
EREC	European Renewable Energy Council
ESTIF	European Solar Thermal Industrial Federation
ETC	Evacuated Tube Collector
EVA	Ethylene-vynil acetate
EU	European Union
FF	Fill Factor
FPC	Flat Plate Collectors
GHG	Greenhouse Gas
IEA	International Energy Agency
IPQ	Instituto Português da Qualidade
JCGM	Joint Committee for Guides in Metrology
LUCF	Land-use Change and Forestry
MMP	Maximum Power Point
NREAPs	National Renewable Energy Action Plans
pc-Si	Polycrystalline silicon

PV	Photovoltaic
PV/T	Photovoltaic and thermal
PV/T-a	Photovoltaic and thermal air collector
PV/T-w	Photovoltaic and thermal water collector
RES	Renewable Energy Sources
RES-E	Renewable Electricity
RES-HC	Renewable Heating and Cooling
R&D	Research and Development
TRNSYS	Transient Systems Simulation Program
UK	United Kingdom
UN	United Nations

List of Symbols

A	Area (m^2)
az	Azimuth (^{o})
C	Speed of light (m/s)
c	Specific heat capacity (J/(kgK))
E	Energy (J)
$\dot{E}$	Electric power (W)
e	Electric power flux (W/m^2)
ET	Equation of time (minutes)
$F´$	Collector efficiency factor (-)
f_S	Solar fraction (%)
F_R	Modified collector heat removal factor (-)
G	Irradiance (W/m^2)
g	Gravitational acceleration (m/s^2)
H	Hour angle (°)
h	Plank´s constant = 6.652×10^{-34} (J s), heat transfer coefficient for convection ($W/(m^2K)$)
I_{El}	Electric current (A)
I	Irradiation (hourly, daily) (J/m^2)
i_{Cell}	ideality factor of the PV cell
k	Thermal conductivity (W/(mK))
L	Length (m)
LT	Legal Time (hh:mm:ss)
$\dot{m}$	Mass flow rate (kg/s)

N	Number of tests, number of elements
n	n^{th} day of the year
Nu	Nusselt number
P	Perimeter (m)
Pf	Packing factor (-)
Pr	Prandtl number
$\dot{Q}$	Useful heat (W)
q	Heat flux (W/m^2)
R	Equivalent thermal resistance (m^{2}K/W)
Ra	Rayleigh number
Re	Reynolds number
$s\,(X_i)$	Estimated standard error from N independent repeated observations X_i
$s^2(X_i)$	Estimated variance determined from N independent repeated observations X_i
T	Temperature (ºC, K)
t	student's t-distribution point, elapsing time (s)
T^*	Reduced temperature difference (Km^2/W)
TST	True Solar Time (hours)
u	Standard uncertainty
u_c	Combined standard uncertainty
u_{cA}	combined standard uncertainty determined from standard uncertainties and estimated covariances obtained from type A evaluations
u_{cB}	combined standard uncertainty determined from standard uncertainties and estimated covariances obtained from type B evaluations
U_L	Collector overall heat loss coefficient (W/(m^{2}K))
V	Voltage (V)
$\dot{V}$	Volumetric flow rate (m^3/s)
Vol	Volume
W	Distance between tubes (m)
X	Exergy (J/m^2)

Greek Symbols

α	Absorptivity (-), thermal diffusivity (m^2/s)
β	Collector tilt angle (°)
β'	Coefficient of volumetric thermal expansion (1/K)
β_{Cell}	Temperature coefficient of the PV cells (1/K)
δ	Thickness (m), declination angle of the earth (°)

ε	Emissivity (-)
ϕ	Latitude (°)
γ	Solar height (°)
η	Efficiency (%)
λ	Wavelength (m), longitude (°)
ν	Frequency (s^{-1}), kinematic viscosity (m^2/s)
ρ	Reflectivity (-), density (kg/m^3)
θ	Angle of incidence between the beam radiation and the collector (°)
σ	Stefan-Boltzmann constant, = 5.67×10^{-8} $W/(m^2K^4)$, standard deviation
τ	Transmissivity (-)
τ_{max}	Maximum no dimensional deviation from the mean, in a sample of tests

Subscripts

abs	Absorber
amb	Ambient
B	Bottom
b	Beam
bb	Blackbody
Cell	Cell
Col	Collector
cond	Conduction
conv	Convection
d	Diffuse
El	Electric
eq	Equivalent
f	Fluid
G	Combined
GC	Glass cover
H	High temperature
i	Index of elements along *z* direction
IN	Inlet
j	Index of elements along *x* direction
L	Low temperature
M	Module
max	Maximum
MG	Module glass
MBG	Module bottom glass
MTG	Module top glass
n	Normal
o	Optical
OUT	Outlet
P	Absorber plate
Ph	Photon
rad	Radiation
ref	Reference conditions
S	Sun
St	Structure
T	Tube
Th	Thermal
W	Wind
x	Along *x* axis
z	Along *z* axis

Chapter 1.

Introduction

This research focuses on the study of solar hybrid photovoltaic/thermal ("PV/T") collectors. This designation comes from the association of the thermal and electrical outputs of incident solar energy, in the same equipment. In terms of construction, they consist in simply applying photovoltaic cells to a solar thermal collector.

Renewable energy sources and a sustainable development have been on the international agenda for the last two decades. A broader application of renewable energy technologies brings environmental benefits, by reducing CO_2 emissions and saving natural fossil fuel resources, such as oil, coal, and natural gas. The contribution to a stronger energetic independence is also a key factor to boost political measures that encourage the use of renewable energy sources. In this context, the Kyoto Protocol was adopted on 11 December 1997, extending the 1992 United Nations Framework Convention on Climate Change. For a first commitment period, 2008-2012, the Protocol has set an average target of 8% reduction in CO_2 emissions for the EU compared to 1990 (UN Framework Convention on Climate Change, 2014). Because of its less developed economy, Portugal was allowed to further increase their emissions by 27%. According to the latest data, the increase did not exceed 13.1%, excluding CO_2 emissions from land-use change and forestry (LUCF), on a carbon equivalent basis (APA, 2014). In the current context, the European Union (European Comission - DG Climate Action, 2015) established average targets for a second commitment period, elapsing from 2013 to 2020, as:

- 20% reduction of greenhouse gases (GHG) emissions, relative to 1990 levels;

- 20% share of Renewable Energy Sources (RES) in gross final consumption;

- 20% reduction in primary energy consumption, in relation to the consumption projection for 2020 (made from Baseline 2007 by application of the PRIMES model of the European Commission).

According to the National Renewable Energy Action Plans (NREAPs), the share of renewable energies in the final consumption of electricity (RES-E) and heating and cooling (RES-HC) should reach 34.3 % and 21.3 %, respectively, in 2020, in the EU (European Forum for Renewable Energy Sources, 2011). Regarding estimates of electricity consumptions in 2020, wind energy will represent 14.1%, hydropower 10.5%, biomass 6.5%, photovoltaics 2.35%, concentrated solar power 0.5%, geothermal energy 0.3% and ocean energy 0.15%, as referenced by EREC (2011). According to the 27 NREAPs (EREC, 2011), energy from solar thermal should account for 1.2% of the total heating and cooling energy demand in 2020. Austria, Germany, Cyprus, Greece and Malta represent at the moment the stronger solar thermal markets in Europe. The solar thermal market is expected to grow in countries like Sweden, Denmark, Poland, France, Italy, Spain and UK. On average, in Europe, solar thermal is expected to grow by 10 to 15% per annum between 2010 and 2020.

According to the EU Roadmap (EREC, 2011), the NREAP for Portugal has specified an overall target of 31% for share of energy from renewable sources in gross final consumption, split into 55.2% for electricity, 30.6% for heating and cooling and 10% for the transport sector. By 2020, Portugal intend to pass the landmark figure of 1 GWp of PV power installed, together with countries like Spain, Italy, France, the United Kingdom, Greece, the Czech Republic, Belgium, and namely Germany. It is expected that 1475 GWh of electricity generation comes from PV, representing 2.3% of the total electric consumption. Regarding heating consumption, NREAP projections for 2020 indicate 160 ktoe from solar power source, representing 2% of total heat consumption. There is no specific information about energy consumption for cooling.

The extensive application of solar energy technologies, including solar thermal and photovoltaics, is particularly advantageous in a country with high levels of insolation such as Portugal. The average number of hours of sunshine is 2200-3000 per year, in contrast to Germany, for instance, where it is at most 1800 h/year (Portal das Energias Renováveis,

2015). However, the use of this potential has only become significant in recent years, driven by financial incentives launched by institutional programs, like partial tax deduction on the acquisition cost and high feed-in tariff for electricity production.

The production of renewable electricity and heat from PV/T collectors can significantly contribute to meet the EU targets, namely in Portugal. Additionally, the local production of thermal and electrical energy for self-consumption can represent a considerable saving in the energy bill for the end user, which is particularly interesting when the initial investment is compensated by the savings during the lifetime of the system. If the same equipment enables the simultaneous production of thermal and electrical energy, there are also benefits associated to the space required by the installation.

1.1 The present energy context and targets

Increasing the share of renewables in the energy consumption is an important strategy for achieving economic and environmental sustainability, through energy independence, rationalization of natural resources and reduction of greenhouse gas emissions. In this context, the production of heat and electricity from renewable resources is an important issue. The energy consumption in the world has been increasing, mainly due to the contribution of emerging national economies, such as Brazil, Russia, China and South-Africa (BRIC countries), and the dynamics of CO_2 emissions is in line with these trends. The share of renewables in primary energy consumption has been growing in the EU countries, from a value of about 6% in 2000, reaching 12.7% in 2013. In contrast, an opposite tendency is observed in China and other BRIC countries, till the beginning of this decade (Enerdata, 2014), as shown in Figure 1.1. Considering the evolution for EU countries, the goal of 20% share from RES in gross final consumption in EU can only be reached by 2023, considering the linear trend observed since 2005.

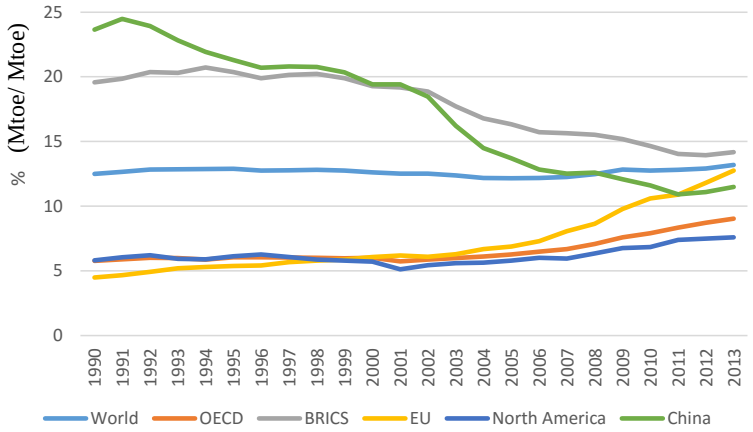

Figure 1.1 - Share of renewables in primary consumption (%), including hydro (data adapted from Enerdata (2014))

The evolution of the share of renewable energies, including big hydro, in the total electricity generation in Portugal is presented in Figure 1.2, between 1999 and 2014. It can be seen from the figure that there is a constant increase of the weight of RES-E since 2002. In 2014, the share of RES in electricity generation in Portugal, not including big hydro, was 32.5%, of which 1.2% came from solar photovoltaic (APREN, 2015c).

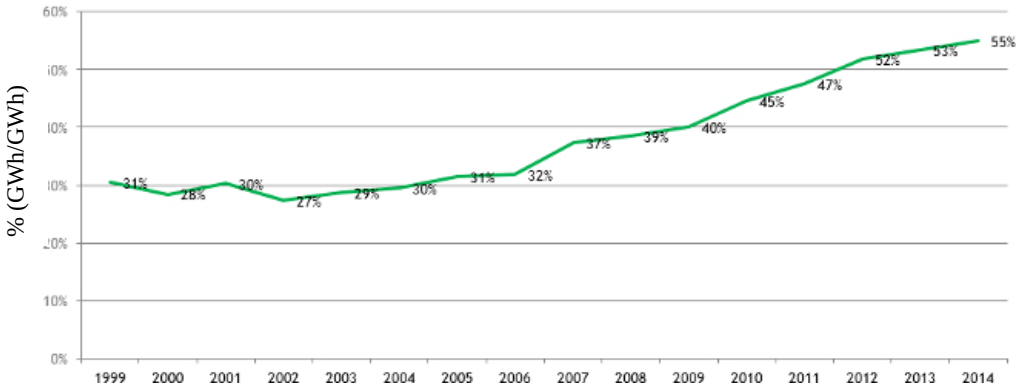

Figure 1.2 - Evolution of the share of electricity generation from renewable energies in Portugal between 1999 and 2014, including big hydro (with hydro correction) (APREN, 2015b)

The annual growth of the installed capacity of four technologies (wind, small hydro, solar and biomass) is shown in Figure 1.3. It can be observed that the newly installed capacity from renewables had a significant increase between 2004 and 2009, mainly due to wind power installations. This technology represented a large share, compared to the small hydro, solar and biomass. This growing trend was inverted in 2009, mainly because of the economic crisis. The data in Figure 1.3 seems to contradict the tendency presented in Figure 1.2. This can be explained by the reduction of the total installed capacity since 2011 in Portugal, presented in Figure 1.4.

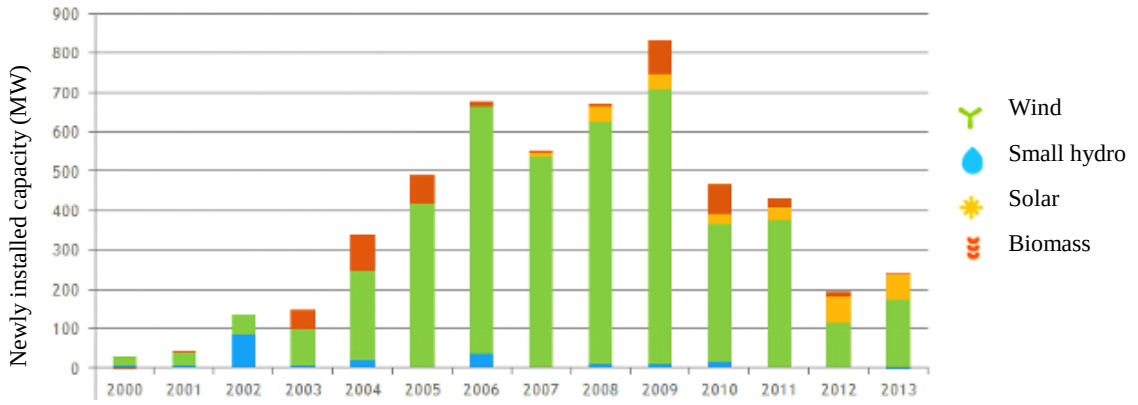

Figure 1.3 – Evolution of newly installed capacity from renewable energies, in Portugal (continental) between 1999 and 2013 (APREN, 2015a)

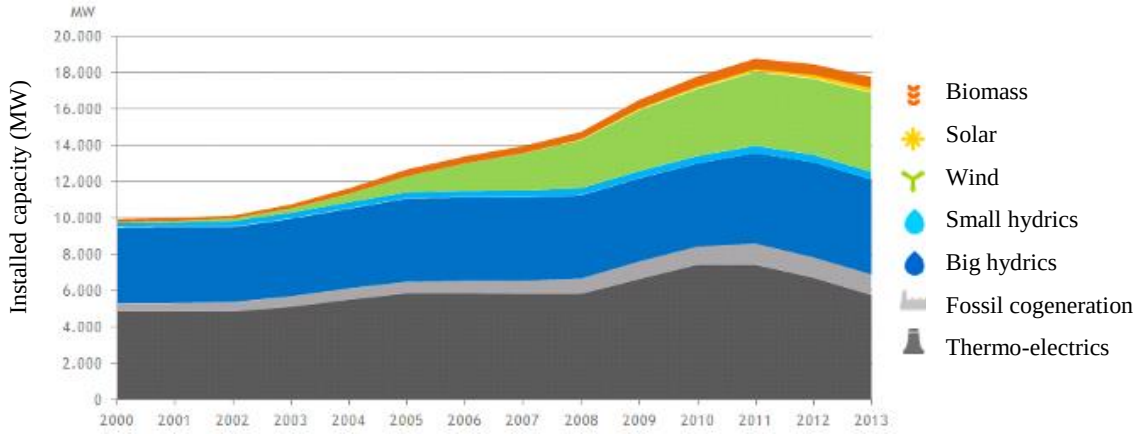

Figure 1.4 - Evolution of installed capacity in Portugal (continental) between 1999 and 2013 (APREN, 2015d).

The evolution of the annual capacity from photovoltaics and the total production of RES-E, between 2006 and 2014, in Portugal, is presented in Table 1.1. The electricity production from PV increased, but it is not possible to identify a regular relative increase trend. The PV share on the total RES-E production only decreased in 2010 and 2013, by 0.09% and 0.37%, respectively. Those periods corresponded to changes in the policy of incentives to the installation of photovoltaic equipment, with reduction of the feed-in tariffs for micro-generation.

Table 1.1 – Evolution of annual production from photovoltaic and total RES-E, in Portugal, from 2006-2014 (Direcção Geral da Energia e Geologia, 2015)

	2006	**2007**	**2008**	**2009**	**2010**	**2011**	**2012**	**2013**	**2014**
PV, GWh	5	24	41	160	215	282	393	479	631
RES-E, GWh	16188	16593	15140	19016	28754	24692	20410	30610	32461
PV share (%)	0.03%	0.14%	0.27%	0.84%	0.75%	1.14%	1.93%	1.56%	1.94%

Regarding heating and cooling, renewable energy accounted for 16.5 % of the total energy use in 2013 in the EU-28, a significant increase from 9.9% in 2004, as stated in

Eurostat (2015b). Mainly the industrial sector, services and residential use (building sector) contributed to this growth. Aerothermal, geothermal and hydrothermal heat energy captured by heat pumps are taken into account, to the extent reported by member states.

In contrast with the electrical production from renewables (RES-E), the weight of clean technologies in heating and cooling in Portugal has decreased. In 2011 renewable technologies accounted 35% for heating and cooling, while in 2013 this was only about 30% (Grupo About Media, 2015). Portugal was one of the 6 Member States that did not meet their planned 2013 renewable energy deployment level in the heating and cooling sector, together with Denmark, Ireland, France, the Netherlands and Slovakia (EC, 2015).

The heat production from solar thermal source was 1.9 Mtoe in 2013 in the EU, that is well below the trajectory expected from NREAP´s (EC, 2015). This has to be viewed from the perspective of low economic growth and moribund construction market. According to the Renewables energy progress report (EC, 2015), the 2020 indicative targets for solar thermal, reflected in the NREAPs, are likely to be missed by 41.8% - 45.6%. Data from the European Solar Thermal Industrial Federation reveal that in 2013 (ESTIF, 2014) and 2014 (ESTIF, 2015) the European market maintained a contraction trend for the newly installed capacity, with annual decrease of 11.8% and 7.1%, respectively. This corresponds to an increase in the total installed capacity of 6.2% in 2013 and 5.3% in 2014. In 2014, the total collector area was 45.4 million m², producing 31.8 GWth energy.

In 2013, the Portuguese solar thermal market shrank by 37%, decreasing almost to the same level as that of 2007 (ESTIF, 2014), as shown in Figure 1.5. This decline continued, and was equal to 11% in 2014 (ESTIF, 2015). The goal set by the National Plan for Energy Efficiency and Renewable Energy is 2.2 million m² of solar thermal systems installed by 2020, corresponding to an average annual growth of 11.5% between 2010 and 2020 (ESTIF, 2015). Considering the annual installed capacity, and the present tendency of small increase in new construction, the market should stabilize around 55000 m^2/year. The current trends clearly reveals an insufficient growth of the total collector area in Portugal. Unless the annual installations reach 150000 m^2/year, the target will be down by 50% (ESTIF, 2015).

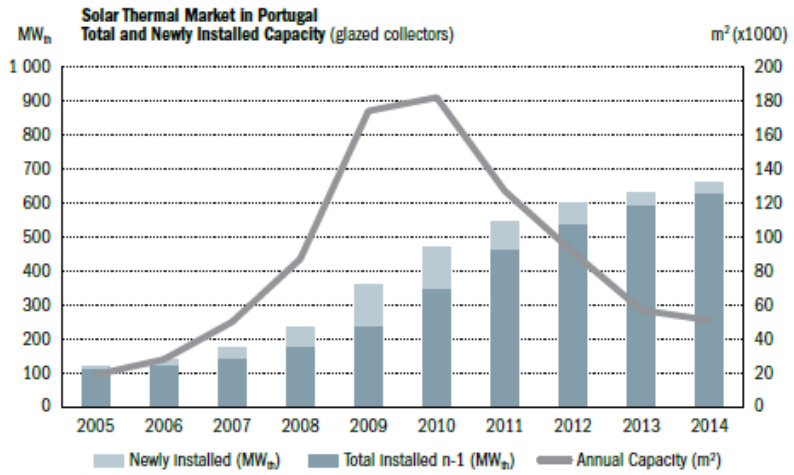

Figure 1.5 – Evolution of the total and newly solar thermal capacity in Portugal since 2005 (ESTIF, 2015)

Financial support for the installation of solar thermal collectors was in place in 2009 and 2010. However, there are currently no new specific measures foreseen to promote this technology, besides the ones already included in the Energy Efficiency Action Plan, and a revision of the building regulation code (EREC, 2011). According to this scenario, the goal of 30.6% share for RES-HC may not be reached.

The installation of hybrid PV/T solar collectors fits into an urgent strategy of diffusion of renewable energy technologies, with decisive implications for the institutional goals at national, European and global level. The wider application of hybrid PV/T collectors can provide a solution for maintaining the current growth of the electricity sector from solar energy, while boosting the solar thermal market. New products are needed, especially to change the dynamics of the solar thermal market. The investigation carried out in this thesis aims to create added value for characterizing the performance of hybrid PV/T panels, showing the advantages of their application in energetic and economic terms.

1.1.1 Use of solar energy in buildings

Buildings are responsible for about one third of the total final energy consumption, and about 40% of primary energy consumption in most of the 29 member countries of International Energy Agency (IEA) (IEA, 2015). The European Commission (EC) and the national governments have realized that the maximum potential for energy-saving and CO_2 reduction lies by far within the building sector (Buildings Performance Institute Europe, 2011).

In 2010, buildings consumed about 35% of the end-use energy, as shown in Figure 1.6. They are also responsible for about 36% of CO_2 emissions in Europe. Residential buildings, the largest segment of the building stock in the EU, are responsible for the majority of the energy consumption. About 70% of total final energy is spent on space heating. By 2050, the EU aims to cut its GHG emissions by 80-95% compared to 1990 levels (European Comission - DG Climate Action, 2015). Because of the significant contribution of the building sector, this target can only be met if buildings demonstrate very low carbon emission levels and very low energy usage from carbon based sources. For most buildings in Europe, this means improving the current average energy efficiency by a factor of four or five and broad installation of renewable based technology (Buildings Performance Institute Europe, 2011). The presence of renewables in building energy consumption was only 30% in 2010, as also indicated in Figure 1.6.

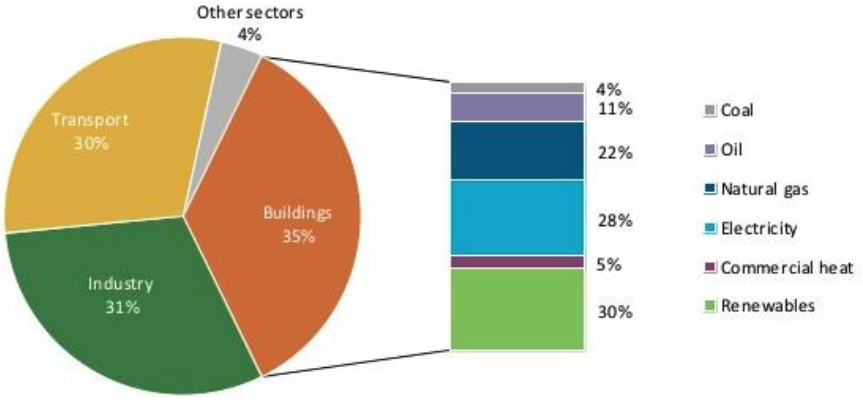

Figure 1.6 - Final energy consumption by sector and buildings energy mix, 2010 (IEA, 2013)

The establishment of adequate legislation framework is a key tool to assure that the targets are met. Through the introduction of the Energy Performance of Buildings Directive (Directive 2002/91/EC, EPBD), requirements for certification, inspection, training or renovation are now imposed in the EU Member States. The installation of solar collectors is a prescriptive requirement in building codes, such as in Portugal, Spain and Cyprus (Buildings Performance Institute Europe, 2011). The directive was modified in 2010 (European Parliament, 2010) with more ambitious provisions, namely that all newly constructed buildings should be energetically nearly self-sustainable and their energy should come from renewable sources 'to a very large extent', by the end of 2020. For old buildings, that represent a substantial share of the stock in Europe, the major renovations

should always include an improvement of the energy performance (European Parliament, 2010).

Heating applications (space heating and domestic hot water) in residential buildings are of low temperature range (50-60 °C). These needs can be easily satisfied by existing and available technologies using renewable energy sources. Simple systems such as thermosiphons with flat-plate or evacuated tube collectors can be installed on terraces and horizontal rooftops in mild climates. Building integration of pumped systems allows heat storage for several days in stratified water tanks, where a back-up from another energy source is often installed. The most cost-effective systems cover 40% to 80% of the heating loads for domestic hot water (IEA, 2011).

The European PV Industry Association (EPIA) calculates that a total ground floor area over 22000 km^2, 40% of all building roofs and 15% of all facades are suited for PV applications in the EU. Building-Integrated Photovoltaic Systems (BIPV) can cover from 15% to 58% of electricity demand (IEA, 2011). According to EPIA, a 20 m^2 PV system in a sunny region (global irradiance at least 1200 kWh/m^2/year) would produce enough electricity to fulfil the specific electricity need of a two to three people household on a yearly basis, with an excess during spring and summer, and a deficit in the winter (IEA, 2011). An eventual surplus of electricity production can be sold to the public grid with economic benefits, since in most developed countries there are incentives to encourage the deployment of renewable energy technologies. A report by IEA (2010) forecasts that more than half of the global PV capacity will be installed in residential and commercial buildings until 2050, producing a little less than half the total PV electricity generation.

Typical obstacles for a wider deployment of solar systems until recent years were the lack of evidence about their economic advantage, and their high initial price of acquisition and installation. The prices vary greatly according to the associated levels of complexity, as well as other factors such as labour. A DWH thermo-siphon system for one family unit consisting of a 2.4 m^2 collector and 150 litre tank costs 700 € in Greece, but 150 € in China (with no government support) (IEA, 2011). The effective cost of a system includes its price, but also the operation and maintenance cost and benefit of the generating plant over its life cycle period. Solar domestic hot water system cost in Europe ranges from 85 €/MWh to 190€/MWh, which is competitive with retail electricity prices in some countries, if not yet with natural gas prices. These costs are expected to decline until 2030 to 50€/MWh to 80 €/MWh for solar hot water systems (IEA, 2011). Cost reductions will

result from the use of less expensive materials, improved manufacturing processes, mass production and the direct integration of collectors into buildings as functional components and development of modular, easy-to-install systems.

Hybrid PV/T collectors allow for the improved conversion per unit collector surface area, by combining thermal and electric energy production. This is an interesting option when the available surface area is limited, such as in densely populated regions. Another possible application of water PV/T modules is the cooling of buildings through radiative heat exchange with the sky during the night by circulation of the cold water stored through a concrete floor slab, during the day (Eicker and Dalibard, 2011).

An adequate combination of solar options with other renewable technologies and energy-efficiency strategies into buildings are also very important. That most suitable scenario depends on local factors like climatic conditions, economic framework, available space and use of the building. In the last two decades, scientific and R&D advances have enabled a reduction of manufacturing costs. The market expansion led to larger scale production and consequently to price reductions. Nevertheless, the economic crisis felt in EU affected the building sector, and in turn it led to the regression of the solar thermal market over the last 5 years. The implementation of solar technologies through the building and industry sectors is mandatory (DR, 2006), in the context of the current legal measures towards the reduction of greenhouse gas emissions (GHG) and improvement of energy efficiency. Thus, institutional incentives, together with the continuity on the cooperation between the scientific research and the industry, are important paths for successfully achieving the ambitious goals of a sustainable development.

1.2 Combined thermal and electric conversion in solar collectors – the hybrid photovoltaic/thermal collector

According to Chow (2010), a common photovoltaic module converts between 4 to 17% of the incident solar radiation into electricity, while more than 50% of it is ultimately transformed into heat. This may lead to operating temperatures 50°C above ambient temperature. The electric conversion efficiency (η_{El}) can be defined as the electric power output ($\dot{E}$) produced over the total incident radiation in the photovoltaic module. There is a linear reduction of the electrical conversion efficiency with cell temperature (Wysocki and Rappaport, 1960, Saidov, 1995), relative to its value registered for reference conditions of

temperature and radiation. The operation of photovoltaic modules at high temperatures can eventually cause undesired damage of the modules.

The temperature dependence of the cell performance is primarily a characteristic of the material used. The effect of cell temperature on electrical efficiency is typically in the range of 0.4%/°C for monocrystalline silicon cells (c-Si) (Zondag, 2008, Chow, 2003, Kalogirou and Tripanagnostopoulos, 2006, Chow, 2010) and polycrystalline silicon cells (pc-Si) (Kalogirou and Tripanagnostopoulos, 2006). In amorphous silicon (a-Si) modules this reduction is more moderate, about 0.26%/°C (Chow, 2003, Yamawaki *et al.*, 2001, Kalogirou and Tripanagnostopoulos, 2006). Reviews on correlations between PV module performance and operating temperature can be found in Skoplaki and Palyvos (2009a), Skoplaki and Palyvos (2009b) and Dubey *et al.* (2013).

The electrical efficiency can be improved by removing the excess heat with, for example, a heat transfer fluid. This led to the concept of a hybrid collector. Bergene and Lovvik (1995) found that the electrical efficiency was in a range of 10.4% to 12.7% for flat-plate PV/T collectors using water. This represents a relative increase of 10-30% compared to the values obtained for uncooled conventional cells of the same type (9.5% to 10.5%). A reduction of 20°C in cell operating temperatures was achieved in ventilated roof and wall integrated photovoltaic collectors by air circulation, resulting in improved electrical and thermal performance of the building (Brinkworth *et al.*, 1997). Kalogirou (2001) reported that the average annual efficiency of photovoltaic power production increased from 2.8% to 7.7% with a hybrid system. More recently, Teo *et al.* (2012) found that electrical efficiency of a photovoltaic panel increased from 8.6% to 12.5%, when integrated with a solar air collector. Results from the numerical model developed by Siddiqui *et al.* (2012) showed that the performance of a PV panel with cooling varied very little with incident radiation (200–1000 W/m^2) at a constant ambient temperature (25°C), and also with ambient temperature (0–50 °C), at an incident radiation of 800 W/m^2. For the same variation in the operating conditions, the performance of the panel without cooling reduced significantly. It was concluded that the use of hybrid collectors is more advantageous in climates with high solar radiation and ambient temperature, such as in the Middle-East region.

There are also benefits regarding the installation costs of hybrid collectors. Applying the same device for heat and electric production immediately enables savings by avoiding duplication of common elements such as the transparent cover and the support structure

(Loferski *et al.*, 1982). Building integrated photovoltaics (BIPV), where thin films are used, allows for the reduction in installation costs and helps controlling the thermal loads on buildings (Agrawal and Tiwari, 2010). Van Helden *et al.* (2004) reviewed the existing literature and compared the performance of conventional and hybrid collectors from a number of aspects. Their major selected conclusions can be highlighted as follows:

- Two adjacent collectors with areas of 1 m^2 each, one thermal and another photovoltaic, can produce 520 kWh of useful thermal energy and 72 kWh of electrical energy. A hybrid collector of 2 m^2 would supply 700 kWh heat and 132 kWh electrical, respectively under the same conditions (Zondag *et al.*, 2002), representing an increase of 34% in total energy output. By reducing the collector area while keeping the same output, the use of PV/T collectors increases the average yield per m^2, with a corresponding decrease in manufacturing and installation costs.

- The energy payback time for PV/T collectors was found to be considerably shorter than for individual systems. For example, the pay-back time reduced to 2 years from the original 4.3 years for solar thermal and 3.4 years for a PV system in the Italian climate (Frankl *et al.*, 2000). Considering Greece, the payback time shortened to 10 years for c-Si modules and 6 years for a-Si modules (Tselepis and Tripanagnostopoulos, 2002).

Kalogirou (2001) included an economic analysis in his study based on the daily and monthly performance of a hybrid water PV/T system. The results indicated a reduction on life cycle system cost of 790 Cy£ (about 1360 €), with a payback period of 4.6 years. Calculations made by Energy Research Centre of the Netherlands (ECN) show that by using PV/T collectors instead of side-by side-systems, it is possible to reduce the collector area by 40% and still generate the same amount of energy (IEA, 2007).

In order to evaluate the performance of a photovoltaic/thermal (PV/T) collector, the amount of electricity compared to the useful heat from the collector is an important factor. The performance of a PV/T collector can also be evaluated in terms of exergy efficiency. PV/T collectors are thermodynamically advantageous as they simultaneously generate high-grade (electrical) and low-grade (thermal) energy. Joshi and Tiwari (2007) concluded that there is an increase of about 2–3% in exergy due to thermal energy, in addition to 12% for the electrical exergy from a PV/T system, which leads to an overall exergetic efficiency of about 14–15% for a PV/T system. Sarhaddi *et al.* (2010) reviewed the literature for PV/T

exergy efficiency. It was found that the working fluid has a strong effect on the modified exergy efficiency, which can be increased if an incompressible fluid (water) is used in a PV/T collector system.

In conclusion, the use of PV/T collectors can lead to both energetic and economic benefits. However, research is still needed, particularly on optimizing the PV cells layout, in terms of the fraction of the surface collector area covered by PV cells, and its preferable placement. An economic assessment of the PV/T collector performance is essential to assert this technological option.

1.3 Scope of the study

The aim of this research is to identify the optimum design of a PV/T collector for domestic hot water (DHW) applications, under the perspective of the fraction of the absorber surface area that is covered by PV cells ("packing factor", *Pf*), and its location. This is accomplished through the experimental and numerical assessment of the thermal and electrical performance, for different layouts of the collector. The best option for the collector configuration is also addressed through the perspective of the economic and environmental interest of PV/T collectors, in the Portuguese context. A comprehensive parametric study on the dependence of efficiency on the most relevant environmental, operating and design parameters is implemented, and constitutes another objective of the thesis.

A PV/T collector prototype was adapted for the experimental determination of the thermal and electrical efficiency curves. The curves are obtained for different values of *Pf*. A mathematical model was developed and applied in the parametric study. The studied parameters include ambient temperature (T_{amb}), solar irradiation (G), inlet temperature of the fluid ($T_{f,IN}$), packing factor (Pf) and PV cell layout on the absorber plate surface. The main focus is in the effect of the two latter parameters. The experimental results were used for validating the mathematical model.

Based on the performance characteristics obtained through the mathematical model, an economic and environmental evaluation of the implementation of a PV/T system is developed. This approach focusses on optimizing the PV/T packing factor, using a typical

scenario of energy costs for domestic installations, and two different typical climates in Portugal.

1.4 The structure of the thesis

The dissertation is divided into six chapters. After the introduction (Chapter 1), where the energy problem and the objectives of the thesis are presented, the trajectory and the present state of the art of hybrid PV/T technology is discussed through chapter 2. After introducing the PV/T background, concerning solar thermal and photovoltaic technologies, the different types of hybrid solar PV/T collectors and some of their relevant performance aspects are reviewed. An overview of their main characteristics and evolution is made, and the different forms of accounting hybrid collectors performance are presented. A detailed description of the development of hybrid water collectors, through analytical models, experimental studies, and economic aspects of its application, is issued. The existing PV/T commercialized models are listed.

The experimental PV/T prototype accessed in this work is presented in Chapter 3. The characterization of the collector and system components is made, and the experimental procedure is described. The criteria for selection of the experimental results under steady state conditions are defined. Three sets of tests with the application of three different PV to total area ratios were performed. The results for thermal, electrical, and combined efficiency are analysed.

Chapter 4 deals with the development of a mathematical model for the simulation of the performance of a PV/T collector, depending on different environmental, operational, and design conditions. The model is based on the energy and mass balance equations applied to the different parts of the PV/T collector. The model is validated in this chapter using the experimental results presented in Chapter 3. A parametric analysis is then performed, using the mathematical model. The analysis includes evaluation of the effect of environmental conditions (G, T_{amb}) and other operating conditions, such as inlet temperature of the thermal fluid ($T_{f,IN}$). Different design options, focused on the packing factor (Pf) and cells layout, are compared in terms of system performance.

An economic assessment of the implementation of the studied PV/T collector in a residential building is presented in Chapter 5. Upon a typical economic scenario, a methodology to define the optimum packing factor is described. This methodology is based

on the collector efficiency characteristics experimentally determined in Chapter 3 and numerically determined in Chapter 4. Yearly performances were obtained by a dynamic simulation tool using local weather data of the collector installation, in this case the TRNSYS software.

The most important conclusions of the thesis are summarized in Chapter 6. Special attention is given to suggestions for future research in the field of the PV/T technology.

Chapter 2.

A state of the art of PV/T technology

The potential of PV/T collectors is recognized since the 1970´s. There was however an intensification of studies over the past 20 years, in order to fully exploit their possibilities for contributing to the needs of heat and electricity of today´s society.

This chapter is dedicated to the characterization of the hybrid photovoltaic/thermal (PV/T) solar collectors, through the evolution from their early development stage to the present state of the art. The fundamental characteristics of solar radiation, reason for the existence of solar collectors, are first presented. After a brief introduction to photovoltaic and thermal collectors, the different types of PV/T collectors are presented. The main results from relevant numerical and experimental studies are also discussed, with a special attention to flat-plate PV/T water collectors. Different methodologies used for the economic evaluation of PV/T systems are presented. The primary application of PV/T collectors is water and air heating, although they are also relevant, for instance, in heat pump systems. These and other applications of hybrid collectors are exposed. Finally, a survey on the existing commercial models of hybrid PV/T collectors is also carried out.

2.1 Topics on solar and thermal radiation

This subsection summarises basic concepts related to solar energy and thermal radiation. Typical references of the literature concerning solar energy (Duffie (1991) and Kalogirou (2009)) provided the basis for the following topics and equations (2.1 to 2.7).

The sun emits a total of 3.8×10^{20} MW of power that radiates outward in all directions. The earth receives a small part: 1.7×10^{14} kW. The energy from the sun received per unit time on a unit area of surface perpendicular to the direction of propagation of the radiation at mean earth-sun distance outside the atmosphere is called the solar constant (G_{sc}). The latest value of G_{sc} is 1366.1 W/m^2, adopted in 2000 by the American Society for Testing and Materials (ASTM). The definition of this value was based on an Air Mass Zero reference spectrum (ASTM E-490) (NREL), developed from data collected from satellites, space shuttle missions, rocket soundings, ground-based solar telescopes, and modelled spectral irradiance. The spectral distribution of extra-terrestrial solar radiation ate the mean sun-earth is shown in Figure 2.1.

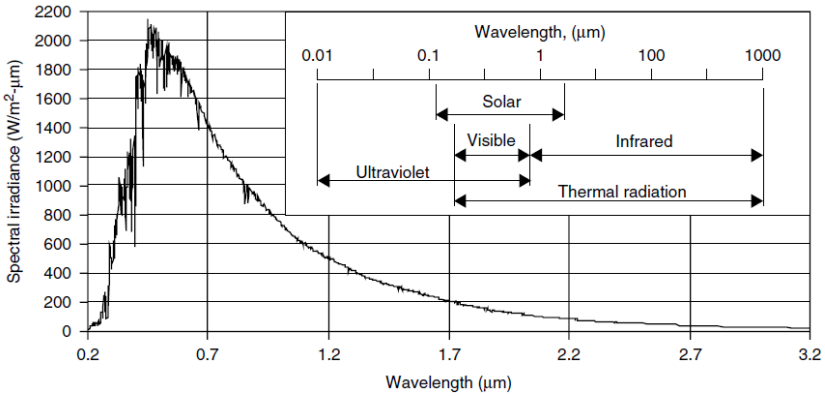

Figure 2.1 – Standard curve giving a solar constant of 1366.1 W/m^2 and its position in the electromagnetic radiation spectrum (Kalogirou, 2009)

The extra-terrestrial radiation measured on the plane normal to the radiation varies during the year, depending on the sun-to-earth distance. The solar heat at any point on earth depends on the ozone layer thickness, the distance travelled through the atmosphere to reach that point, the amount of haze in the air and the extent of cloud cover. Measured data of the solar radiation reaching earth´s surface in a certain location is usually available in energy rates, from a specified and calculated direction such as the ‘‘beam’’ radiation that comes directly from the sun, and the ‘‘diffuse’’ radiation that has been scattered in some generally unknown manner over all parts of the sky. A pyranometer is an instrument typically used to measure total hemispherical solar (beam plus diffuse) radiation. The solar,

or short wave, radiation in the wavelength range of 0.3 to 3 μm includes both beam and diffuse components.

Thermal radiation is a form of energy emission and transmission that depends entirely on the temperature characteristics of the emissive surface. It is in fact an electromagnetic wave that travels at the speed of light (*C*). It is, thus, characterized by a wavelength (λ) and a frequency (ν), as expressed in the following equation:

$$C = \lambda \nu \tag{2.1}$$

Thermal radiation corresponds to the region in the electromagnetic spectrum from approximately 0.2 to approximately 1000 μm (see Figure 2.1). An elementary particle, with zero mass and zero electric charge, is called a photon. The energy contained in a photon (E_P) of a photon is given by:

$$E_{Ph} = h\nu \tag{2.2}$$

where *h* is the Planck´s constant (=6.625×10^{-34} J.s). Combining eq. 2.1 and 2.2, it results in the definition of the energy of the photons in terms of the wavelength, as it follows:

$$E_{Ph} = h\,{}^{C}/_{\lambda} \tag{2.3}$$

This fact is particularly significant where a minimum photon energy is needed to bring about a required change (e.g., the creation of a hole–electron pair in a photovoltaic device).

The total thermal energy that is incident on a surface can then be reflected, absorbed, or transmitted. Each one of those fractions corresponds, respectively, to the reflectivity (ρ), absorptivity (α) and transmissibility (τ), and are related by the following expression:

$$\rho + \alpha + \tau = 1 \tag{2.4}$$

Each material is characterized by those radiation properties just defined, also called optical properties. However, they can change with the direction and wavelength of the incident radiation. The term generally used for radiation properties at a particular wavelength is “monochromatic”. A blackbody is a hypothetical idealization of a body that absorbs the total received radiation, and, thus, has α = 1, regardless of the spectral or directional characteristics of the incident radiation. A blackbody is also considered as a perfect emitter of radiation, although, in this case, it depends on its temperature and wavelength. The total emissive power results of the integration of the emitted energy for all the electromagnetic spectrum, and is defined by the Stefan-Boltzmann law:

$$E_{bb} = \sigma T^4 \tag{2.5}$$

In eq. 2.5, σ is the Stefan-Boltzmann constant = 5.67×10^{-8} W/m^2 K^4. The emissivity (ε) of a real surface is defined by the reason of its emissive power to the one of a blackbody. The Kirchoffs law of radiation for the monochromatic emissivity of any surface in thermal equilibrium, states that:

$$\varepsilon_\lambda(T) = \alpha_\lambda(T) \tag{2.6}$$

This can be generalized for the entire wavelength, as:

$$\varepsilon(T) = \alpha(T) \tag{2.7}$$

This generalization, however, is strictly valid only if the incident and emitted radiation have, in addition to the temperature equilibrium at the surfaces, the same spectral distribution. Such conditions are rarely met in real life; to simplify the analysis of radiation problems, however, the assumption that monochromatic properties are constant over all wavelengths is often made. Such a body with these characteristics is called a graybody.

2.2 The first stage of the development of thermal collectors and photovoltaic panels

In the last 60 years, technology research for the use of solar energy focussed on different applications, such as water heating, space heating and cooling, or electricity production. Among it, solar thermal collectors and photovoltaic panels are perhaps with the largest deployment in the market-ready energy technologies.

The photovoltaic effect has already been known since 1839, discovered by Becquerel. However, the first solar cell was only manufactured by Adam and Day in 1876. This cell was made from selenium, and had an efficiency (η_{El}) of about 1-2%. It was the discovery of the production process of pure crystalline silicon by Jan Czochralski in 1916 that led to a major advance for electronics (Kumar and Rosen, 2011a). In 1954, Daryl Chapin, Calvin Fuller and Gerald Pearson developed the first “high efficiency” silicon cell (Chapin *et al.*, 1954), which meant 6% by that time. However, the elevated production cost limited its application almost only to aerospace science. It was applied to ensure the operation of radio stations in the space satellite Vanguard I in 1958 (Riffat and Cuce, 2011). Research in the 1960s resulted in the discovery of new photovoltaic materials such as gallium arsenide (GaAs), which could operate at higher temperatures than silicon, but it

was even more expensive (Kalogirou, 2009). The energy crises of 1970s spurred a new found of initiatives in many countries to make photovoltaic systems affordable, especially for off-grid applications (Kumar and Rosen, 2011a). This resulted in a broader application of the use of photovoltaic panels.

PV cells, usually connected in series, are packed into modules through encapsulation resins, such as Ethylene-vinyl acetate (EVA), to produce a specific voltage and current when illuminated. PV modules can then be connected in series or in parallel in order to produce, respectively, larger voltages or currents. Applications powered by PV systems include communications (both on earth and in space), remote power, remote monitoring, lighting, water pumping, and battery charging. Besides those stand-alone applications, PV systems can also be grid connected, enabling selling the electricity, which can be economically interesting.

Regarding thermal collectors, flat plate collectors (FPC) with single glass cover are the most common type. They are mainly used in domestic hot water (DHW) systems with temperatures up to 60 °C, and thus often referenced as “low temperature” applications. The schematic pictorial view with the main parts of a typical water flat plate collector is represented in Figure 2.2. The operating principle is simple and well known. The incident solar radiation passes through a transparent cover and hits a blackened absorber surface. A large portion of the radiation is absorbed by the plate and then transferred to a transport medium into the channels, which are in physical contact to the absorber plate, to be carried away for storage or use. Normally the channels are copper tubes, named “risers”, arranged in parallel (“*harp”*), and are connected at both ends by larger diameter header tubes. Such configuration is often referred to as “sheet and tube” type. The underside of the absorber plate and the side of the casing are well insulated to reduce conduction losses. The liquid tubes can be welded to the absorbing plate, or they can be an integral part of it. The most used material for the cover is low iron glass, with a high transmissibility (τ) of the incident radiation (Kalogirou, 2009).

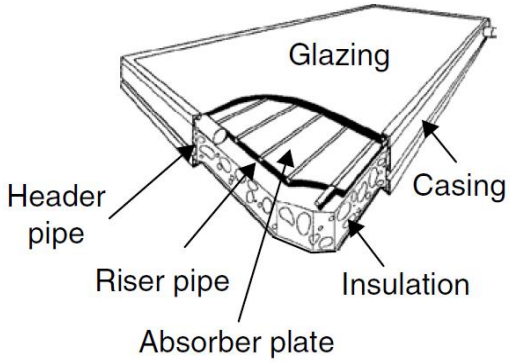

Figure 2.2 – Pictorial view of a typical flat plate collector with sheet and tube harp configuration (Kalogirou, 2004)

The performance of thermal collectors is evaluated through the thermal efficiency, (η_{Th}), defined as the ratio of the heat transferred to the fluid to the total incident radiation on the collector area (A_{Col}) (Duffie, 1991):

$$\eta_{Th} = \frac{\dot{m}c\left(T_{f,OUT} - T_{f,IN}\right)}{A_{Col}G} \tag{2.8}$$

In eq. 2.8, $\dot{m}$ and c are the mass flow rate and specific heat of the working fluid, and $T_{f,IN}$ and $T_{f,OUT}$ are its temperatures at the inlet and outlet, respectively.

The thermal efficiency (η_{Th}) decreases with the average collector temperature from a maximum value, called *optical efficiency* (η_o). This maximum value is verified when the ambient, the absorber plate, and the working fluid are in thermal equilibrium, and thus, losses are associated only to the optical properties of the cover and the absorber plate. Heat losses to the ambient through various modes of heat transfer occur in a thermal collector. The thermal losses result from the temperature differences that exist between the ambient, the cover, the absorber plate, the tubes, the insolation, and the fluid. An essential parameter of the collector is thus its *overall heat loss factor* (U_L), that represents the magnitude of that heat loss. η_{Th} can be expressed as a function of the temperature difference between the absorber plate and the ambient:

$$\eta_{Th} = \eta_o - U_L \frac{(T_P - T_{amb})}{G} \tag{2.9}$$

The performance testing procedure of solar thermal collectors is well defined in standards (IPQ, 2007). The tests should be carried out in order to cover different ranges for solar irradiance (G), ambient temperature (T_{amb}) and fluid inlet temperature ($T_{f,IN}$). A typical efficiency curve of a flat plate thermal collector working with liquid is presented in Figure 2.3. The variable in abscissa is called the *reduced temperature difference* (T^*), and can be defined as:

$$T^* = \frac{T_{f,IN} - T_{amb}}{G} \tag{2.10}$$

T^* can also be expressed according to the temperature of the plate (resulting on eq. 2.9), the average fluid temperature ($\overline{T_f}$), or $T_{f,OUT}$. The correspondence between the different references for T^* and η_{Th} is obtained through the use of different factors, that are defined according to the heat transfer processes between the different components. The collector overall heat loss factor can now be easily associated to the negative slope of the efficiency curve represented in Figure 2.3. Referring to the same figure, the thermal efficiency is there expressed as a linear function of T^* (Duffie, 1991):

$$\eta_{Th} = F_R\eta_o - F_R U_L T^* \tag{2.11}$$

In eq. 2.11, F_R is the *modified heat removal factor*, and accounts for the ratio of the actual useful heat transfer to the maximum possible useful heat transfer.

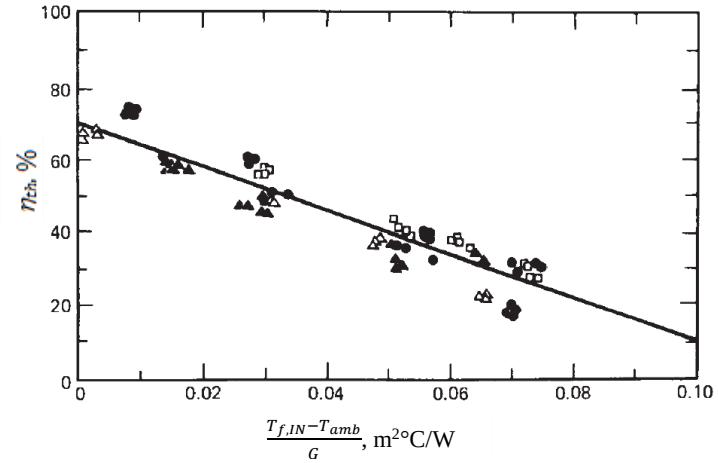

Figure 2.3 - Experimental collector efficiency data measured for a liquid flat-plate collector with one glass cover and a selective absorber (Duffie, 1991)

FPC are built in a wide variety of designs and from many different materials. The thermal fluids can be water, water-antifreeze solutions, or air. The most common constructive design is the sheet and tube, with harp channel configuration, as presented in Figure 2.2. A serpentine design for the absorber can also be found. In this case, the total flow is not divided into a number of streams inside parallel riser tubes, but it flows in a single tube on the underside of the absorber plate, in a serpentine path. This collector does not present the potential problem of an uneven flow distribution in the various riser tubes of the header and riser design. However, as the flow rate through the tube is higher, serpentine collectors cannot work effectively in thermosiphon mode (natural circulation) and need a pump to circulate the heat transfer fluid (Kalogirou, 2009).

Besides sheet and tube collectors, there are also concentrator type collectors, with different designs, but all being able to achieve higher temperatures, and thus they can be used in industrial applications, like, for example, for preheating water. The objective of concentrating the solar radiation into a smaller absorber area is to minimize convective losses and maximize incident radiation per unit surface area, so that higher operating temperatures can be obtained. Compound parabolic collectors, often referred to as *"CPC"*, have a reflector surface, constituted by pairs of parabolic cavities that allow multiple reflection of solar beams into the absorbers. The absorbers can be either fins over the fluid pipe or evacuated tubes. In the first configuration, a glass cover is needed, such as in the case of a flat plate collector. A schematic diagram of this design is presented in Figure 2.4.

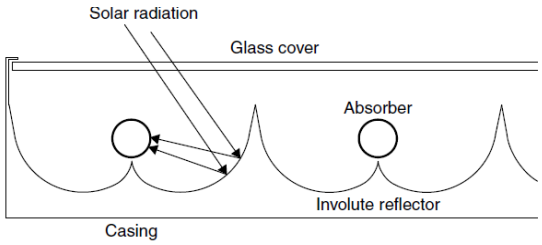

Figure 2.4 – Schematic diagram of a panel CPC collector with cylindrical absorbers (Kalogirou, 2009)

Along with concentration, the vacuum technique is also used in solar collectors, in order to minimize convective losses, and also reach higher temperatures. Direct flow evacuated tube collectors (ETC) with U-type copper tubes are often used combined with compound parabolic concentrator reflectors. Vacuum is maintained in the space between two concentric glass tubes, where the outer one is transparent, in order to transmit solar radiation. Inside the inner glass tube, a copper tube bended in U is connected to a cold water distributer pipe, in the inlet side, and to a hot water collector, on the outlet side, as shown in Figure 2.5 a). The entering cold water flows down, gradually heats, and returns up to the hot water collector tube. Direct flow ETC can also be found with coaxial absorber tubes, as presented in Figure 2.5 b). In this case, the vacuum is created between the outer glass and the absorber tube, which has another concentric tube inside, creating two separated sections. The cold fluid enters in the inner tube, flows down while heats, and returns through the outer annular section. The inlet and outlet are connected also to separate annular zones in the same tube. This configuration has the advantage that the heat lost from the hot fluid is transferred to the cold flow, reducing the overall heat losses. In heat pipe ETC configuration, presented in Figure 2.5 c), one copper heat pipe is assembled together with the inner tube with a small amount of high purity water, or alcohol. When heated, it

vaporizes, and the vapour rises along the heat pipe to a heat pipe bulb, which is in contact with the water collecting tube area, placed in the top of the collector. There, the heat it transferred to the cold water, causing the condensation of the vapour and the downward flow of vapour and the restoring of the system. The main advantage of heat pipe tube collectors is of practical order, once the absorber plate and the manifold does not require any process of bonding, making installation much easier than with direct flow collectors. Also, as the tubes are separated, any eventual damage in one tube just requires its substitution, without emptying or dismantling the entire system. This flexibility makes heat pipe ETC collectors ideal for closed loop solar designs as the modular assembly allows for easy installation and ability to easily expand by adding as many tubes as you want. On the other hand, in direct flow evacuated tube designs there isn't a heat exchange between fluids, contributing to minor heat losses (Jack *et al.*, 2011).

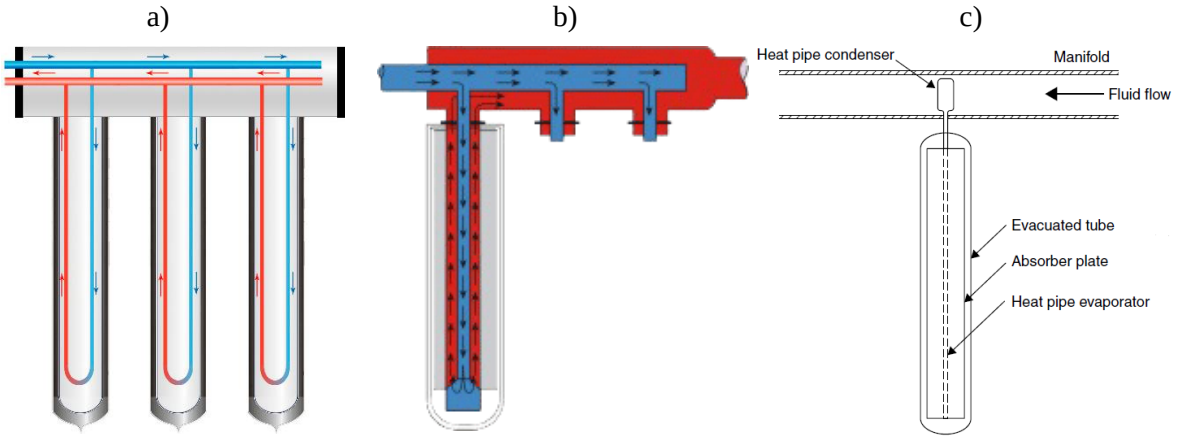

Figure 2.5 – Schematics of three types of design for evacuated tube collectors: a) Direct flow with U-type absorber (ArchiExpo, 2015) b) Direct flow with coaxial-type absorber (Sunda Solar, 2015) c) Heat pipe (Kalogirou, 2009)

The performance characteristics of some examples of the different types of solar thermal collectors just presented are listed in Table 2.1, according to its certification documents (Água Quente Solar, 2015).

Table 2.1 – Performance characteristics for different types of solar thermal collectors for water heating available in the market

Collector type	Intercept (η_0)	a_1 (W m^{-2} K^{-1})	a_2 (W m^{-2} K^{-2})	Ref.
Flat plate, selective	0.757	4.0	0.015	Agua Quente Solar (2015b)
	0.744	4.162	0.014	Agua Quente Solar (2015c)
CPC	0.727	3.948	0.022	Agua Quente Solar (2015d)
Evacuated tubes	0.518	2.08	-	Agua Quente Solar (2015a)
Evacuated tube with heat pipes	0.694	2.118	0.004	Agua Quente Solar (2015e)

The procedure most recently adopted by the certification entities accounts for the dependence of the heat loss coefficient (U_L) on the average fluid temperature ($\overline{T}_f$), and ambient temperature. The parameter a_2 in Table 2.1 reflect that influence. The thermal efficiency function can be rearranged in order to reflect that dependence, resulting on the following expression (IPQ, 2007):

$$\eta_{Th} = \eta_o - a_1 \frac{\left(\overline{T}_f - T_{amb}\right)}{G} - a_2 \frac{\left(\overline{T}_f - T_{amb}\right)^2}{G} \tag{2.12}$$

From the analysis of Table 2.1 it is possible to note that FPC and CPC collectors can reach higher values of η_0, but the heat losses coefficient is almost halved for evacuated tube collectors, because of the vacuum insulation.

The collectors mentioned before are mostly suitable for domestic and small-scale applications. Large installations, such as solar thermal power plants, for energy production at high temperatures (250-2500°C), comprise mirrored parabolic format devices, associated in large numbers, with concentration of energy at a point or along a line. They can be arranged aligned rectangular, around a solar tower, or forming a parabolic dish. For those applications, the systems use also tracking systems, to follow the sun beams.

The collectors with concentration are not in the scope of this study, so, this subject will not be further detailed.

2.2.1 Photovoltaic technology

Photovoltaic cells are made of semiconductor materials. The most commonly used are silicon (Si) and cadmium sulphide compounds (CdS), cuprous sulphide (Cu_2S), and gallium arsenide (GaAs). The largest part of the PV market continues to be crystalline

silicon based, either polycrystalline (pc-Si) or monocrystalline (c-Si), with a share of about 83.5% (Chen and Riffat, 2011).

The c-Si modules are made of cells of about 0.2-0.3 mm thickness, saw-cut from a single cylindrical crystal of silicon. Although their average electrical efficiency is about 10-17%, its manufacturing process is also more expensive, resulting in a higher price for the modules. The pc-Si modules are made of cells cut from an ingot of melted and recrystallized silicon. They are cheaper to produce, but have slightly lower electrical efficiency, in the range of 11-15% (Chen and Riffat, 2011).

Instead of a crystalline structure, amorphous silicon (a-Si) modules use Si atoms deposited on a thin and homogeneous layer substrate with better light absorption capacity. Therefore, they can be manufactured with thinner thicknesses, of about 1 μm. For the same reason, amorphous silicon cells are also known as a *thin film PV technology*. This feature, when combined with the variety of possible substrates, makes them a flexible option in terms of applications (for example, curved surfaces). Although their efficiency is inferior to crystalline silicon (in the range of 4-7%), their cost is also lower and are less sensitive to efficiency losses at high temperatures. This type of modules has about 5.8% of market share (Chen and Riffat, 2011). An important disadvantage of thin film technology is the rapid performance degradation with time. Therefore, further growth in the PV market is not expected.

New materials are emerging for manufacture of photovoltaic modules at competitive costs and higher efficiency than that of the a-Si, such as cadmium telluride (CdTe) and the CIS cells ($CuInSe_2$) (Kalogirou, 2009). Currently, the efficiency of commercial photovoltaic panels is about 15%, in average. It should be noted that laboratory models have achieved efficiency values superior than 40%, for multijunction (three-junction, four-junction or more) concentrator cells (NREL, 2015a). A multijunction cell works with different semi-transparent layers: the top cell produces electricity from the higher-energy portion of the solar spectrum, and the lower-energy sunlight passes through to the lower cells to be converted into electricity, resulting in a highly efficient production of power. To make it work, the stacked cells need to absorb complementary wavelengths of sunlight, and those absorption wavelengths are determined by the material's bandgaps (NREL, 2013). The photo-absorption layers are made from compounds of multiple elements, from which the most typical are InGaP, GaAs and InGaAs (Sharp, 2013). The recent significant reduction in the prices of photovoltaic cells has led to annual growth of

PV products. 2013 was a record year for PV installations with at least 38.4 GW of newly-added capacity around the globe and 11 GW in Europe (EPIA, 2014). In 2014, system prices for utility-scale solar PV fell below $1.8 per watt in the USA - 59% lower than in 2010, according to NREL and Lawrence Berkeley National Lab. Prices for distributed solar PV systems dropped 12-19% in the USA during 2013 (Sustainable Business.com, 2014). Since 2010, installed prices are down 46%, because of lower equipment costs and streamlined installation practices. Residential solar averaged $3.29 per watt in 2014, according to NREL (Sustainable Business.com, 2014). A study on the PV costs evolution and forecasts is made by Candelise *et al.* (2013). The growth in solar photovoltaic technologies including worldwide status, materials for solar cells, efficiency, factor affecting the performance of PV module, overview on cost analysis of PV and its environmental impact are reviewed in a study by Tyagi *et al.* (2013). The evolution of PV panel cost by material from 1995 to 2012 with prediction for price up until 2020 was presented, confirming that PV price dropped drastically since 1995 to 2012. The solar PV module production shares by technology are shown in Figure 2.6 (SolarBuzz, 2015). The production of pc-Si PV modules is set to dominate PV manufacturing during 2014, accounting for 62% of all modules produced.

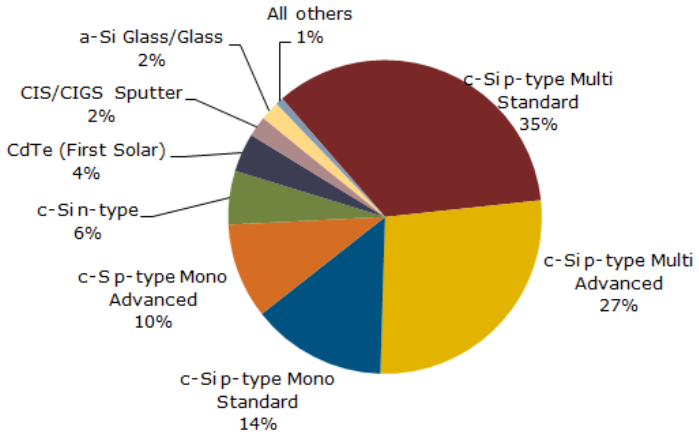

Figure 2.6 - Solar PV module production by technology in 2014 (SolarBuzz, 2015)

For a typical commercial PV panel, 13-20% of the solar radiation is converted into electricity (Armstrong and Hurley, 2010). The electrical efficiency of photovoltaic modules depends, besides the type of cells, on the intensity of radiation of the climate region where they are installed, the module packing factor and module temperature. The packing factor is the fraction of the area effectively occupied by the cells, compared to the area occupied by the module.

As previously stated on section 1.2, cell efficiency decreases with its operating temperature according to the following relation (Skoplaki and Palyvos, 2009a):

$$\eta_{Cell} = \eta_{El,ref}\left[1 - \beta_{ref}\left(T_{Cell} - T_{ref}\right)\right] \tag{2.13}$$

The rate of the reduction in η_{Cell} characteristics is given by the temperature coefficient, β_{ref}. $\eta_{El,ref}$ represents the electrical efficiency under reference conditions of temperature (T_{ref}) and radiation (G_{ref}), normally corresponding to 25°C and 1000 W/m^2, respectively. The effect of the temperature coefficient upon the efficiency of various types of silicon-based PV module is shown in Figure 2.7. It can be seen from the figure that the influence of the operating cell temperature on the electrical efficiency is especially relevant for monocrystalline modules, indicated by a steeper decline of the curves, compared to pc-Si and a-Si. Therefore, the benefits of cooling the cells in hybrid collectors is expected to be more pronounced for these type of modules.

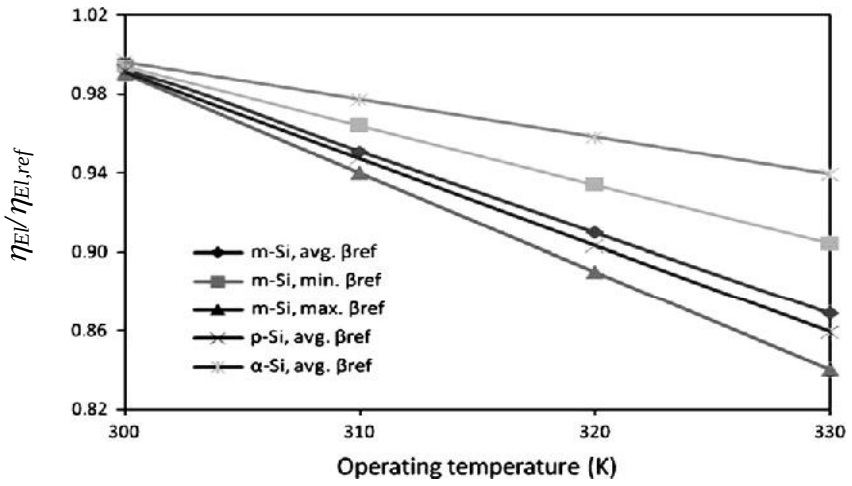

Figure 2.7 – Influence of operating temperature on the electrical efficiency for typical silicon-based PV module types (c-Si, pc-Si and a-Si) (Skoplaki and Palyvos, 2009a)

2.2.2 The role of selective coatings used in absorber plates

Absorber plates are made of good thermal conductive materials, such as copper, in order to reduce the thermal resistance between the plate and the working fluid. An absorber plate should also have high absorptivity, typically achieved by a black colour surface on the receiver side. The thermal efficiency is further improved if the coating material is selective. This means that its optical properties change depending whether it receives or emits radiation to the environment. A good selective coating easily absorb radiation, with an absorptivity (α) higher than 95% in the visible range (400 nm ≤ λ ≤ 700 nm), while

presents a low emissivity (ε), lower than 15%, in the infrared range ($\lambda \geq 0{,}8\ \mu$m). Selective absorbers often consist of a very thin black metallic oxide on a bright metal base.

Optical properties of some important selective coatings are listed in Table 2.2. Black copper oxide coating on copper or aluminium is the most commonly used selective surface and is extensively commercialized in solar collector industries. Before application of the black coating, the copper sheet undergoes a deep cleaning process. It is then dipped for different times in the blackening bath containing sodium hydroxide (NaOH) and sodium chlorite ($NaClO_2$), at a solution temperature between 140-145°C. However, the most successful and stable selective surfaces developed so far are made of black chrome. It is obtained by electroplating a layer of bright nickel on absorber plate, then electrodepositing an extremely thin layer of chromium oxide (black chrome) on the nickel substrate. Black chrome on copper shows good selectivity and resistance for humidity. Their feasibility is however limited because of the high cost of copper substrate (Madhukeshwara and Prakash, 2012). Other typically used selective coatings are black nickel, applied on polished nickel, or galvanized iron and cobalt oxide fixed on bright nickel-plated steel substrate.

Table 2.2 - Properties of selective coatings (Madhukeshwara and Prakash, 2012)

Selective Coatings	α	ε	α/ε
Black Chrome	0.93	0.10	9.3
Black Nickel on polished Nickel	0.92	0.11	8.4
Black Nickel on galvanized Iron	0.89	0.12	7.4
CuO on nickel	0.81	0.17	4.7
Co_3O_4 on silver	0.90	0.27	3.3
CuO on Aluminium	0.93	0.11	8.5
CuO on anodized Aluminium	0.85	0.11	7.7
Solchrome	0.96	0.12	8.0
Black paint	0.96	0.88	1.09

Besides the aforementioned coatings, used mainly in mid-temperature applications, such as solar hot water and industrial process heat, there are also high-temperature absorber coatings, suitable for concentrated solar power applications. Transition metal based *cermets* have emerged as novel high temperature solar selective coatings (Selvakumar and Barshilia, 2012). A *cermet* is a composite material formed by ceramic (*cer*) and metallic (*met*) materials. The metal is used as a binder for an oxide, boride, or carbide. Generally, the metallic elements used are nickel, molybdenum, and cobalt. Those applications are not within the scope of this thesis.

2.3 General aspects of photovoltaic/thermal collectors

In this section the global aspects thorough the comprehension of PV/T collectors operation are presented, including its performance characterization and discussion of recent advances within this subject.

The thermal efficiency (η_{Th}) and electrical efficiency (η_{El}) of a PV/T collector represent, respectively, the useful heat ($\dot{Q}$) and electric power output ($\dot{E}$) produced over the total incident radiation in the absorber plate, as defined in the following expressions:

$$\eta_{Th} = \frac{\dot{Q}}{GA_P} \tag{2.14}$$

$$\eta_{El} = \frac{\dot{E}}{GA_P} \tag{2.15}$$

According to IPQ standard (IPQ, 2007), η_{Th} can also be defined with reference to collector aperture area, instead of the absorber area. A typical indicator of the global performance of a PV/T collectors is the *global efficiency* (η_G), defined as the ratio of the sum of the useful heat and electrical power output over the total incident radiation:

$$\eta_G = \frac{\dot{Q} + \dot{E}}{GA_{GC}} \tag{2.16}$$

Other terms are also commonly used for the global efficiency, as "*combined efficiency", "overall efficiency"* or "*total efficiency*".

The simplest way to build a flat-plate PV/T absorber is to connect mechanically a standard PV module over the top surface of the absorber plate of a flat collector. The PV laminate can either be mechanically pressed (Tripanagnostopoulos *et al.*, 2002) or glued using an additional adhesive layer with good thermal properties (Fraisse *et al.*, 2007, Zondag *et al.*, 2003). In this particular configuration, the thermal resistance between the PV cells in the module and the absorber plate was estimated to be about 0.01 (m^2 K/W) by Van Helden *et al.* (2004). Subsequently, the PV/T absorber is inserted in the frame of a standard collector and covered by a glass cover.

According to Chow (2010), the calculated maximum thermal efficiency of PV/T-liquid systems ranges generally from 45% for unglazed collectors to 70% for glazed designs. For PV/T-air systems, the thermal efficiencies can be up to 55% for optimized collector design. The thermal efficiency of air type PV/T systems depends strongly on the air flow rate, air duct depth and collector length. For higher values of air flow rate, small

air duct depth and long PV/T systems, thermal efficiencies up to about 55% are predicted by the theoretical models (Tripanagnostopoulos *et al.*, 2002). However, for a building integrated system studied by Ricaud and Roubeau (1994) higher values for efficiency (66%) were achieved. Through transient analysis of Prakash (1994) it was pointed out that an hybrid air collector (PV/T-a) design has a lower thermal efficiency than an water collector (PV/T-w), because of the reduction of heat transfer coefficient between the thermal absorber and the airflow stream. Their advantage is most relevantly due to low construction and operative cost, whereby they are frequently used in PV applications in buildings at locations with low insolation and ambient temperatures, space heating is necessary for almost all the year. PV cooling by air circulation in combination with space heating can also be more useful and cost effective compared to liquid cooled PV (Tripanagnostopoulos *et al.*, 2002).

Regarding the solar cell technology in conventional c-Si PV modules, the absorption coefficient is usually optimized for the wavelength range $300 \leq \lambda \leq 1100$ nm for silicon. However, in the case of PV/T collectors, it is relevant for the thermal function to consider the absorption coefficient for the entire range of the solar spectrum ($300 \leq \lambda \leq 2500$ nm). Because of their homogenous surface texturing, monocrystalline silicon solar cells (c-Si) have lower reflection losses than polycrystalline silicon (pc-Si) solar cells and present a better absorption properties. In order to check the difference between pc-Si and c-Si, experimental measurements were carried out by (Dupeyrat *et al.*, 2011b). The absorption coefficients for pc-Si and c-Si cells were found to be 0.85 and 0.90 respectively. The corresponding electrical efficiency was 0.13 and 0.15. Therefore, it may be preferable for both thermal and electrical perspective to use c-Si solar cells instead of pc-Si solar cells. This could make even obvious with a specific low-reflecting encapsulation in order to increase the PV/T plate absorption coefficient.

The comparison between amorphous silicon (a-Si) cells and polycrystalline cells is integrated into the extensive parametrical study by Tripanagnostopoulos *et al.* (2002). The results showed that the use of pc-Si PV module can be considered more effective, taking into account its higher electrical efficiency and also its lower relative system cost. Amorphous silicon was compared to single-crystalline module types by Daghigh (2011), for a water-based PV/T collector in a Building Integrated Photovoltaic Thermal (BIPVT) system. The effect on thermal and overall efficiencies are shown in Figure 2.8. The behaviour of a-Si cells is better in both thermal and overall perspectives.

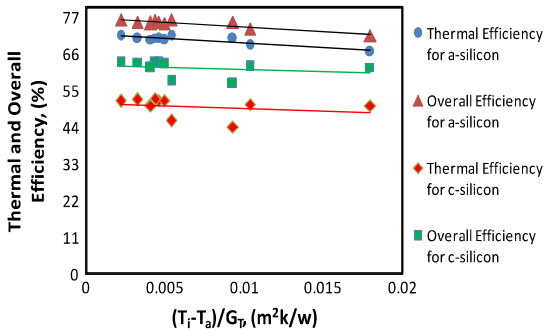

Figure 2.8 – Comparison of thermal and overall efficiencies of c-Si and a-Si PV cells in a water BIPVT system (Daghigh, 2011)

Sandnes and Rekstad (2002) refer a loss of about 10% in the solar energy absorbed by pasting solar cells on the absorbing surface, due to lower optical absorption in the solar cells ($\alpha \approx 75\%$), when compared to the absorber plate ($\alpha \approx 90\%$), and due to the increased thermal resistance for the thermal fluid. Numerical studies to improve these characteristics on thin-films used in PV/T collectors were carried out by Johnston (2010), through the optimization of the different layers that compose solar thin film PV/T cell.

2.3.1 Estimating hybrid collector efficiency

The useful heat ($\dot{Q}$) and electric power ($\dot{E}$) produced by a PV/T collector are obtained through the following equations:

$$\dot{Q} = \dot{m}c\left(T_{f,OUT} - T_{f,IN}\right) \tag{2.17}$$

$$\dot{E} = V_{MPP} I_{MPP} \tag{2.18}$$

In eq. 2.18, V_{MPP} and I_{MPP} are the voltage and electric current output of the PV module, respectively, at *maximum power point* (MPP) operating conditions.

The Hottel–Whillier–Bliss model, modified by Florschuetz for hybrid collectors (Florschuetz, 1976), express the thermal efficiency as:

$$\eta_{Th} = F_R\left[(\tau\alpha)_e(1-\eta_{El}) - U_L\left(\frac{T_{f,IN} - T_{amb}}{G}\right)\right] \tag{2.19}$$

In eq. 2.19, $(\tau\alpha)_e$ is the *effective transmittance-absorptance product* ($\tau\alpha$) (Duffie, 1991), that accounts for the reduced thermal losses due to absorption of solar radiation by the glass, and η_{El} is the electrical efficiency evaluated at cell operating temperature (T_{Cell}). Eq. 2.19 can be modified in order to use the average fluid temperature in the collector ($\overline{T_f}$), defined as:

$$\overline{T_f} = \frac{T_{f,IN} + T_{f,OUT}}{2} \tag{2.20}$$

The definition of thermal efficiency as a function of $\overline{T_f}$ follows the expression (Chow, 2010):

$$\eta_{Th} = F' \left[(\tau\alpha)_e \, (1 - \eta_{El}) - U_L \left(\frac{\overline{T_f} - T_{amb}}{G} \right) \right] \tag{2.21}$$

The factor F_R in eq. 2.20 is replaced in this last definition by the *collector efficiency factor* (*F´),* that is the ratio of the actual useful energy gain to the useful gain that would result if the entire collector absorber surface was at the local fluid temperature. Firstly, a solar collector should absorb most of the incident irradiance, in order to achieve a high level of useful heat, *i.e.* $(\tau\alpha)_e$ needs to be high. Secondly, the heat transfer from the absorber to the working fluid should be much higher than the heat loss to the surroundings, represented by the overall heat loss coefficient (U_L). The *collector efficiency factor* describes the relationship between these two processes. Eisenmann *et al.* (2004) pointed out that the value of *F'* strongly depends on the distance between the tubes (*W*) and the absorber plate thickness (δ_P).

Traditionally, the thermal efficiency of solar thermal and PV/T collectors is expressed as a linear function of the reduced temperature difference (*T**) similarly to the formulation used for thermal collectors, as expressed previously in eq. 2.11.

Precaution should be taken into considering when using this approach for the estimation of efficiency of hybrid collectors, since electricity and heat are not qualitatively equivalent (Bergene and Lovvik, 1995). Heat can only be converted into work if there is a temperature difference between the hot temperature source (T_H), and the low temperature sink (T_L) (Fujisawa and Tani, 1997). Through the use of an exergy analysis, it is possible to quantitatively access that difference, based on the same standard. One can define electrical (X_{El}) and thermal (X_{Th}) exergy, as:

$$X_{El} = \eta_{El} I \tag{2.22}$$

$$X_{Th} = \left(1 - \frac{T_L}{T_H}\right) \eta_{Th} I \tag{2.23}$$

In the previous equations, *I* is the hourly irradiation. The overall exergetic efficiency (η_X) of the PV/T collector will then be taken as:

$$\eta_X = \frac{X_{El} + X_{Th}}{G} \tag{2.24}$$

The study of Fujisawa and Tani (1997) shows that, despite the thermal annual earnings are much higher than the electrical gains (548 kWh/66 kWh), the annual electric power exergy is about ten times higher than the thermal (66 kWh/5.6 kWh) for a liquid PV/T collector with one glass cover. The output density of exergy in combined utilization was also determined by dividing exergy gain (thermal + electrical) by the installation area. With the hybrid PV/T collector, an output of 102.1 kWh/m^2 was achieved in comparison with 65 kWh/m^2 for a standalone PV module and thermal collector. However, it was found that a PV/T collector with no cover had a better output density of exergy than a PV/T collector with one cover. A similar exergetic analysis was carried out by Morita *et al.* (2000). For the same conditions of irradiance, wind and ambient temperature, the results for a glazed hybrid collector were slightly better than for an unglazed collector.

Another approach is proposed by Huang *et al.* (2001), defining an energy-saving efficiency (η_{PES}) in terms of the primary-energy saving, as:

$$\eta_{PES} = \frac{\eta_{El}}{\eta_{\dot{E}}} + \eta_{Th} \tag{2.25}$$

In eq. 2.25, $\eta_{\dot{E}}$ is the electric power generation efficiency for a conventional power plant, taken as 0.38. This reference value can change, depending on the method of electric energy generation. It was observed that the primary energy saving efficiency of water heating a system that integrates an unglazed PV/T collector exceeds 0.60, which is better than the result for a stand-alone solar hot water heater or PV system. The study of Bhattarai *et al.* (2012) presents a one-dimensional mathematical model for simulating the transient process of sheet and tube type PV/T system and compared it to conventional type solar collectors. It was found that the energy saving efficiency was 16% higher for the PV/T system.

2.3.2 Evolution and characterization of hybrid PV/T solar collectors

The concept of hybrid collectors was first introduced in the 1970s, as a coincidence with the oil crisis. The first hybrid PV/T system was integrated in 1973 by Boer and Tamm (2003) into a test building (Solar One House), operating with air. It was the first building which enabled direct conversion of sunlight into both electricity and heat for domestic use. The first liquid PV/T collector was investigated by Wolf (1976). The performance of a combined solar PV and water heating system for a single-family residence over a full year was analysed. The main concept was further improved by Kern Jr and Russell (1978), studying its application suitability in four different typical USA climates. Hendrie (1979)

presented a model and experimental results for the thermal and electric performance of an air and a liquid type of combined photovoltaic/thermal solar collector. Two separate one-dimensional analyses were carried out by Raghuraman (1981) for the prediction of the thermal and electrical performance of both liquid and air flat-plate PV/T collectors. The analysis account for the temperature difference between the PV cells and the flat plate absorber. Some design recommendations were made to maximize the total energy obtained from the collectors, mainly focusing on the thermal component. Their suggestions can be summarized as follows:

- glass cover with crisscrossing grooves reduce convective losses and the use of anti-reflective coatings reduce reflection losses;
- optimal cell-to-glass-cover air-gap height for cell-to-glass temperature difference between 8-17°C should be higher than 5 cm;
- use of high thermal conductivity epoxy bonds between PV cells and the thermal collector to ensure a low thermal resistance and electrical isolation;
- in liquid PV/T collectors, minimize heat resistance between the plate and the tubes by integrating the two elements during the manufacturing process,;
- improve the interior heat transfer coefficient by using rough tube (PV/T-w) or channel (PV/T-a), and also by placing fins along the flow direction;
- use of selective black coatings of black nickel or chrome on the thermal collector

Cox and Raghuraman (1985) carried out their numerical work on the improvement of the absorber characteristics to enhance the performance of air flat plate collectors employing c-Si PV cells. It was found that, for PV cells covering more than approximately 65% of the total collector area, a selective absorber actually reduces the thermal efficiency when used with a gridded-back cell. The requirements for the low emissivity coating are less than 0.25 and a solar transmissivity greater than 0.85 for the infrared radiation range.

A hybrid a-Si PV/T-w solar collector was developed by Lalovic *et al.* (1986). The electric characteristics of the photovoltaic modules showed only a small increase with the adaptation to the hybrid configuration, but the unit performed well as a thermal solar collector. In addition, space saving and cost saving of the photovoltaic generator was obtained with the PV/T adaptation. In order to improve the thermal efficiency, a novel

transparent type of a-Si cell was integrated and tested in the hybrid unit. The results obtained showed the possibility of constructing simple and cheap hybrid systems with good photovoltaic and thermal efficiencies.

Bhargava *et al.* (1991) presented a study on hybrid forced air systems for optimizing the area of the solar cells necessary to generate electrical energy for the circulation fan, for different configurations of the air heater. The hybrid system was proven to be self-sufficient only for specific design parameters and flow rates. The study was extended by Garg *et al.* (1991), adding a plane booster reflector to a hybrid flat-plate solar air heater. Concentrating sunlight is a key technique in order to reduce the system cost. With this solution, the area required for the PV modules decreased, and therefore payback time becomes shorter. However, PV module temperature increases with concentration which is disadvantageous for the electrical efficiency (Riffat and Cuce, 2011). It was verified that the minimum required cell area decreases with the use of boosters, and that high cost cells could be replaced by low cost reflectors. The improvement on the total efficiency of applying a booster diffuse reflector and glazing in a water hybrid system with pc-Si cells was registered by Tripanagnostopoulos *et al.* (1996), as well as the use of the glazing. Brogren *et al.* (2000) analysed the optical efficiency of a water-cooled hybrid PV/T system with a low-concentrating aluminium CPC, determining a value for the optimum efficiency η_o= 0.71.

An important issue to achieve high thermal performance in a PV/T collector is to ensure a good thermal contact between the photovoltaic element and the absorber plate (Raghuraman, 1981), as previously mentioned. Usually, a layer of an adhesive with high conductivity is applied to bond the two parts. Zakharchenko *et al.* (2004) evaluated different materials and application methodologies to assess the thermal contact between the PV panel and the collector. It was concluded that commercial PV panels failed due to the poor thermal conductivity of the panel substrate material. Therefore, a PV prototype panel was constructed using metallic substrate with a thin insulating layer. It was noted that the power output of the PV panel increased 10% with the new design. In order to enhance the heat transfer between PV cells and the metal sheet, more advanced techniques can be used, consisting on laminating together all the components in one step: the transparent front glazing (not necessarily glass), the encapsulated material, the PV cells and the absorber (Zondag, 2008). Dupeyrat *et al.* (2011a) obtained better results of thermal and electrical performance for this type of improved laminated absorber. Numerical results obtained are

shown in Figure 2.9. The experimental data also indicated a significant improvement for both thermal and electrical performance in comparison with other PV/T concepts. Thermal and electrical efficiency for zero reduced temperature were 79% and 8.8%, respectively, using pc-Si PV cells.

The effect of thermal contact was also studied by Siddiqui *et al.* (2012), through a range of contact resistance from 0.005-0.05 ºC m^2/W. From the case of ideal contact to the case of maximum contact resistance considered, the PV cell temperature increased around 18 °C. The absolute drop in efficiency was around 2% and about 19% of electrical power was lost due to the contact resistance. Khandelwal *et al.* (2007) proposed a non-contact Photovoltaic-Thermal collector, which consists of a PV panel separated by a conventional sheet and tube solar thermal collector. At high values of PV transmissivity ($\tau > 0.75$), the thermal efficiency of the non-contact type system exceeds that of the contact type collector at higher values of inlet temperatures.

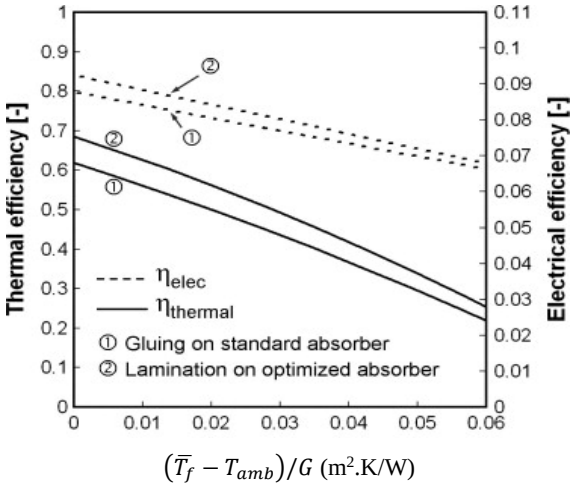

Figure 2.9 - Thermal and electrical efficiency curves of a PV/T collector for two different bonding methods as a function of the reduced temperature. (Dupeyrat *et al.*, 2011a)

The application of thermal collectors, photovoltaic panels, and hybrid collectors on buildings, according to many sensitivities entails a negative aesthetically overload, despite its energetic and environmental advantages. Therefore, the potential for the PV/T collectors can be increased by developing aesthetically more attractive solutions, which can be applied into buildings, integrated on the facades and roofs. This technology is known as building integrated Photovoltaic/Thermal (BIPVT) systems, and have been studied by various authors (Clarke *et al.*, 1996, Sandberg and Moshfegh, 1998, Posnanky *et al.*, 1992, Posnanky *et al.*, 1994, Brinkworth *et al.*, 1997), cited in Riffat and Cuce (2011). This technology evolved from the building integrated photovoltaics (BIPV) technology

(Posnanky *et al.*, 1992). Structural elements can be used also for energy management purposes, providing savings in material and installation costs (Anderson *et al.*, 2009). Typically, air systems are used, for convenience of installation and integrated with ventilation units, but also water collectors can be adapted, providing hot water and space heating simultaneously. Tripanagnostopoulos (2007) carried out an experiment to improve the performance of a PV/T system at University of Patras, Greece. A dual heat extraction operation system was investigated, through a combination of water and air PV/T. Three alternative models of passing the water inside the air channel were tested. For improving heat extraction using air, the modifications included placing a thin corrugated metallic sheet into the middle of a flow channel, as well as attaching small ribs on the opposite wall of PV module and installation of light weight pipes along the channel. In order to enhance the operation on a horizontal roof, a booster diffuse reflector was also combined with the PV/T system.

Moradi *et al.* (2013) compiled and reviewed the major control parameters on the thermal/electrical performance of PV/T collectors, such as packing factor, mass flow rate, PV solar cell materials, heat transfer fluids and geometries. Regarding the compiled information on the influence of the packing factor, it was found that a comprehensive knowledge about the variation of packing factor and its effects with different fluids in different PV/T systems still does not exist. So, the study developed in this thesis contributes to fill in the research on this aspect, with respect to water PV/T collectors.

2.4 Relevant characteristics of the components of PV/T flat plate water collectors

Most of the hybrid flat plate water collectors are sheet and tube type, originating from the most widely spread technology of thermal collectors. In this section, some major issues concerning the different components of a PV/T collector are presented, which are correlated to the wide range of constructive designs of the hybrid collectors. Advantages and fragilities of different existing options will be addressed.

2.4.1 Use of transparent covers

The option for the number of transparent covers used in the sheet and tube configuration (none, one and two) has been extensively studied (Fujisawa and Tani (1997),

Morita *et al.* (2000), Zondag *et al.* (2003), Tripanagnostopoulos (2010)). Single glazed PV/T collector presents higher thermal output than an unglazed one. Nevertheless, its electrical output is reduced, due to additional optical losses (Fraisse *et al.*, 2007). An exergy analysis was presented by Morita *et al.* (2000). It was found that the exergetic efficiency increases with the flow temperature up to a maximum value of about 13.36% for glazed and 11.92% for unglazed PV/T collectors, and the optimum flow temperature is, respectively, 83.6ºC and 38.8ºC. Chow *et al.* (2009) carried out outdoor measurements on two similar sheet-and-tube thermosiphon PV/T water collector systems in Hong Kong, in one glazed and another unglazed. The influence of six selected operating parameters was evaluated. The first law analysis indicated that the glazed design is always more suitable if either the thermal or the overall energy output is to be maximized. However, from the exergy analysis it was found that an unglazed system is more advantageous for high values of PV cell efficiency, packing factor, water mass to collector area ratio, and wind velocity, whereas the increase of solar radiation and ambient temperature are favourable for a glazed system. The use of more covers create additional losses by reflection. Instead of glass, other lighter, cheaper and stronger materials, such as polycarbonate, polymethylmethacrylate, polyvinyl fluoride, can be adopted for the cover. However, the use of glass is the best option, because of its good optical properties, resistance to UV and high temperatures (Zondag *et al.*, 2003). The air gap between the PV laminate and the cover material must be thin enough to benefit from the insulating properties of air, and preventing at the same time convective flows and micro turbulence. Generally the gap with should be between 15 and 40 mm. ((Gordon, 2001), cited by Aste *et al.* (2014)).

2.4.2 PV modules

The photovoltaic modules applied to an absorber typically use EVA for the encapsulation of the cells. However, there are some technical difficulties related to standard EVA lamination of PV modules. It can decompose in the presence of acetic acid (delamination, coloration, degradation of PV cells by acid) at temperatures above 80°C. Thus, conventional PV laminates cannot withstand stagnation temperatures in glazed collectors usually operating between 120 and 180 °C. A novel glazed PV/T collector concept based on PV laminate with siloxane gel is now under development at the Czech Technical University in Prague. Application of siloxane gel instead of EVA lamination compound offers several important advantages, such as high temperature resistance, high

transparency, compensation of thermal dilatation stresses and favourable heat transfer from PV to heat exchanger in PV/T collector ((Matuska, 2014), (Poulek *et al.*, 2012)).

2.4.3 Absorber plate structures

In a PV/T solar collector, the absorber plate is an important functional element, since it transfers the solar energy, that was not converted to power by the photovoltaic element, to the fluid. Its desirable properties are high thermal conductivity and low specific heat capacity. For these reasons, absorber plates for water PV/T are generally metallic, such as copper, aluminium or more rarely steel. The upper side of the plate should allow the perfect adhesion of the cells or the PV laminate, thus enhancing the heat removal from the photovoltaic component. Besides the most usual sheet and tube arrangement, other structures can be found for absorbers in water hybrid FPC, as shown in Figure 2.10.

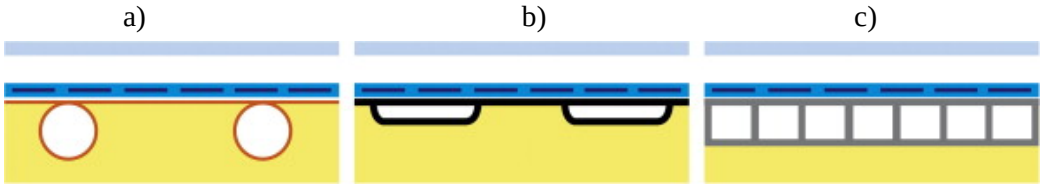

Figure 2.10 - Thermal absorber structures: sheet and tube, roll bond and box channel (Aste *et al.*, 2014)

The designation of “roll bond” comes from its production process. In this manufacturing technique, a sandwich of two aluminium sheets is formed by means of a special hot or cold rolling process. Before pressing together the aluminium sheets, the desired pattern of channels is printed with a serigraphic process on the inner surface of one sheet. A special ink is applied to prevent subsequent welding of the surfaces along the pattern. This allows flexibility to configure the desired channels profile, according to various configurations, while maintaining a low production costs (Aste *et al.*, 2014).

The “box channel” structure is formed by parallel ducts with a rectangular cross section. It can be made from an extruded or pultruded profile, that is generally aluminium, or, occasionally, using polymeric materials, such as rubber or fiberglass (Cristofari *et al.*, 2002, Cristofari, 2012). However, the relatively large coefficient of thermal expansion of plastics hinders the binding with the PV laminate (Van Helden *et al.*, 2004), and their low thermal conductivity and temperatures resistance makes their limited to this application. Special components are required to connect the inlet and the outlet manifolds to the rectangular channel, which greatly increases the costs and the technical issues. The

manufacturing process of the box channel configuration is relatively expensive (Aste *et al.*, 2014).

A strategy to strengthen the deployment of hybrid collectors is by reducing its production cost, without prejudice of the performance. With a numerical model developed and validated, Charalambous *et al.* (2011) optimized the absorber plate configuration, by reducing the size of the tubes and the amount of metal worn in the flat panel construction, for both harp and serpentine configuration. Based on their results, the cost on expensive raw materials such as copper can be reduced.

2.4.4 Configurations of the collector structure

Beyond the traditional "sheet and tube" type of water hybrid collectors, some other designs have been evaluated by Zondag *et al.* (2003). The performance was studied by varying the layout of the different parts (PV module, absorber, fluid flow). Four main types of PV/T were identified according to the water flow pattern and the heat exchange method, as shown in Figure 2.11: sheet and tube, channel, free flow and double absorption.

It is clear that a more efficient heat transfer is obtained when the mean distance between heat generation and heat collection is minimal. This is the case when the liquid flows directly over, or below, the PV cells, in the channel concept. Figure 2.11 b) shows channel flow over the PV cells. In channel PV/T collectors the absorption spectrum of the fluid should be sufficiently different from the absorption spectrum of the PV. The existence of an additional glass cover turns the assembly heavy, and fragile.

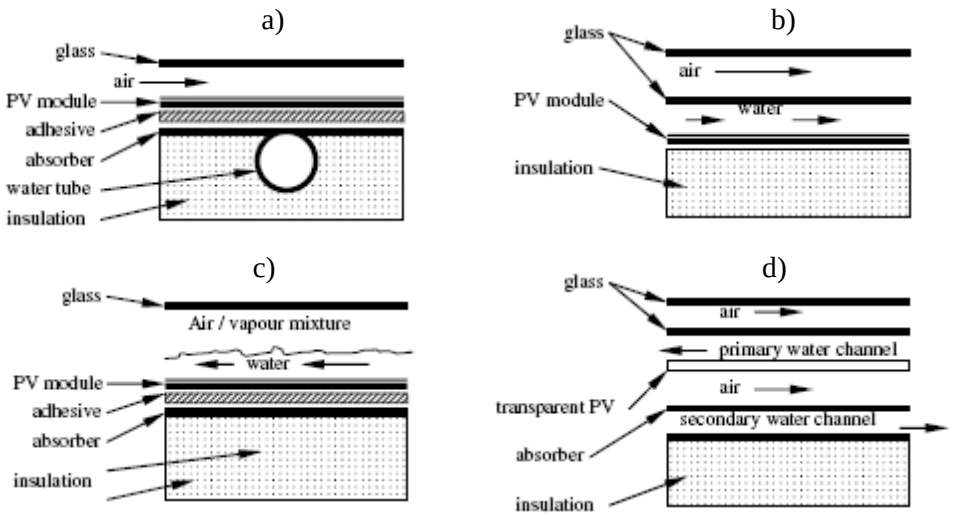

Figure 2.11 – Different configurations for flat plate water hybrid collectors
a) sheet and tube; b) Channel; c) Free flow; d) Double absorption (Charalambous *et al.*, 2007)

The concept of drawing heat beneath the PV cells is depicted in Figure 2.12. Here, the PV module can be opaque, or transparent with a separate black thermal absorber underneath the channel. This geometry is better suited to withstand water pressures in the channels than in the case of a broad channel. The absorber "box channel" structure is applied in this configuration. Sandnes and Rekstad (2002) have used this type of design, filing the square-shape box-type absorber channels with ceramic granulates, in order to improve the heat transfer to flowing water. The results for applications to low-temperature water-heating systems were promising.

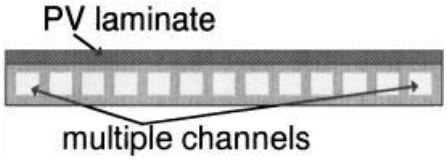

Figure 2.12 - Channel PV/T with liquid flow beneath the PV cells (Van Helden *et al.*, 2004)

The channel design with liquid flow under the PV cells has been used in the BIPV/T technology, for facades (Ji, 2006). With the use of wall-mounted water-type PV/T collectors, the system not only generates electricity and hot water simultaneously, but also improves the thermal insulation of the building envelope. The simulation results indicated that there is an optimum water mass flow rate for the desired energy performance. A dynamic simulation model of a building-integrated photovoltaic and water heating system, was developed by Chow *et al.* (2008), using the same absorber design. Their study was further developed by Chow (2009), analysing the annual energy performance of a BIPV/T water system, in both natural and forced circulation modes. Compared to a normal building

facade, both modes of operation were able to reduce the thermal transmission through the PV/T water wall by about 72% and 71%, respectively. An economical evaluation was also performed by determining the payback period, and the economic advantage of the BIPV/T water system was proved to be much better than a simple BIPV. Cristofari *et al.* (2009) also developed a simulation model for a channelled type water PV/T collector manufactured in a copolymer material. The system was suitable for wall integrated water heating.

Recently, the use of flat-box absorber design on PV/T systems has become more frequent ((Chow *et al.*, 2006), (He *et al.*, 2006)). A model for flat-box aluminium-alloy photovoltaic and water-heating system designed for natural circulation was developed by Ji *et al.* (2007). The simulated results indicated that the higher the packing factor and the glazing transmissivity, the better the overall system performance.

In a free flow design (see Figure 2.11c)), the cooling effect of the thermal fluid moves towards the front surface of the PV panel. One glass layer is eliminated, compared to the top channel flow design, whereby reflection losses and material costs are reduced, as well as the mechanical problem of breaking the glass cover is avoided. A disadvantage of this design is the increased heat loss due to evaporation. As in the case of the channel flow type, the fluid flowing over the PV panel has to be transparent for the solar spectrum (Zondag *et al.*, 2003). Until today, this configuration had only been studied on a theoretical basis.

The two-absorber panel in Figure 2.11d) combines, to a certain extent, the channel and the free flow solutions. A transparent PV laminate is used as a primary absorber below the primary water channel. A black metal plate is installed as a secondary absorber, separating air from the secondary water channel. The water passing through the upper channel is returned through the lower channel. Hendrie (1982) examined this design, and reported a high thermal efficiency (Zondag *et al.*, 2003). A main advantage of this concept is that a lower mean PV cell temperature is maintained, compared with geometries with heat and electricity generation in one plane (Figure 2.11 a) to c)). A disadvantage, however, is the complexity of the geometry, that makes the module difficult to manufacture.

Zondag *et al.* (2003) evaluated nine design concepts of hybrid water collectors, based on the four types showed on Figure 2.11. The numerical results revealed better thermal efficiency for the two absorber design (Figure 2.11 d)). Regarding the total annual yield for a domestic hot water system, the best option was the channel-below-transparent-

PV design. The one-cover sheet-and-tube design was also proved to be a good alternative, since its efficiency was only 2% inferior. As this latter design is by far the simplest to manufacture, the single cover sheet-and-tube design seems the most promising of the examined concepts for domestic hot water production.

Seven configurations of serpentine collectors with single glazing were designed, investigated and compared through simulation methods by Ibrahim *et al.* (2008). Different type of paths for the flow were considered: direct, oscillatory, serpentine, web flow, spiral, parallel-serpentine, and modified serpentine-parallel. The best results for the efficiency were observed for the spiral flow design shown in Figure 2.13.

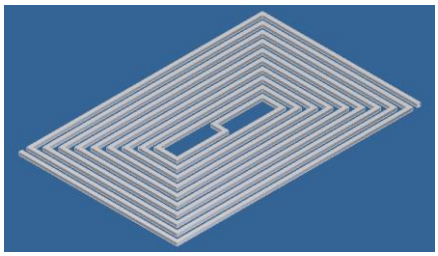

Figure 2.13 - Spiral flow configuration (Ibrahim *et al.*, 2008)

The pressure drop across the flow is also an important factor, because of mechanical and thermal aspects. A larger pressure drop requires higher energy demand on the circulation pump. If the PV/T collector uses natural circulation a higher pressure drop lows the flow rate, and thus the heat transfer. Experimental results carried out by Pieper and Klein (2011) and Hermann (2011) with a configuration called “bionical”, were compared to the harp and serpentine configurations. The plate used in the “bionical” configuration replicates the structure and morphology of the blood vessels: small size parallels channels connected together in pairs into a bigger channel and then they are all collected in the manifold, as shown in Figure 2.14. The results showed that the harp configuration gives a better response than the serpentine arrangement, and slightly worse than the bionical, for high flow rate.

Figure 2.14 - First generation BIONICOL prototype collector (© Fraunhofer ISE) (ISE, 2015)

2.5 Parameters affecting the performance of PV/T flat plate water collectors

The development of theoretical and empirical models is an essential tool in engineering to predict the performance, such as from solar PV/T collectors, over a wide range of operating conditions. After validation, these models can be used, e.g. for design purposes. Analytical models of PV/T collectors are developed based on energy balance equations, considering the relevant heat transfer modes and adequate boundary conditions. Several software tools are available for solving the governing equations, such as EES (F-Chart software, 1975), or ANSYS Fluent (ANSYS). EES is a general equation-solving program that simultaneously solves a set of non-linear algebraic equations. ANSYS Fluent software uses finite volume method discretization of a set of differential equations to m, typically describing fluid flow and heat transfer problems. TRNSYS (Transient System Simulation Tool) (TRNSYS) is used for unsteady analysis, simulating the performance of a modelled system over a period of time. It integrates information of the variation of several environmental conditions, such as radiation, wind and ambient temperature, for a certain geographic location.

It is important, within the context of this thesis, to identify the most important parameters that affect the performance of hybrid PV/T water collectors. In this section, some conclusions from the baseline investigations previously published in the field of hybrid photovoltaic/thermal water systems will be following discussed. Although efficiencies depend on several parameters, a summary of published values of electrical and thermal efficiencies of water PV/T collectors is listed on Table 2.4, according to studies selected by Aste *et al.* (2014). Table 2.4 was outlined evidencing the influence of the flow rate by surface area of the absorber, absorber plate configurations and existence of cover. The reported efficiency values correspond to zero reduced temperature, except when otherwise indicated.

Table 2.3 – Thermal and electrical efficiencies from selected works on water PV/T collectors (adapted from Aste *et al.* (2014))

Plate type	PV/T Type	Flow rate (kg/s m^2)	Thermal efficiency	Electrical efficiency	Analysis type	Refs
Sheet and tube	Uncovered	0.02	66%	14%	Experimental	Kim (2012)
	Covered	0.02	58%	8.90%	Numerical	Zondag et al. (2003)
	Uncovered	0.02	52%	9.70%	Numerical	
Box channel	Uncovered	0.02	70%	15%	Experimental	
	Covered	0.02	57%	12%	Numerical	Chow et al. (2006)
	Covered	n/a	45% daily	10.15% daily	Experimental	Ji et al. (2007)
	Covered	0.02	60%	9%	Numerical	
	Covered	n/a	71%	n/a	Experimental	Sandnes and Rekstad (2002)
	Uncovered	n/a	76%	n/a	Experimental	
Roll bond	Covered	0.01	49.3% yearly	10.3% yearly	Numerical	Bai et al. (2012)
	Covered	0.02	79%	8.70%	Experimental	Dupeyrat et al. (2011b)

In this subsection, relevant conclusions of numerical and experimental studies on the influence of the most important parameters affecting the performance of hybrid flat plate water collectors are presented. Studies dedicated to the impact of the packing factor and the PV cells layout are emphasized.

2.5.1 Packing factor (P_f) and PV cells layout

The application of PV cells over an absorber plate obstructs the incident radiation, causing a reduction on the energy conversion to useful heat, as confirmed in several studies. Figure 2.15 shows the electrical and the thermal efficiency of a PV/T collector obtained through a numerical model by Dupeyrat *et al.* (2011a) for an absorber plate covered by pc-Si solar cells for packing factors of 65%, 80% and 100%. The results confirm that a higher packing factor has a positive impact on the PV efficiency, with an increase of about 3.5%, but impairs the thermal efficiency. Wu *et al.* (2011) developed a model to study the performance of a heat pipe PV/T system, and used it for carry out a parametric investigation on several parameters, including *Pf*. It was found that the solar cell temperature decreased, by increasing *Pf* from 0.7 to 0.9.

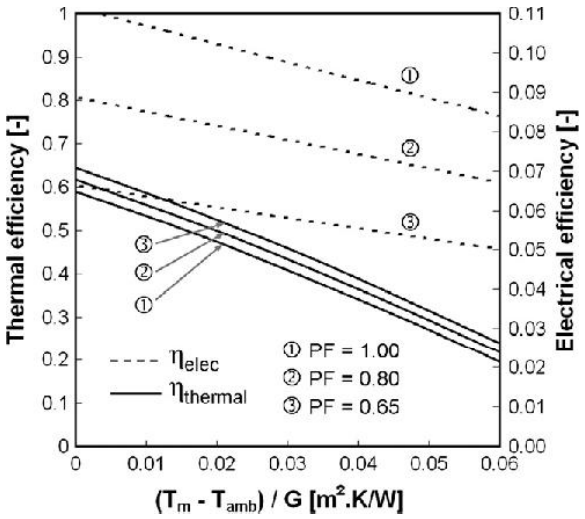

Figure 2.15 - Thermal and electrical efficiency curves of a typical PV–T collector for different PV packing factors (Dupeyrat *et al.*, 2011a)

Garg and Agarwal (1995) analysed the performance of a direct forced flow hybrid system for domestic hot water production, using a simulation model. The total thermal energy was extracted from the useful heat stored in a tank. They concluded that increasing the packing factor from 50% to 100%, the total daily efficiency increased. The efficiency was defined as the ratio between the total thermal plus electrical energy over the total solar insolation. Dubey and Tiwari (2008) developed a thermal model of a PV/T solar water heating system and applied it for different values of *Pf*: 30.56%, 50% and 100%. The PV modules were applied at the water inlet side of the collector, where they substituted the glass cover, since the PV cells were encapsulated in glass. A decrease in thermal efficiency was observed with the increase of the area covered by PV cells. This study was later complemented by testing a similar collector covered with PV cells on the water outlet side of the absorber (Dubey and Tiwari, 2009). The results were integrated and compared by Tiwari *et al.* (2011) through analysis of the hourly variation of the cell temperature and solar cell efficiency during one day. The application of the PV cells in the lower part was shown to be more advantageous. The investigation by Dubey and Tiwari (2009) included a detailed analysis of energy, exergy and electrical energy yield by varying the number of collectors connected in series. It was concluded that partially covered collectors are beneficial in terms of annualized uniform cost, if the primary requirement of the user is the thermal energy yield. Fully covered collectors are however beneficial when the primary requirement is electrical energy yield. Chow *et al.* (2006) used an experimentally validated numerical model to compare thermal and electrical efficiencies of a photovoltaic-thermosiphon collector system, for different packing factors of 0, 50% and 100%. A box

channel structure was built from a multiple of extruded aluminium alloy modules for the absorber. The solar cells were encapsulated between 2 layers of EVA and tedlar-polyester-tedlar. The position of the PV module was also evaluated. The results for thermal and electrical efficiencies were better with the application of the PV module in the lower part of the collector than in the superior one.

The results of Herrando *et al.* (2014) with low solar irradiance and low ambient temperatures in the UK show that a complete coverage of the solar collector with PV, and a lower collector flow-rate, benefit both heat and electrical conversion achieved with the PV/T collector, while maximising the CO_2 emissions savings. It was found that with a fully covered collector and a flow-rate of 20 l/h, 51% of the total electricity demand and 36% of the total hot water demand over a year can be supplied by a hybrid PV/T system. The electricity demand coverage value was only slightly higher than an equivalent PV-only system (49%).

Despite studies on the influence of the packing factor in the thermal and electrical already exist, references on the effect on the overall efficiency are scarce (Chow *et al.*, 2006), and more particularly the specific influence on the loss coefficient of hybrid collectors.

2.5.2 Geometric characteristics, environmental and operating conditions

Bergene and Lovvik (1995) defined a physical model for a hybrid flat plate collector with finned water channel. A parametric study was performed to study the influence of factors such as fin width to tube diameter ratio, inlet temperature and mass flow rate, on the thermal and electrical efficiency. They verified that the thermal efficiency is approximately halved when the fin width to tube diameter ratio is increased from 1 to 10. The flow rate and the inlet fluid temperature were identified as the most important parameters affecting electrical efficiency, while the total efficiency was strongly dependent on the fin size.

The existence of an optimal mass flow rate for maximum thermal, electrical and total efficiency was identified in the already referred study by Garg and Agarwal (1995). The effect of the capacity of a water storage tank was also studied. It was concluded that a smaller volume improved the thermal efficiency only, but the electrical and total daily efficiency decreased. Other authors also reported the existence of an optimum flow rate

(Garg and Adhikari, 1997, Garg and Agarwal, 1995, Kalogirou, 2001, Morita *et al.*, 2000). Daghigh *et al.* (2011) studied solar PV/T modules integrated into the building structure (BIPV/T). The effect of mass flow rate on the system efficiencies was evaluated, for different types of cells. Although an optimum value was not verified, it was found that efficiencies increased up to a given value of flow rate, and then stabilized. The effect of the collector flow rate on the performance of PV/T systems was also studied by Herrando *et al.* (2014). It was observed that the electrical performance did not change notably (<5% variation) with the collector flow-rate, whereas the hot water production was significantly affected. It decreased by about 35% as volumetric flow rate increased from 20 l/h to 200 l/h. Aste *et al.* (2014) reviewed published optimum flow rate values reported in the literature, for different absorber plate structures and PV/T types, as showed in Table 2.4.

Table 2.4 - Suggested optimum flow rates by selected authors (Aste *et al.*, 2014)

Channel type	PV/T type	Flow rate (kg/sm²)	Refs.
Parallel channel	Glazed	0.0027	(Nualboonrueng et al., 2013)
Parallel channel	Glazed	0.0014	(Kalogirou, 2001)
Roll Bond	Glazed	0.0014-0.0049	(Morita et al., 2000)
Parallel channel	Glazed	0.005	(Chow, 2003)
Parallel channel (square)	-	0.0054-0.0064	(Gao, 2010)
Parallel channel	Glazed	0.015	(Garg and Agarwal, 1995)
Box channel	Glazed BiPVT	0.025-0.04	(Ji, 2006)

Morita *et al.* (2000) developed an analytical model in order to investigate the design parameters for optimizing PV/T hybrid collector energy performance using a second law approach. Besides the presence of the cover glass, the mass flow rate was identified as a key parameter affecting the exergy efficiency. Respecting thermal and global exergetic efficiencies, there is a relatively low value of the optimum flow rate of 2.3 g/(s m^2) for glazed PV/T collectors. The photovoltaic conversion efficiency under a wide range of environmental conditions decreased with the solar radiation intensity (3.6%/kWm^{-2} at T_a = 20 °C); however, it was observed that the exergy efficiency of PV/T-l increased 3.6%/ kWm^{-2} (at T_a = 20°C). Therefore, the advantage of PV/T will be more remarkable with the solar radiation.

As solar energy is intermittent, many algorithms and electronics were developed to identify the maximum power generation from PV/T collectors. Nevertheless, no control systems have been developed in order to track maximum power generation from PV/T system. A study by Ammar *et al.* (2013) suggests a PV/T control algorithm based on Artificial Neural Network (ANN) to adjust the Maximum Power Operating Point (MPP)

by considering PV/T model behaviour. An optimum mass flow rate is computed for a considered irradiation and ambient temperature. Simulation results demonstrate great concordance with ANN outputs.

Another parameter that affects thermal and electrical performance of hybrid collectors is the operating water temperature. The electricity production from PV cells is favoured by low temperatures, whereas the value of the thermal energy is higher at higher temperatures. Evola and Marletta (2014) demonstrated that, for any operating condition of solar irradiance and flow rate, it is possible to calculate an optimum water inlet temperature that maximizes the total exergy generated by the system. The optimum temperature falls within the range commonly occurring in solar thermal systems, and can be achieved in practice through a simple feedback control system.

The effect of water inlet velocity and inlet temperature on the performance of a PV/T collector were analysed by Siddiqui *et al.* (2012). Figure 2.16 shows the results of thermal and electrical performance for the variation of the inlet velocity in a range from 0.01 m/s to 0.1 m/s. For this range, the average PV cell temperature decreased from 41.1 °C to 30.6 °C and the water outlet temperature dropped from 30.7 °C to 25.7 °C (Figure 2.16 a)). The increase in electrical efficiency for this range was of about 1.2%, with a minimum value of 9.4%. The results for the influence of inlet temperature of the fluid, ranging from 4-45ºC, are shown in Figure 2.17. Average PV cell temperatures increased from 14.5°C to 50.1°C (Figure 2.17 a)) and the electrical efficiency dropped from 12.28% to 8.4% (Figure 2.17 b)). It would be interesting to complete this study with results for the global efficiency, to understand the relative weight of each parameter.

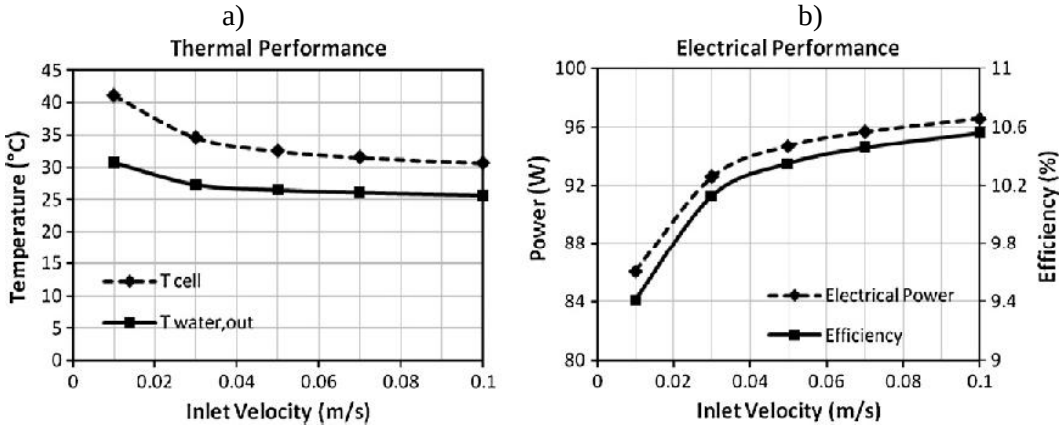

Figure 2.16 - PV/T collector performance variation with heat exchanger inlet velocity (Siddiqui *et al.*, 2012)

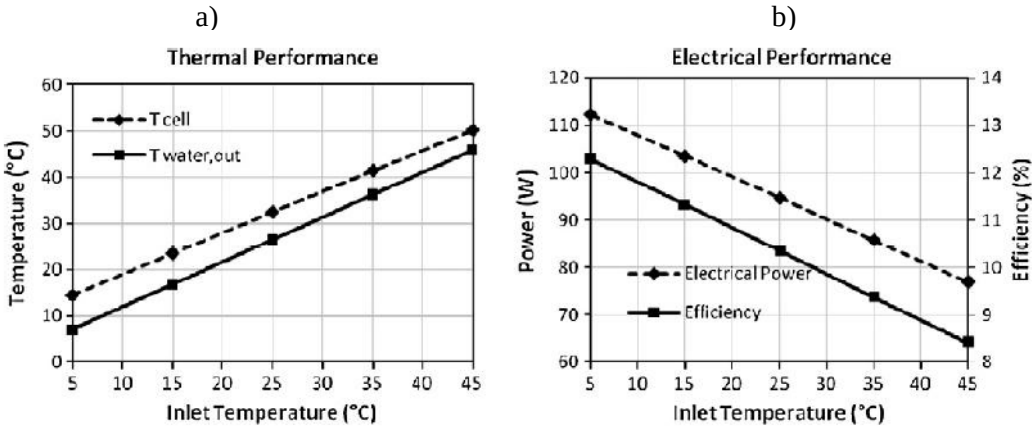

Figure 2.17 - PV/T collector performance variation with heat exchanger fluid inlet temperature (Siddiqui *et al.*, 2012)

2.5.3 Methods to optimize PV/T performance

The problem of optimizing design parameters that affect the performance of PV/T collectors frequently leads to conflicting solutions to fit a given application. The results of the studies that follow this approach are not the aim of this subsection, but the presentation of the methods itself.

A genetic algorithm has been used by Sobhnamayan *et al.* (2014) to optimize the exergy efficiency of PV/T water collector, for a selected group of environmental and design conditions. Effects of water inlet velocity at the, pipe diameter, solar radiation intensity and wind velocity were studied. The exergy efficiency has extremum points and showed points of global maximum, for a pre-selected range of operational and design conditions. The optimum conditions were identified by the maximum values of exergetic efficiency for each parameter, with values for inlet water velocity and pipe diameter of 0.09 m/s and 4.8 mm, respectively. Maximum exergy efficiency was found to be 11.36%.

Recently, mathematical techniques were integrated into algorithms for *Multi-Objective Optimization (MOO)*, in order to overcome the generic problem of global optimization. Vera *et al.* (2014) studied simultaneously the design and performance of water cooled PV/T systems, using an elitist multi-objective evolutionary algorithm non-dominated sorting genetic algorithm-II (NSGA-II). NSGA-II derives a Pareto optimal set, which illustrates the trade-off between solutions. The study focused in the following selected parameters: water mass flow rate, length of the collector, packing factor and air gap thickness. PV/T glazed and unglazed configurations were modelled. Electrical and thermal efficiencies are the two objectives functions to be maximized. The mathematical

analysis was performed based on results for a 24 h simulation obtained using a dynamic simulation tool, TRNSYS. The dynamics of the results is complex, but proves that this approach can provide a good tool to understand the relative weight of each parameter in optimizing a scenario.

2.6 Hybrid air collectors

PV/T modules working with air are used when there is a demand on hot air for applications like drying and preservation of agricultural crops, dehydration of industrial products and space heating, increased ventilation, as well as electricity generation. Some advantages over water collectors are the reduced corrosion and leakage, no freezing, no need for high pressure protection, lighter weight and easiness of installation (Kumar and Rosen, 2011a). However, the thermal output is inferior to the water collectors because of poor heat transfer between the absorber plate and the flowing air (Prakash, 1994) and lower density per unit mass. Flat plate air collectors exist in different designs, which of the most common models are shown in Figure 2.18. They basically differ in terms of the position of the cells relative to the air channel and the number of streams. The photovoltaic cells are placed over the black absorber plate, that should not be selective (Hegazy, 2000).

Bhargava *et al.* (1991) proposed a single-pass PV/T air heater, with air flux under the absorber, similar to the represented in Figure 2.18 b). Sopian *et al.* (1996) compared its performance to a new collector, using steady-state models with a double passage design, as shown in Figure 2.18 d). Performance analysis showed that the double-pass photovoltaic thermal solar collector produced better performance over the single-passage design within normal collector mass flow rate range 100-300 kg/h. However, the increased in energy demand for circulating the air through double-pass model was not considered. In a later work by Sopian *et al.* (2000) a mathematical model for the evaluation of the performance of the double collector p was developed and experimentally validated.

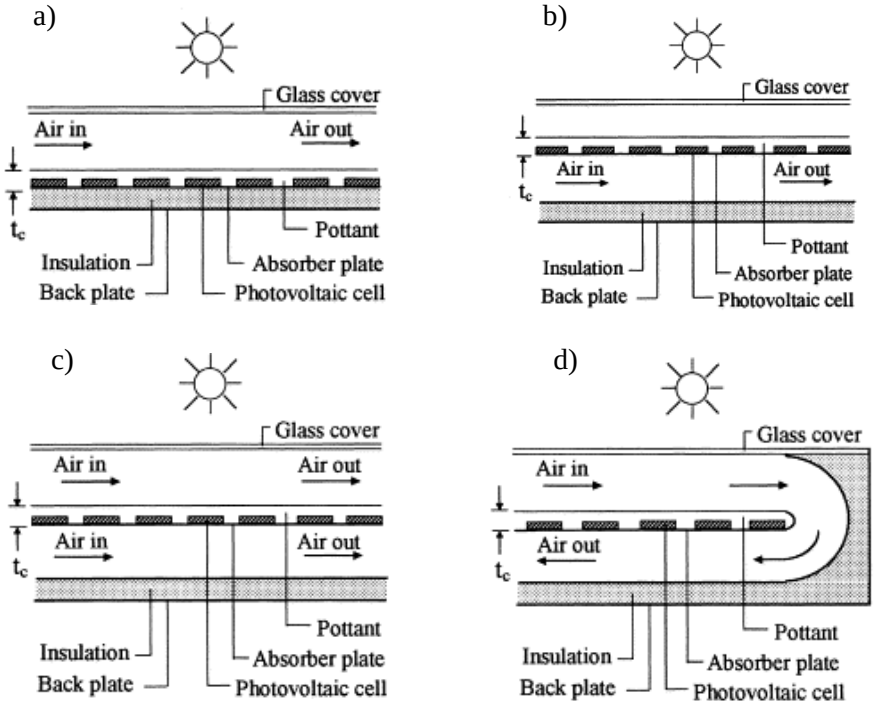

Figure 2.18 – Schematics of the various PV/T models (adapted from (Hegazy, 2000)):
a) Single pass, air flow over absorber; b) Single pass, air flow under absorber;
c) Single pass, both sides of absorber; d) double pass

Hegazy (1999) defined a simple criterion for maximizing the useful heat based on the channel geometry, for thermal collectors with single pass configuration, with flow under the absorber. An optimal value for channel depth-to-length ratio of 0.025 was determined. An extended investigation was carried out by Hegazy (2000), comparing the thermal, electrical, hydraulic and overall performances of the designs presented in Figure 2.18. The effects of air flow rate per collector surface unit area and selectivity of the absorber plate and PV cells on the performances were analysed, based on the developed models. The main conclusions were:

- for a particular design, the thermal efficiency is enhanced with the increase of the air specific mass flow rate. The available net electrical energy, resultant from the deduction of the power needed for circulating the air, from which , available net electrical energy, significantly decreases with air specific flow rate;
- design corresponding to Figure 2.18 a) present the lowest overall performance, while the other configurations exhibit comparable performance up to a specific mass rate of 0.02 kg/(s m^2). For higher values of $\dot{m}/A$, design c) has the highest overall performance, followed by the layout d). For each design, there is an

optimal mass flow rate beyond which overall performance of the collector decreases;

- performance comparisons indicate that the design c) is the most suitable for converting solar energy into low grade heat and high quality electrical energy, while also it is of simple construction.

Tonui and Tripanagnostopoulos (Tonui and Tripanagnostopoulos, 2007a, b, 2008) worked on the improvement of the heat transfer rates for air hybrid collectors by the enhancement of the air channel layout (see Figure 2.19). In Figure 2.19 a), a thin flat metal sheet is suspended in the middle of the air channel. Within Figure 2.19 b), fins with rectangular profiles are attached to the back wall of the air duct parallel to the flow direction. Glazed and unglazed versions were analysed. Both experimental and theoretical results showed that the suggested modifications improve the performance of the PV/T air system. Parametric studies were conducted (Tonui and Tripanagnostopoulos, 2008) to analyse the influence of channel depth, channel length, air flow rate and temperature, incident radiation, collector tilt angle and exit vent on the thermal and electrical performance of the hybrid collector. The parametric analysis showed that the induced mass flow rate and hence thermal efficiency decreases with increasing inlet temperature and increases with tilt angle for a given insolation level. The results also showed that there is an optimum channel depth for which the mass flow rat and the thermal efficiency are maximum. For the studied systems, the optimum channel depth occurred between 0.05 and 0.1 m, with both modified systems showing slightly higher optimum depth. The thermal performance also increased with exit area of the channel, which should not be restricted and made as large as possible, or equal to the duct cross-sectional area.

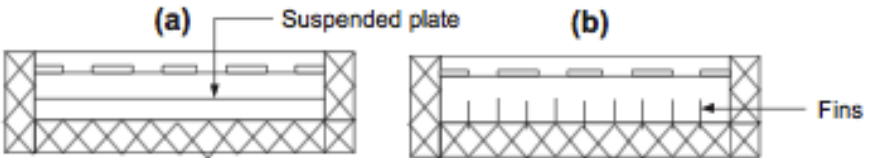

Figure 2.19 – Configuration improvements to single pass inferior flux air PVT collectors (Kumar and Rosen, 2011a, Skoplaki and Palyvos, 2009a)

The effect of the fins, depth of the ducts, flow rate, inlet temperature and packing factor in thermal and electrical efficiencies was also evaluated by Kumar and Rosen (2011b) for a double pass configuration, but with the fins arranged perpendicular to the direction of air flow to enhance the heat transfer rate and efficiency. The extended fin area

reduced the cell temperature from 82°C to 66°C. The advantage of a high packing factor was also proved, as it led to a better electrical output per unit collector area, and better control of the cell temperature, despite marginally reducing thermal output.

Tiwari and Sodha (2007) studied different layouts for the single pass configuration with air flow under the absorber. Single glazing, and the use of tedlar on the back of the solar cells was also considered. It was observed that a glazed hybrid PV/T without tedlar gave the best performance. Dubey *et al.* (2009a) and Dubey *et al.* (2009b) developed in their works analytical models to evaluate electrical efficiency of air PV/T collectors, as a function of climatic and design parameters. They compared the difference in the behaviour of glass to glass modules with glass to tedlar modules with no glazing. They also studied the effect of an inferior air flow and found that the best electrical efficiency was achieved with glass-to glass modules with channels.

A theoretical analysis has been presented by Garg and Adhikari (1999) for acessing thermal and electrical processes of a hybrid PV/T air heating collector coupled with a compound parabolic concentrator (CPC) with a layout presented in Figure 2.20. A parametric analysis on the thermal and electrical performances of the system showed that the thermal and electric output increased with the collector length, air mass flow rate and packing fraction, and decreased with the channel depth. It was It was also observed that the system coupled with CPC always performs better in terms of both the thermal and electric output.

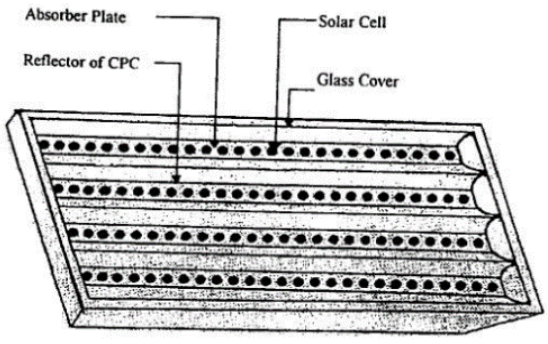

Figure 2.20 - Air hybrid collector with CPC´s application (Garg and Adhikari, 1999)

The combination of alternative techniques that enhance system performance is a good strategy to find improved solutions. Othman *et al.* (2005) studied the inclusion of CPC throughs and fins in a double pass configuration of a PV/T-air collector with a layout presented in Figure 2.21 a). The fins are attached to the back side of the absorber plate. It was observed that the electrical performance was significantly influenced by the air flow

rate and temperature. The work was extended to a similar configuration, without the CPC throughs (Othman *et al.*, 2007), as shown in Figure 2.21 b). The height of the upper channel was fixed, but the height of the channel below the absorber plate could be adjusted to observe its effect on the system performance. The experiments indicated that using fins as the integral part of the PV module increased the overall efficiency.

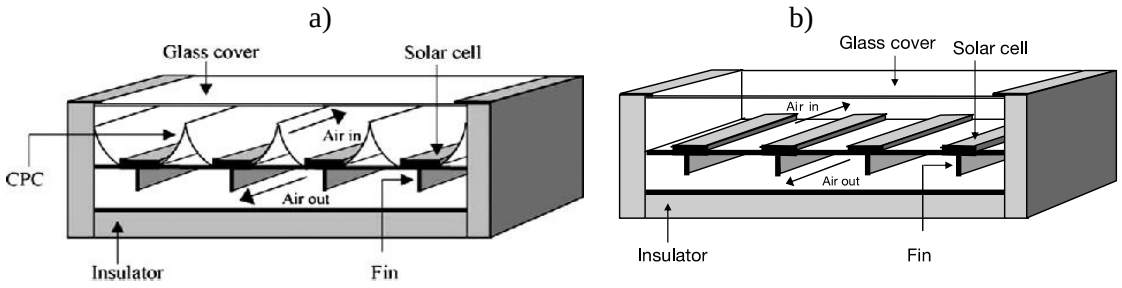

Figure 2.21 - Double pass PV/T air heater improved configurations:
a) with CPC and fins (Othman *et al.*, 2005); b) with fins (Othman *et al.*, 2007)

An unglazed, single pass configuration with air flow under the absorber was also tested by Othman *et al.* (2009). This unit had an aluminium ∇-grooved absorber plate in the air channel, as depicted in Figure 2.22. Results from the experiment showed that, although the electrical efficiency had been only improved by 1%, the thermal efficiency enhancement was high, by 30%. The use of a porous media was applied by Sopian *et al.* (2009) to a double pass prototype at the lower channel. Experimental data proved that this technique led to the increase of the thermal efficiency of the system as high as 60% to 70%. Such design was concluded to be suitable for drying applications.

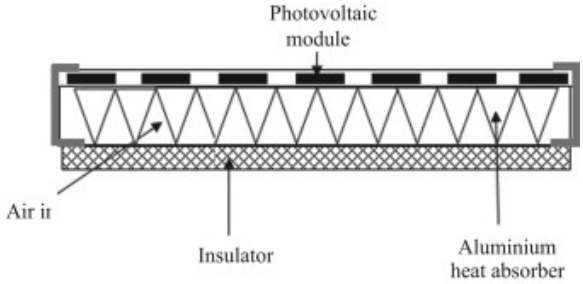

Figure 2.22 - PV/T system with aluminium ∇-grooved absorber plate (Hussain, 2013)

Exergy analysis of a solar hybrid collector for air heating was conducted by Sarhaddi *et al.* (2010). The thermal, electrical and overall energy efficiency were found to be about 17.18%, 10.01%, 45%, respectively. The exergy efficiency was 45% under a sample climatic, operating and design parameters. Optimized values of the air inlet velocity and irradiance was identified. It was observed that the modified exergy efficiency depended

slightly on air inlet temperature or duct length, while increasing wind speed led to an increase in the exergy efficiency.

The use of air for building integrated hybrid collectors (BIPV/T) is more usual than water. Sandberg and Moshfegh (2002) studied characteristics of the air gaps behind solar cells located on vertical facades. Mass flow rate, velocity, temperature rise and location of the air gap were the parameters being verified and measured. Muresan *et al.* (2006) also developed detailed models for describing the heat transfer modes in the air channel of PV module integrated in facades. A parametric study was performed for a case of a vertical channel heated at one side, as a function of the channel width, wall heat flux, and dimensionless turbulent intensity. PV/T hybrid exterior clapboard-shaped wallboards have been tested experimentally by Nagano *et al.* (2003), permitting modular assembly, which simplifies the installation. A scheme of the system is shown in Figure 2.23.The air gap created between the hybrid wallboard and the thermal insulation of the exterior wall can be utilized for solar heating the ventilation air as well as the tap water feed of a hot water system. The study presented an analytical and experimental evaluation of both the electrical power generating ability and the solar heat collection capacity of six variations of the experimental PV/T hybrid wallboard during winter. In addition, exergy analysys were conducted.

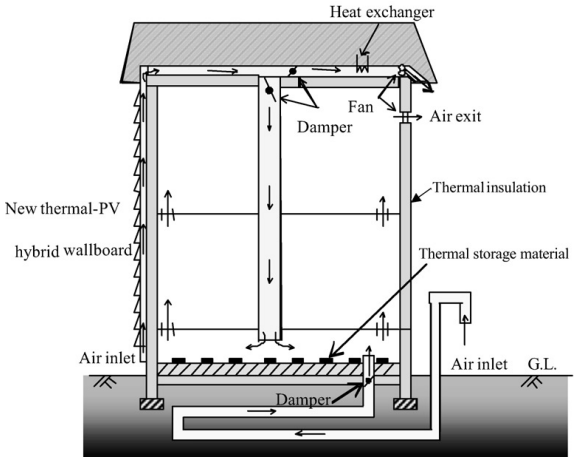

Figure 2.23 - System concept of hybrid wallboard with air (Nagano *et al.*, 2003)

Recent R&D in PV technology developed transparent PV cells. The use of this type of cells is particular interesting in BIPV/T applications. Research study carried out by Guiavarch and Peuportier (2006) pointed out that, by using semi-transparent pc-PV modules as a cover for an air collector, the ventilation air can be pre-heated and the global efficiency can reach 20%, 6% higher than the reference case. Vats *et al.* (2012) studied the

effect of packing factor of semi-transparent PV modules integrated to the roof of a building. Different PV technologies for the PV module were analysed, in energetic and exergetic basys: mono-crystalline silicon (c-Si), poly crystalline silicon (pc-Si), amorphous silicon (a-Si), cadmium telluride (CdTe), copper indium gallium diselenide (CIGS), and a heterojunction with thin layer (HIT). Maximum annual electrical and thermal energy conversion was measured for a-Si PV module with packing factor of 0.62. It was observed that a decrease in packing factor from 0.83 to 0.42 led to a decrease of the module temperature by 10.0°C and increase of its efficiency by 0.2–0.6%. A PV module with 0.62 packing factor was found to perform better than the one with 0.83 packing factor, for both electrical and thermal conversion.

Currently, there are commercially available unglazed air types of PV/T collectors. However, the application of air heating in the residential market is limited. A market study was carried out by Hussain (2013) and showed that the air collectors have a market share of less than 1% of the worldwide solar collector market. Even though PV/T collectors are able to produce more energy compared to stand alone system, the market share for such system is still negligible due to lack of proper public awareness. However, this situation should change since several institutes and manufacturers are making an effort to promote these systems.

In reviewing by Hussain (2013) the perspective for future development of a PV/T collector and BIPV/T system are discussed. It clearly shows that, by appropriate architectural design and configuration, the future of a PV/T collector can be encouraging as an alternative application in the residential, industrial and commercial buildings.

2.7 Approaches and metrics for the economical assessment of PV/T collectors

The analysis presented until now concerned with characterization of the performance of hybrid systems in terms of energy and exergy efficiencies. Conclusions on the economic advantages of using hybrid collectors have not yet been particularly addressed. An economic assessment is conditioned by the application context: the local weather conditions and the demands on heat to electric power ratio by the PV/T system; local economic development and policy matters. Nevertheless, an economic approach must always be preceded by an energy analysis of the system. Moreover, as the results that are

involved in this analysis do not refer to instantaneous or steady state conditions, in order to achieve a comprehensive analysis it should be based a long term assessment. Thus, simulation tools that include detailed local climate data and provide dynamic response of the model are necessary to carry out this type of analysis.

The approach to this issue arises with the first studies on hybrid collectors. Kern Jr and Russell (1978) were one of the firsts to perform an economic analysis of PV/T systems. After an evaluation of the useful energy and backup energy needs, it was concluded that hybrid systems were more attractive in situations of large heating needs, while for more temperate climates or with cooling needs the PV systems were the most appropriate. Ricaud and Roubeau (1994) developed an economic study of the combined generation of solar electricity and hot air in a residential and a commercial building. It was found that the use of the considered hybrid system for the domestic application is in the limit of being competitive.

Different metrics can be used to the economic evaluation of the application of hybrid PV/T collectors. One of the most common is the *payback time* (PBT) of the system that can be determined by considering installation and operating costs, energy prices and economical figures, such as financial costs of loans, or inflation rate. The *energy payback time* (EPBT) is the total time period required to recover the total energy spent to prepare the materials (embodied energy) used for fabrication of the systems. A life cycle analysis can also be performed in order to obtain the total cost (or *life cycle cost*) and the *life cycle savings* (LCS) of the systems. This approach is followed in several studies (Kalogirou and Papamarcou (2000), Brogren and Karlsson (2001), (Kalogirou, 2001), (Chow *et al.*, 2007), (Erdil *et al.*, 2008), (Chow, 2009)). With the *Lyfe Cycle Savings* (LCS) method all costs and benefits are accounted for as their present values. General conclusions are not necessarily relevant, since are limited to a certain geographic application. However, some methodologies can be highlighted.

Kalogirou and Tripanagnostopoulos (2006) studied PV/T domestic hot water solar systems using a-Si and pc-Si modules in three locations at different latitudes (Nicosia (35 degrees), Athens (38 degrees) and Madison (43 degrees)). The economic analysis indicated better results of *LCS* for lower latitudes and a-Si modules. A similar study was extended to industrial applications by Kalogirou and Tripanagnostopoulos (2007). Aste *et al.* (2012) calculated the optimal value of solar fraction (f_S) for hybrid PV/T-water systems, from energetic end economic point of views. Applying an economic scenario, the PBT was

determined as a function of. Mishra and Tiwari (2013) evaluated and compared the energy matrices of a hybrid PV/T water collector applied in New Delhi under constant collection temperature mode with five different types of PV modules: c-Si, p-Si, a-Si (thin film), CdTe and CIGS. The highest annual overall thermal energy and exergy was obtained with the use of c-Si PV module. The maximum and minimum EPBT of 1.01 and 0.66 years was obtained for c-Si and CIGS respectively, whereas on exergy basis maximum EPBT of 5.72 years was obtained for a-Si and minimum of 3.44 for CIGS PV module.

The concept of payback time was applied in an environmental perspective by Tripanagnostopoulos *et al.* (2005), in a study on the annual performance of water cooled PV/T solar systems, combining different configurations (glazed/unglazed, horizontal/tilted, different operating temperatures). The study included the estimation of costs and payback time, and determined the *energy payback time* (EPBT) and *CO_2 payback time*.

When performing an economic assessment of hybrid systems, thermal and electrical outputs are accounted for separately, since they have different costs and energy savings. An approach focusing on methods to develop a ratio between electrical and thermal output from a domestic PV/T system was carried out by Coventry and Lovegrove (2003). Methods discussed included thermodynamic analysis using exergy, market analysis for both an open market and a renewable energy market, and environmental analysis using savings in greenhouse gas emissions. A discounted cash flow method was used to determine levelized energy costs from both electrical and thermal renewable energy sources, giving a ratio between electrical to thermal value of 4.24. Levelized energy cost was plotted against the energy value ratio to compare different options, like using a-si or c-Si cells, or identifying critical points. System performance was simulated using TRNSYS, and the calculations were carried out using US financial data.

In order to assess the economic viability of water heating PV/T systems installed in three cities of different longitudes and climatic conditions (Athens, Munich and Dundee), Axaopoulos and Fylladitakis (2013) performed a simple economic analysis based on the LCS method. Since most of the economic parameters change in relation to time and geographic area, it is difficult to make reliable predictions about future trends on the value of money. Therefore, a sensitivity analysis, based on the *Net Present Value* (NPV) method was performed to evaluate the economics of energy produced under various investment costs, feed-in tariff prices and energy price fluctuations. In all three areas and with the energy prices of that period, the installation of a PV/T system appears to be a more

advantageous investment when the auxiliary water heating energy source comes from electricity, followed by heating oil and then natural gas.

The price of the thermal energy delivered by a water PV/T collector was calculated by Evola and Marletta (2014) to be ranging from 1 to 10 c€/kWh, for an assumed price of the electricity ranging from 0.18 to 0.24 €/kWh.

In conclusion, there are different approaches for the analysis of economic performance of hybrid systems. Economical techniques are just one tool that can be used to identify situations for an advantageous application of PV/T systems.

2.8 Space heating and cooling applications of PV/T collectors

The most typical applications of hybrid collectors, a water heating and BIPVT systems combined with production of electricity. However, PV/T technology presents good potential for other important applications. Its use can be particular successful for reducing the operation cost of space heating and cooling units, through solar heat pumps integrated with air/conditioning. PV/T concepts can also be used in solar green-houses and solar stills. Sometimes the innovation may not mean innovative or cutting-edge expensive technologies, but taking advantage of the right combination of the strengths of each one for some particular purpose. Van Helden *et al.* (2004) highlighted some possible examples. The available roof area, the demands of electricity and heat, and the temperature levels determine the PV/T system set-up that is most suited for a given house or building. For instance, an array of PV/T collectors can be connected to an earth-coupled heat exchanger, so that the low-temperature heat gained in the summer is stored in the ground and used in the winter. The PV modules can provide the electricity to the heat pump that transfers energy from a low-temperature heat source to higher temperatures sink for either room heating or for DHW. This strategy can highly improve the solar fraction and over all efficiency of solar systems.

In this section the characterization of the state of the art for hybrid collectors is conducted with a presentation of its application for space heating and cooling, and other novel perspectives, such as tri and poligeneration.

2.8.1 Heat pump systems

A heat pump is used to take energy from low temperature source and promote this energy to a suitable temperature range for different applications. The coefficient of performance (COP) is used to measure the heat pump efficiency, defined as the ratio of the amount of energy provided by the heat pump (Q) to electrical energy consumed. The COP of a heat pump becomes better with increasing evaporating temperature (for fixed condensing temperature) (Kamel *et al.*, 2015). The integration of a PV/T system with a heat pump provides both thermal energy and electrical power to run the cycle, e.g., for space heating. The common potential advantage to the solar collector and the heat pump performance is to depress the collector temperature and boost the heat pump evaporator temperature, enhancing the performance of both systems, and thus improving the heat pump COP. The integrated system is called Solar Assisted Heat Pump (SAHP). If properly incorporated, SAHP systems can cover the heating load in cold climates. A solar system could deliver a relatively high-temperature source for a heat pump compared to a traditional heat pump using outdoor air and ground source heat exchanger. (Kamel *et al.*, 2015).

Solar assisted heat pumps are categorized, based on the integration scheme between the solar system and the heat pump, into *Direct Expansion Solar Assisted Heat Pump* (DX-SAHP) and *Indirect Expansion Solar Assisted Heat Pump* (IDX-SAHP) (Kamel *et al.*, 2015). Most research and development of solar assisted heat pump systems consist of a solar thermal collector, which produce only thermal energy, linked with the evaporator of a heat pump, i.e., thermal energy is extracted from the solar thermal system for heating purposes only. The only integrated PV/T system with a heat pump, which provides both thermal energy and electrical power, is the PV-evaporator type. (Kamel *et al.*, 2015)

In DX-SAHP, the heat pump and the solar system work together as one combined system. The PV/T collector in the DX-SAHP system works as the evaporator low temperature heat source of the heat pump. A schematic diagram of the working principle of a direct expansion system is depicted in Figure 2.24. In this arrangement, liquid refrigerant vaporizes at the tubing underneath the flat-plate collector. Solar energy is absorbed at the PV/T evaporator that operates at a lower temperature than the ambient environment, and released later at the water-cooled condenser at a higher temperature. Cell efficiency is then higher than the standard operating efficiency. Based on this working principle, a PV/T–SAHP system with pc-Si aluminium roll-bond panels was constructed

and studied (Ito *et al.*, 1997, Ito *et al.*, 1999). The experimental results indicated that the COP of the heat pump is able to reach 6.0, and with hot water supplying to the condenser at 40 °C. A DX-SAHP system was also proposed by Chow *et al.* (2010). Numerical analysis was carried out making use of a dynamic simulation model developed for the Hong Kong climate. It was found that the proposed system, working with R-134a, is able to achieve a yearly-average COP of 5.93 and PV output efficiency of 12.1%, thus with an energy output considerably higher than the conventional heat pump plus PV "side-by-side" system. The results for the monthly average COP for DX-SAHP using solar thermal collector and a PV-SAHP system, using a PV/T collector, are shown in Figure 2.25. *COPpt* definition referenced in the figure corresponds to:

$$COP_{pt} = \frac{Q + {}^{E}/_{\eta_P}}{W} \tag{2.26}$$

where Q is the heat transferred in the condenser (see Figure 2.24), E is the output power of the solar cells per unit area, and η_P is the average electricity generation efficiency of the power plant as a conversion factor (= 0.38).

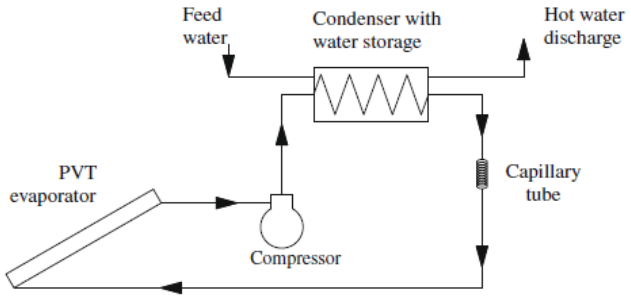

Figure 2.24 - Schematic diagram of the DX-SAHP system (Chow *et al.*, 2010)

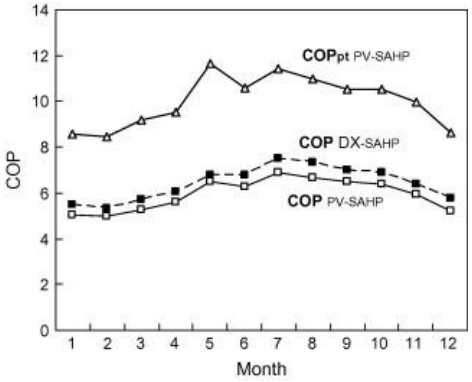

PV-SAHP – Solar Assisted Heat Pump with PV/T collector

DX-SAHP - Solar Assisted Heat Pump with solar collector

Figure 2.25 - Comparison of monthly average COP between traditional DX-SAHP and PV/T SAHP (Chow *et al.*, 2010)

During the day, there is a possibility of liquid refrigerant remaining at the outlet of the PV-evaporator because solar radiation changes; consequently, the system works

inefficiently and will require control of the mass flow rate of the refrigerant. In addition, the system works only when evaporator temperature is above a certain value. It may be beneficial to overcome this issue by separating the PV/T unit from the heat pump evaporator. (Kamel *et al.*, 2015).

In indirect expansion heat pumps, the heat pump and the solar collector are combined together, but work as two individual systems, that can be arranged in parallel, in series, or dually. Air and water PV/T collectors can be used in SAHP systems. Kamel *et al.* (2015) presents a review on the application of hybrid PV/T to heat pumps systems. A summary of studies referring to IDX-SAHP systems and the specific application of SAHP for cold climates is pointed out.

2.8.2 Solar Cooling with PV/T technology

In climates with high insolation and high outdoor temperatures, there is a need to lower the indoor temperature considerably in order to provide thermal comfort. Solar cooling of buildings is one of the most attractive solutions. This is an application in which the demand for cooling energy closely matches the availability of solar energy, both in the seasonal and the daily variations. One of the technologies of solar cooling is based on absorption cycle, depicted in Figure 2.26. Absorption is the process of attracting and holding moisture by substances called desiccants. Absorption systems are similar to vapour-compression air conditioning systems but differ in the pressurisation stages. In general an absorbent on the low-pressure side absorbs an evaporating refrigerant. The most usual combinations of fluids include lithium bromide–water (LiBr–H_2O), where water vapour is the refrigerant, and ammonia–water (NH_3–H_2O) systems where ammonia is the refrigerant. The pressurisation is achieved by dissolving the refrigerant in the absorbent in a absorber section. Subsequently, the solution is pumped to a high pressure with an ordinary liquid pump. The addition of heat in the generator is used to separate the low-boiling refrigerant from the solution. In this way the refrigerant vapour is compressed without the need of large amounts of mechanical energy that a vapour-compression air conditioning system demands (Florides *et al.*, 2002). Therefore, the absorption chillers can be powered by solar collectors. The COP for conventional absorption cycles is about 0.6-0.7 for NH_3–H_2O systems (Florides *et al.*, 2002) and between 0.6 and 0.8 for LiBr–H_2O systems (Duffie, 1991). This solution, however, needs electricity to drive the pump, despite the power is very small.

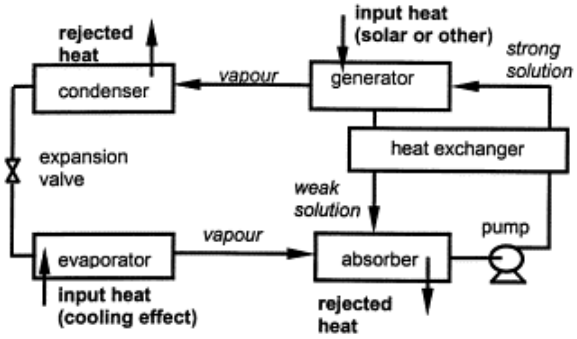

Figure 2.26 - Basic principle of the absorption air conditioning system (Florides *et al.*, 2002)

Simultaneous production of electrical and high grade thermal energy is proposed with a concentrating photovoltaic/thermal (CPVT) system operating at elevated temperature by Mittelman *et al.* (2007). CPVT collectors may operate at temperatures above 100 °C, and the thermal energy can drive processes such as refrigeration, desalination and steam production. The performance and cost of a CPVT system with single effect absorption cooling was investigated in detail. An example of a thermal application that can be coupled to the CPVT collectors, a single effect absorption chiller, was analyzed under different scenarios. The results show that under a reasonably wide range of conditions, the CPVT cooling system can be comparable in costs to a conventional alternative. Under some conditions, the solar cooling is even significantly less expensive than conventional cooling. This is in contrast with solar cooling based on thermal collectors, which is usually found to be significantly more expensive than conventional cooling. The range of conditions where CPVT cooling is competitive depends on the prevailing local costs of conventional energy.

2.8.3 Tri-generation and polygeneration

As new applications for hybrid collectors are studied, new possibilities for the integration of different technologies arise. A further possible use of both medium-temperature and high-temperature PV/T collectors is the integration with solar heating and cooling (SHC) technology. SHC systems can use solar radiation to provide space heating during the winter and space cooling in the summer, by using a heat-driven chiller, which can either work by absorption or adsorption process (Calise *et al.*, 2012). The heat needed for that process is provided by a solar collector field. The use of PV/T collectors, instead of solar thermal ones, can provide electricity additionally. An energy supply system which delivers simultaneously more than one form of energy to the final user is the basis of the

polygeneration concept. The association of cooling, heating and power in one system is also known as Combined Cooling, Heat and Power (CCHP), or *trigeneration*.

A SHC system with photovoltaic/thermal collectors was studied by Calise *et al.* (2012), applied to a university building located in Naples. The system integrated PV/T collectors, a single-stage LiBr–H_2O absorption chiller, storage tanks and auxiliary heaters. The electricity generated through PV/T collectors was partially consumed in the building, by electric appliances, lighting and system parasitic loads. The surplus was sold to the grid. Simultaneously, the PV/T system provides the heat required to drive the absorption chiller. The system performance was analysed from both energetic and economic perspectives, using a transient simulation model developed in TRNSYS. The economic results showed that the system under investigation could be profitable, provided that an appropriate funding policy is available. In addition, the overall energetic and economic results are comparable to those reported in literature for similar systems.

A coupled system is proposed by Mittelman *et al.* (2009), comprised of a concentrating PV/T collector field and a multi-effect evaporation desalination plant. A desalination process using solar energy is a logical combination, since regions with abundant solar radiation are often also short in potable water supply. Three processes are commercially available for large-scale desalination plants: Reverse Osmosis (RO), Multi-Stage Flash distillation (MSF), and Multiple Effect Evaporation (MEE). RO requires electricity, a high-grade form of energy; however, MEE and MSF consume thermal energy, and can readily operate with alternative low-grade heat sources such as solar energy. PV/T collectors can thus be used also for this application, with such a great importance for sustainability. However, large scale of desalination plants use high inlet temperatures are required, in order to provide reasonable performance and reasonable heat exchanger sizes. These higher temperatures can be achieved with a concentrating collector field. The combined system studied by Mittelman *et al.* (2009) produces solar electricity and simultaneously exploits the waste heat of the photovoltaic cells to desalinate water. A detailed simulation was performed to compute the annual production of electricity and water. The cost of desalinated water was estimated and compared to that of alternative conventional and solar desalination plants, under several economic scenarios. The cost was found to range from 0 to 4 \$/m^3, for 4 scenarios considering minimum and maximum electricity and natural gas prices, and installation cost of the system. The results indicate that the proposed coupled plant can have a significant advantage relative to other solar

desalination approaches. For a scenario with higher electricity prices, considered of ¢15/kWh, CPVT desalination is even more cost-effective than conventional desalination. with results of zero or even negative cost of the desalinated water.

Calise *et al.* (2014) investigated the integration of renewable energy sources and water systems, presenting a novel solar PV/T system producing simultaneously electrical energy, thermal energy, cooling energy and desalinized water. The system is designed for small communities in European Mediterranean countries, rich in renewable sources and poor in fossil fuels and water resources. It includes PV/T collectors, a MED system for seawater desalination, a single-stage LiBr–H_2O absorption chiller and additional components, such as storage tanks, auxiliary biomass-fired heaters and devices for the balance of plant. Since absorption chillers and MED process requires for high temperature water, it is needed the use of concentrating PV/T collectors. The system is dynamically simulated by means of a zero-dimensional transient simulation model. A thermo-economic analysis is also presented, aiming at determining the optimal values of the most important design variables, making use of TRNSYS. A numerical case study was developed and widely discussed, putting in evidence the significant potential of energy savings achievable by such system, also due to the opportunity of maximizing the utilization factor of the thermal energy produced by the CPVT, especially during the summer. On the other hand, the winter performance was by far less satisfactory, since CPVT thermal and electrical productions dramatically decrease; as a consequence, in such periods a large amount of heat must be produced by an auxiliary heater to drive the MED.

2.8.4 Solar stills and solar greenhouses

The solar stills are small-scale, decentralized, environmental friendly solution for getting pure water through desalination. However, conventional single basin passive solar stills are not widely used because of their low yield (approximately 2–3 l/m^2 day), low thermal efficiency (max. around 30%) dependent on solar intensity which varies with location. A hybrid (PV/T) active solar still is a combination of solar still and flat plate collector integrated with glass–glass photovoltaic module. A PV/T solar still was proposed by Kumar and Tiwari (2009). An analysis of the annual performance and cost of distilled water produced was carried out and compared with passive solar stills for the climate of India. The comparative cost of distilled water produced from passive solar still was found to be less than hybrid (PV/T) active solar still for 30 years life time of the systems. The

payback periods of the passive and PV/T active solar still are estimated to be in the range of 1.1–6.2 years and 3.3–23.9 years, respectively. Despite the higher price, the use of PV/T solar still can be advantageous when electricity is unavailable. The main objective of the work of Singh (2011) was enhancing the productivity of a double slope solar still to provide distilled water for isolated communities, facing electricity problems and good quality of water for commercial use. To increase the temperature of feed water in the solar still, a double slope solar still was connected to two flat plate collectors with one of them photovoltaic (PV) integrated. It was found that energy payback time is significantly reduced by almost 30% in present design with less capital investment.

An energy and exergy analysis for the prediction of performance of a photovoltaic/thermal (PV/T) collector integrated with a greenhouse at I.I.T, Delhi, India was performed by Nayak and Tiwari (2008). The analysis is based on quasi-steady state conditions. Experiments for the annual performance and numerical computation were carried out for a typical day only for validation. Exergy analysis calculations of the PV/T integrated greenhouse system showed an exergy efficiency level of approximately 4%. Sonneveld *et al.* (2009) presented a greenhouse with a spectral selective coating on the covering. This coating reflects the near infrared radiation (NIR), containing about 50% of the solar heat load which is not required for crop production, and transmits the PAR. Because the NIR reflection is performed with a bent surface, the whole covering worked as a solar concentrator PV module located in the focal line. This concentrator technology reduces the surface area required by the expensive PV cells, so only a small PV area is needed. The module is cooled with water so the system delivers both electrical and thermal energy. Further performance results on this type of systems were presented by Sonneveld *et al.* (2010). After the description of the construction of this greenhouse, the peak power for Dutch climate circumstances is determined based on the amount of electrical and thermal energy (hot water) produced. The typical yearly yield of this greenhouse system is determined as total electrical energy of 20 kW h/m^2 and a thermal energy of 160 kWh/m^2.

2.9 PV/T models available on the market

Despite the general acceptance of the PV/T technology in the scientific community, its deployment on the market is still reduced. The position of PV/T Systems was analysed from the market point of view by 2004 in the PVT Roadmap (Affolter *et al.*, 2006). For all

of the principal types of PVT systems, commercial and near-commercial products were presented, although they were recent and in a small number. In its review study, Zondag (2008) published the timeline of hybrid collectors, from the research background to the position in the market. It was showed that the only product with a market share was air type collectors for autonomous applications, even if modest. Ventilated PV systems existed almost only as specific solutions for individual projects, while PV/T concentrators as well as glazed and unglazed PV/T-liquid collectors commercially available were still not produced in significant quantities.

A comprehensive overview on commercially available PV/T products with technical and economic information for building projects is made by Treberspurg and Djalili (2011). The report includes PV/T-air collectors, PV/T-Liquid collectors and concentrator type. The referred manufacturers and types are listed in Table 2.5, as well as its continuity at the present.

Table 2.5 - Existing commercialized PV/T collectors in 2011 (Treberspurg and Djalili, 2011)

Manufacturer	Type of collector	PV/T product still on market?
SolarVenti	Air/ BIPVT facades	No
Grammer Solar	Air/ BIPVT roofs	Yes
Solarwall	Air/ BIPVT roofs	Yes
PVTWins	Liquid	No
Millenium Electric	Liquid	No
RES Energy kombimodul	Liquid	No
Arontis solar solutions	Concentrator	No
Menova Engineering Inc	No	No

The performance of a variety of commercially available systems, in terms of the ratio of thermal over electrical outputs per surface area is shown in Figure 2.27. It can be observed that just one air PV/T collector is included, and the most are water PV/T equipment. The ratio of thermal to electrical output for water collectors range from about 2, for the Millenium Electric model, to 4.8, for PVTWins model. At the moment, PVTWins manufacturer no longer exists, and Energy-Sol just commercializes solar thermal collectors.

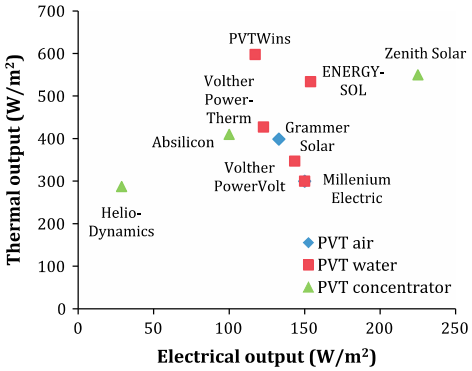

Figure 2.27 - Summary of commercially available hybrid PVT systems, in terms of their ratio of thermal over electrical output per surface area (Herrando *et al.*, 2014)

An economic analysis was developed by Matuska (2014), based on the performance results for domestic hot water application in an apartment block in Wurzburg, energy prices and conventional PV and thermal collector prices. The market price of solar PV/T liquid collectors achieved extremely high level (450 to 950 €/m^2) in comparison with standard glazed solar thermal collectors and PV modules. The prices for the most typical types were 350 €/m^2 and 120 €/m^2, respectively. Competitive price of unglazed PVT collector is negative in most of variants. The competitive specific price for the marketed hybrid collectors, range from 200-250 €/m^2. If the market price of novel spectrally selective glazed PV/T collectors would be maintained under 420 €/m^2, a large potential would open for substitution of standard solar thermal applications in buildings for domestic hot water and space heating systems.

From a research in the worldwide web, some FPC PV/T models were found, and are listed in Table 2.6. Only few collectors are commercialized, but more models are available, suggesting that PV/T technology is gaining some market. Once again, more models working with liquid are commercialized. Just one of the flat plate models have a glass cover, since the glass layers where PV cells are encapsulated work as cover. The different models of RenOn P2300 series (RenOn Energie, 2014) result from different packing factors. This way, the manufacturer can offer a product adapted to different balances of thermal vs electrical needs.

Table 2.6 - PV/T marketed models at the present

Company	Product reference	Fluid/ Design	Country	P_{elMax} (W)	η_0 (%)	A (m^2)
DualSun	DualSun	Glicol+Water, no glass cover	France	250	55	1.66
Grammer Solar	Hybrid air collector	BIPV/T, no glass cover	Switzerland	230	40	1.732
Meyer Burger	FS Hybrid	Water, no glass cover	Switzerland	285, 275	60	1.641
Millenium Electrics	MSS-MIL PVT	No-glass cover	Israel	190		1.277
NES	SUNSYSTEM PVT 240	Propylene glycol	Bulgaria	240	0.9	1.62
RenOn	RenOn P2300 series	Water, no glass cover	Germany	140, 180, 240	76.7, 77.7, 85.0	2.253
SolarWall	SolarWall PV/T SolarDuct PV/T	Air Air/BIPVT	Canada/USA /France	-	-	-
SOLIMPEKS	Volther series	Water, with/without glass cover	Turkey	180, 200	69.0, 62.9	1.427, 1.37
TES Group	TESZEUS PV-T series	Water, no glass cover	Greece	240, 250, 280, 300	65.1	1.637, 1.949

Although PV/T market has been developing in a monotonous rate, stronger efforts are still needed to get the reliable data to the solar equipment manufacturers. In particular, there are no Portuguese manufacturers/models. Pragmatic studies on economic evaluation of the installation of hybrid collectors are important to a growth in the market. This thesis fits into that perspective, by the optimization of the PV/T cells layout, in energetic and economic perspectives.

As in the case of other expensive technologies, strategical measures from the governments to support the development in research and the application of PV/T systems by consumers are also an important way to go. Strategic incentives and policies can contribute to a wider deployment of the technology and consequent reduction of production costs.

2.10 Gaps in literature on PV/T-w collectors

A wide range of knowledge on PV/T solar collectors have been brought to light in the last 20 years, as presented in the former sections. However, there still exist some gaps of information that worth to be deepen. This thesis focusses on some of that gaps, concerning water PV/T collectors at low temperatures.

It already are known studies on the global influence of control parameters like the PV cells positioning, packing factor, ambient temperature, fluid inlet temperature, absorber plate length or solar irradiation on the thermal and electrical efficiencies of a PV/T collector. The results for the combined efficiency are scarcer. The work developed in this thesis characterizes quantitatively those effects, for a wide range of operating conditions, according to results from experimental tests and a numerical model. The influence of the packing factor is particularly developed, in order to define its effect on the thermal and combined efficiency curve parameters: zero reduced temperature efficiency and loss overall factor. The numerical model was used to develop an extensive and exhaustive parametric study, aiming a comprehensive characterization of the simple and combined effects of the parameters afore mentioned, assuming a degree of detail still not present in the literature. For example, results of η_G were obtained as a function of the *Pf*, for the different positioning of the PV cells at the inlet side and outlet side of the collector. A similar comprehensive parametric study, based on the exergetic analysis of PV/T collectors, could be of great interest to complete the studies conducted in this thesis, contributing to a wider optimization perspective of PV/T collectors. The impact of the flow rate should also be included in future studies.

Chapter 3.

Experimental determination of the hybrid PV/T collector prototype performance

Within this chapter the experimental results of a PV/T collector prototype are presented. Thermal, electrical and combined efficiencies were obtained for different conditions of inlet fluid temperature ($T_{f,IN}$), under climatic conditions that were registered. The efficiency curves were determined for different PV to thermal area ratios of the collector. The tests were performed based on indications defined by NP EN 12975-2 standard (IPQ, 2007). The standard specifies criteria for the installation and position of the collector, measuring equipment, testing set up and procedure. Summarily, at least four test points should be obtained for each of four water temperatures in the operating range. During the tests, the total solar radiation on the collector plane should be higher than 700 W/m^2. An experimental setup was assembled on the rooftop of Building L at FEUP. Environmental variables, including ambient temperature (T_{amb}) and solar irradiance (G), were monitored through a data acquisition system. The collector prototype was instrumented so that efficiency curves could be determined, according to the readings of fluid temperature at the inlet ($T_{f,IN}$) and outlet ($T_{f,OUT}$). In the following sections, the collector, photovoltaic modules, and equipment used for the work will be characterized. The experimental procedure will be described, detailing how the parameters for the calculation of thermal and electrical gains were obtained. Only test values which respected stationary conditions were used, and the

criteria followed are defined. The operation of a solar collector can be assumed as steady state, since, during the period of the day when there is water circulation, the effects of intermittence of sunshine, ambient temperature and wind speed are negligible (Duffie, 1991). The results for thermal, electrical, and combined efficiencies are presented and discussed, and the associated uncertainty is evaluated.

3.1 Experimental setup

The collector and the feed water circuit from the supply point on the roof mainly compose the experimental setup. Since the required water flow rate is low, of about 0.01 kg/s, an open circuit was used to simplify installation and operation. The data acquisition system was designed in order to measure environmental variables, including solar irradiance (G) and ambient temperature (T_{amb}), and operational temperatures (water temperatures at the inlet ($T_{f,IN}$) and outlet ($T_{f,OUT}$)).

3.1.1 Layout of the solar thermal collector

The tested collector prototype was adapted from a solar thermal commercial collector, in order to simplify installation and handling. This original collector was supplied by the thermal technology division of BOSCH group in Portugal. The collector was unglazed, with a selective absorber plate composed of 9 equal size segmented fins of 124 mm width each and 1912 mm length. The prototype was built with only four absorber fins, of reduced length 1 m, as shown in Figure 3.1. The fins slightly overlap on the edges.

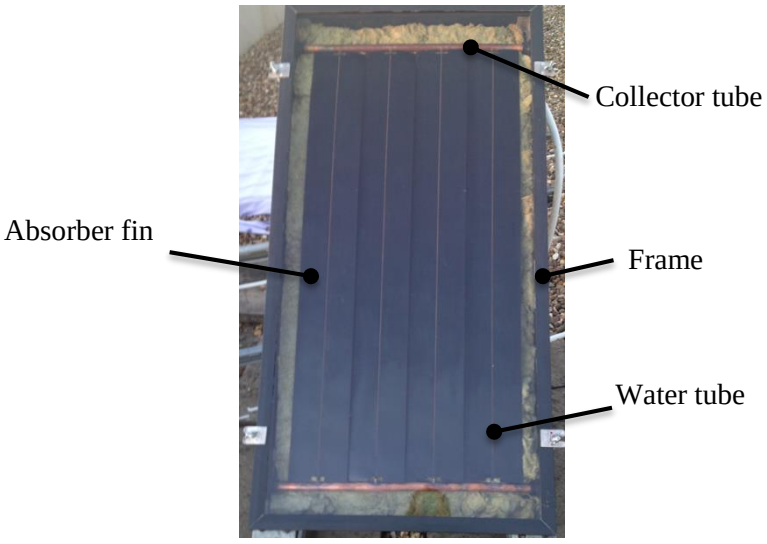

Figure 3.1 - View of the collector prototype (without instrumentation)

The individual copper tubes have an external diameter of 6 mm, while the collector pipes have 22 mm. The original PVC frame was replaced by an aluminum profile. A low-iron tempered glass cover was added to the aluminium frame, and sealed. Handles were also added, so that the glass cover could be easily removed when necessary. The collector was insulated on the bottom pane to avoid undesired thermal losses, with 50 mm thick rockwoool, resulting on a global heat loss coefficient of about 0.6 W/(m^{2}K). Typical values of the back surface heat loss coefficient are 0.3–0.6 W/(m^{2}K) (Kalogirou, 2009). Rockwool is an efficient insulating material, since the influence on the heat loss coefficient is less dependent of the thickness used (Ferdous, 2012). The detailed collector geometry is presented in Figure 3.2.

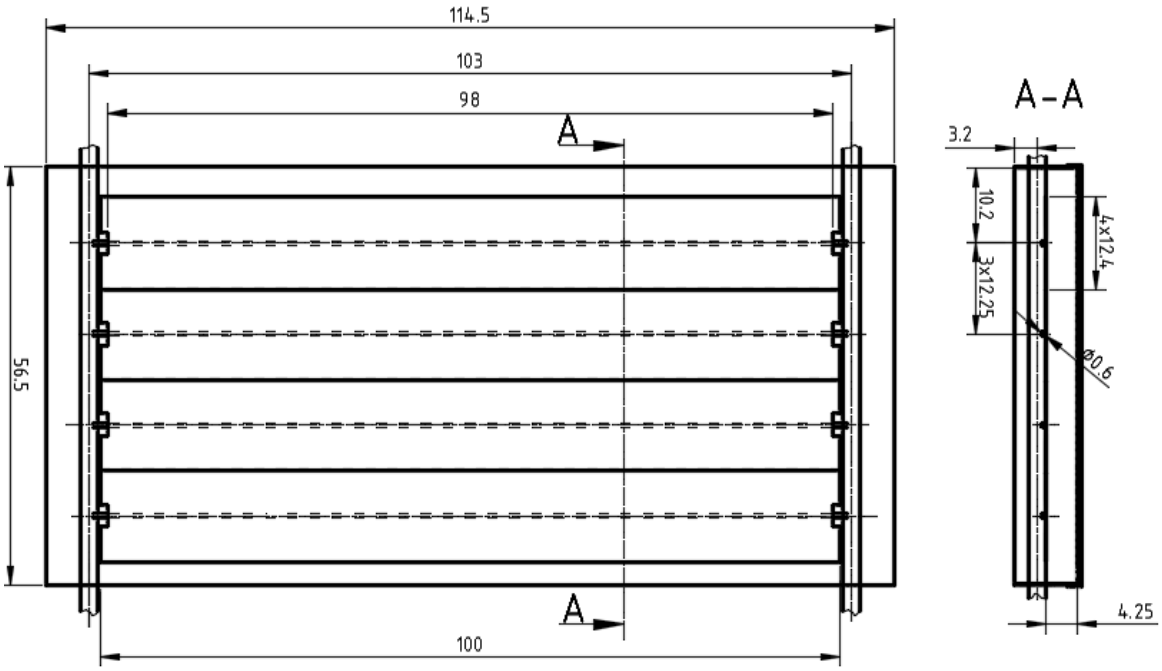

Figure 3.2 - Collector geometry (dimensions in cm)

3.1.2 Position of the collector

The collector is mounted on a structure, oriented southwards. At the location no shadow was projected on the collector surface during testing, nor collector horizon was obstructed. The surrounding buildings were sufficiently far, so that the measured incident solar radiation conditions imposed by the standard regarding the vicinity of other buildings were fulfilled.

The support structure allowed adjustment of collector tilt angle (β), within the limits imposed by its dimensions (30º-45º). The tests were conducted between July and

September, for which the ideal tilt would be of 26° for the latitude of Porto ($\phi = 41.178°$), respecting the indication by Água Quente Solar (2004):

$$\beta = \phi - 15 \tag{3.1}$$

As it was not possible, by the geometric limitations, to use that slope, it was fixed at the minimum possible, 30º.

3.1.3 Water circuit

The necessity of testing different inlet temperatures in the collector required the existence of equipment to heat the supply water. In this case, an electrical water heater was used, with 2000 W heating power and 80 l capacity. The circuit was adapted from an existing network in the rooftop, only adding the heating element, designated as (H) in Figure 3.3. The tubes are multilayer, with a diameter of 16 mm on segment AB and 14 mm from B to the water outlet.

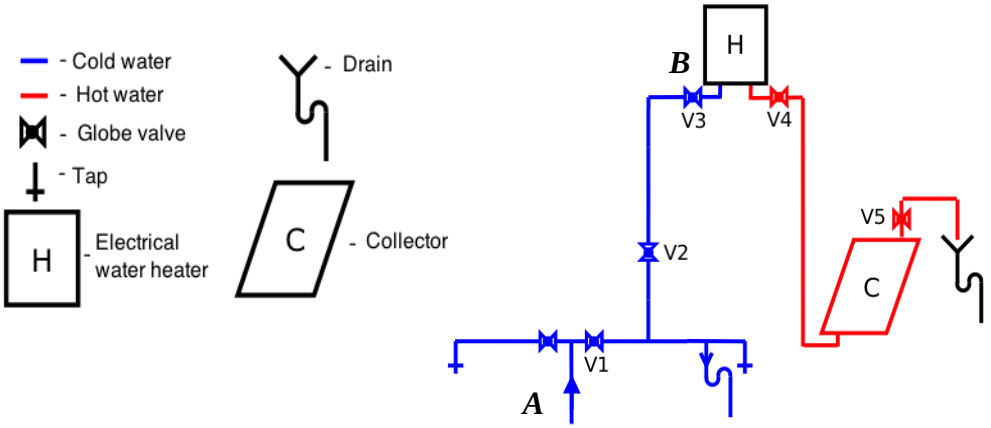

Figure 3.3 - Collector feed water circuit

Originally, the temperature at the inlet of the collector was controlled by the thermostat of the electric heater. However, preliminary tests indicated that the thermostat was not able to provide a stable water temperature during the experiments, registering variations of about 15°C, for a set point temperature of 50ºC. It was therefore necessary to include a PID power controller (Shinko Brand, Model ACS-13A), equipped with a T thermocouple probe, installed before valve V4.

There are several references on how to select the flow rate of the heat transfer fluid for the performance tests. The standard IPQ (2007) recommends a flow rate according to:

$$\dot{m} = 0.02\, A_{Col} \tag{3.2}$$

In eq. 3.2 the flow rate $\dot{m}$ is expressed in kg/s. Another relation is indicated by Água Quente Solar (2004) for selective collectors, for a flow rate expressed in kg/h:

$$\dot{m} = 46\, A_{Col} \tag{3.3}$$

The mass flow rate corresponding to eq. 3.3 is 0.013 kg/s. In practice, flow rate values lie in the range of 15 to 20 g/s/m^2, which will be considered in this work. Thus, for an aperture area of 1.127x0.55 (m^2), the mass flow rate can vary between 0.0093 kg/s and 0.0124 kg/s. For the tests a flow rate of about 0.01 kg/s was used.

The water flow rate was controlled by adjusting different valves of the circuit (V1, V4 and V5 in Figure 3.3). The mass flow rate was determined according to the equation:

$$\dot{m} = \dot{V}\, \rho(T) \tag{3.4}$$

In eq. 3.4, the volumetric flow rate ($\dot{V}$) was obtained by measuring the time that was required to fill up a 1000 ml beaker. The collecting point was after valve V5. The measurements were made before each experiment start, and along each test, to verify the flow rate stability. The density of the water was obtained as a function of the outlet temperature $T_{f,OUT}$ according to the following equation (IPQ, 2007):

$$\rho(T) = 999.85 + 6.187 \times 10^{-2} T - 7.654 \times 10^{-3} T^2 + 3.974 \times 10^{-5} T^3 - 1.110 \times 10^{-7} T^4 \tag{3.5}$$

In eq. 3.5 T is expressed in °C, and corresponds to the outlet water temperature. A continuous

3.1.4 Instrumentation of the experimental setup

The measurements of solar irradiance and ambient temperature were carried out with a pyranometer (CM6B, Kipp & Zonen), and a temperature (and humidity) sensor with radiation shield (SKH 2013, Skye), as shown in Figure 3.4. They were located in the rooftop of the building, and the pyranometer was directed to the south, with the same slope as the collector, 30º. The output from both devices is in voltage, measured in the data acquisition board 34901A (section 3.1.6). The signal was then converted to solar radiation and temperature through a software developed in LabView 2011.

a) b)

Figure 3.4 - Sensors used in the measurements
a) Pyranometer b) Temperature and humidity sensor

The water temperatures at the inlet and outlet of the collector were measured with type t thermocouples. Before installation, all the thermocouples were calibrated using a thermal bath (JULABO EH5, class III according to DIN 12876) with a PT100 reference probe. A range of setpoint temperatures has been selected, according to the operational conditions: 20°C, 30°C, 40°C, 50°C, 60°C, 70°C. For each one, after stabilizing bath temperature, the data for the calibration procedure were recorded at intervals of 3 seconds, over 6 minutes. The calibration lines for the thermocouples installed at the collector inlet ($T_{f,IN}$) and outlet ($T_{f,OUT}$) are presented in Figure 3.5.

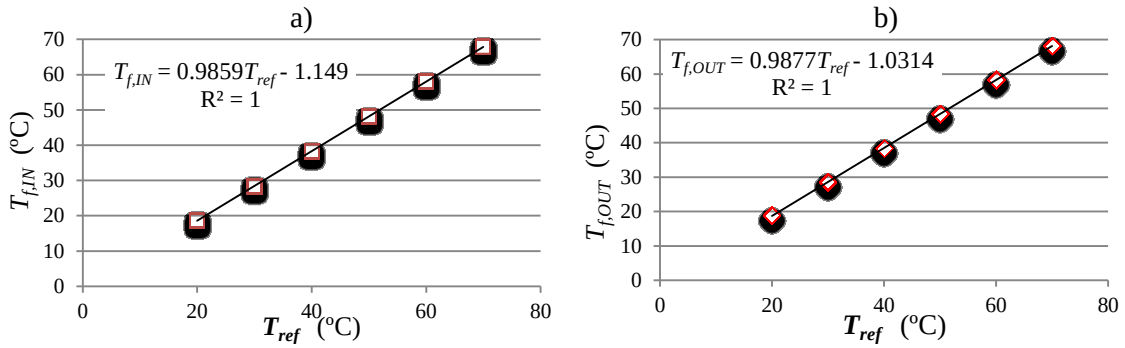

Figure 3.5 - Thermocouple calibration curves
a) $T_{f,IN}$ b) $T_{f,OUT}$

Table 3.1 presents the regression lines, the standard error and determination coefficient that characterize the approximation to the temperatures read by the thermocouples, based on the least squares method. The linear regression function was later used to correct the water temperature values read through the data acquisition system.

Table 3.1 - Thermocouple characterization

Thermocouple	Linear regression	Standard error	R^2
$T_{f,IN}$	$T_{f,IN}$ = 0.9859 T_{ref} – 1.1490	0.04557	0.99999
$T_{f,OUT}$	$T_{f,OUT}$ = 0.9877 T_{ref} – 1.0314	0.05669	0.99999

3.1.5 Photovoltaic component: characterization of cells and measurement procedure

The selection of photovoltaic cells has been limited by the size of the fins, thereby opting for 5" cells (c-Si), associated in 4x2 series arrangements to enable module manufacture, resulting in the geometry shown in Figure 3.6. It was, thus, a custom made solution, supplied by Onyx Solar (2015). Cells are encapsulated into EVA layers, with a total 0.5 mm thickness, and laminated between two layers of 4 mm thick glass. Because of the dimensions of the modules, the experiments were carried out applying up to three modules to the collector prototype.

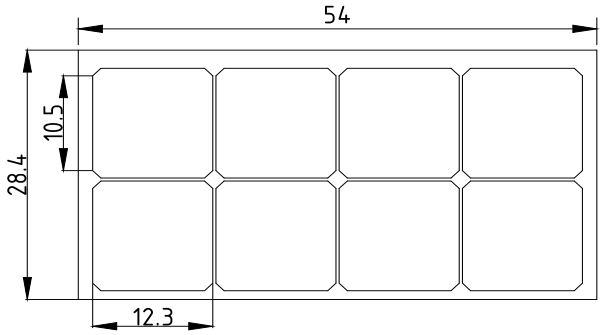

Figure 3.6 - Layout of photovoltaic modules (dimensions in cm)

The reference characteristics of the cells, provided by the manufacturer, are summarized in Table 3.2, for a radiation level of 1000 W/m^2.

Table 3.2 - Reference electrical characteristics of the PV cells

Dimension/ type	**Efficiency (%)**	**Power (W)**	**V_{OC} (V)**	**I_{SC} (A)**	**V_{MPP} (V)**	**I_{MPP} (A)**	**R_S (Ωcm^2)**	**R_{SH} (Ωcm^2)**
5"/c-Si	17.75-18.00	2.6	0.631	5.59	0.52	5.24	0.9	120

In Table 3.2, I_{SC} refers to the *shortcut-circuit* current, that is the maximum current (I_{El}) generated by the cells when the voltage (V) is 0, and V_{OC} represents the *open-circuit* voltage. The manufacturer also refers that the final module efficiency is about 10% lower than for separated cells, because of the glass encapsulation and resistance from cell interconnections. The generated voltage values does not vary significantly with irradiance (G) above 100 W/m^2, which does not happen with the current, that is very sensitive to G.

Another characteristic of the cells is their parasitic resistance, resulting from two different components: the series resistance R_S, and the shunt resistance R_{SH} (on Table 3.2). The series resistance of a cell arises from different phenomena: the movement of the current through the emitter and the base of the cell, the resistance between the metal contacts and

the silicon and by the resistance of the top and rear metal contacts (Honsberg and Bowden). The shunt (parallel) resistance is associated with the leakage current across the junctions, especially on the top of the cell area, through resistive surface conduction pathways, or due to micro short-circuits (Ferreira, 1999).

For this study, it is need to know the power produced by the PV modules for each set of test conditions. In order to correctly measure it, it is important to ensure that the module is operating at maximum power. The typical *I-V* curve of solar cell is represented in Figure 3.7, along with the power ($\dot{E}$) curve, where the maximum is easily identified ($\dot{E}_{max}$), corresponding to the conditions I_{MPP} and V_{MPP}.

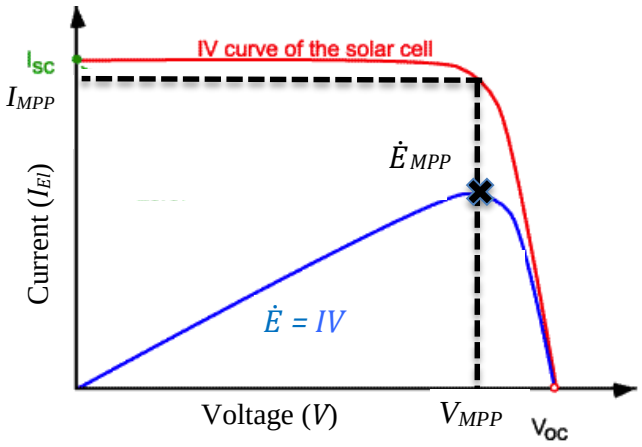

Figure 3.7 - Typical *I-V* and power curves of PV cells (adapted from Honsberg and Bowden)

In the common utilization of photovoltaic systems, an equipment called Maximum Power Point Tracker (MPPT) is needed to ensure the operation under maximum power conditions. MPPT checks the output of PV module, compares it to battery voltage, and then fixes the best power that the PV module can produce to charge the battery and converts it to the best voltage to get maximum current into battery. In this experimental case, it was not possible to operate this way, because there was not any commercial model operating for this range of low voltage values. Another way of determining $\dot{E}_{MPP}$ as a function of operation conditions is through the characteristics V_{OC} and I_{SC} (Table 3.2) as:

$$\dot{E}_{MPP} = I_{MPP} \times V_{MPP} = I_{SC} \times V_{OC} \times FF \tag{3.6}$$

In eq. 3.6, *FF* represents the cells *Fill Factor*. It is an indicator of the "quality" of the cells, since it is the ratio between the maximum power ($\dot{E}_{MPP}$) and the maximum theoretical power ($\dot{E}_{max,Th}$), expressed in the following equation:

$$\dot{E}_{max,Th} = I_{SC} \times V_{OC} \tag{3.7}$$

It can be more easily understood graphically as the ratio between the rectangular areas of the point of maximum power and maximum area of the graph, as shown in Figure 3.8.

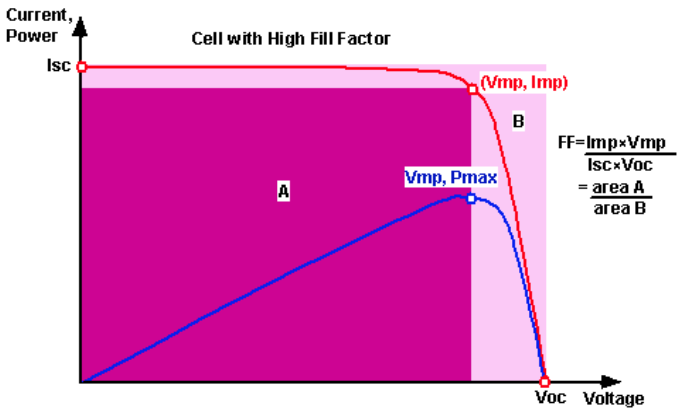

Figure 3.8 – Graphical interpretation of the Fill Factor of solar cells based on *I-V* and $\dot{E}_{El}$ curves (Honsberg and Bowden)

The previously referred parasitic resistances, R_S and R_{SH}, induces a reduction of the fill factor. The value of the fill factor is characteristic of the cells, as well as the series resistance R_S, and the shunt resistance R_{SH}.

Irradiance is a key parameter for photovoltaics, affecting characteristics of the PV cells like I_{SC}, V_{OC}, R_S, R_{SH} and *FF*. Figure 3.9 shows the influence of irradiance on *I*, *V* and *FF* for the range of radiation 700 W/m^2 (0.7 sun) - 1000 W/m^2 (1 sun), for the characteristic cell values of R_S and R_{SH}.

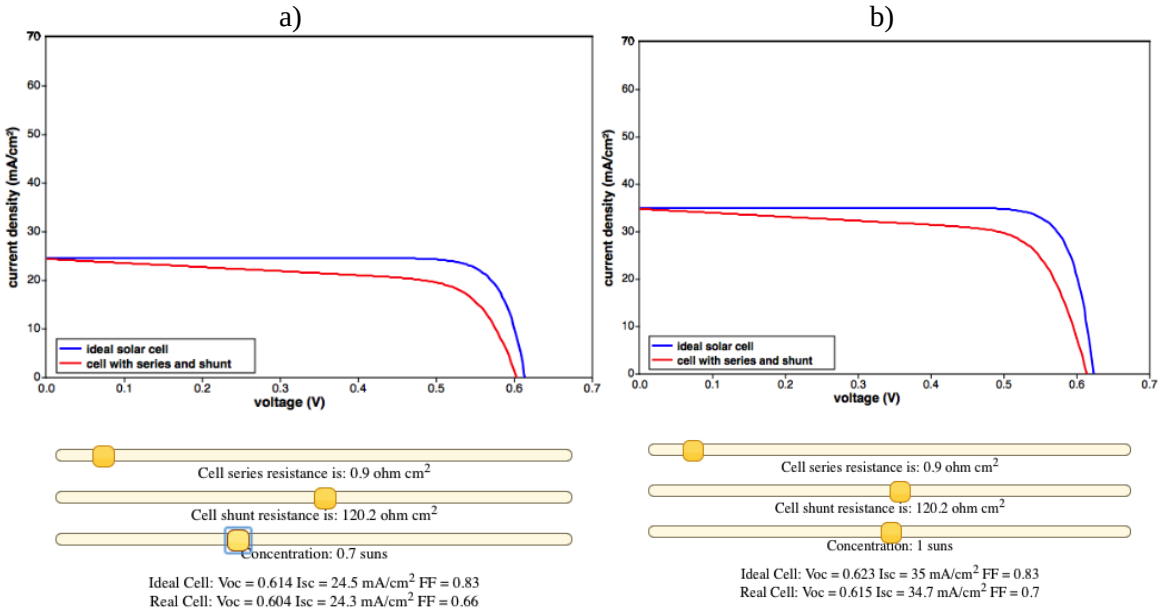

Figure 3.9 - Influence of irradiance on cell characteristics (*I, V, FF*) (Honsberg and Bowden)
a) G = 700 W/m^2 b) G = 1000 W/m^2

The *FF* values used in this study (eq. 3.6) were estimated through the interactive graphics represented in Figure 3.9, for the measured values of *G*.

Running the experiments, electric power in eq. 3.6 was determined by the continuous measurement of V_{OC}, registered by the acquisition system, and the indirect measurement of I_{SC}. The short circuit current (I_{SC}), that varies with irradiance, was estimated indirectly through a process of approximation by linear regression. The regression lines were obtained previously to the tests, for each one of the tested serial module association (one, two and three PV modules), and are presented in Figure 3.10. The results of I_{SC} were obtained with a multimeter Agilent U1252A, connected in series to the circuit. The linear functions of I_{SC} with *G* were applied for the test values of *G* to determine I_{SC}.

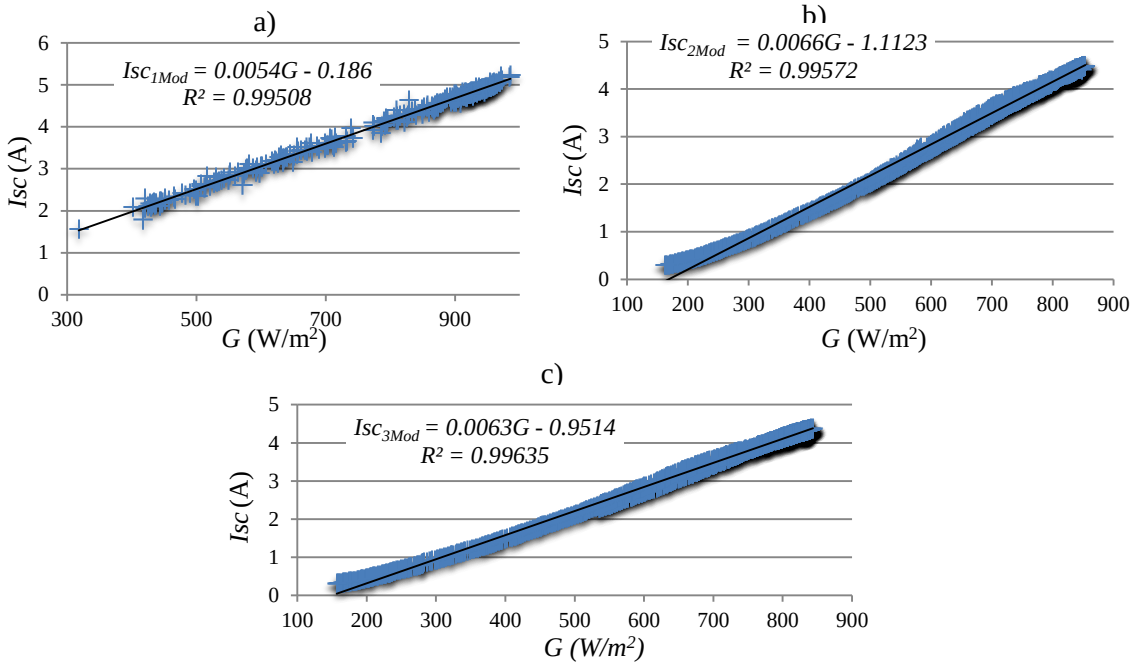

Figure 3.10 – $I_{SC} = f(G)$, for different number of PV modules connected in series
a) 1 PV module b) 2 PV modules c) 3 PV modules

3.1.6 Data acquisition

In order to monitor the system performance, a number of instruments were installed. Values of solar irradiance, ambient temperature, inlet and outlet fluid temperature have been acquired during each test. The sensitivity of the specified sensors of radiation and ambient temperature had to be considered, and is listed in Table 3.3.

Table 3.3 - Sensors sensitivity

Quantity	Sensivity
Solar radiation	13.2 μV/(W/m²)
Ambient temperature	10 mV/°C

The data acquisition system integrated a data logger module (HP Agilent 34970A, USA) with a board 34901A connected to a personal computer. A monitoring program was developed in LabView 2011 (National Instruments, USA). That data were sampled every 30 seconds and saved for subsequent analysis, which was carried out using MS EXCEL. The presentation and discussion of the experimental results is made in section 3.3.

3.2 Experimental procedure

Summarizing, three sets of experiments have been performed, respectively with one, two and three applied PV modules, connected in series. For each set, tests were conducted for different setups of inlet temperature ($T_{f,IN}$), ranging from 25°C to 65°C (25°C, 35°C, 45°C, 55°C and 60°C). The tests were carried out during periods when the sun incidence angle was adequate (respecting the testing standard). The tests were conducted based on information set forth in the standard NP EN 12975-2, for testing the thermal performance of collectors with one cover under stationary conditions, as further specified in the following points. Since the purpose of the tests was not collector certification, certain restrictions have been alleviated, as will be also referred in due time.

3.2.1 Angle of incidence of direct solar radiation

The angle of incidence of direct solar radiation on the collector aperture should be such that the incidence angle modifier for the collector does not vary more than ± 2% of its value at normal incidence, which, for flat plate collectors with single cover, will usually be satisfied if the angle of incidence (θ) of direct solar radiation on the collector aperture is less than 20° (IPQ, 2007). This rule was updated in this version of the standard, but had been considered as 30° in previous versions. Thus, for this study, all periods with incidence angles of direct solar radiation on the collector aperture lower than 30° were considered.

In order to determine the period of each day of tests with adequate angle of incidence (θ), it was necessary to know the variation of the sun position along the day. It can be determined according to a local coordinate system, defined by solar azimuth (az_S) and sun height (γ_S). The collector position is defined, according to the same system, by the azimuth (az_C) and the tilt angle (β_C). The solar geometry parameters involved are

represented in Figure 3.11. In the same figure, azimuth angles are referenced to the North. Some authors, like Duffie (1991), consider the azimuth angles referenced to South.

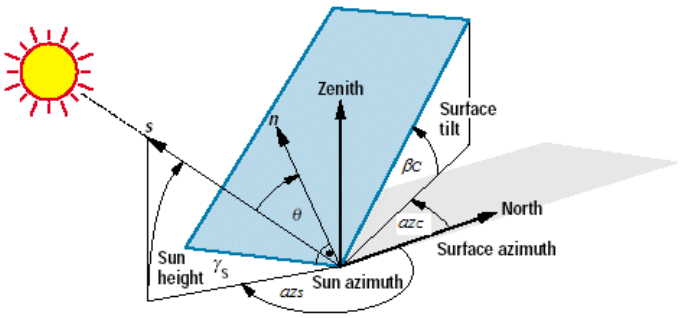

Figure 3.11 – Solar geometry coordinates, in relation with the solar collector position (adapted from Quaschning (2003))

The solar geometry angles are calculated for each day of tests, according to a generally accepted formulation (Duffie, 1991). The angle of incidence θ can then be obtained applying a set of useful geometrical relations, resulting on eq. 3.8, using azimuths referenced to the South:

$$cos(\theta) = sin(\gamma_S)cos(\beta_C) + cos(\gamma_S)\, sin(\beta_C)\, cos(az_S - az_C) \tag{3.8}$$

Throughout the day, for a location with latitude ϕ, it is possible to determine solar azimuth az_S and solar height γ_S, by relating local coordinate system with the spherical coordinates (δ, H) through equations 3.9 and 3.10. For a given day of the year (n), the declination angle of the earth (δ) represents the angular position of the sun at the solar noon, with respect to the plane of equator, and is given by eq. 3.11. H, the hour angle, represents the angular displacement of the sun, east or west of the local meridian, due to the rotation of the earth on its axis at 15º per hour, as expressed in eq. 3.12. *True solar time* (TST) is the time based on the apparent angular motion of the sun across the sky, with solar noon at the time the sun crosses the observer´s meridian, corresponding to H =0.

$$sin(\gamma_S) = sin(\delta)\, sin(\phi) + cos(\delta)\, cos(\phi)\, cos(H) \tag{3.9}$$

$$sin(az_S) = \frac{-cos(\delta)\, sin(H)}{cos(\gamma_S)} \tag{3.10}$$

$$\delta = 23.45\, sin\left(360\frac{(284+n)}{365}\right) \tag{3.11}$$

$$H = 15\,(TST - 12) \tag{3.12}$$

In order to determine the time of day respecting the correct angle of incidence ($\theta <$ 30°), it is necessary to make the correspondence between *TST* and the *Legal time* (LT).

That correspondence depends on the local longitude, λ, and varies daily according with one adjustment, named *equation of time* (*ET*). The formulation is expressed in the equations 3.13 and 3.14:

$$\begin{cases} October - March: TST = LT + ET + \dfrac{\lambda}{15} \\ April - September: TST = LT + ET + \dfrac{\lambda}{15} - 1 \end{cases} \tag{3.13}$$

$$ET = 9.87\ sin\left(2\frac{360(n-81)}{364}\right) - 7.53\ cos\left(\frac{360(n-81)}{364}\right) - 1.5\ sin\left(\frac{360(n-81)}{364}\right) \tag{3.14}$$

Thus, for each day of tests, the time of day respecting an angle of incidence $\theta < 30°$ was previously calculated, through equations 3.8 to 3.14. The tests were performed during the periods determined.

3.2.2 Application of photovoltaic modules

The process of application of photovoltaic modules over the absorber plate was carried out with attention to a good thermal contact between both elements. In order to correct small irregularities of the absorber surface, a sufficiently thick layer of thermal mass was applied on the fins before applying the PV modules. The thermal mass used has, according to the supplier's information (Fixapart, 2015), a thermal conductivity of about 3.2 W/mK and a thermal impedance less than 0.06°C/W, for a working temperature range of -50°C to 180°C.

Another practical issue came across, since the absorber fins presented some warpage, which compromised thermal contact with the photovoltaic modules. A wood plate has been applied under the absorber fins, with rips to house the individual water tubes. The plate forced the fins up against the PV modules, by placing wooden blocks under it. On the opposite side wooden guides were also added on the border of the frame to press the PV modules downwards against the fins.

3.3 Results and discussion of experimental tests

As mentioned before, the tests were performed for three arrangements: with one, two and three photovoltaic modules applied to the absorber plate, corresponding to packing factors 0.24, 0.49 and 0.73, respectively. Photographs of the configurations are presented in Figure 3.12.

a) b) c)

Figure 3.12 - Views of the three tested arrangements:
a) with one PV module b) with two PV modules c) with three PV modules

The three different arrangements will be furthered referenced as "*PV/T1*", "*PV/T2*" and "*PV/T3*", with the index indicating the number of PV modules applied. For each case, experiments were performed with five set up collector inlet temperatures. The data have been registered during the day, always with sun incidence angles up to 30°, after a stabilization period for the flow rate and the set up temperature.

The data analyses were carried out on the results that fulfilled steady conditions imposed by the IPQ (2007) standard for G and T_{amb}, based on the average values registered over a 10 minute period, respectively $\bar{G}$ and $\overline{T_{amb}}$. The criteria applied to $T_{f,IN}$ was adapted. The attended criteria are expressed as follows:

$$|G - \bar{G}| \leq 50\ W/m^2 \tag{3.15}$$

$$|T_{amb} - \overline{T_{amb}}| \leq 1.5\ K \tag{3.16}$$

$$\frac{\left|T_{f,IN} - \overline{T_{f,IN}}\right|}{\overline{T_{f,IN}}} \leq 0.5\% \tag{3.17}$$

The fluid inlet temperature stability was the most critical condition to obtain a valid test. As the temperature in the water heater was controlled by a PID controller, the variation of $T_{f,IN}$ during a test was due to the change in the mass flow rate. Therefore, the test points selected for the analysis under the steady state $T_{f,IN}$ condition also respected the steady state condition for the mass flow rate, according to $|\dot{m} - \bar{\dot{m}}| \leq 1\%$. The continuous measurement of the flow rate would assure directly this steady state criteria.

3.3.1 Thermal efficiency

The thermal efficiency (η_{Th}) was calculated for the set of experimental results that verified the stability conditions, according to the formerly presented eq 2.8. The mass flow rate was obtained from the average of the volumetric flow rate (eq. 3.4) for each test, determined experimentally as explained in subsection 3.1.3. A continuous measurement of $\dot{m}$ would allow the determination of the thermal efficiency exclusively from direct measured values of the variables in equation 2.8, for each test point. The data from the selected tests have been then considered for a regression analysis, applied to the estimated thermal efficiency values for each arrangement (PV/T_1, PV/T_2 and PV/T_3), obtaining a typical linear equation, in the form:

$$\widehat{\eta_{Th}} = F'\eta_o - F'U_L T^* \tag{3.18}$$

According to the procedure indicated in IPQ (2007), T^* is here defined as a function of the average fluid temperature ($\overline{T_f}$), expressed in eq. 2.20, as:

$$T^* = \frac{\overline{T_f} - T_{amb}}{G} \tag{3.19}$$

On a first approach, some test results have been discarded, based on the application of the criterion of Chauvenet (Young, 1996). This criterion states that all data points that fall within a band around the mean that corresponds to a probability of 1-1/(2N) should be retained, where N is the total number of tests. That probability can be related to a maximum deviation away from the mean by using the Gaussian probabilities, and a no dimensional maximum deviation τ_{max} can be determined. The values of τ_{max} are related with the size of the sample, and are normally listed in tables. A corresponding critical value of thermal efficiency, $\eta_{Th,max}$ can thus be determined, by applying the usual relation for a normal distribution:

$$\tau_{max} = \frac{\left|\eta_{Th,max} - \overline{\eta_{Th}}\right|_{max}}{\sigma_{\eta Th}} \tag{3.20}$$

In eq. 3.21 $\sigma_{\eta Th}$ is the standard deviation estimate for η_{Th}, defined as:

$$\sigma_{\eta Th} = \sqrt{\frac{\sum_{i=1}^{N}\left(\eta_{Th,i} - \widehat{\eta_{Th,i}}\right)^2}{N-2}} \tag{3.21}$$

This selection of eligible results for final analysis was performed on the basis of thermal efficiency values, since it is the predominant factor in the overall efficiency of the collector.

In order to characterize the reliability of the results, confidence intervals were determined for the remaining sample, with a 95% confidence level, defined as (Guimarães):

$$\widehat{\eta_{Th}} \pm t_{N-2}^{2.5\%}\sigma_{\eta Th}\sqrt{1 + \frac{1}{N} + \frac{(T^* - \overline{T^*})^2}{\sum(T^* - \overline{T^*})^2}} \tag{3.22}$$

where $t_{N-2}^{2.5\%}$ is the critical value for the student-t distribution with *N-2* degrees of freedom, and significance level of 5%.

The results for thermal efficiency curve and confidence interval with 95% probability are presented for the three arrangements in Figure 3.13, Figure 3.14 and Figure 3.15. In the graphics, *Y-* and *Y+* represent the limits of the confidence interval defined by eq. 3.22.

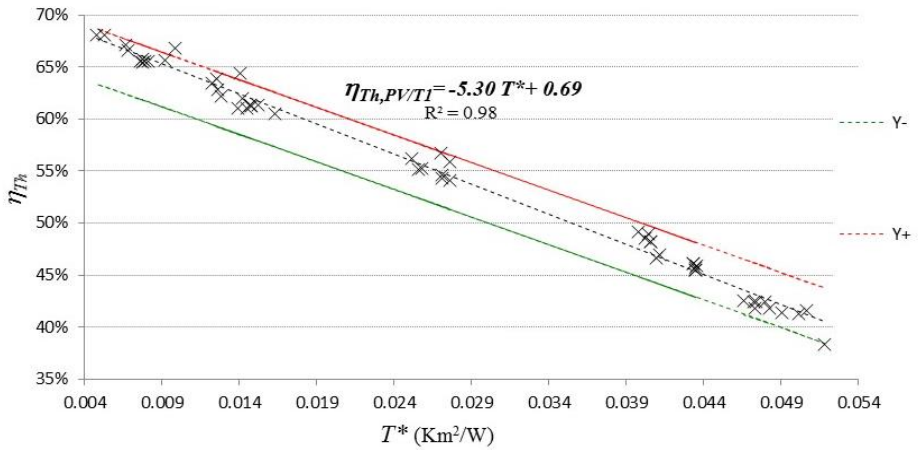

Figure 3.13 - Thermal efficiency curve ($\eta_{Th} = f(T^*)$) and 95% confidence interval for PV/T_1 arrangement

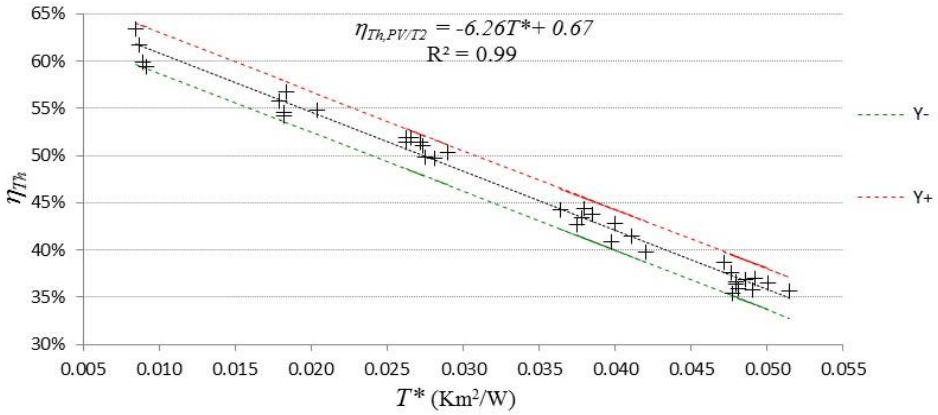

Figure 3.14 - Thermal efficiency curve ($\eta_{Th} = f(T^*)$) and 95% confidence interval for "PV/T_2" arrangement

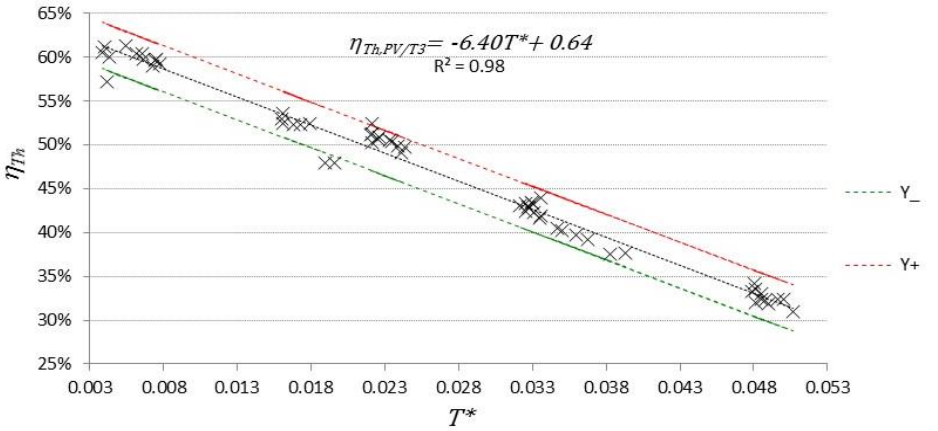

Figure 3.15 - Thermal efficiency curve ($\eta_{Th} = f(T^*)$) and 95% confidence interval for "PV/T_3" arrangement

It is expected that the optical efficiency, $F'\eta_0$, is reduced with the obstruction of the incident radiation, caused by application of the PV modules over the absorber plate. It is confirmed by the experimental results. The results are presented for the three cases in Figure 3.16, to ease comparison. The regression analysis coefficients obtained for the three cases are presented in Table 3.4.

Table 3.4 - Regression analysis coefficients and standard error for η_{Th} obtained with one, two and three PV modules applied

	Pf	Intercept ($F'\eta_{Th,0}$)	Slope ($F'U_L$)	Standard Error (σ)
PV/T_1	24%	0.69	-5.30	0.013
PV/T_2	49%	0.67	-6.26	0.010
PV/T_3	73%	0.64	-6.40	0.013

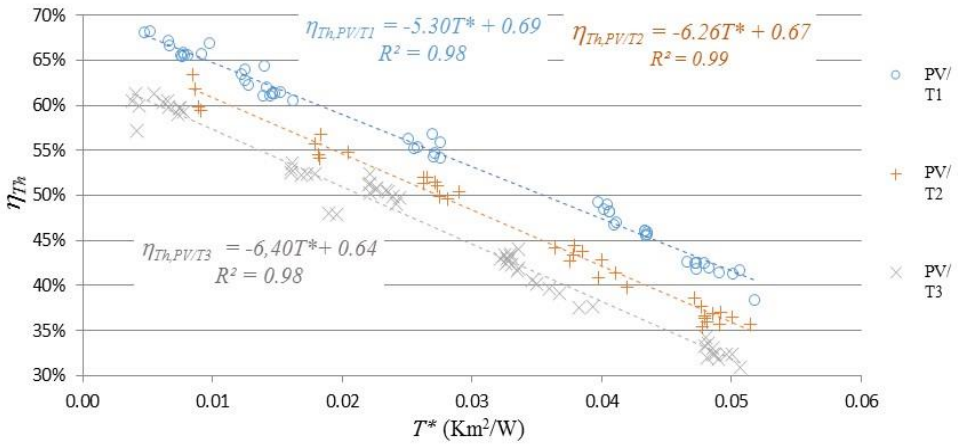

Figure 3.16 - Thermal efficiency curves ($\eta_{Th} = f(T^*)$) for 1, 2 and 3 modules applied

The reduction of thermal efficiency with the number of photovoltaic modules applied is clear from Figure 3.16, but a conclusion regarding the effect on loss overall factor $F'U_L$ is not as straightforward. It is therefore necessary to resort to a complementary approach, as statistical techniques, in order to grant an objective analysis.

Regression coefficients (intercept and slope) from Table 3.4 were compared for the three configurations using statistical approaches. T-tests for the mean values of the intercepts and slopes were performed, assuming equal variances, with a significance level of 5%, to verify if the coefficients could be assumed significantly different for the three cases, or not (Guimarães, 2009). It was proved that the intercept values were significantly different for the three cases. Regarding the slope values, it was verified that the slope for two and three modules were not significantly different, but, the results of the test were inconclusive, when comparing the slope for one and two applied modules.

It is a fact that, with the application of PV modules, the temperature of the absorber is not so high, and so, the heat loss factor, $F'U_L$, representing the losses due to the temperature difference between the plate and the ambient, would decrease. However, the glass of the PV modules has a higher emissivity than that of the selective absorber surface (0.8 for the glass compared to 0.2 for the selective absorber), leading to higher radiation losses. Studies on the influence of the P_f in the overall heat loss coefficient still do not exist. Reporting to the performance characteristics of selective FPC listed in Table 2.1, it can be noticed a decrease in the optical efficiency from traditional values over 0.74 to 0.69 for PV/T_1 arrangement. The heat losses, reflected mainly in parameter a_1 in the same table, are in the order of 4 W m^{-2} K^{-1} in solar thermal collectors, and increase to 5.3 with one PV/T module applied.

3.3.2 Determination of the combined collector efficiency

The analysis presented in the previous section only concerns the thermal efficiency of the collector. It is necessary to analyse the electrical component and the resulting combined efficiency. The selected set of test results previously presented will now be studied, in terms of those contributions.

Electrical efficiency is calculated for each test following eq. 2.15. The results are presented, for the three situations, in Figure 3.17.

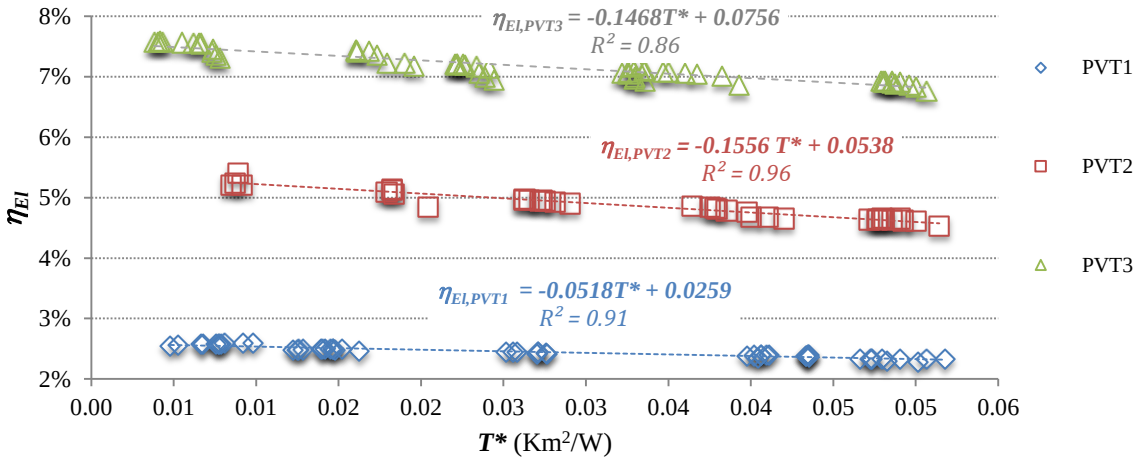

Figure 3.17 - Electrical efficiency ($\eta_{El} = f(T^*)$) for configurations PVT_1, PVT_2 and PVT_3

It can be seen in Figure 3.17 that the electrical gain increases roughly in proportion to the number of modules applied, of about 2% per 25% of *Pf* increase. The increase in the reduced temperature difference, *T**, is associated to an expected decrease in the electrical efficiency.

The global effect of *Pf* on η_{Th} and η_{El} follows the expected tendency reported in literature, in references such as Dupeyrat *et al.* (2011a). Thermal and electrical efficiencies determined by Zondag *et al.* (2003) at zero reduced temperature for single covered PV/T-w collectors are 58% and 8.9%, as listed in Table 3.5. Given that those results correspond to a complete coverage of the collector with PV modules, the values obtained in this work for *Pf* = 73%, $\eta_{Th,o}$ = 64% and $\eta_{El,o}$ = 8%, are in line with them. The results obtained by Chow *et al.* (2006) are also summarized in Table 3.5, for *Pf* = 50% and *Pf* = 100%. Regarding thermal efficiency, and reporting to Table 3.4, the zero reduced efficiency values also in agreement with the tendency in the reference, but the variation with *Pf* is lower. The values found by Chow *et al.* (2006) regarding the electrical efficiency are higher than the

ones obtained with the experiments, and in less agreement than the ones by Zondag *et al.* (2003), but reveal a similar tendency for the effect of *Pf*.

Table 3.5 – Characteristic values for η_{Th} and η_{El} referenced in literature, for PV/T-w collectors

Reference	*Pf*	$\eta_{Th,o}$	$\eta_{El,o}$
Zondag et al. (2003)	100%	58%	8.9%
Chow et al. (2006)	50%	66.8%	12.1%
Chow et al. (2006)	100%	57.4%	12.3%

Another approach was applied to the electrical component analysis, using the concept of electrical efficiency for PV cells, calculated based on the area with cells (A_{PV}):

$$\eta_{El}{}^{*} = \frac{\dot{E}_{MPP}}{A_{PV} G} \tag{3.23}$$

The results are presented in Figure 3.18 for the three configurations. It shows that the increase of *Pf* has a global reducing effect on η_{El}*, despite generating an increase in electrical output in absolute terms. There is a gain when increasing from one to two PV modules, for low values of *T**. The PV cells efficiency is, reporting to Table 3.2, around 18%, which is higher than the values obtained experimentally. The method used for estimating the values of the electrical output may introduce some error in the experimental results.

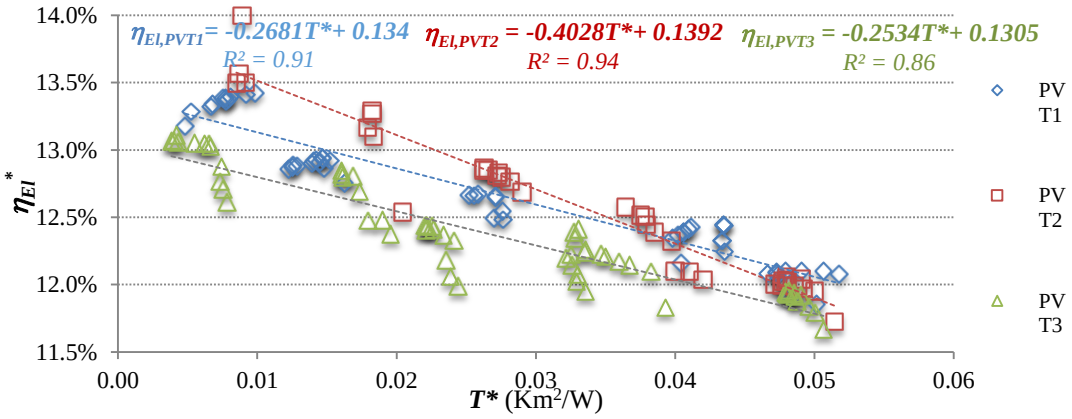

Figure 3.18 - Electrical efficiency* (η_{El}*= *f*(*T**)) for PVT_1, PVT_2 and PVT_3 configurations

The combined efficiency definition used in this work was previously presented in eq. 2.16. The results obtained for the experimental tests are shown in Figure 3.19, and it can be observed that the electrical gain does not compensate the loss in thermal gain caused by the application of PV modules, and thus η_G reduces with *Pf*.

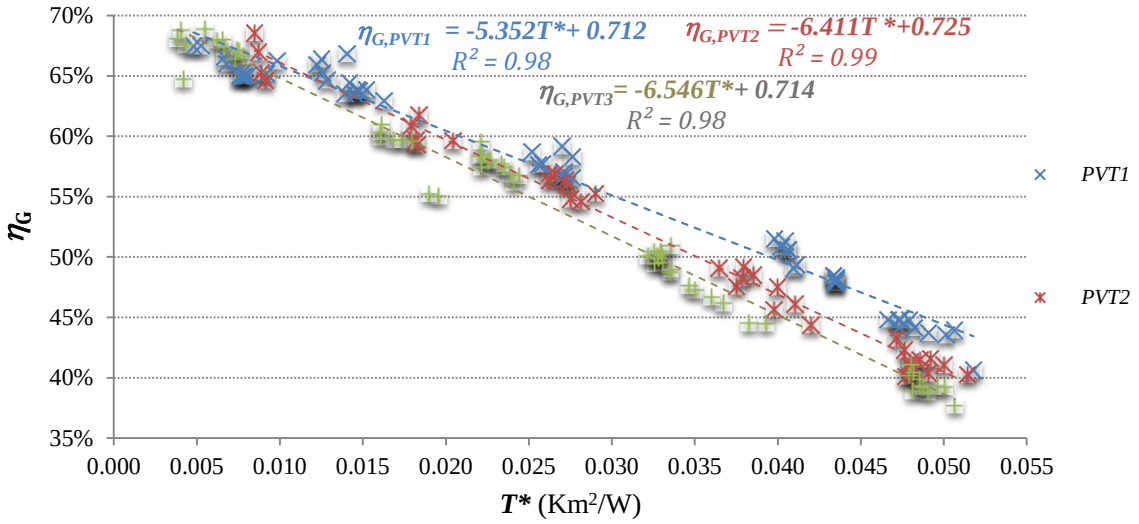

Figure 3.19 - Combined efficiency ($\eta_G = f(T^*)$) for PVT_1, PVT_2 and PVT_3 configurations

Analysing the regression parameters for the efficiency curves in Figure 3.19, it can be also verified that the decrease of the combined efficiency with the packing factor is mainly due to the increase in the loss overall factor, represented by the slope parameter.

Despite some references can be found regarding the effect of *Pf* in η_{Th} and η_{El}, the information on the effect in η_G is scarcer. The influence of the packing factor, fluid inlet temperature and solar radiation on thermal, electrical, and overall efficiencies of PV/T collectors is reviewed by Moradi *et al.* (2013). The global impact of *Pf* summarized confirms the tendencies already identified for η_{Th} and η_{El}, but the results regarding η_G are opposite. This last conclusion is based on some studies such as Garg and Agarwal (1995) and Wu *et al.* (2011). The numerical model developed by Garg and Agarwal (1995) for a system with a PV/T-w collector accounted for thermal and electrical outputs differently than the formulation used in this work. The results found by Wu *et al.* (2011), mentioned by Moradi *et al.* (2013), refer to exergy efficiency, which is not also the standard for the analysis carried out in this work. However, the results obtained by Sopian *et al.* (1996) with a numerical model for PV/T-a collectors showed also a decreasing effect of *Pf* in η_G.

3.3.3 Uncertainty analysis

It is necessary to estimate the uncertainty associated to the efficiency calculations, η_G, η_{Th} and η_{El}. This uncertainty is originated from different sources:

i. The output quantities, η_{Th}, η_{El}, or η_G, are not directly measured quantities, but are instead obtained from others, directly measured or also calculated. This corresponds

to the "*combined standard uncertainty*" (u_C). Each individual uncertainty will contribute to the uncertainty of the output depending on their relative weight.

ii. The experimental data points obtained form a sample, with a dispersion that can be determined applying statistical tools. This is often referred to as "*type A standard uncertainty*" (u_{cA}), which is associated to a random component of the error in the measurements.

iii. For an estimate of an input quantity that has not been obtained from repeated observations, the standard uncertainty is evaluated by scientific judgement based on all of the available information on the possible variability of that quantity. This corresponds to "*type B standard uncertainty"* (u_{cB}), and is obtained from an assumed probability density function based on the degree of belief that an event will occur (JCGM, 2008).

The formulation used in this subsection follows the rules established by JCGM (2008).

The combined efficiency (η_G), as shown in equation 2.16, can be rewritten as follows:

$$\eta_G = \eta_{Th} + \eta_{El} \tag{3.24}$$

The uncertainty of combined efficiency ($U\eta_G$) can be estimated from the results uncertainty, depending on the uncertainty of thermal efficiency ($U\eta_{Th}$) and electrical efficiency ($U\eta_{El}$),, according to the following expression:

$$u_c(\eta_G) = \sqrt{u_c^2(\eta_{Th}) + u_c^2(\eta_{El})} \tag{3.25}$$

Since η_{Th} is a calculated quantity, type A and type B combined uncertainties, $u_{CA}(\eta_{Th})$ and $u_{cB}(\eta_{Th})$ should be considered in the determination of the uncertainty $u_c(\eta_{Th})$, resulting on the following similar expression:

$$u_c(\eta_{Th}) = \sqrt{u_{cA}^2(\eta_{Th}) + u_{cB}^2(\eta_{Th})} \tag{3.26}$$

The type A combined uncertainty of η_{Th} ($u_{CA}(\eta_{Th})$) will be given by:

$$u_{cA}(\eta_{Th}) = t_{N-1,2.5\%}u(\overline{\eta_{Th}}) \tag{3.27}$$

where $t_{N-1,2.5\%}$ is the corresponding value of the student's t-distribution point for 95% confidence level, with *N-1* degrees of freedom.

The *standard deviation of the sample average* ($u(\overline{\eta_{Th}})$) can be estimated from:

$$u(\overline{\eta_{Th}}) = \sqrt{\frac{s^2(\eta_{Th})}{N}} \tag{3.28}$$

The *estimated variance*, s^2, characterizing type A uncertainty, is calculated from a sample of *N* observations of a random variable. Applying to η_{Th} we can obtain:

$$s^2(\eta_{Th}) = \frac{1}{N-1}\sum_{j=1}^{N}\left(\eta_{Th,j} - \overline{\eta_{Th}}\right)^2 \tag{3.29}$$

The referred statistical properties, expressed in equations 3.27, 3.28 and 3.29 for the three PV/T configurations are summarized in Table 3.6, including the *estimated standard deviation*, $u(\eta_{Th})$.

Table 3.6 - Statistical characteristics of η_{Th}, for PV/T1, PV/T2 and PV/T3 configurations

	PVT$_1$	**PVT$_2$**	**PVT$_3$**
$\boldsymbol{u(\eta_{Th})}$	9.39%	8.59%	9.485%
$\boldsymbol{u(\overline{\eta_{Th}})}$	1.27%	1.39%	1.235%
$\boldsymbol{u_{CA}(\eta_{Th})}$	2.54%	2.82%	2.47%

The combined standard uncertainty ($u_c(\eta_{Th})$) is an estimated standard deviation and characterizes the dispersion of the values that could reasonably be attributed to the measurand (JCGM, 2008). The type B uncertainty for thermal efficiency, ($u_{cB}(\eta_{Th})$), which is a combined uncertainty, depends on the individual uncertainties of each variable X_i intervening in the calculation of thermal efficiency. Assuming that the variables X_i are not correlated, $U_{B,\eta Th}$ can be obtained as:

$$u_{cB}^2(\eta_{Th}) = \sum_{i}^{M}\left(\frac{\partial \eta_{Th}}{\partial X_i}\right)^2 u^2(X_i) \tag{3.30}$$

where $u(X_i)$ is a standard uncertainty of type A or type B for the variable X_i.

The thermal efficiency is calculated by formerly presented eq. 2.8. Applying eq. 3.30, results in:

$$u_{cB}^2(\eta_{Th}) = \left(\frac{\partial \eta_{Th}}{\partial \dot{m}}\right)^2 u^2(\dot{m}) + \left(\frac{\partial \eta_{Th}}{\partial c_P}\right)^2 u^2(c_P) + \left(\frac{\partial \eta_{Th}}{\partial T_{f,OUT}}\right)^2 u^2\left(T_{f,OUT}\right) + \left(\frac{\partial \eta_{Th}}{\partial T_{f,IN}}\right)^2 u^2\left(T_{f,IN}\right) + \left(\frac{\partial \eta_{Th}}{\partial G}\right)^2 u^2(G) + \left(\frac{\partial \eta_{Th}}{\partial A}\right)^2 u^2(A) \tag{3.31}$$

Developing eq. 3.31, each uncertainty is obtained according to the appropriate considerations, weather X_i is a measured or derived variable. The definition of each parcel, corresponding to the uncertainty of each variable, is presented next.

Irradiation (G) is directly measured, therefore its uncertainty ($u(G)$), in equation 3.31, results only from the uncertainty of the equipment. The most relevant specification is the error associated to the non-stability correction per year, with a value of 0.5 to 1%, according to the manufacturer. So, $u_c(G)$ will be of 11%. The usual value for this type of pyranometer would be of 4.7%, according to the manufacturer.

The temperatures $T_{f,IN}$ and $T_{f,OUT}$ are measured by thermocouples, for which the standard errors s were calculated during the calibration process (Table 3.1). This type A uncertainty was estimated with 95% confidence level, for N readings:

$$u_{cA}(T) = t_{N-2,2.5\%}\, s(T) \tag{3.32}$$

It is also necessary to consider the uncertainty of the thermal bath temperature used for the thermocouple calibration, with an error (u) of ±0.03 °C (information on the technical data of the equipment). A uniform probability distribution was assumed for the thermal bath error, which can be written in a general form:

$$u_{cB,uniform} = \frac{u}{\sqrt{3}} \tag{3.33}$$

Thus, based on the calculated type A and type B uncertainties, it is possible to obtain the temperatures uncertainty, to include in eq. 3.31, by applying the traditional Root Sum Square methodology, resulting on the combined uncertainty for T:

$$u_c(T) = \sqrt{\left(t_{N-2,95\%} s_T\right)^2 + \left(\frac{u_{Thermal\ bath}}{\sqrt{3}}\right)^2} \tag{3.34}$$

The definition of the area of the glass cover (A_{GC}) and specific heat (c) result are derived quantities determined as:

$$A_{GC} = L_{GC} H_{GC} \tag{3.35}$$

$$c = a_0 + a_1\bar{T} + a_2\bar{T}^2 + a_3\bar{T}^3 + a_4\bar{T}^4 + a_5\bar{T}^5 \quad \text{(IPQ, 2007)} \tag{3.36}$$

where $\bar{T}$ is average fluid temperature, calculated according to eq. 2.20. L_{GC} and H_{GC} are the length and height of the glass cover. So, a similar method to the one described for η_{Th} (eq. 3.30) has to be applied. For the area (A_{GC}), it results in:

$$u_{cB}^2(A_{GC}) = \left(\frac{\partial A_{GC}}{\partial L_{GC}}\right)^2 u^2(L_{GC}) + \left(\frac{\partial A_{GC}}{\partial H_{GC}}\right)^2 u^2(H_{GC}) \tag{3.37}$$

The uncertainties $u(L_{GC})$ and $u(H_{GC})$ are related to the resolution of the measuring equipment used, that is 0.5 mm. It is, then, a symmetric, uniform probability distribution, and so, they are determined by:

$$u_{cB}(L_{GC}) = u_{cB}(H_{GC}) = \frac{0.0005}{\sqrt{3}} \tag{3.38}$$

Regarding for the estimation of *u(c)*, the standard IPQ (2007) identifies the largest deviation of the polynomial as 0.02%, and so, as a uniform probability distribution, the uncertainty can be obtained as:

$$u_{cB}(c) = \frac{0.02c}{100\sqrt{3}} \tag{3.39}$$

The uncertainty of the mass flow rate ($u_c(\dot{m})$) has a statistical component and a type B component, according to the equation:

$$u_c(\dot{m}) = \sqrt{u_{cA}^2(\dot{m}) + u_{cB}^2(\dot{m})} \tag{3.40}$$

The instantaneous variability of $\dot{m}$ during a testing day (type A uncertainty, $u_{CA}(\dot{m})$) in eq. 3.40 is determined by the equation:

$$u_{cA}(\dot{m}) = t_{N-1,2.5\%}u(\bar{\dot{m}}) \tag{3.41}$$

The mass flow rate ($\dot{m}$) is obtained for each test point by the following equation:

$$\dot{m} = \frac{Vol}{t}\rho\left(T_{f,OUT}\right) \tag{3.42}$$

where *Vol* is the volume discharged during approximately one minute (t), which was measured several times during each test with a graduated beaker. Therefore, the type B combined uncertainty can be then obtained as:

$$u_{cB}^2\,(\dot{m}) = \left(\frac{\partial \dot{m}}{\partial Vol}\right)^2 u^2(Vol) + \left(\frac{\partial \dot{m}}{\partial t}\right)^2 u^2(t) + \left(\frac{\partial \dot{m}}{\partial \rho}\right)^2 u^2(\rho) \tag{3.43}$$

The standard deviation for the volume was considered to be half the beaker resolution, $u(Vol) = \pm 5 \times 10^{-6}\ m^3$. As it is in this case a uniform probability distribution, the standard uncertainty will be calculated as:

$$u_{cB}(Vol) = \frac{u}{\sqrt{3}} \tag{3.44}$$

The uncertainty for the time results on the experimental standard deviation of the average for an experience of 10 timings, considering the time lag after stopping the chronometer, calculated as:

$$u_{cA}(t) = t_{N-1,2.5\%} s(\bar{t}) \tag{3.45}$$

The density $\rho(T_{Out})$ was determined using a polynomial function of temperature $T_{f,OUT}$ (eq. 3.4). A maximum deviation of the polynomial of 0.02% was indicated for a rectangular probability distribution. Thus, a standard uncertainty will be obtained similarly to eq. 3.41:

$$u_{cB}(\rho) = \frac{0.02\rho}{100\sqrt{3}} \tag{3.46}$$

The different isolated uncertainties contributing to combined standard uncertainty of thermal efficiency ($u_c(\eta_{Th})$), in equation 3.31, and mass flow rate ($u_c(\dot{m})$), in equation 3.43, were presented through equations 3.34, 3.37, 3.39, 3.44, 3.45 and 3.46, and are summarized in Table 3.7.

Table 3.7 - Estimated uncertainties of the variables affecting determination of thermal efficiency

Xi	u(Xi)	Xi	u(Xi)
G	11%	c	0.012% (eq. 3.39)
$T_{f,IN}$	0.09 (eq. 3.34)	Vol	2.89×10^{-6} (eq. 3.44)
$T_{f,OUT}$	0.11 (eq. 3.34)	t	0.0475 (eq. 3.45)
A_{GC}	0.0004 (eq. 3.37)	ρ	0.012% (eq. 3.46)

The type B uncertainty of $\dot{m}$ ($u_{CB}(\dot{m})$) was determined through equation 3.43, using the results of the isolated uncertainties defined in equations 3.44 to 3.46.

After developing each term in eq. 3.31 and eq. 3.40, the maximum combined standard uncertainty, $u_c(\eta_{Th})$ was estimated for each case. The results are presented in Table 3.8. A continuous measurement of $\dot{m}$ would have contribute to a smaller error associated to the type A uncertainty of $\dot{m}$.

Table 3.8 - Contribution of the uncertainty determined for each variable to the thermal efficiency of the collector

	$\left(\frac{\partial \eta_{Th}}{\partial \dot{m}}\right)u(\dot{m})$	$\left(\frac{\partial \eta_{Th}}{\partial c}\right)u(c)$	$\left(\frac{\partial \eta_{Th}}{\partial T_{fOut}}\right)u(T_{fOut})$	$\left(\frac{\partial \eta_{Th}}{\partial T_{fIn}}\right)u(T_{fIn})$
PVT_1	1.16%	0.01%	1.05%	0.85%
PVT_2	0.32%	0.01%	1.05%	0.85%
PVT_3	0.28%	0.01%	1.00%	0.81%

	$\left(\frac{\partial \eta_{Th}}{\partial G}\right) u(G)$	$\left(\frac{\partial \eta_{Th}}{\partial A}\right) u(A)$	$u_{CB}(\eta_{Th})$
PVT$_1$	7.14%	0.04%	7.36%
PVT$_2$	6.97%	0.04%	7.11%
PVT$_3$	6.74%	0.04%	6.86%

It is clear that the radiation uncertainty parcel represents the main source of uncertainty. That high value is due mainly from the non-stability uncertainty, arising for the used pyranometer has not been recalibrated for a long period. If a recently calibrated pyranometer CM6B had been used, we would be talking of a typical uncertainty of 5% (information from the supplier). The final value for thermal efficiency uncertainty can be obtained, applying eq. 3.28. Table 3.9 presents the final results for $u_c(\eta_{Th})$, using the typical value for pyranometer uncertainty:

Table 3.9 - Thermal efficiency uncertainty

	$u_{cA}(\eta_{Th})$	$\left(\frac{\partial \eta_{Th}}{\partial G}\right) u(G)$	$u_{cB}(\eta_{Th})$	$u_c(\eta_{Th})$
PVT$_1$	2.54%	3.24%	3.77%	4.57%
PVT$_2$	2.86%	3.17%	3.46%	4.47%
PVT$_3$	2.47%	3.06%	3.33%	4.14%

A similar procedure for the calculation of the uncertainty of electrical efficiency, $u_c(\eta_{El})$, can be applied, addressing to eq. 2.15. It is necessary to calculate the type A and B components, $u_{cA}(\eta_{El})$ and $u_{cB}(\eta_{El})$, according to following equations:

$$u_c(\eta_{El}) = \sqrt{u_{cA}(\eta_{El})^2 + u_{cB}(\eta_{El})^2} \tag{3.47}$$

$$u_{cA}(\eta_{El}) = t_{N-1,95\%} u(\overline{\eta_{El}}) \tag{3.48}$$

$$u_{cB}(\eta_{El})^2 = \left(\frac{\partial \eta_{El}}{\partial I_{SC}}\right)^2 u^2(I_{SC}) + \left(\frac{\partial \eta_{El}}{\partial V_{OC}}\right)^2 u^2(V_{OC}) + \left(\frac{\partial \eta_{El}}{\partial FF}\right)^2 u^2(FF) + \left(\frac{\partial \eta_{El}}{\partial G}\right)^2 u^2(G) + \left(\frac{\partial \eta_{El}}{\partial A}\right)^2 u^2(A) \tag{3.49}$$

However, comparing the relative importance of both components (thermal and electrical) on the global efficiency, the value obtained through this exhaustive process would result in a residual value, compared to the one concerning the thermal component. Just for a matter of checking, the example for 3 modules will be presented, which is the one with a bigger impact on η_{El}, corresponding to the most probable significant independent variable, G in Table 3.10.

Table 3.10 - Illustrative example for electrical efficiency uncertainty

	$u_{cA}(\eta_{El})$	$\left(\frac{\partial \eta_{El}}{\partial G}\right) u(G)$	$u_c(\eta_{El})$
PVT$_3$	0.07%	0.38%	0.39%

According to this negligible contribution of the electrical component to the global efficiency uncertainty, just the uncertainty associated to the thermal efficiency will be considered, listed in Table 3.8.

3.4 Relevant aspects and findings of the experimental work

The experimental work exposed throughout this chapter is the end product of a process that has progressed, between successively surpassed downtimes and setbacks. A procedure of uncertainty analysis was applied to the experimental results, and it was determined that the most important contributor to the uncertainty of thermal efficiency was irradiance (G), as a result of the period since the last calibration of the pyranometer. The results of thermal efficiency are, thus, affected with an uncertainty of about 7% (see Table 3.8). The uncertainty associated to electrical efficiency values was of about 0.39% (see Table 3.10).

The tests were carried out for fluid inlet temperatures in the operational range from 25ºC – 60ºC. The environmental conditions corresponded to the registered values for T_{amb} and G for summer conditions, ranging globally from 19ºC-30ºC and 727 W/m^2 – 873 W/m^2, respectively. Those conditions resulted in a reduced temperature difference (T^*) ranging globally from 0.0036 Km^2/W – 0.0506 Km^2/W. The results of thermal, electrical, and combined efficiency were analysed, for 1, 2, and 3 PV modules applied over the absorber plate, corresponding to Pf of 0.24, 0.49 and 0.73, respectively.

It was verified that the addition of the PV modules caused a reduction in η_{Th}, and some details can be highlighted regarding the thermal component:

- ✓ the optical efficiency ($F'\eta_0$) decreases from typical values for flat plate selective solar collectors of 75% to 69% with Pf = 24%;
- ✓ the impact of Pf in $F'\eta_0$ is almost linear, and corresponds to a reduction of about 2% per 24% of Pf increase. This represents, on average, about 3% of the thermal efficiency.

- ✓ The thermal losses characterized by $F´U_L$ increase from typical values for flat plate selective solar collectors of 4 W/(m^{2}K) to 5.3 W/(m^{2}K) with Pf = 24% and 6.26 W/(m^{2}K) for Pf = 49%. This can be explained by the increased emissivity of PV cells, of 0.837, compared with the one of the absorber plate, of 0.2. It was not registered a significantly further increase for Pf = 73%. The effect of Pf in $F´U_L$ has still not been identified in existing experimental works, and constitutes a new finding for the PV/T characterization.

Regarding electrical efficiency of the tested PV/T prototype, it increased almost linearly with *Pf*, of about 2.5% per 24% of *Pf* increase, reaching maximum values of about 7.5% for Pf = 74% (see Figure 3.17). However, if electrical efficiency is calculated with respect to the real area of PV cells (η_{El}*), it is verified a slight decrease of about 0.35% in η_{El}* between PVT_1 and PVT_3 arrangements. This finding is of practical interest, when accessing the cost to benefit ratio of considering arrangements with different *Pf*. Further analysis will be addressed over this matter in chapter 5. Considering η_{El}* concept of efficiency, values of about 13.5% are reached for PVT_2 arrangement. Nevertheless, the results obtained for η_{El}* (see Figure 3.18) are lower than the reference ones of the PV modules, of 17.75% (Table 3.2). This can result from the followed procedure used for the estimation of $\dot{E}$, instead of using a MPPT to measure it directly, as discussed in subsection 3.1.5.

The results of combined efficiency (η_G) range approximately from 35% to 70% (see Figure 3.19). It was verified that the loss overall factor, represented by the slopes obtained through linear regression curves, increased with *Pf*, from 5.352 W/(m^{2}K) to 6.546 W/(m^{2}K) with *Pf* increase from 24% to 73%. So, globally, it was found that η_G decreases with *Pf*, mainly due to the losses increase. The benefit of PV/T lies, between other possible analyses, in the quality improve of the total output, resulting for better exergy efficiency of the electric power obtained.

Chapter 4.

Numerical model for the simulation of a hybrid solar collector

In this chapter, the mathematical model used for simulating the performance of a hybrid collector (thermal, electrical and combined) is presented. The model is a useful tool to the determination of the PV/T collector efficiency, under different operational conditions, and will be applied in the parametrical study that is carried out afterwards. The model takes into account the existing heat transfer mechanisms between the components of the collector model and the environment. Input variables are the solar radiation (G), external air temperature (T_{amb}) and fluid inlet temperature ($T_{f,IN}$). Steady-state, an even distribution in the water riser tubes and negligible dust effect were assumed.

First, the developed mathematical model is presented in detail. The heat transfer modes are adapted to the particular geometry of the experimentally tested collector, considering the specific construction of the photovoltaic modules. The resulting equations constitute a set of non-linear algebraic equations that were solved using iterative methods, using EES software (F-Chart software, 1975). This software, by being generic, allows flexibility of application, leaving to the user all the options for the construction of the model. The integration of energy fluxes analyses into the numerical model and the resulting system of equations allow the determination of the temperature distribution (in the collector

plate, in the PV cells, and in the fluid). Additionally, useful heat and power outputs are also calculated, in order to obtain the efficiency parameters of the hybrid collector.

The mathematical model is then validated, by quantifying the level of agreement with the experimental results obtained.

A parametric and systematic study on the performance of a generic photovoltaic/thermal collector is then carried out. The study focus on separated and combined effects of environmental and operational variables, with a special relevance for the ratio of area covered with PV cells and its preferred location. This analysis uses a simplified version of the previously developed mathematical model.

4.1 Mathematical model

The mathematical model was based on the specific geometry of the experimentally tested hybrid collector, presented in Figure 3.12. Details of a local cross-section of the assembly are represented in Figure 4.1. The model takes into account the existence of two layers of glass, between which the cells are encapsulated. This way, the energy fluxes that reach the cell will be affected by the optical properties of the glass, leading to higher energy losses, and a relatively complex model. The cell/EVA layer thickness is of 0.5 mm.

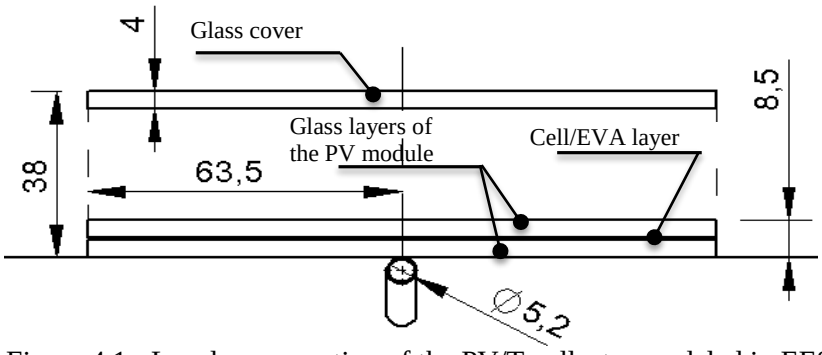

Figure 4.1 - Local cross-section of the PV/T collector modeled in EES

The thermal and optical characteristics used for modelling followed the data from the supplier, as listed in Table 4.1. The copper alloy used for the solar tubes and the absorber plate was C12200, containing a minimum of 99.9% copper, and so the values used for thermal conductivity k_T and k_P correspond to pure copper at 20 °C. The emissivity of the selective coating of the absorber was measured in the laboratory of Associação Rede Competência em Polímeros (Parque de Ciência e Tecnologia da Universidade do Porto, 2015), a company integrated in UPTEC.

Table 4.1 - Values of physical and optical properties for the collector prototype components used in the numerical model

Element	Material	Property
Glass Cover (Planilux Saint Gobain)	Tempered glass	Absorptivity α_{GC} = 0.07 Emissivity ε_{GC} = 0.89 Transmissivity τ_{GC} = 0.9
Absorber plate	Copper covered with selective coating	Absorptivity α_P = 0.93 Emissivity ε_P = 0.2 (tested) Thermal conductivity k_P = 387.6 W/mK
Tubes	Copper	Thermal conductivity k_T = 387.6 W/mK
Photovoltaic module (ONIX)	Glass	Absorptivity α_{MG} = 0.07 Transmissivity τ_{MG} = 0.839 Thermal conductivity k_{MG} = 1 W/mK
	Cells	Absorptivity α_C = 0.9 Thermal conductivity k_C = 0.5737 W/mK Emissivity ε_M = 0.837
	Characteristic values at T_{ref} = 25 °C:	η_{Elref} = 0.18, β_{ref} = 0.0045 K^{-1}

In order to favour the model explanation, first the heat transfer mechanisms regarding a thermal-only collector will be presented. This corresponds to the area of the hybrid collector with no cells applied.

4.1.1 Heat transfer mechanisms in a typical solar thermal collector

The development of such a mathematical model is always based on the identification of the heat transfer processes affecting a thermal system. The scheme presented in Figure 4.2 illustrates the existing heat transfer mechanisms between the various parts along the cross-section of a solar thermal collector.

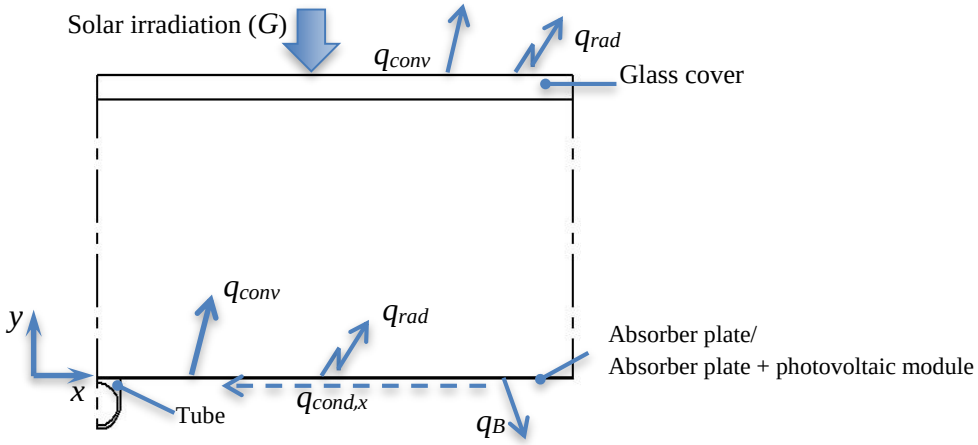

Figure 4.2 - Heat fluxes in a solar collector cross-section (half distance between tubes)

The detailed description of the each heat flux within the module will be presented later on sections 4.1.3 to 4.1.6. In Figure 4.2 the heat fluxes presented are:

G – solar irradiance incident on the collector;

q_{conv} – heat loss by convection;

q_{rad} – heat loss by radiation;

$q_{cond,x}$ – heat transferred by conduction along the cross-section of the plate, from the midplane to the tubes;

q_B – heat loss from the plate to the bottom side of the collector.

The water enters the solar collector through the tubes at a lower temperature ($T_{f,IN}$) than the absorber plate (T_P). The existence of the convective flow in the thermal fluid, at a lower temperature than the absorber plate, arouses a convergence of conductive thermal fluxes in the plate, along the two surface directions:

- q_{condx}, conductive heat fluxes in cross-sectional direction, x, from the midplane between two tubes towards the tubes (Figure 4.3 a) and b);

- q_{condz}, conductive heat fluxes along the direction of the flow, z, (Figure 4.3 b.).

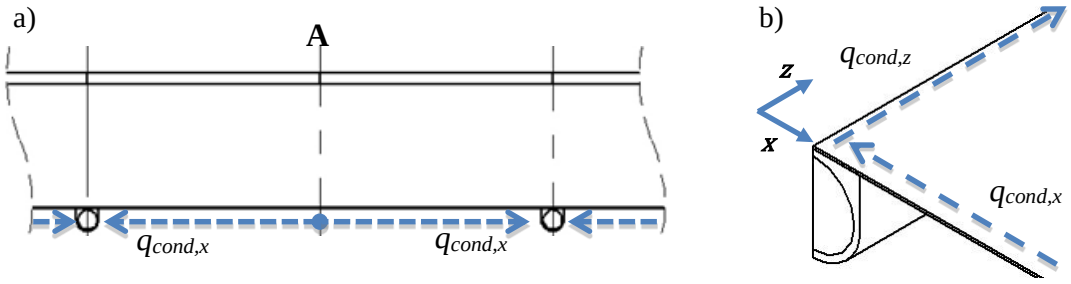

Figure 4.3 - Conductive heat fluxes in the absorber plate
a) Along transversal direction (x) b) along transversal (x) and longitudinal direction (z)

In order to consider the temperature variation on the plate along both the transversal and longitudinal directions, it is necessary to create a two-dimensional model. For such, in the mathematical model, the plate (plate/module) is divided into a number of elements, as shown in Figure 4.4: N_x elements along x and N_z elements along z. This discretization scheme does not apply to the glass cover, which is simply treated as one element. Note that the temperature variation along the plate thickness (y axis) will be disregarded, since the plate is very thin.

The following assumptions were made for the development of the mathematical model:

- all the surfaces, except the absorber plate, are treated as grey (optical properties are independent of the wavelength) and diffuse;

- the incident radiation on the surfaces is uniform (isotropic).

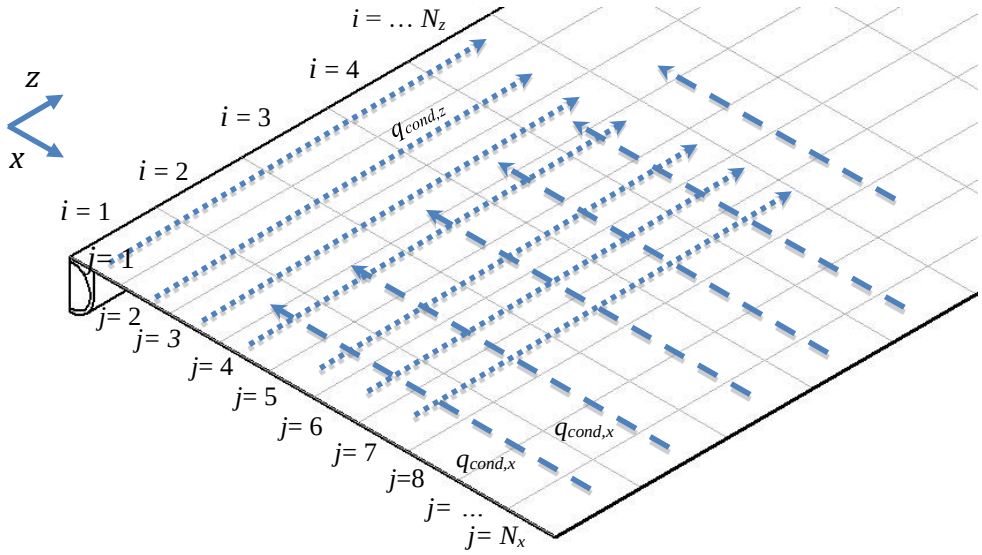

Figure 4.4 - Outline of conductive heat fluxes on the plate/photovoltaic module

4.1.2 Model simplifications: characteristic geometry

The symmetrical conductive heat fluxes through the *x* direction cause a maximum temperature location along the cross-section in the mid-distance between two tubes (plane A in Figure 4.3 a.) and a minimum temperature over the tubes, and so the modelled geometry consists only in half the cross-section between two consecutive tubes, as represented in Figure 4.2.

Conductive heat fluxes along the y axis for the glass cover, absorber plate and tube are neglected, since their thicknesses are small (4 mm, 0.8 and 0.15 mm, respectively) and their thermal conductivity is relatively high. The work by Smith (1986), cited by Zondag et al. (2002), confirms that modelling the temperature variation through the glass cover had no significant impact on the calculation of the thermal efficiency. It was found that the temperature difference between the fluid and the tube wall was the determinant factor. Thus, in the present model a constant temperature through the thickness of the glass, plate and tube is considered.

4.1.3 Thermal balance over the glass cover

The different types of heat transfer on the glass cover are presented in Figure 4.5. The glass cover receives heat from the exterior, through solar radiation (G), and from the module and plate, through convection ($q_{conv(P+M)/GC}$). It also releases heat to the environment by radiation ($q_{rad\text{-}amb}$) and convection ($q_{conv\text{-}amb}$). The radiative fluxe to the glass cover was treated differently whether it was coming from the absorber plate ($q_{rad\text{-}P/GC}$) or the PV module ($q_{rad\text{-}M/GC}$), since the optical properties and temperatures are different.

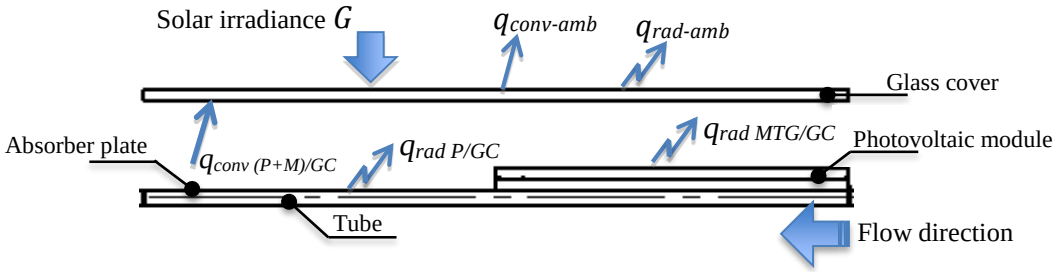

Figure 4.5 - Glass cover heat fluxes

The heat balance equation for the glass cover can be written as:

$$q_{rad-abs} + q_{radP/GC} + q_{radMTG/GC} + q_{conv(P+M)/GC} = q_{conv-amb} + q_{rad-amb} \quad (4.1)$$

For the development of the balance equation (eq. 4.1) it was considered that the glass cover, module top glass and absorber plate have uniform temperatures, T_{GC}, T_{MTG} and T_P, respectively, taken as their average temperatures. Each term in equation 4.1 is defined next, through equations 4.3 to 4.13.

i. Absorbed heat through radiation, $q_{rad\text{-}abs}$

The total solar radiation G, results from the direct, or beam (G_b), and diffuse (G_d) radiation as:

$$G = G_b + G_d \quad (4.2)$$

From the incident solar radiation on the glass cover, one fraction is absorbed (α_{GC}), another is reflected (ρ_{GC}) and the rest is transmitted (τ_{GC}). The heat gain of the glass in eq. 4.1 is defined as:

$$q_{rad-abs} = \alpha_{GC} G \quad (4.3)$$

ii. Heat loss to the ambient by convection, $q_{conv\text{-}amb}$

The convective heat transferred between the glass surface and the ambient air ($q_{conv-amb}$ in eq. 4.1) represents a portion of the thermal losses to the environment. It is characterized by the heat transfer coefficient (h_W), as:

$$q_{conv-amb} = h_W(T_{GC} - T_{amb}) \tag{4.4}$$

There are many correlations for the estimation of h_W (Duffie, 1991), depending on the specific application. Watmuff et al. (1977) cited by Duffie (1991), reported a correlation that is most suitable for this case, directly dependent on the wind speed, V, as:

$$h_W = 2.8 + 3.0\,V \tag{4.5}$$

This equation was developed for a flat plate with characteristic length (L) of 0.5 m, according to:

$$L = \frac{4A_{GC}}{P_{GC}} \tag{4.6}$$

In Eq.4.6 A_{GC} is the glass cover surface area and P_{GC} is its perimeter.

iii. Radiation heat flux from the glass cover to the environment, $q_{rad\text{-}amb}$

The glass cover emits radiation to the environment, corresponding to the parcel $q_{rad-amb}$ in eq. 4.1, according to the following equation:

$$q_{rad-amb} = \sigma\varepsilon_{GC}\left({T_{GC}}^4 - {T_{amb}}^4\right) \tag{4.7}$$

This equation takes into account the approximation of the sky temperature to ambient temperature, $T_{amb,}$ since sky temperature does not have great influence on the top heat loss (Duffie, 1991).

iv. Radiation between glass cover and absorber plate ($q_{rad\ P/GC}$)/PV module top glass ($q_{radMTG/GC}$)

These radiation heat fluxes, in equation 4.1, can be obtained from the radiation equation between two infinite parallel plates (Holman, 1989), resulting in:

$$q_{rad\ P/GC} = \frac{\sigma(\overline{T_P}^4 - {T_{GC}}^4)}{\frac{1}{\varepsilon_{GC}} + \frac{1}{\varepsilon_P} - 1} \tag{4.8}$$

$$q_{rad\ MTG/GC} = \frac{\sigma(\overline{T_{MTG}}^4 - {T_{GC}}^4)}{\frac{1}{\varepsilon_{GC}} + \frac{1}{\varepsilon_{MG}} - 1} \tag{4.9}$$

In Eq. 4.8 and 4.9, temperatures, $\overline{T_P}$, and $\overline{T_{MTG}}$, were taken as averages of the "local" temperatures $T_{P(i,j)}$ and $T_{MTG(i,j)}$ determined for each element *(i,j)* as:

$$\overline{T_P} = \frac{\sum_{i=1}^{Nz,P} \sum_{j=1}^{Nx} A_{i,j}\, T_{P\,i,j}}{A_P} \tag{4.10}$$

$$\overline{T_{MTG}} = \frac{\sum_{i=1}^{Nz,M} \sum_{j=1}^{Nx} A_{i,j}\, T_{MTG\,i,j}}{A_M} \tag{4.11}$$

A_M and A_P in eq. 4.11 are the areas of the module and the plate with no module applied, respectively.

v. Convection between glass cover and plate/PV module, $q_{conv-(P+M)/GC}$

The temperature difference between the set "absorber plate/PV module" and the glass cover results in a natural convection heat transfer, considered in eq. 4.1, which can be estimated by:

$$q_{conv(P+M)/GC} = h_{(P+M)/GC}(\overline{T_{(P+MTG)}} - T_{GC}) \tag{4.12}$$

In Eq.4.12 it is assumed that the temperature on the absorber surface and the PV module top glass are represented by an average value, given by:

$$\overline{T_{(P+MTG)}} = \frac{\overline{T_{MTG}}\, A_M + \overline{T_P}\, A_P}{A_M + A_P} \tag{4.13}$$

The heat transfer coefficient ($h_{(P+M)/GC}$) can be obtained, through the determination of the *Nu* number in eq. 4.14, from empirical correlations for natural convection in confined spaces, composed of two infinite parallel plates at a distance δ heated from below. It was used for the model a pre-defined function available on EES. This function is based on the calculation of the *Nu* number as a fraction of *Ra* number and the tilt angle of the surface (β), as Duffie (1991), for tilt angles between 0º and 75º, expressed in eq. 4.15. The *Ra* number is defined in eq. 4.16.

$$Nu = \frac{h_{(P+MTG)/GC}\,\delta}{k_f} \tag{4.14}$$

$$Nu = 1 + 1{,}44\left[1 - \frac{1708(sin1{,}8\beta)^{1,6}}{Ra\ cos\beta}\right]\left[1 - \frac{1708}{Ra\ cos\beta}\right]^{+} + \left[\left(\frac{Ra\ cos\beta}{5830}\right)^{1/3} - 1\right]^{+} \tag{4.15}$$

$$Ra = \frac{g\beta'\left(\overline{T_{(P+MTG)}} - T_{GC}\right)\delta^3}{\nu\alpha} \tag{4.16}$$

In eq. 4.16, β' is the coefficient of volumetric expansion and α is the thermal diffusivity of the fluid, defined as follows:

$$\beta' = \frac{1}{\frac{(\overline{T_{(P+MTG)}} + T_{GC})}{2}} \tag{4.17}$$

$$\alpha = \frac{k_f}{\rho_f c_f} \tag{4.18}$$

Beyond a critical value of the temperature difference between the two surfaces, corresponding to a Rayleigh number Ra = 1708, bi-dimensional circulation eddies begin to form. These eddies become three dimensional with the increase in Ra, ending, at some point, in the transition to turbulent flow regime. It should be noted that the formulation exposed above represent, however, an approximation, since it is not dealing with infinite plates. Nevertheless, it is an acceptable assumption since δ/L = 0.04.

4.1.4 Heat balance equations on the photovoltaic module

In order to develop a mathematical model for the heat fluxes within the PV module, it is necessary to consider the following components: (1) top glass, (2) PV cell encapsulated with EVA and (3) bottom glass.

The conductive fluxes along *x* and *z* that were mentioned for a simple thermal collector also have to be considered when the PV module is added. Thus, the discretization scheme represented for the absorber plate of a thermal collector in Figure 4.4 is also valid for each component of the PV module. Thus, the temperature of each component is indexed to the specific "location" *(i,j).* The main heat fluxes existing in the PV module are represented in Figure 4.6. No discretization was applied along the *y* direction, within each component. However, there is a gradient of temperature between the cell and the surfaces of the top and bottom glass, resulting on conductive fluxes from the cell, upward and downward, along the *y* direction ($q_{cond\ Cell/MTG}$ and $q_{cond\ Cell/MBG}$ in Figure 4.6).

In this subsection the balance equations for each component of the PV module will be detailed, leading then to the determination of the temperature distributions for all the discretized elements T_{MTG} *(i,j)*, T_{Cell} *(i,j)* and T_{MBG} *(i,j)*. However, it is necessary to apply proper boundary conditions to solve the system of equations. The boundary conditions are:

- ✓ Symmetry at the mid plane: $\frac{dT}{dx}|_{x = Lfin/2} = 0$;
- ✓ Zero conductive heat flux along *x* for *x*=0: $q_{cond,x} = 0$;
- ✓ Zero conductive heat flux along z for *z*=0 and *z*=*L*: $q_{cond,z} = 0$;

- ✓ Temperature of the tube is the same as the plate (where no PV module is applied): $T_T|_{x=0} = T_P$;
- ✓ Temperature of the tube is the same as the bottom module glass (where PV module is applied): $T_{Tx=0} = T_{MBG}$.

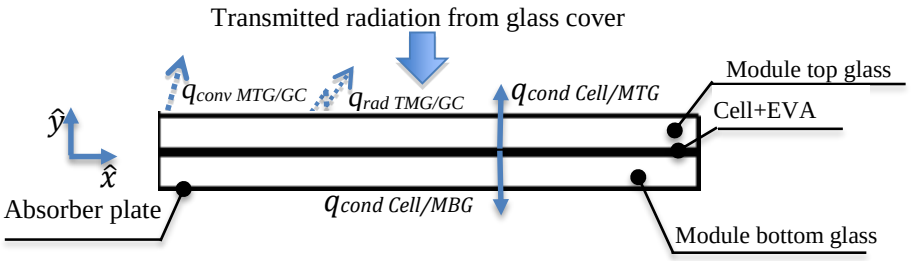

Figure 4.6 - Main heat fluxes in the photovoltaic module (except transversal q_{condx} and axial q_{condz} conductive fluxes)

In the boundary conditions just presented L_{fin} is the distance between two tubes and T_T is the temperature of the tube.

The thermal balance equations applied to each element of the PV module will then be presented.

i. Module top glass

As already accounted before, the photovoltaic module transfers heat to the glass cover by convection and radiation (see Figure 4.5 and eq. 4.12) through its top glass (see Figure 4.6), The general balance equation can be written as:

$$q_{rad-abs,MTG} + q_{condCell/MTG}\ (+q_{condxMTG} + q_{condzMTG}) = q_{convMTG/GC} + q_{radMTG/GC}\ (+q_{condxMTG} + q_{condzMTG}) \quad (4.19)$$

This equation was applied for each element *(i,j)*, after discretization of the complete domain. For the elements on the boundaries (x=0, x=L_{fin}/2, z=0, z=L) some of the terms corresponding to conductive fluxes are null, according to the boundary conditions. Those fluxes, when present, are calculated by the following equations:

$$q_{condx,MTG} = \frac{k_{MG}}{L_x}\left(T_{MTG\ i,j} - T_{MTGi,j-1}\right) \quad (4.20)$$

$$q_{condz,MTG} = \frac{k_{MG}}{L_{z,M}}\left(T_{MTG\ i,j} - T_{MTGi+1,j}\right) \quad (4.21)$$

L_x and $L_{z,M}$ in eqs 4.20 and 4.21 represent the dimensions of each discretized element (i,j) of the PV module along x and z, respectively.

The convective and radiative fluxes to the glass cover, respectively $q_{convMTG/GC}$ and $q_{radMTG/GC}$ in Figure 4.6, are equivalent to those stated in equations 4.8 and 4.9, but are now applied for each element *(i,j),* with temperature $T_{MTG\,i,j}$:

$$q_{conv\,MTG/GC} = h_{(P+M)/GC}(T_{MTG\,i,j} - T_{GC}) \tag{4.22}$$

$$q_{rad\,MTG/GC} = \frac{\sigma({T_{MTG\,i,j}}^4 - {T_{GC}}^4)}{\frac{1}{\varepsilon_{GC}} + \frac{1}{\varepsilon_{MG}} - 1} \tag{4.23}$$

From the total incident solar radiation, the top module glass absorbs the fraction determined by the transmissivity of glass cover and its absorption coefficient ($\tau_{GC}\ \alpha_{MTG}$). The successive reflections and absorptions existing between the glass cover and a surface bellow, results in the following approximation for most practical solar collectors (Duffie, 1991):

$$(\tau\alpha) \equiv 1.01\ \tau_{GC}\alpha_{MTG} \tag{4.24}$$

The diffuse component of the solar radiation incident on the top glass of the module must be treated differently, since the values of the absorption and transmission coefficients depend on the angle of incidence (Duffie, 1991). Considering an isotropic incident radiation, and integrating the radiation transmitted in all directions, one could define an incidence equivalent angle such that the direct radiation would result in the same transmittance that the diffuse radiation. For horizontally placed collectors, this angle is equivalent to 60° (Duffie, 1991).

The absorptivity and transmissivity depend on the angle of incidence of the incident radiation. (Duffie, 1991) also presents curves for determining $(\tau\alpha)$ as a function of incidence angle, relative to the normal incidence, $(\tau\alpha)/(\tau\alpha)_n$. For the equivalent angle of 60º for diffuse radiation:

$$\frac{(\tau\alpha)_d}{(\tau\alpha)_n} = 0.9 \tag{4.25}$$

Therefore, the absorbed radiation flux to consider is given by the following equation:

$$q_{rad-abs,MTG} = (\tau_{GC}\alpha_{MTG}G_b + 0{,}9\tau_{GC}\alpha_{MTG}G_d)1.01 \tag{4.26}$$

The temperature differences between the three elements of the module imply conductive fluxes along the y axis, leading to the referred fluxes from the cell ($q_{cond\ Cell/MTG}$ and $q_{cond\ Cell/MBG}$ in Figure 4.6). The flux concerning the top glass of the module can be quantified as:

$$q_{condCell/MTG} = \frac{k_{MG}}{\delta_{MG}}\left(T_{Cell\,i,j} - T_{MTG\,i,j}\right) \tag{4.27}$$

In the latter equation δ_{MG} represents the thickness of the module glass.

ii. Cell+EVA layer

The cell layer receives the radiation transmitted by the top glass of the module, as represented in Figure 4.7. This absorbed radiation will contribute to the electric and thermal gains of the cell. By the obstruction caused and the deduction of the electrical gain, there is a reduction to the heat transferred to the absorber plate and thermal fluid.

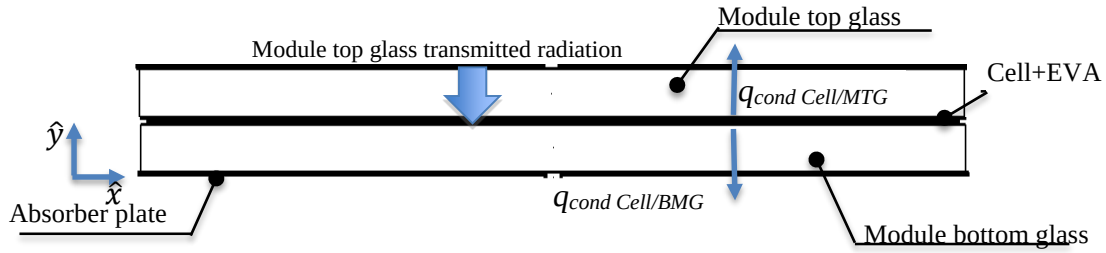

Figure 4.7: Main heat fluxes in the cell layer
(except transversal q_{condx} and axial q_{condz} conductive fluxes)

Thus, the electric flux generated is given by:

$$e = (\,G_b + 0.9G_d)\tau_{GC}\,\tau_{TMG}\alpha_{Cell}\,1.01\,\eta_{El\,i,j} \tag{4.28}$$

The heat gain by radiation is estimated from:

$$q_{rad} = (\,G_b + 0.9G_d)\tau_{GC}\,\tau_{MTG}\alpha_{Cell}\,1.01\,(1 - \eta_{El\,i,j}) \tag{4.29}$$

The electrical efficiency (η_{El}) reduces linearly with the increase of the cell temperature, according to eq 2.13.

The parameters were provided by the cell manufacturer, as presented in Table 4.1.

Since the cell electrical efficiency depends on $T_{Cell,(i,j)}$, it varies along the layer Cell/EVA. Total electrical gain can be calculated from:

$$\dot{E} = \sum_{i=1}^{Nz,M}\sum_{j=1}^{Nx}\eta_{El\,i,j}\,(\,G_b + 0.9G_d)\tau_{GC}\,\tau_{MTG}\alpha_{Cell}\,1.01L_xL_{zM} \tag{4.30}$$

The energy balance fluxes in the cell layer is:

$$e + q_{rad}\,(+q_{condxCell} + q_{condzCell}) = q_{condCell/MTG} + q_{condCell/MBG}(+q_{condxCell} + q_{condzCell}) \tag{4.31}$$

As mentioned before in section 4.1.2, the temperature variation along the absorber plate below the PV module glass was not considered, since the plate is very thin and has a

high thermal conductivity. Instead, an equivalent thermal conductivity k_{eq1} is calculated for the set *bottom module glass/plate*:

$$\frac{\delta_{MBG} + \delta_P}{k_{eq1}} = \frac{\delta_{MBG}}{k_{MG}} + \frac{\delta_P}{k_P} \tag{4.32}$$

The conductive heat flux from the cell to the bottom glass of the module is given by:

$$q_{condCell/BMG} = \frac{k_{eq1}}{\delta_{MG}} \left(T_{Cell\ i,j} - T_{BMG\ i,j}\right) \tag{4.33}$$

The conductive fluxes will be considered all, or not, by applying the boundary conditions. Each parcel is calculated as:

$$q_{condx,Cell} = \frac{k_{Cell}}{L_x} \left(T_{Cell\ i,j} - T_{Cell\ i,j-1}\right) \tag{4.34}$$

$$q_{condz,Cell} = \frac{k_{Cell}}{L_{z,M}} \left(T_{Cell\ i,j} - T_{Cell\ i+1,j}\right) \tag{4.35}$$

iii. Bottom glass of the module

This component exchanges heat by conduction with the PV cell, and loses heat to the insulation along *x* and *z* directions (Figure 4.8), resulting in eq. 4.36.

$$q_{condCell/MBG}\ (+q_{condxMBG} + q_{condzMBG}) = q_{B,M}\ (+q_{condxMBG} + q_{condzMBG}) \tag{4.36}$$

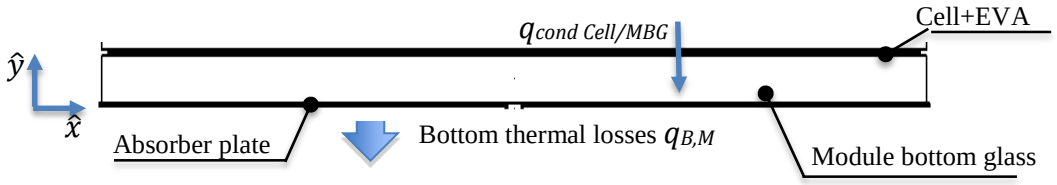

Figure 4.8 - Main heat fluxes in the bottom glass of PV module
(except transversal q_{condx} and axial q_{condz} conductive fluxes)

The thermal losses through the lower surface ($q_{B,M}$), combine conductive flux through insulation and aluminium structure, and convective/radiative loss to the exterior. The radiative flux is usually neglected (Duffie, 1991), given its insignificant contribution to the heat balance. As referred in section 3.2.2, a plywood plate was applied under the absorber plate. The impact of considering this additional resistance on the bottom thermal losses was also evaluated, to understand its significance.

The series resistance, using the electrical circuit analogy, is obtained with eq. 4.37, considering 1 cm of plywood plate, 3 cm of rock wool, 1 mm for the aluminium structural back plate, and an exterior convection coefficient of 10 W/m^{2}K.

$$R_{eq} = \frac{\delta_{Plywood}}{k_{Plywood}} + \frac{\delta_{Ins}}{k_{Ins}} + \frac{\delta_{St}}{k_{St}} + \frac{1}{h_{amb}} \tag{4.37}$$

The heat flux $q_{B,M}$ is treated as a convective heat flux, and is calculated by:

$$q_{B,M} = \frac{(T_{MBG\ i,j} - T_{amb})}{R_{eq}} \tag{4.38}$$

The equivalent global heat transfer coefficient will round ≈ 1 W/m^{2}K, so it can be neglected in the model.

With respect to conductive fluxes along the bottom glass of the module, *x* and *z* directions, it is necessary to account for the dependence on the plate thermal conductivity, because it has a significant impact. In one discretized element, the plate thermal conduction (k_P = 387.6 W/mK) affects 0.15mm, corresponding to the thickness of the plate, compared to the thermal conductivity of the glass (k_{MG}= 1 W/mK), applied to a 4 mm thickness. To find the equivalent conductivities for the total thickness of the element, the following equations are expressed for *x* and *y* direct:

$$\hat{x}\colon \frac{k_{eqx}}{L_x}(\delta_{MBG} + \delta_P)L_{zM} = \frac{k_{MBG}}{L_x}\delta_{BMG}L_{zM} + \frac{k_P}{L_x}\delta_P L_{zM} \tag{4.39}$$

$$\hat{z}\colon \frac{k_{eqz}}{L_{zM}}(\delta_{MBG} + \delta_P)L_x = \frac{k_{BMG}}{L_{zCell}}\delta_{MBG}L_x + \frac{k_P}{L_{zCell}}\delta_P L_x \tag{4.40}$$

Solving 4.39 and 4.40 for k_{eq} will result in the same expression for this equivalent thermal conductivity:

$$k_{eqx} = k_{eqz} = \frac{k_{MBG}\delta_{MBG} + k_P\delta_P}{(\delta_{MBG} + \delta_P)} \tag{4.41}$$

The conductive heat fluxes can then be written as:

$$q_{condx,BMG} = \frac{k_{eqx}}{L_x}\left(T_{MBG\ i,j} - T_{BMG\ i,j-1}\right) \tag{4.42}$$

$$q_{condz,BMG} = \frac{k_{eqz}}{L_{z,M}}\left(T_{MBG\ i,j} - T_{BMG\ i+1,j}\right) \tag{4.43}$$

To conclude the presentation of the heat fluxes in the bottom glass of the PV module, it should be mentioned that, for the elements at the left boundary (*x =0*), that are in contact with the collector tube, an additional term in the balance equation should be added, representing half of the heat transferred to the fluid, on that element (*i,j*). This will be discussed in more detail in section 4.1.6.

4.1.5 Thermal balance on the absorber plate

The analysis regarding the absorber plate, for the part of the hybrid collector not covered by the photovoltaic module is slightly simpler. Some of the concepts already presented for the photovoltaic module will be adapted. For the schematic representation of the heat transfer mechanisms, the reader is referred to Figure 4.2.

As for the module, the collector area is divided into a number of elements, N_x and N_{ZP} in the x and z directions, respectively, resulting in a system of equations, that should be simultaneously solved for $T_{P(i,j)}$.

Applying the energy balance for the absorber plate gives:

$$q_{rad-abs,P}\ (+q_{condxP} + q_{condzP}) = q_{convP/GC} + q_{radP/GC}\ + q_B\ (+q_{condxP} + q_{condzP}) \tag{4.44}$$

The equations for each term were already presented for the photovoltaic module, for what they will only be adapted, using the physical properties for the absorber plate:

$$q_{rad-abs,P} = (\tau_{GC}\alpha_P G_b + 0.9\tau_{GC}\alpha_P G_d)1.01 \tag{4.45}$$

$$q_{convP/GC} = h_{(P+M)/GC}(T_{P\,i,j} - T_{GC}) \tag{4.46}$$

$$q_{rad\,P/CG} = \frac{\sigma({T_{P\,i,j}}^4 - {T_{GC}}^4)}{\frac{1}{\varepsilon_{GC}} + \frac{1}{\varepsilon_P} - 1} \tag{4.47}$$

$$q_{B,P} = h_{eqB,P}(T_{P\,i,j} - T_{amb}) \tag{4.48}$$

Once again, the heat conduction along x and z axis can be approximated by:

$$q_{condx,P} = \frac{k_P}{L_x}\left(T_{P\,i,j} - T_{P\,i,j-1}\right) \tag{4.49}$$

$$q_{condz,P} = \frac{k_P}{L_{z,P}}\left(T_{P\,i,j} - T_{P\,i+1,j}\right) \tag{4.50}$$

Similarly as for the bottom glass of the PV module, an additional term in the balance equation has to be accounted for the elements in the left boundary ($j = 1$) that are in contact with the tube, representing half of the heat transferred to the fluid. This will be presented in more detail in section 4.1.6.

For the boundary elements that form the transition interface between the bottom glass of the PV module and the plate, the conductive fluxes along z were derived from equations 4.36 and 4.44 to obtain:

$$q_{condz,MBG\ NzM,j} = \frac{k_P}{L_{z,M}/2}\left(T_{MBG\ NzM,j} - T_{P\ 1,j}\right) \quad (4.51)$$

$$q_{condz,P\ 1,j} = \frac{k_P}{L_{z,M}/2}\left(T_{MBG\ NzM,j} - T_{P\ 1,j}\right) \quad (4.52)$$

4.1.6 Convection heat transfer along the fluid flow in the collector tubes

The main objective of applying solar thermal collectors is to heat a thermal fluid circulating in the tubes with the absorbed solar radiation incident on the plate. Thus, for each element on the left boundary (*j =1*), an additional heat parcel has to be considered, in equations 4.36 for the bottom module glass elements ($q_{T,Mi}$), and in eq. 4.44, for the absorber plate elements, respectively. q_{Ti} represents the heat that is transferred to the fluid through the tube, by a convection mechanism. The formulation of the equations for this term, for the bottom glass of the PV module and the absorber plate, are:

$$q_{T,M\ i} = \frac{\dot{Q}_{T,M\ i}}{L_{zM}L_{xM}} \quad (4.53)$$

$$\dot{Q}_{T\,M\ i} = h_{f\ i}\left(T_{BMG\ \ i,1} - \overline{T_{f,\imath}}\right)(2\pi r)L_{zM} \quad (4.54)$$

$$q_{T,P\ i} = \frac{\dot{Q}_{T,P\ i}}{L_{zP}L_{xP}} \quad (4.55)$$

$$\dot{Q}_{T\,P\ i} = h_{fi}\left(T_{P\ i,1} - \overline{T_{f,\imath}}\right)(2\pi r)L_{zP} \quad (4.56)$$

In order to estimate the local average water temperature ($T_{f,i}$) in equations 4.54 and 4.56, the following approximation was applied:

$$\overline{T_{f,\imath}} = \frac{T_{f\ i} + T_{f\ i-1}}{2} \quad (4.57)$$

The heat fluxes through the tubes leads to temperature rise along the flow path:

$$\dot{Q}_{T_i} = \dot{m}\ c_f(T_{f\ i} - T_{f\ i-1}) \quad (4.58)$$

The resulting system of equations can be solved after providing the inlet temperature of water, which is an input variable.

The internal convection coefficient depends largely on the flow regime (Re), that is usually laminar in solar collector applications, and on the thermal boundary condition. The thermal boundary condition for a solar collector can be understood as a constant resistance between the flowing fluid and the surroundings at a constant temperature. Constant heat flux or constant wall temperature conditions can be assumed. It is recommended a constant-

wall-temperature assumption for the boundary, since it yields lower heat transfer coefficients than a constant heat flux condition (Duffie, 1991). For fully developed laminar flow, thermally and dynamically, and for isothermal wall condition, the *Nusselt* number is constant and takes a value of 3.66 (Bejan, 1993). From the *Nusselt* number it is possible to determine the convection coefficient by expression 4.14. For non-developed flow conditions, Rohsenow (1961), cited by Duffie (1991), presents a graph for the dependence of Nu on the dimensionless group $Re\ Pr\ Dh/L$, as shown in Figure 4.9.

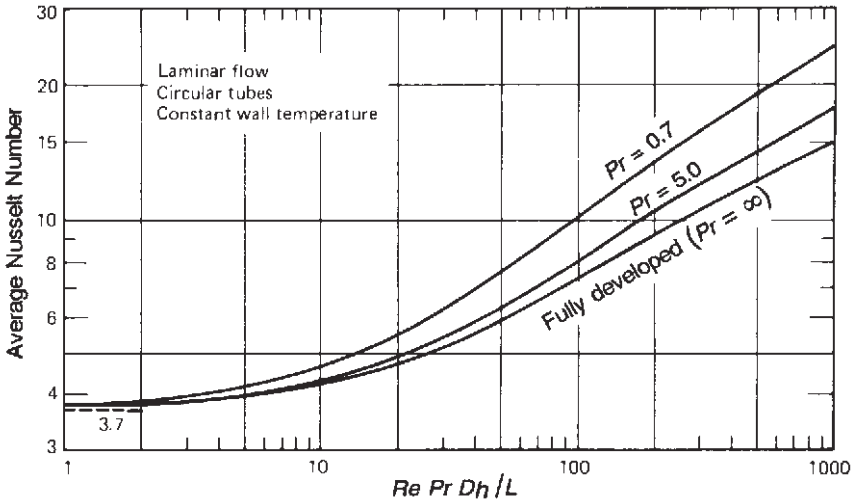

Figure 4.9 - Average Nusselt numbers in short tubes for various Prandtl numbers (Duffie, 1991)

The *Prandtl* number is given by:

$$Pr = \frac{\nu_f}{\alpha_f} \tag{4.59}$$

where ν_f and α_f are the kinematic viscosity and thermal diffusivity of the fluid, respectively.

The EES program, used to solve the system of equations, treated the determination of the convection transfer coefficient for each element ($h_{f,i}$) in a dedicated subroutine.

4.1.7 Model verification

Before validation, a verification process accompanied the development of the model, by monitoring some results. Verification is the process of determining that a model implementation accurately represents the developer's conceptual description of the model and its solution (Thacker *et al.*, 2004). The following expected aspects were checked:

- ✓ The average temperature in the plate was higher than the one in the cells;

- ✓ In the photovoltaic module elements, the higher temperature was always verified in the cell;
- ✓ The temperature increases, for each part, along *x* and *z* directions.

After assuring, on a first phase, that the model confirms those prerequisites, the validation with the experimental results can be carried out.

4.2 Validation of the developed model with experimental results

Model validation is essential for assuring a significant level of confidence and predictive accuracy of the mathematical model, providing evidence that it is sufficiently accurate for its intended use. Validation is the process of determining the degree to which a model is an accurate representation of the real world from the perspective of the intended uses of the model (Thacker *et al.*, 2004).

The experimental results are used for the validation procedure that is presented throughout this section. The validation assessment is applied to the values of the thermal, electrical and combined efficiencies, for all the tested conditions selected in section 3.3 concerning the application of 1, 2, and 3 PV modules. Variables that were not measured during the tests, as wind speed (eq. 4.5), and the distinction between the values of diffuse and beam radiation (equations 4.26, 4.28 to 4.30 and 4.45), are consulted from climate data of TRNSYS for Porto, for the testing periods. The incidence angleThe total process of validation for one PV module applied is taken for example, and then the analysis for all the tests is summarized.

4.2.1 Comparison of numerical and experimental results for efficiencies, with one PV module applied

Taking for example the case with one module applied, Figure 4.10 and Figure 4.11 include comparative results for thermal and electrical efficiencies. The observation shows a generally good agreement between both results.

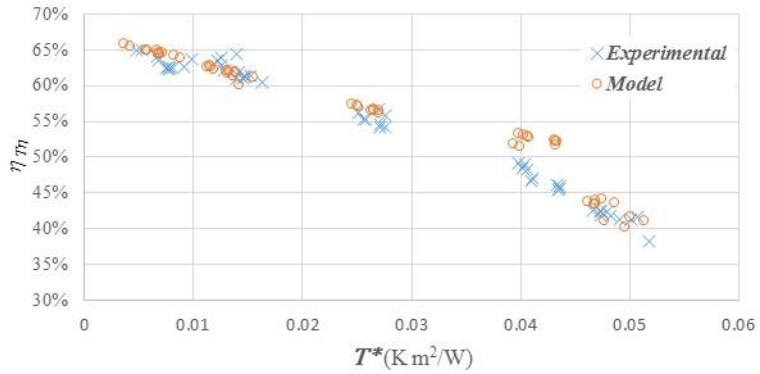

Figure 4.10 - Comparison of model and experimental values of thermal efficiency, with one PV module applied

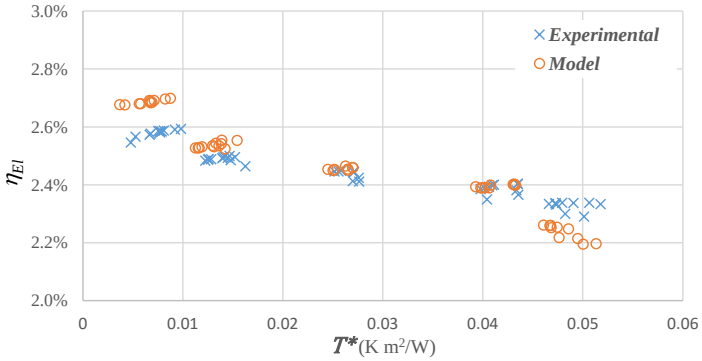

Figure 4.11 - Comparison of model and experimental values of electrical efficiency, with 1 PV module applied

For the same configuration, with one PV module applied (PVT_1), the degree of agreement for the results of thermal and electrical efficiencies was evaluated, through the determination of the linear regression parameters. Figure 4.12 and Figure 4.13 present the comparison for model efficiencies (thermal and electrical), relative to experimental values. The "*ideal*" named case represents an ideal fit, with slope = 1. Similar analysis was extended to the results obtained with 2 and 3 PV modules applied, for thermal, electrical, and combined efficiencies.

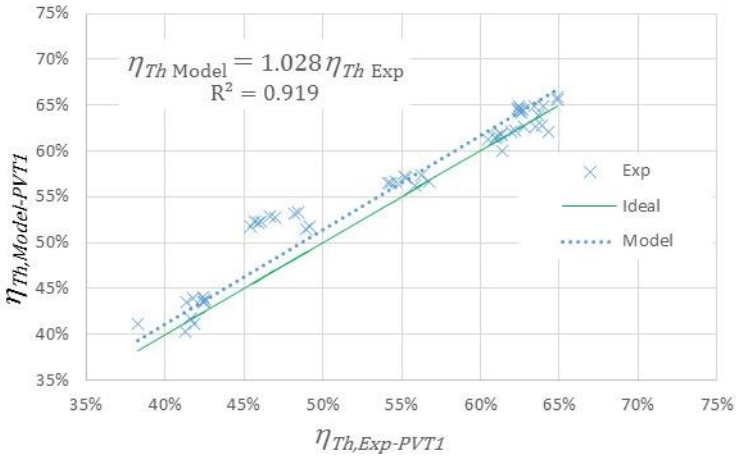

Figure 4.12 - Agreement between model and experimental thermal efficiencies, with 1 PV module applied

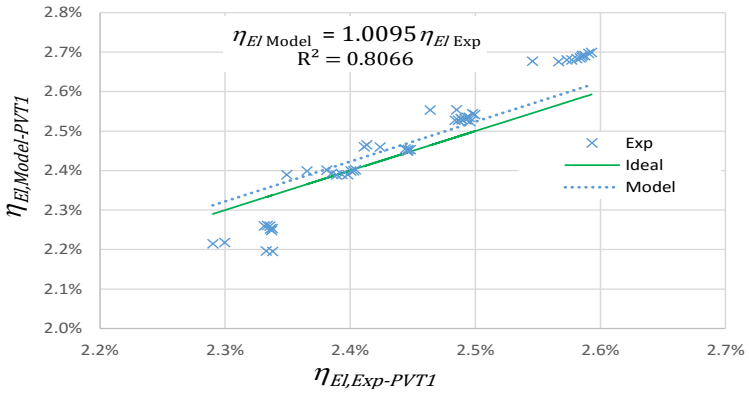

Figure 4.13 - Agreement between model and experimental electrical efficiencies, with one PV module applied

4.2.2 Statistical analysis for a validation assessment

A similar analysis was extended to the results obtained with 2 and 3 PV modules, for thermal, electrical, and combined efficiencies. For a more exhaustive validation of the agreement between the model and experimental results, a statistical analysis was applied. Based on the regression lines obtained for all the tested conditions, similarly to the procedure presented in section 4.2.1, statistical tests were applied to the slope values that have been determined. Confidence intervals were then estimated with 95% confidence level, and are listed in Table 4.2.

Table 4.2 – Confidence intervals for regression lines slopes, with 95% confidence level, for validation of results of thermal, electrical and combined efficiencies

N. PV modules	***η_{Th}, slope***	***Low limit***	***High limit***	***η_{El}, slope***	***Low limit***	***High limit***	***η_{G}, slope***	***Low limit***	***High limit***
1	1.028	1.017	1.040	1.009	1.002	1.017	1.028	1.017	1.039
2	1.007	0.984	1.030	1.013	1.003	1.023	1.008	0.987	1.029
3	0.932	0.922	0.941	1.035	1.030	1.041	0.946	0.937	0.954

It is confirmed that the confidence interval includes unity, or is very near, namely for one and two modules applied. In case of three photovoltaic modules, the values for thermal efficiency present a higher deviation. In this case, the area with only thermal gains is small, and the temperature rise in the fluid is also lower, and so, there is a higher probability of experimental reading values presenting a higher error.

Considering the level of approximation achieved, this model can be used as a reference, representing the thermal and electrical behaviour a PV/T collector with reasonably high accuracy.

4.3 Parametric analysis of the performance of an hybrid PV/T collector

In this section, it is intended to evaluate the effect of some selected environmental variables and operating conditions on the performance of the hybrid PV/Thermal collector, besides quantifying the effect of PV cell area (packing factor). The impact of the packing factor (P_f), fluid inlet temperature ($T_{f,In}$), irradiation level (G) and ambient temperature (T_{amb}) on the thermal (η_{Th}), electrical (η_{El}) and overall (η_G) efficiency is characterized, through an extensive and systematic analysis. The parametric study will focus on the preferred positioning for the PV cells, by comparing the differences between applying cells at collector inlet or collector outlet. This study can be further used to support a study for optimizing the extent of the application of PV cells, or other constructive practical options for an hybrid PV/T collector.

The installation of photovoltaic cells over the absorber plate causes a reduction of the heat gain of the thermal fluid. In general, this loss is not compensated by the electrical gain, since the electrical efficiency of the cells is around 15% (relatively to the area of the cells applied), which is significantly lower than the thermal efficiency. Therefore, the hybrid collector design manages two opposite outputs: the electrical and the thermal gains. The optimization issue can be explored under various perspectives, focusing, for example, in the global efficiency of the collector, the electrical efficiency per area of PV cells, primary energy savings, etc. The purpose of this parametric study is to explore different approaches. The first one is to confirm the best positioning for installing the PV cells, comparing the installation at the inlet side with the outlet side of the collector. It is expected to find better electrical efficiencies when the PV cells are placed near the inlet, since the plate absorber temperatures are lower. The effects of positioning and percentage of the collector with PV cells are analysed separately and combined. The question is whether it is possible to maximize the outputs (electrical or total), and to identify how the different parameters can be used to optimize the efficiencies.

The analysis is based on the results for thermal, electrical and overall efficiencies obtained through simulation, using the mathematical model. Some simplifications were introduced in the model presented in section 4.1, to adapt it to more realistic dimensions and conditions (for instance, no plywood plate would be used), and to make it more flexible to the systematization needed, reducing simulation time. The adapted model used for this

parametric study considers for the photovoltaic module just the PV cells, instead of a PV module, without any encapsulation material of finite thickness and absorptivity. This is possible through the use of alternative encapsulating technologies, like dye-sensitized solar cell or other thin-film methods. Moreover, the glass cover complies with the traditional function of protection from diverse weather conditions or mechanical damages. Only the simplification details that were introduced to the original model will be referred, together with the particular geometric conditions and material properties. This concerns mainly the heat balance in the photovoltaic element.

Some conclusions of this study have already been published (João and Oliveira, 2015).

4.3.1 Characterization of the geometry and physical properties of materials considered for the model

The collector geometry used for this study is based on the original dimensions of the thermal collector, 1.125 m × 2 m, before the adaptation made for experimental tests. The characteristic geometry modelled, corresponding to half the collector section between two tubes, is represented in Figure 4.14. The photovoltaic cells are directly attached to the absorber plate. The collector has 9 tubes in total, and the absorber plate surface area is 2,1 m^2. The total water flow rate is 40 g/s, which is in agreement with the typical values verified in thermal collectors (15-20 g/s/m^2), and close to the ASHRAE standard flow rate per unit area for glazed liquid flat plate collectors of 20 g/s/m^2.

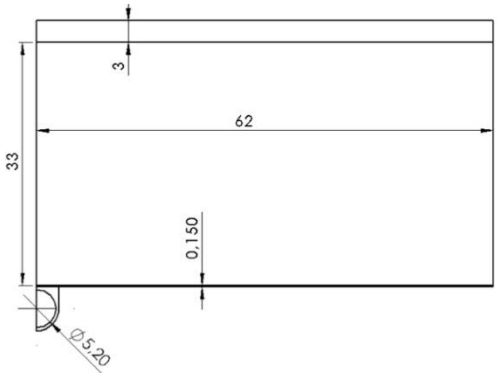

Figure 4.14 - Geometric details of the computational domain

The materials used for the different components in the model and their physical characteristics are listed in Table 4.3. The values were chosen from literature (Duffie, 1991) and commercial references.

Table 4.3 – Physical and optical properties of the collector components used in the simulation

Element	Material	Property
Glass cover	Low iron glass (Solatex)	Absorptivity α_{GC} = 0.02 (Guardian Industries Corp.) Emissivity ε_{GC} = 0.88 (Duffie, 1991) Transmissivity τ_{GC} = 0.90 (Also Media Ltd, 2013)
Absorber plate	Copper covered with selective coating	Absorptivity α_P = 0.96 (Duffie, 1991) Emissivity ε_P = 0.10 (Duffie, 1991) Thermal conductivity k_P = 387.6 W/mK
Tubes	Copper	Thermal conductivity k_P = 387.6 W/mK
Photovoltaic cells		Absorptivity α_C = 0.90 (Dupeyrat *et al.*, 2011a) Emissivity ε_C = 0.90 (Dupeyrat *et al.*, 2011a) Characteristic values at reference temperature T_{ref} = 20 °C: $\eta_{Cellref}$ = 0.15; β_{ref}= 0.04 K^{-1} (Skoplaki and Palyvos, 2009a)

4.3.2 Particular adjustments to the mathematical model

In order to simplify the application of the model to the parametric study focused on the positioning of the cells, two versions of the mathematical model were created, considering, for the same ratio of area covered by the cells, its application at the inlet side (*"IN"*) and at the outlet side ("*OUT"*) (for example, for 10% of area with cells, two situations were evaluated, considering these 10% at the entrance, "10%$_{IN}$", and at the outlet, "10%$_{OUT}$").

Comparing to the mathematical model formerly presented in section 4.1.4, the formulation of heat fluxes here will be is much simpler, since the photovoltaic module only consists of the cells. The adaptations that need to be considered are presented next.

Regarding the thermal balance over the glass cover (see eq. 4.1), the term for radiation heat flux has to be rewritten:

$$q_{rad\ Cell/GC} = \frac{\sigma(\overline{T_{Cell}}^4 - {T_{GC}}^4)}{\frac{1}{\varepsilon_{GC}} + \frac{1}{\varepsilon_{Cell}} - 1} \tag{4.60}$$

The average cell temperature ($\overline{T_{Cell}}$) is now:

$$\overline{T_{Cell}} = \frac{\sum_{i=1}^{Nz,M} \sum_{j=1}^{Nx} A_{i,j}\, T_{Cell_{i,j}}}{A_{Cell}} \tag{4.61}$$

The convection heat transfer between the glass cover and the cells can be defined as:

$$q_{conv(P+Cell)/GC} = h_{(P+Cell)/GC}(\overline{T_{(P+Cell)}} - T_{GC}) \tag{4.62}$$

$\overline{T_{(P+Cell)}}$ is the average value for temperature for the total area of the surface below the glass cover, and can be determined as:

$$\overline{T_{(P+Cell)}} = \frac{\overline{T_{Cell}} A_{Cell} + \overline{T_P}\, A_P}{A_{Cell} + A_P} \tag{4.63}$$

The convective heat transfer between the cells and the glass cover is analogous to the one obtained for the top glass of the module:

$$q_{convCell/GC} = h_{(P+Cell)/GC}(T_{Cell\,i,j} - T_{GC}) \tag{4.64}$$

The heat balance for the photovoltaic cell can be written as:

$$e + q_{rad}\ (+q_{condxCell} + q_{condzCell}) \tag{4.65}$$
$$= q_{convCell/CG} + q_{radCell/CG}\ (+q_{condxCell} + q_{condzCell}) + q_B$$

where the electric power flux and the radiation heat flux are redefined as:

$$e = (\ G_b + 0.9G_d)\tau_{GC}\ \alpha_{Cell}\ 1.01\ \eta_{El\,i,j} \tag{4.66}$$

$$q_{rad} = (\ G_b + 0.9G_d)\tau_{GC}\ \alpha_{Cell}\ 1.01\ (1 - \eta_{El\,i,j}) \tag{4.67}$$

The calculation of electrical efficiencies for each element *(i,j)* can be obtained from eq. 2.15 The conductive fluxes along the PV cells, $q_{condx,Cell}$ *(i,j)* and $q_{condZ,Cell}$ *(i,j)*, are similar to eq. 4.34 and 4.35.

For the determination of the heat loss through the lower surface (q_B) it will just be included the convection coefficient to the exterior, and, thus:

$$q_{B\,i,j} = h_{eq,B,Cell}(T_{Cell\,i,j} - T_{amb}) \tag{4.68}$$

The heat transferred to the fluid has also to be considered in the heat balance equation applied for the PV cells, in the boundary elements *j=1*, for the zone of the plate with PV cells. To be determined, eq. 4.53 can be combined with:

$$\dot{Q}_{T,i} L_{z,Cell}\ L_x = h_{f\,i}\left(T_{Cell\,i,1} - \overline{T_{f,i}}\right)(2\pi r) L_{z,Cell} \tag{4.69}$$

The model described corresponds to the one presented in the work by João and Oliveira (2015).

4.3.3 Analysis of the performance for a solar thermal-only collector

Despite the study focussing on the performance of hybrid collectors, the case of a thermal-only collector was modelled, for reference and verification of the adapted model. The temperature distribution along the plate absorber and the effect of the water inlet temperature in the thermal efficiency are presented.

Figure 4.15 shows the temperature distribution obtained for the absorber plate, without the application of photovoltaic cells, for input conditions: $T_{f,IN}$ = 20°C, G_b = 800

W/m^2, G_d = 200 W/m^2, T_{amb} = 20 °C. It can be seen that the temperature increases in cross-sectional direction from the tube axis (x = 0) into the plane of symmetry, (x = 0.053) and also along the flow (z axis). Under these conditions the plate temperature ranges from 21.9 °C (point A) to 53.8 °C (point B).

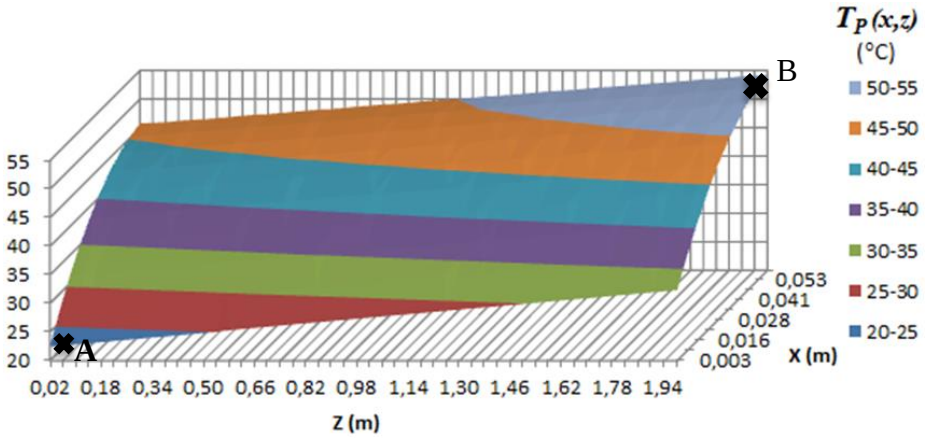

Figure 4.15 - Plate temperature distribution without PV cells
($T_{f,IN}$ = 20°C, G_b = 800 W/m^2, G_d=200 W/m^2, T_{amb}= 20 °C)

The effect in thermal efficiency of increasing the water inlet temperature, ($T_{f,IN}$) from 20ºC to 60ºC can be verified in Figure 4.16.

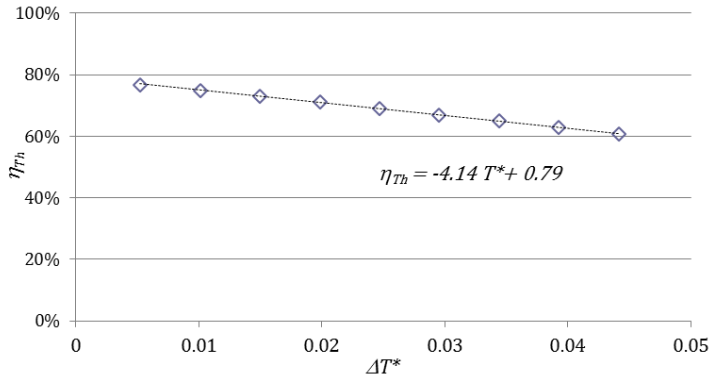

Figure 4.16 – Thermal efficiency curve for a solar thermal-only collector
(G_b = 800 W/m^2, G_d=200 W/m^2, T_{amb}= 20 °C)

The coefficients of the regression line in Figure 4.16 represent the thermal yield at zero thermal losses, η_{Th0}, and thermal loss factor, $F'U_L$, according to eq. 2.11. The values obtained are acceptable, for sheet and tube selective collectors (η_{Th0} reaches 76%, and $F'U_L$ assume values of about 4 W/m^{2}K for market available models, as said in section 2.1).

4.3.4 Baseline characterization of the effect of different parameters

Through this study, the influence of several parameters on the hybrid collector performance is analysed. If the separated effects may not look clear from the start, the analysis of their combined effects becomes more relevant.

In order to establish a clear starting point, the effects of some parameters can be already pointed out, based on results accepted from the practice and from literature. For example, increasing fluid inlet temperature ($T_{f,IN}$) causes a reduction in the thermal (η_{Th}), electrical (η_{El}) and global (η_G) efficiencies. On the other hand, increasing the area covered with PV cells causes an increase in η_{El}, and a decrease in η_{Th} and η_G. When the area of PV cells does not cover all the surface of the plate absorber, it is better for electrical efficiency to place them near the inlet side of the collector, because it is the area of the absorber plate with lower temperatures, and where the desired cooling effect of the PV cells is more intense. Table 4.4 summarizes this baseline scenario.

Table 4.4 - Effect of the different parameters on efficiencies of the hybrid collector

Parameter:	η_{Th}	η_{El}	η_G	η_{El}^*
$T_{f,In}$	⇓	⇓	⇓	⇓
P_f	⇓	⇑	⇓	?
In vs Out	?	⇑	?	⇑

Legend: ⇓: causes decrease; ⇑: causes increase; ?: uncertain

In Table 4.4, the unknown effects of the parameters are classified as "?". In the same table, the electrical "intensive" efficiency (η_{El}*) is also considered, since it is an important feature for evaluating the performance of the hybrid collector. η_{El}* can be relevant to isolate the effect of different parameters on the electrical performance itself.

It is, thus, interesting, to focus the analysis in parameters with opposite effects, or with an impact which is not clear from the start. It is expected that the decrease in thermal and global efficiencies caused by increasing $T_{f,IN}$ is enhanced by the effect of the packing factor.

4.3.5 Influence of PV cell positioning (Inlet vs Outlet), ratio of area covered with cells (*Pf*), and fluid inlet temperature ($T_{f,IN}$)

The analysis presented in this subsection is carried out considering the following environmental conditions: ambient temperature (T_{amb}) of 20°C, and direct (G_b) and diffuse (G_d) radiation of 800 W/m^2 and 200 W/m^2, respectively.

It is not simple to completely separate the different parameters. First, the best option for positioning the PV cells is analysed, according to thermal and global efficiency, in order to complete Table 4.4. For this purpose, different values of the packing factor (*Pf*) were considered for the simulations (25%, 35%, 50% and 75%), for configurations with the PV cells starting from the flow entry zone, noted by "*IN*", and from the exit zone, noted by "*OUT*". The graphical representation of the thermal (η_{Th}), and global (η_G) efficiencies, is shown in Figure 4.17 and Figure 4.18, for $T_{f,IN}$ varying from 20°C to 60°C. According to linear trend lines coefficients determined according to Figure 4.18, the decrease with $T_{f,IN}$ was in average of about 5/(Km^2/W) for η_G. The values for *Pf* = 75% were not included in Figure 4.17 and Figure 4.18, for a better perception of the graphic. Selected results from simulation, for values of $T_{f,IN}$=20ºC, 40ºC and 60ºC are shown in Table 4.5 and 4.6.

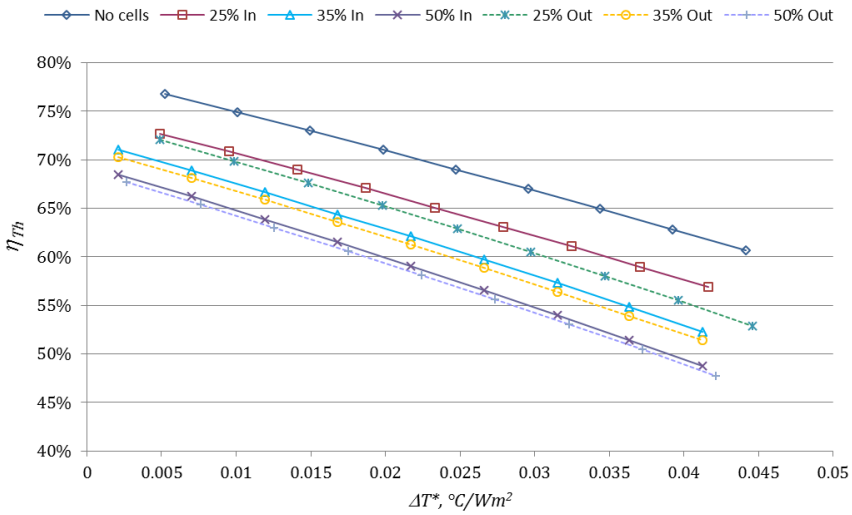

Figure 4.17 - Thermal efficiency of PV/T collector:
Influence of $T_{f,IN}$, *Pf* and layout ("*In*" *vs* "*Out*") (G_b = 800 W/m^2, G_d = 200 W/m^2, T_{amb} = 20 ºC)

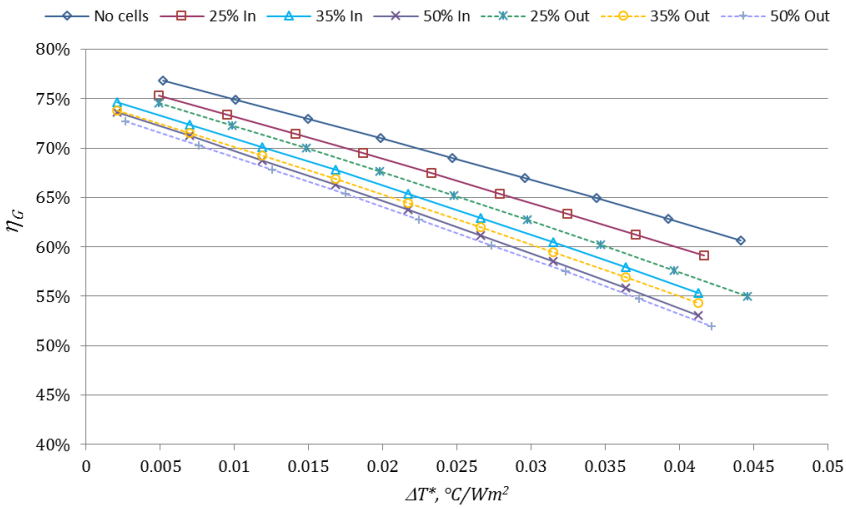

Figure 4.18 - Global efficiency of PV/T collector:
Influence of $T_{f,IN}$, *Pf* and layout ("*In*" *vs* "*Out*") (G_b = 800 W/m², G_d = 200 W/m², T_{amb} = 20 ºC)

It is clear that a larger area with PV cells causes the reduction of both thermal (Figure 4.17) and global (Figure 4.18) efficiencies, as expected (see Table 4.4). This reduction is also confirmed in Table 4.5 and Table 4.6, where the thermal and combined efficiencies for zero reduced temperatures, respectively, are presented. The η_{Th} reduction with *Pf* is enhanced with the increase of $T_{f,IN}$, ranging, with the "*Inlet*" layout, from 8.6% for $T_{f,IN}$=20ºC to 14% for $T_{f,IN}$=60ºC.

In terms of thermal efficiency, it can be observed that the application of the cells at the inlet side is better. It can be concluded from the results in Table 4.5 that the effect of positioning is more pronounced for higher values of the fluid inlet temperature ($T_{f,IN}$), namely for *Pf* = 25%.

Table 4.5 –Thermal efficiencies at zero reduced temperatures,
for different values of *Pf*, $T_{f,IN}$ and layout *In vs Out*

η_{Th}	P_f = 25%		P_f = 35%		P_f = 50%		P_f = 75%	
$T_{f,IN}$	IN	OUT	IN	OUT	IN	OUT	IN	OUT
20ºC	72.7%	72.1%	71.0%	70.3%	68.5%	67.7%	64.1%	63.6%
40ºC	65.1%	63.4%	62.1%	61.2%	59.1%	58.1%	54.0%	53.3%
60ºC	56.9%	53.9%	52.3%	51.4%	48.8%	47.7%	42.8%	42.0%

Analysing the results for global efficiency, installing the PV cells at the inlet is also convenient, as can be seen in Figure 4.18. On the other hand, that effect is intensified by the increase $T_{f,IN}$ only for *Pf* ≤ 50%, as can be confirmed through Table 4.6. The added effects of $T_{f,IN}$ and *Pf* in the decrease of global efficiency can also be confirmed, *i.e.*, the η_G decrease caused by the increase of PV cells area becomes stronger with $T_{f,IN}$, ranging from 3.5% for $T_{f,IN}$=20ºC to 9.9% for $T_{f,IN}$=60ºC, in the "*Inlet*" layout.

Table 4.6 - Global efficiencies at zero reduced temperature, for different values of *Pf*, $T_{f,IN}$ and layout *In vs Out*

η_G	P_f = 25%		P_f = 35%		P_f = 50%		P_f = 75%	
$T_{f,IN}$	IN	OUT	IN	OUT	IN	OUT	IN	OUT
20ºC	75.3%	74.6%	74.6%	73.8%	73.7%	72.7%	71.8%	71.1%
40ºC	67.5%	65.7%	65.4%	64.5%	63.8%	62.8%	61.0%	60.3%
60ºC	59.1%	56.0%	55.3%	54.3%	53.1%	52.0%	49.2%	48.4%

In Figure 4.19 it is possible to observe the combined effects of positioning and P_f, in terms of global efficiency. It is clear that the global efficiency decreases with the percentage of collector area covered with PV cells, and confirms the best results for PV cells applied at the inlet side. So, applying the PV cells preferentially at the inlet will reduce, although in a small scale, the decrease in global efficiency caused by the increase in packing factor. The effect of positioning will have more impact for hybrid collectors with balanced areas with, and without, PV cells. Even though the installation of PV cells at the inlet side is objectively proved to favour the hybrid collector performance, its impact on global efficiency is very small.

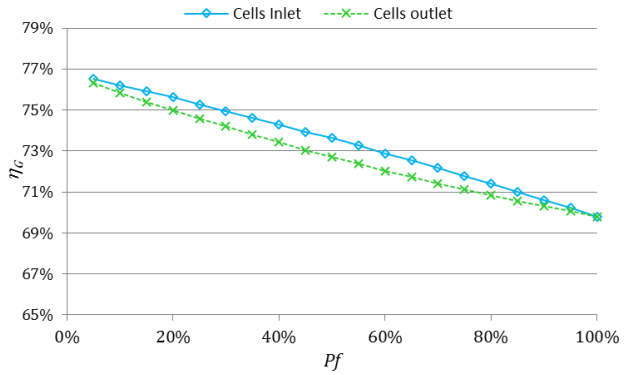

Figure 4.19 - Global efficiency – Influence of *Pf* and location ("*In*" vs "*Out*") ($T_{f,IN}$ = 20°C, G_b = 800 W/m^2, G_d = 200 W/m^2, T_{amb} = 20 °C)

The effect of the location of PV cells in the electric efficiency, both with reference with the total area of collector (η_{El}) and the area with cells (η_{El}^*), will not be referred, because it is already known. The combined effects of the positioning of PV cells in electrical efficiencies with $T_{f,IN}$ will also not be mentioned, because of its very small value.

The packing factor (*Pf*) is a very important parameter in this analysis, especially with the aim of optimizing the hybrid collector. Its effect on the decrease in thermal (η_{Th}) and global (η_G) efficiencies can be noticed in Figure 4.17 and Figure 4.18, respectively. In Figure 4.20 the influence of *Pf* in η_{Th} and η_G can be more clearly observed. It can be verified that the increase in *Pf* is not enough to compensate the decrease in thermal efficiency, but

attenuates that effect: the linear decrease of η_{Th} and η_G with Pf is of 17% and 7%, respectively.

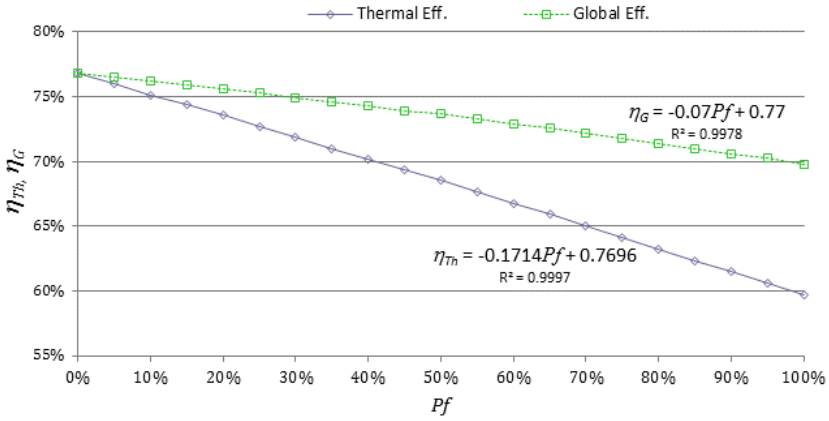

Figure 4.20 - Influence of Pf in η_{Th} and η_G, for $T_{f,IN}$ = 20°C, G_b = 800 W/m^2, G_d = 200 W/m^2 and T_{amb} = 20 °C

Referencing to Table 4.4, the analysis of the combined effects of Pf and $T_{f,IN}$ in electrical efficiency is seen in Figure 4.21. By application of linear trend lines, the effect of Pf in can be quantified in about 2.7% per 25% Pf increase, which is significant, attending to the average values of η_{El}. It can be observed that, despite the increase in $T_{f,IN}$ causing a reduction in electrical efficiency (η_{El}), this effect is so small that can be neglected.

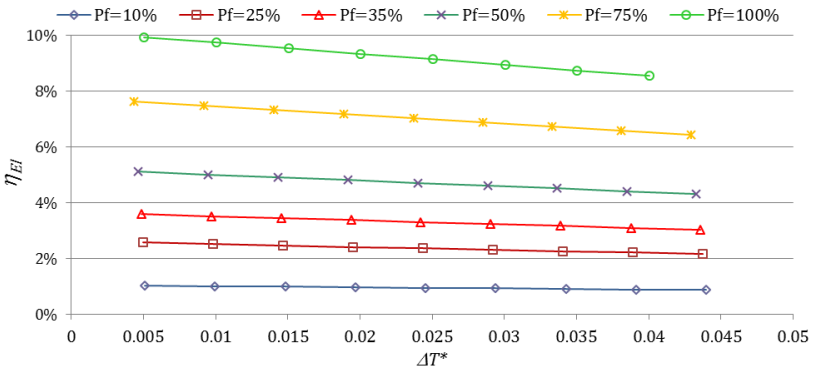

Figure 4.21 - Influence of Pf and $T_{f,IN}$ in the electrical efficiency of an hybrid collector, for G_b = 800 W/m^2, G_d = 200 W/m^2 and T_{amb} = 20 °C

In Figure 4.22 the influence of Pf and $T_{f,IN}$ can also be observed, regarding the electric power generated per area of PV cells, which can be understood as the average efficiency of the PV cells (η_{El}*). By application of linear trend lines, the effect of Pf can be quantified in about 0.04% per 25% Pf increase. Thus, Pf has no significant influence in η_{El}*. An increase of the inlet fluid temperature causes a decrease in the average efficiency of the PV cells, of about 0.4/(Km^2/W). The combined influence of both parameters is not clear.

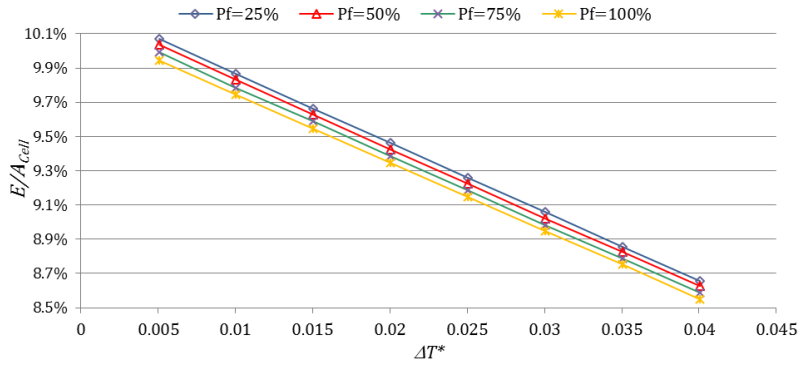

Figure 4.22 - Influence of $T_{f,IN}$ and Pf in electric PV cells efficiency (G_b = 800 W/m^2, G_d = 200 W/m^2, T_{amb} = 20 ºC)

Table 4.4 can now be completed, and the update is seen in Table 4.7.

Table 4.7 - Effects of different parameters on hybrid collector efficiencies

Parameter:	η_{Th}	η_{El}	η_G	η_{El}^*
$T_{f,IN}$	⇓	-	⇓	⇓
Pf	⇓	⇑	⇓	-
In vs Out	⇑	⇑	⇑	⇑

Legend: ⇓: causes decrease; ⇑: causes increase; -: no significant effect

In conclusion, an absolute optimization for the ratio of the area of the hybrid collector with PV cells is not possible, in terms of efficiencies. The results obtained through this developed model can be complemented with the inclusion of design variables, as the energy needs, climatic data, together with values of local energy costs, in order to quantify the effect of the packing factor.

4.3.6 Combined effects of incident radiation and ambient temperature

In this subsection the influence of the climatic variables (solar radiation (G), and ambient temperature (T_{amb})) on the performance of the hybrid collector is analysed, together with the effect of the packing factor (Pf) and fluid inlet temperature ($T_{f,IN}$). It is expected that the efficiencies improve with higher values of G and T_{amb}, because the energy received by the system is higher, and the heat loss through the glass cover reduces.

The influence of solar radiation and ambient temperature on thermal and global efficiencies are presented in Figure 4.23, considering values for the global incident solar radiation from 400 to 1000 W/m^2, and ambient temperature of 10°C, 20°C and 30°C. The results refer to simulations for Pf= 40%, with PV cells installed at the inlet, and a fluid inlet temperature of 40°C.

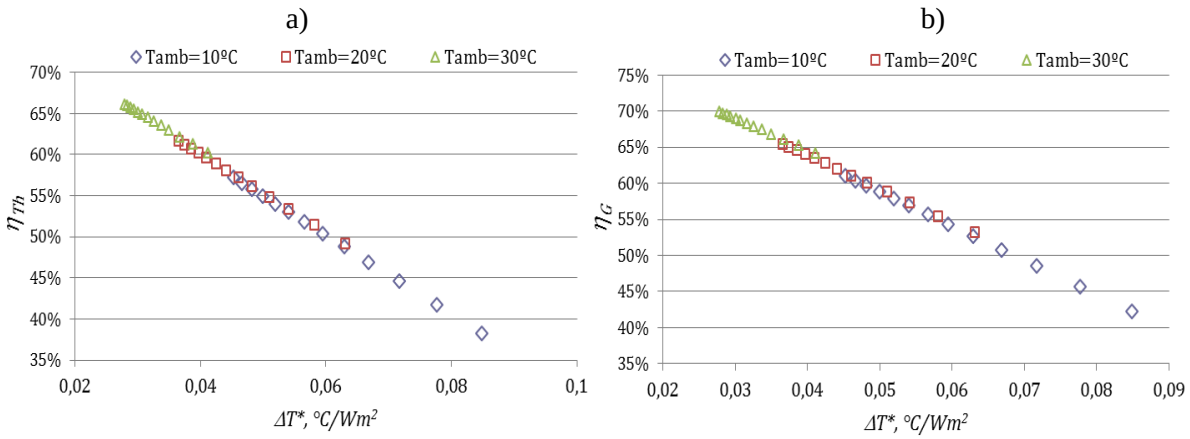

Figure 4.23 - Effect of G and T_{amb} on thermal (a) and global (b) efficiency, for Pf=40% and $T_{f,IN}$ = 40°C

The results in Figure 4.23 confirm the expected effect of G and T_{amb} in the increase of thermal and global efficiencies. The thermal efficiency ranges from 38.2% to 57.2%, for T_{amb} = 10ºC, and from 60.2% to 66.2% for T_{amb} = 30ºC. The values of η_G, for the same conditions, range from 42.2% to 61.0% and from 64.1% to 70.0%, respectively. The values of the efficiency are more affected by G for a low ambient temperature. This is expected, because both parameters cause an increase in the efficiencies, and, for high values of both G and T_{amb}, their effects are added, concentrating the range of values of the efficiencies. As the difference between the values of η_G and η_{Th} is almost constant, the electrical efficiency (η_{El}) seems not to be significantly affected by T_{amb} and G.

In order to get a more detailed overview of each factor, G and $T_{f,IN}$, in the global efficiency, the results have been organized with G in the x axis for values of fluid inlet temperature of 40ºC and 60ºC, with Pf = 40% and T_{amb} =20ºC, as shown in Figure 4.24. It can be confirmed that η_G decreases with $T_{f,IN}$. Regarding the effect of solar radiation on η_G, Figure 4.24 shows that it depends on $T_{f,IN}$. For values of G ranging from 400 to 800 W/m^2, η_G ranges from 53.2% to 65.5% for $T_{f,IN}$ = 40ºC and from 28.6% to 55.2 % for $T_{f,IN}$= 60ºC. For $T_{f,IN}$ =25ºC, the effect of solar radiation on η_G is very small, with values for η_G ranging from 70.2% to 72.6%, for the same range of G. Thus, the influence of solar radiation in the global efficiency increase is enhanced by the effect of $T_{f,In}$.

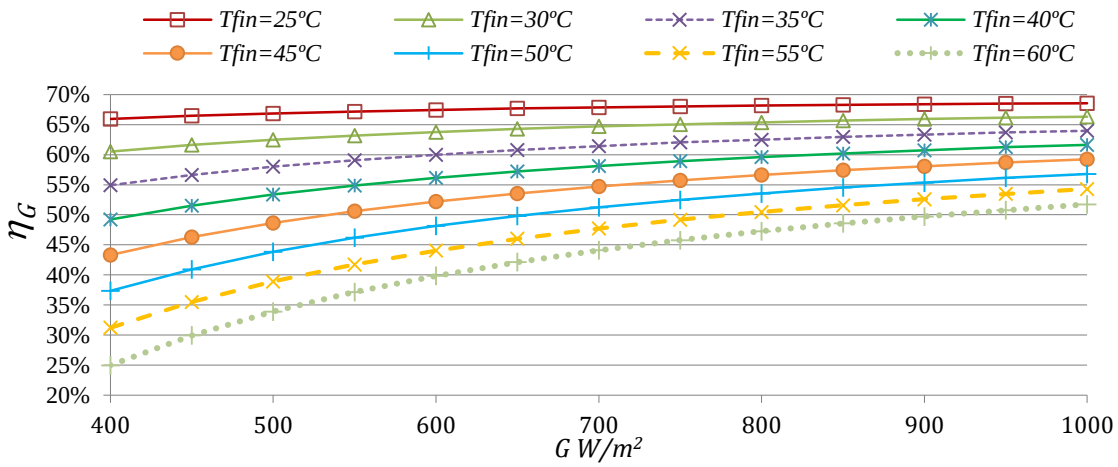

Figure 4.24 - Influence of G and $T_{f,IN}$ in global efficiency (η_G), for Pf=40% and T_{amb} = 20°C

The combined effects of $T_{f,IN}$ (40ºC and 60ºC), T_{amb} (10ºC, 20ºC and 30ºC) and G can be verified in Figure 4.25.

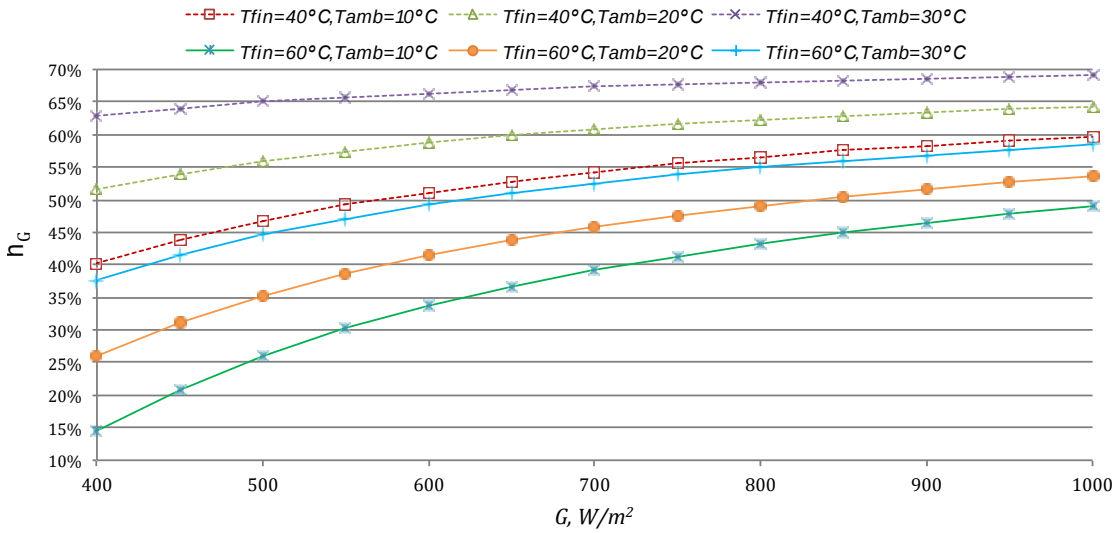

Figure 4.25 - Influence of G, $T_{f,IN}$ and T_{amb} in global efficiency, for Pf=50%

The results from Figure 4.25 confirm the effects of all the parameters in the global efficiency, already mentioned: the influence of the solar radiation in the increase of global efficiency is enhanced by an increase of the fluid inlet temperature and reduced by an increase of the ambient temperature. Analysing the influence of T_{amb} in the global efficiency with $T_{f,IN}$ =40ºC, it is verified that η_G varies from 40.2% to 62.9% for a range in T_{amb} from 10ºC to 30ºC, with G = 400 W/m^2. For G = 1000 W/m^2, global efficiency varies from 59.8% to 69.3%, for the same range of T_{amb}. That can be explained because, with low radiation, the thermal losses through the glass cover will have great influence in the thermal efficiency. As G increases, the relative influence of those losses will decrease.

The analysis of the effect of the packing factor (*Pf*) in the global efficiency (η_G) can be observed in Figure 4.26, for values of solar radiation ranging from 400 W/m^2 to 1000 W/m^2, together with the influence of the ambient temperature (T_{amb}), for an inlet fluid temperature ($T_{f,IN}$) of 40ºC. Values for *Pf* of 25%, 50% and 75%, and ambient temperatures of 10ºC, 20ºC and 30ºC were considered. The results confirm that η_G decreases with the packing factor. In order to simplify the text, the corresponding results from the simulations are presented in Table 4.8.

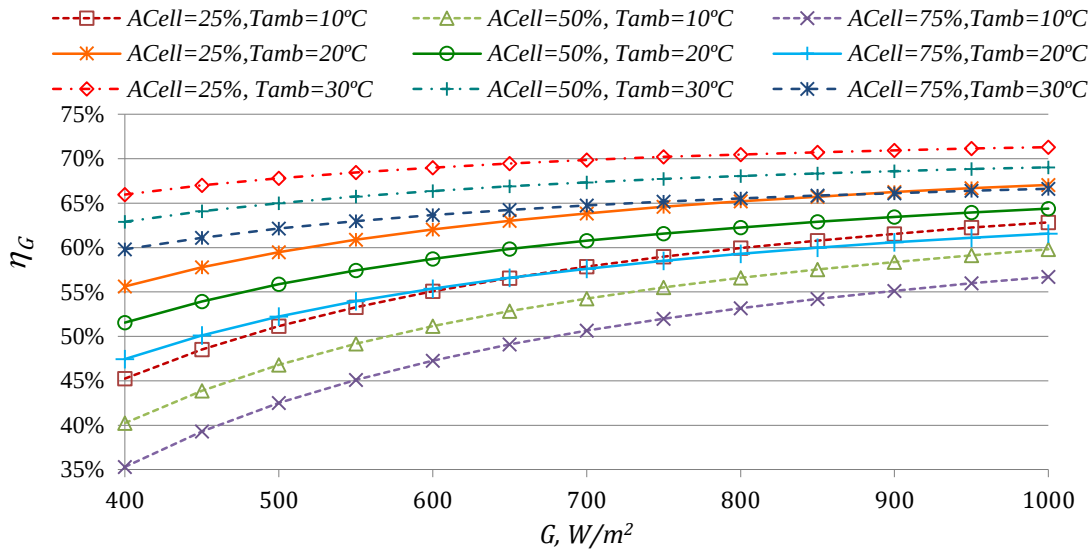

Figure 4.26 - Influence of *G*, *Pf* and T_{amb} in the global efficiency of the hybrid collector, for $T_{f,IN}$= 40°C

Table 4.8 - Influence of T_{amb} and *Pf* in the global efficiency of an hybrid collector, for $T_{f,IN}$= 40ºC

		Pf=25%			*Pf=50%*			*Pf=75%*		
	Tamb:	*10ºC*	*20ºC*	*30ºC*	*10ºC*	*20ºC*	*30ºC*	*10ºC*	*20ºC*	*30ºC*
G (W/m²)	400	45.3%	55.6%	66.0%	40.2%	51.5%	62.9%	35.3%	47.5%	59.8%
	450	48.5%	57.8%	67.0%	43.9%	53.9%	64.1%	39.3%	50.1%	61.1%
	500	51.1%	59.5%	67.8%	46.8%	55.9%	65.0%	42.5%	52.2%	62.1%
	550	53.3%	60.9%	68.5%	49.2%	57.4%	65.8%	45.1%	54.0%	63.0%
	600	55.1%	62.0%	69.0%	51.2%	58.7%	66.4%	47.3%	55.4%	63.7%
	650	56.6%	63.0%	69.5%	52.8%	59.8%	66.9%	49.1%	56.6%	64.2%
	700	57.9%	63.8%	69.8%	54.3%	60.8%	67.3%	50.6%	57.6%	64.7%
	750	59.0%	64.6%	70.2%	55.5%	61.6%	67.7%	52.0%	58.5%	65.2%
	800	59.9%	65.2%	70.5%	56.6%	62.3%	68.1%	53.2%	59.3%	65.5%
	850	60.8%	65.7%	70.7%	57.5%	62.9%	68.3%	54.2%	60.0%	65.8%
	900	61.5%	66.3%	70.9%	58.3%	63.5%	68.6%	55.1%	60.6%	66.1%
	950	62.2%	66.7%	71.1%	59.1%	63.9%	68.8%	56.0%	61.1%	66.4%
	1000	62.8%	67.1%	71.3%	59.8%	64.4%	69.0%	56.7%	61.6%	66.6%

Analysing the results from Table 4.8, it can be verified that the effect of *G* in the increase of the global efficiency is intensified by the increase in packing factor. An increase of *Pf* also enhances the effect of T_{amb} on η_G.

The combined effects of *Pf* and $T_{f,In}$ can be observed in Figure 4.27, for solar irradiation ranging from 400 W/m^2 to 1000 W/m^2, and T_{amb} = 20ºC.

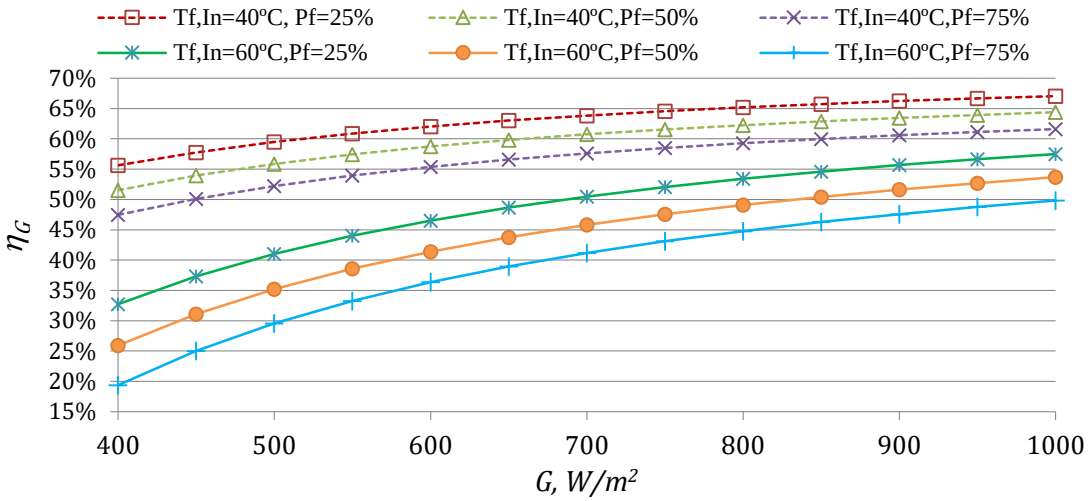

Figure 4.27 - Effect of *Pf* and $T_{f,IN}$ in global efficiency, for T_{amb}= 20ºC

It can be seen from Figure 4.27 that the effect of *Pf* in global efficiency slightly decreases with an increase in solar radiation.

4.4 Concluding remarks

This chapter is devoted to the development of a numerical model to evaluate the performance parameters of an hybrid collector, through values of thermal, electrical and global efficiency, considering input conditions of solar radiation (*G*), ambient temperature (T_{amb}), inlet fluid temperature ($T_{f,IN}$) and different ratios of area covered with PV cells (*Pf*).

The model was validated with the experimental results obtained on chapter 3, and used in a parametric analysis, to characterize the influence of different variables in the efficiency of the hybrid collector.

A detailed analysis was carried out, over the separated and combined effect of the different selected parameters (PV cells layout, *Pf*, $T_{f,IN}$, *G* and T_{amb}), on the hybrid collector performance.

The results from the numerical solution of the model confirm already expected behaviour characteristics:

- the existence of applied PV cells causes a decrease in global efficiency, and η_G decreases linearly with *Pf* about 7%, for $T_{f,IN}$ = 20ºC and T_{amb} = 20ºC.

- a $T_{f,IN}$ increase leads to a decrease in global efficiency, ranging from 4.1/(Km^2/W) for Pf = 0% to 5.3 (Km^2/W) for Pf = 50%.
- an increase in ambient temperature and solar radiation is associated with an increase in the global efficiency.

Those results were complemented with more interesting information about hybrid PV/T collectors. Various conclusions can be highlighted:

- positioning the PV cells near the inlet side of the fluid, where the average temperature in the thermal fluid, the absorber plate, and the PV cells is lower, do not significantly favour global efficiency. However, it has more impact when the areas of the hybrid collector with and without cells are balanced;

- the negative effect of an increase in the inlet fluid temperature is emphasised with the increase of the packing factor;

- the separated effects of T_{amb} and G in the increase of η_G are inhibited mutually by the complementary parameter;

- the η_G increase with G is reduced with $T_{f,IN}$ and increased with Pf;

- the η_G increase with T_{amb} is increased with Pf.

Establishing an optimum value or relation for the area covered with cells is not possible. That analysis will have to be related with the specific purposes of the application of the hybrid collector, taking into account the energy demand profiles, in order to calculate a payback period and perform an economic analysis that would provide an optimum solution. The ecological benefits of using clean and renew- able energy sources that are associated with these hybrid collectors should also been quantified.

The analysis carried out includes extensive information on the influence of significant factors to the performance of the hybrid collectors, that can be used in future works.

Chapter 5.

Optimization of a hybrid solar collector regarding economic performance and environmental impact

The primary application for solar hybrid collectors is in buildings, mainly for hot water systems, with the extra benefit of the electrical output that can be used for supplying the building power needs. Presently, in Portugal there is no economic advantage in selling electricity to the grid, since the governmental incentives allowing high feed-in tariffs no longer exist. Therefore, the first option is to use the electricity generated by the collectors for internal consumption. Then, a surplus can be sold to the grid at 90% of its purchase cost (MINISTÉRIO DO AMBIENTE, 2014). In this chapter, an evaluation of the performance of domestic systems integrating PV/T hybrid collectors is made, taking into account energy, economic and environmental perspectives.

A parameter with direct impact on the costs and savings of hybrid systems is the collector area ratio covered with PV modules, which corresponds to the packing factor (*Pf*). This factor affects in different ways the thermal and electrical efficiencies. The increase of that ratio will cause an almost proportional increase in the electrical power output, and a decrease in the thermal output. As stated several times before, the overall efficiency will decrease. However, it is pertinent and more important to analyse the impact of the packing

factor in terms of energy and cost, by comparison to a consumption scenario using conventional energy sources, like natural gas and grid electricity. The energy savings can be obtained considering the different costs related to the electrical and thermal energy outputs, which have different values for the consumer. The approach presented here aims to help defining the best option for configuring the collector PV area ratio, on the consumer's perspective.

A basic system will be first characterized, suitable for the domestic energy needs of a typical household of 4 persons. The study will be conducted with reference to the application of typical PV modules with 32 cells, covering different area ratios of the solar collectors, corresponding to 1, 2, 3 and 4 PV modules. In order to adapt the system to the Domestic Hot Water (DHW) needs, two collectors will be considered, each one with a typical area, and sufficient to allow the application of 4 PV modules. The volume of the storage tank of the solar collector circuit was determined according to established rules, based on the collector area. It is also considered that all the generated electricity is consumed, instantaneously or at a later time. For the latter situation, the efficiency of the storage equipment is not considered.

The model developed and presented in chapter 4 is used to obtain the thermal parameters of performance of the hybrid collector for different values of the packing factor (*Pf*), corresponding to 1, 2, 3 and 4 PV applied modules. A dynamic analysis of the energetic performance of the system is then performed for two typical Portuguese climatic regions, Porto and Faro, using an adequate dynamic simulation software (TRNSYS). By integrating the hybrid collector efficiency characteristics with climatic data and DHW daily loads, it is possible to estimate the annual thermal and electrical energy supplied by the hybrid collector. Thus, the energy and economic savings can be evaluated, by comparison with a conventional system, which was considered to use a natural gas heater and electricity from the grid. The environmental value of the system is also evaluated, through the calculation of CO_2 saved emissions.

5.1 Applications of hybrid collectors in buildings

Liquid photovoltaic/thermal (PV/T) collectors are used to heat water and simultaneously produce electricity for various domestic and industrial applications (Kumar *et al.*, 2015).

The largest market potential is for domestic hot water (DHW) applications, possibly combined with space heating. Although most collectors are installed on single-family houses, the share of large systems for collective applications is expected to increase. In the PV/T roadmap (Affolter *et al.*, 2006), water heating systems for the residential market are indicated as the main market for glazed PV/T systems, while public pool systems and large hot water systems (both for collective applications and for utility application such as hospitals, campgrounds and homes for the elderly) are presented as interesting niche markets (Zondag, 2008).

The application of hybrid collectors in industry is also an option, once they can partly satisfy the high demand of energy for both heat and electricity in industries. However, the temperature of the cooling medium must not be allowed to be too high as it will have a detrimental effect on the module efficiency. Hence, the system is inherently a low-temperature set-up and will only serve applications where a pre-heated medium is preferably used (Erdil *et al.*, 2008).

Zhang *et al.* (2012) refer that the studies related to economic and environmental analyses of the systems with hybrid collectors done so far are adequate to indicate the performance of the PV/T technology in terms of its economic and carbon benefits, and addressing the following approaches:

(1) PV/T energy saving potential, its cost augment, estimated payback time and life cycle cost saving;

(2) PV/T Energy Payback Time and Greenhouse-gas Payback Time and their relevance with the system's energy and exergy efficiencies.

However, not sufficient studies analyse the influence of the choice of *Pf* on system energetic, economic and environmental performances. This is an important issue for the consumers (and also manufacturers), when deciding the best configuration for the hybrid PV/T collector. This chapter aims to help addressing that issue.

5.2 Performance assessment of systems with hybrid collectors

The evaluation of the performance of PV/T systems is complex and the comparison of the output energy is not a sufficient criterion to assess the performance of the PV/T collectors, due to the interaction of thermal and electrical efficiencies and the different forms and values of the output energy.

As the thermal and electrical outputs depend on the incident radiation, the yield of solar collectors is not only determined by the quality of the collector, but at least as much by the climate and the type of system it is used in. For the effect of the climate, important differences are the annual amount of irradiance and the variation of the irradiance over the year. In particular, cold but sunny winter days are good for solar space/water heating. Due to the very high difference between summer and winter irradiance, the Northernmost climates require a large amount of storage to obtain a significant solar input for space heating, while regions such as the south of Canada, the USA or Japan can cover a much larger share of their heating load with direct solar heating (Zondag, 2008).

Important parameters of system performance are the required temperature level and the solar fraction obtained. In thermal systems the solar savings fraction, or solar fraction (f_S), is the useful energy obtained from solar energy divided by the total energy needs of a conventional system, without solar collectors. The solar fraction can be used to determine the Energy Savings, taking into account the energy consumption of the reference system (Dupeyrat *et al.*, 2014).

The influence of the packing factor and the water flow rate in the overall performance of hybrid PV/T systems applied in a UK domestic building, was considered in a study by Herrando *et al.* (2014). The results show that, for the case of the UK (low solar irradiance and low ambient temperatures), a complete coverage of the solar collector with PV together with a low collector flow-rate are beneficial in allowing the system to achieve a high coverage of the total annual energy (heat and power) demand, while maximising the CO_2 emissions savings. In addition, the emission assessment indicates that a PV/T system can save up to 16.0 tonnes of CO_2 over a lifetime of 20 years, which is significantly (36%) higher than the 11.8 tonnes of CO_2 saved with a PV-only system.

This chapter analyses the impact of the packing factor in the energy, economic and environmental performance of a hybrid DHW/electrical system, for a household of 4 occupants.

5.3 Evaluation of the energetic and economic performance of a Domestic Hot Water system using hybrid solar collectors

The analysis carried out along this section aims the choice/optimization of the packing factor of a hybrid collector, for the given application. The area of the collector is chosen in order to fit 4 PV modules, with 32 5" cells each. The dimensions of the PV module are 1.1 m x 0.6 m, and so the area of each collector will be 1.1 x 2.4 (2.64) m^2. However, in order to represent a more realistic scenario that matches a typical daily load of DHW for a 4 persons' household, the dynamic simulation will be carried out considering the use of two collectors. The Portuguese regulation for energy performance of residential buildings (REH) (DR, 2013), based on the former existing regulation for thermal behaviour of buildings (RCCTE), establishes a domestic hot water consumption of 40 l/occupant and a solar collector area of at least 1 m^2/occupant, which results in the use of two collectors with the aforementioned dimensions.

The primary/solar circuit includes the hybrid solar collectors, connected in parallel, a single speed pump and a controller to turn the flow on/off. A stratified storage tank with a coil heat exchanger is used for transferring the heat to the secondary circuit, which supplies the system for DHW use. An auxiliary heater is considered to fulfil the hot water needs, when the heat from solar collectors is not enough.

The primary circuit flow rate is determined according to IPQ (2007), which specifies a flow rate of 0.02 kg/s/m^2, based on the area of the absorber. Different criteria for the definition of the storage tank volume can be found, some of them based directly on the daily load and others in the collector area. Kalogirou (2009) states that the annual performance of liquid-based solar energy systems is insensitive to the storage capacity, as long as it is higher than 50 litres of water per square meter of collector area. Based on this criteria, a typical tank with 300 litres is used.

The dynamic simulation of the system, performed on an hourly basis for all the days along the year, was modelled using TRNSYS (TRNSYS). A system modelled with TRNSYS comprises the different components that constitute the real system. The TRNSYS library covers a wide range of components already pre-patterned, named as "type", and already includes models for hybrid PV/T solar collectors. The simulation time step was set to 0.1 h. The components used for the system and its main features are described next. The detailed information can be consulted in Appendix A.

5.3.1 Characterization of the components of the DHW hybrid system, according to TRNSYS

Each component in the TRNSYS library is characterized by PARAMETERS. The functions developed internally for each "type" need INPUTS, and calculate OUTPUTS, within its specific application. The parameters are fixed characteristics of the elements. The sequence of the components can be established through links, which make the transposition of the outputs of one element to the inputs of the following element. A scheme of the system is presented in Figure 5.1.

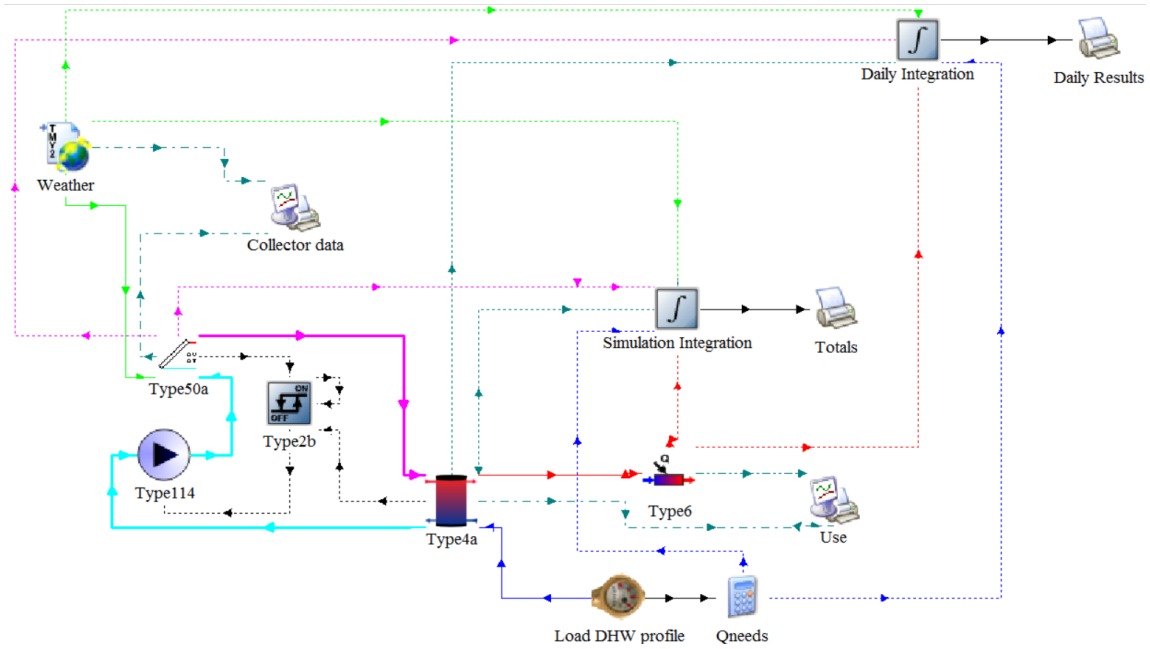

Figure 5.1 – Scheme of the Solar Domestic Hot Water (SDHW) system, developed in TRNSYS

The physical properties of water, specific heat (c) and density (ρ), are considered constants for all the elements of the system, with the values of 4.19 kJ/kg K and 1000 kg/m^3.

The "Load DHW profile" allows to distribute the water needs along the 24 h of a day. It was specified in absolute terms, using l/h. A daily consumption of 160 l for a typical household with 4 occupants was considered, respecting the indication of 40 l/occupant. The daily needs were distributed by the morning period (6h-10h) and in the evening (17h-23h). The type 14b for Water Draw forcing function in the utility menu of TRNSYS was used.

The pump used in the primary closed circuit corresponds to a single speed pump, which is able to maintain a constant fluid outlet mass flow rate ("*type 114*"). According to the specification of 0.02 kg/s/m^2, based on the area of the absorber, by IPQ (2007), the mass flow rate is set to 380 kg/h, which corresponds to the "*rated flow rate*" parameter. Type114 sets the downstream flow rate based on its rated flow rate parameter and the current value of its control signal input. The "*rated power consumption*" parameter is set to 124 W and the "*overall pump efficiency*" input to 0.5. Those values are based on the technical data of a pump used for solar DHW systems, circulation group AGS-10, from Vulcano.

A control element is necessary to command the circulation of the fluid, when the temperature difference between the collector outlet and the cold outlet of the storage tank exceeds an upper dead band value, or turn off the pump when that difference is lower than a lower dead band value. The upper and lower dead bands are defined in this case as 4ºC and 2ºC, respectively. This function is accomplished by a "*type 2b*" differential controller with hysteresis, with a successive distribution control strategy. The output control function is linked to the pump as an input, in order to command turning it on/off, as can be seen in Figure 5.1. This output is on/off type.

The main component of this system is the hybrid PV/T collector, which corresponds to a "*type 50a*", included in the photovoltaic panels group. It is based on the mathematical model of a flat plate collector with constant losses, type 1, adding a PV module. It simulates a hybrid collector and incorporates the analysis and work of Florschuetz (1976) for flat plate collectors operated at peak power. This TRNSYS element treats the instantaneous thermal efficiency of the collector based on the Hottel-Whillier equation (Duffie, 1991), already presented as eq. 2.11. The mathematical model developed and presented in chapter 4 is used to obtain the reference characteristics of the thermal efficiency, F_R and U_L, for the different cases of 1, 2, 3 or 4 PV modules applied, considering cover transmittance (τ_{GC}) of 0.85 and plate absorptivity (α_P) of 0.93.

The glass cover transmittance (τ_{GC}), the plate absorptivity (α_P) and the collector loss coefficient ($F_R U_L$) are given as parameters in the menu for "*type 50a*". It was not accounted for the linear dependency of U_L with the fluid and ambient temperatures. Instead of the overall collector heat removal efficiency factor (F_R), this element of TRNSYS uses as parameter the collector efficiency factor (F'), that represents the ratio of the actual useful energy gain to the useful gain that would result if the collector absorbing surface had been at the local fluid temperature. The parameter F' is determined by the equation (Duffie, 1991):

$$F_R = \frac{\dot{m}c}{A_C U_L}\left[1 - exp\left(-\frac{A_C U_L F'}{\dot{m}c}\right)\right] \tag{5.1}$$

Another important parameter is the *packing factor*, which represents, for this TRNSYS element, the ratio of PV cell area to absorber area.

A summary of those parameters need for the definition of the "*type 50a*" collector is listed in Table 5.1, for the studied cases of 1, 2, 3, and 4 PV modules applied, in order to obtain the TRNSYS parameters U_L and F' through eq. 5.1. The mass flow rate corresponding to one collector is 0.0528 kg/s and the collector area is 2.64 m^2.

Table 5.1 - Characteristic parameters for the calculation of thermal efficiency for the PV/T collector in TRNSYS

	1 PV module	**2 PV modules**	**3 PV modules**	**4 PV modules**
$F_R\,(\tau\alpha)_n$	0.671	0.616	0.564	0.512
$F_R\,U_L$	4.945	5.348	5.739	6.116
U_L	5.826	6.865	8.039	9.450
F'	0.875	0.805	0.739	0.672
P_f	0.188	0.376	0.564	0.752

The electrical efficiency is calculated based on the temperature coefficient of solar cell efficiency (β_{ref}) and the reference temperature for solar cell efficiency (T_{Ref}), that are taken as parameters. The cell efficiency at the reference temperature ($\eta_{El,Tref}$) is taken as an input. Other inputs for *type 50a* element are the inlet fluid temperature, fluid mass flow rate, ambient temperature and incident radiation. The inlet fluid temperature is corrected dynamically by the output of the pump, and the flow rate is the same as for the one taken for the pump. The environmental conditions of temperature and radiation are outputs of the climatic file defined in the element "*weather*". Simulations were run for Porto and Faro.

In the "*weather*" element, the climatic file corresponding to the location that is being simulated is selected from the database. It was defined that there was no tracking, and the

azimuth and slope of the collector were given as an input. The azimuth is always 0, corresponding to the south. The slope for the collectors (β) follows the optimization for all year use, that depends on the latitude of the location (ϕ), indicated also by Água Quente Solar (2004):

$$\beta = \phi - 5 \tag{5.2}$$

The storage tank allows the heat transfer from the hot water leaving the collector in the primary circuit to the utilization circuit. A stratified tank was used, with fixed inlets and uniform losses, corresponding to *type 4a* in TRNSYS library. Six levels of stratification were defined, each one with the same height of 0.3 m. The tank capacity was calculated based on the collector area, with a ratio of 50 L/m^2, resulting on 264 L. This value was approximate to the standard useful capacities of commercialized tanks, that is, in this case, 295 L. The tank loss coefficient parameter was determined based on technical data of commercialized tanks, in this case a Junkers thermal storage tank S-ZB300, with 50 mm insolation of thermal conductivity of 0.034 W/mK. For a better understanding of the terms used in TRNSYS the menu of this element, a scheme is showed in Figure 5.2.

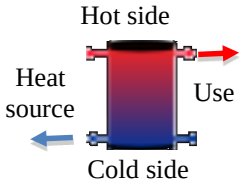

Figure 5.2 - Scheme of the storage tank (TRNSYS type 4a)

In this TRNSYS type, fluid entering the hot side of the tank is added to the tank node below the first auxiliary heater. To disable the operation of that element, the maximum heat rate of that element is set to zero. This parameter disables any value that can be introduced as a parameter for the set point temperature and dead band. This type also allows to consider a second heating element, which heat rate is also set to zero. Fluid entering the cold side of the tank enters the bottom node.

This element receives the outlet temperature and the flow rate of the type 50a as inputs for the inlet at the hot side, and gives information of the temperature and flow rate in the cold side as an output to the pump type 114 input.

The temperature of the cold side inlet corresponds to the temperature of the water grid, which is set to 15ºC, as a constant input. The mass flow rate for this inlet is taken by the "*Load DHW profile*" output, and it corresponds to the hot side outlet flow rate. The

temperature at the hot side outlet results on the heat delivered by the heat source. The ambient temperature is a constant input, which is set to 20 ºC.

An auxiliary heater is applied in the usage circuit after the fluid leaves the storage tank, in order to supply the remaining heat, for the case that the outlet temperature of the tank is lower than the utilization temperature, which is defined as 60 ºC. This value corresponds to the set point temperature input, for "*type 6*" selected element from the existing TRNSYS library. The parameters need are the maximum heating rate, overall loss coefficient for heater during operation, and the efficiency. The maximum heating rate was defined as 24 kW, based on technical data of a commercialized model of a wall mounted boiler, Vulcano AQUASTAR ZWC 24/28. In order to account for the losses when the required heating load is not of 100%, an efficiency of 85% was considered, for a nominal efficiency of 90.6%. The overall loss coefficient for heater during operation accounts for extra losses to the ambient. As the efficiency was under assessed, this value was set to zero.

Graphical outputs to verify an adequate response of the system were added to the system, through online plotters. Through "*Collector data*" plotter, graphics of the solar hybrid collector variables are visualized, including the temperatures at the inlet and outlet of the collector, mass flow rate, incident radiation, rate of useful energy gain and electrical power output. The "*Use*" plotter includes the variation of variables of the utilization circuit and the storage tank: temperatures at the storage tank outlets, in the cold and in the hot side, temperature and flow rate at the auxiliary heater outlet, and rate of energy delivery to the fluid stream, at the auxiliary heater.

5.3.2 Evaluation of the energetic performance of the system

The interest of using a solar hybrid collector for a DHW system can be assessed by the savings in the conventional energy to fulfil the heating needs along the year. Thus, it is necessary to determine those total needs, the fraction that can be obtained through the solar collector, which corresponds to the solar fraction, and the remaining energy that has to be supplied by an auxiliary heater. The extra electrical output that is obtained with the PV modules of the hybrid collector have also to be accounted for. The electrical output from the collector and the heat obtained from the primary circuit in the storage tank represent the annual energy savings. Those energy savings have to be converted on the actual economic savings, depending on the value of the electrical and thermal power.

The thermal and electrical outputs of the solar collector depend on the climate where the collector will be applied, mainly on the radiation and the ambient temperature. The annual savings reached with the use of a hybrid collector are evaluated for two different characteristic Portuguese climates: Porto, with temperate climate, but cloudy and humid, and Faro, with warm climate, sunny and dry.

A dynamic simulation of the DHW system described in the previous section, was run for one year, for both climates: Porto and Faro. The relevant variables were integrated, on an hourly basis, along the period defined for simulation, through Quantity Integrators, of type 24. The outputs were exported to files, through Printers. The variables that are recorded are the incident radiation flux on the tilted surface (G), rate of useful energy gain (Q_{Coll}) and electrical power output (E_{Coll}) in the hybrid collector, energy rate to load in the storage tank ($Q_{Coll\text{-}DHW}$), rate of energy delivery to the fluid stream at the auxiliary heater, (Q_{Aux}) and total needs of heat for the DHW applications (Q_{DHW}).

"Daily integration" calculates the totals for each day, for the 365 days of the year, for the selected variables, and "Simulation integration" for the annual totals.

In tables 5.2 and 5.3 the relevant energy totals along one year are listed, for the two climates, and for the different packing factors considered. The total saved thermal energy ($Q_{TH\text{-}S}$) during one year results from the affectation of thermal energy saved ($Q_{Coll\text{-}DHW}$) with the collectors by the efficiency of a typical boiler, considered 85%:

$$Q_{TH\text{-}S} = Q_{Coll\text{-}DHW}/0.85 \tag{5.3}$$

Table 5.2 - Energy totals and final energy annual savings with the use of hybrid DHW system, in Porto, for different values of *Pf*

	P_f = 19%	P_f = 38%	P_f = 56%	P_f = 75%
G (kWh/m^2/y)	1791	1791	1791	1791
Q_{Coll} (kWh/y)	3090	2619	2211	1834
E_{Coll} (kWh/y)	217	442	677	922
$Q_{Coll\text{-}DHW}$ (kWh/y)	2760	2365	2019	1698
Q_{Aux} (kWh/y)	632	830	1069	1361
Q_{DHW} (kWh/y)	3059	3059	3059	3059
*Saved thermal energy (*kWh/y)	3247	2782	2375	1998
*Saved electrical energy (*kWh/y)	217	443	678	922
*Total energy savings (*kWh/y)	3464	3225	3053	2919

Table 5.3 - Energy totals and final energy annual savings with the use of hybrid DHW system, in Faro, for different values of *Pf*

	P_f = 19%	P_f = 38%	P_f = 56%	P_f = 75%
G (kWh/m^2/y)	2186	2186	2186	2186
Q_{Coll} (kWh/y)	3919	3351	2854	2393
E_{Coll} (kWh/y)	255	521	801	1093
$Q_{Coll\text{-}DHW}$ (kWh/y)	3463	2985	2565	2175
Q_{Aux} (kWh/y)	255	391	591	890
Q_{DHW} (kWh/y)	3059	3059	3059	3059
*Saved thermal energy (*kWh/y)	4074	3512	3018	2559
*Saved electricity (*kWh/y*)*	255	521	801	1093
*Total energy savings (*kWh/y)	4329	4033	3819	3652

It can be verified from Table 5.2 and 5.3, referent to Porto and Faro, respectively, that the increasing of the packing factor causes a reduction on the total energy savings.

This analysis accounts for the thermal and electrical energy equally. Regarding the different cost of thermal energy and electricity, the impact of the packing factor may change when analysing the results from the economic perspective. In the following section an analysis is carried out, considering the economic impact of the different values of the packing factor on the annual energy cost, for the same type of domestic household.

5.3.3 Analysis of the influence of the packing factor on annual energy savings for a DHW system using hybrid solar collectors

The annual energy savings obtained through TRNSYS and listed in Table 5.2 and 5.3 are converted to the equivalent economical savings, considering the domestic tariff for natural gas and electrical power in Portugal, that is 0.093 €/kWh$_{Th}$ and 0.218 €/kWh$_{El}$, respectively, according to average values from eurostat (2015a).

The values for the energetic and economic savings achieved for Porto and Faro are listed in Table 5.4 and Table 5.5, respectively.

Table 5.4 - Energetic and economic annual savings with the use of hybrid DHW system, in Porto, for different values of *Pf*

	P_f = 19%	P_f = 38%	P_f = 56%	P_f = 75%
Saved thermal energy (kWh/y)	3247	2782	2375	1998
Saved electricity (kWh/y)	217	443	678	922
Thermal energy savings (€/y)	302	259	221	186
Electricity savings (€/y)	47	96	148	201
Total annual savings (€/y)	349	355	369	387

Table 5.5 - Energetic and economic annual savings with the use of hybrid DHW system, in Faro, for different values of *Pf*

	$P_f = 19\%$	$P_f = 38\%$	$P_f = 56\%$	$P_f = 75\%$
Saved thermal energy (kWh/y)	4074	3512	3018	2559
Saved electricity (kWh/y)	255	521	801	1093
Thermal energy savings (€/y)	379	327	281	238
Electricity savings (€/y)	56	114	175	239
Total annual savings (€/y)	434	440	455	476

Although the thermal energy savings are higher than the ones for electricity, it can be observed in Table 5.4 and Table 5.5 that the economical balance is mainly influenced by the savings in electrical power, because of the high price of electricity in Portugal. This implies that annual savings depends on the packing factor. The graphic representation of the results for the annual savings is showed in Figure 5.3 and 5.4, for a better perception of the tendencies.

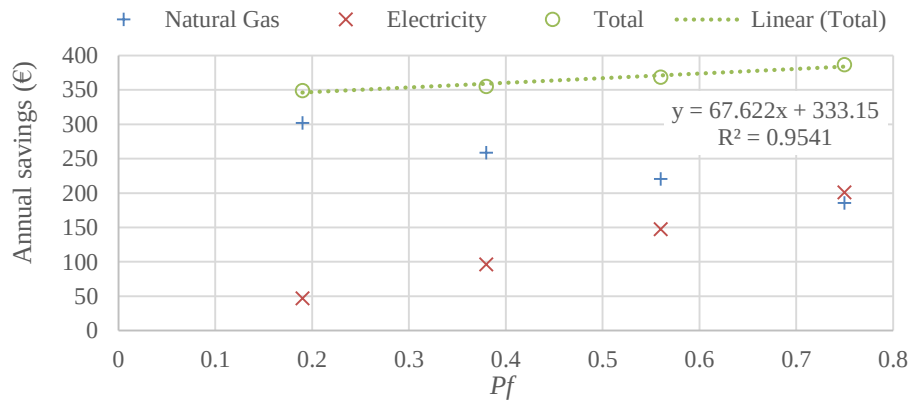

Figure 5.3 - Annual savings with the hybrid solar DHW system, for costs with natural gas and electricity, in Porto

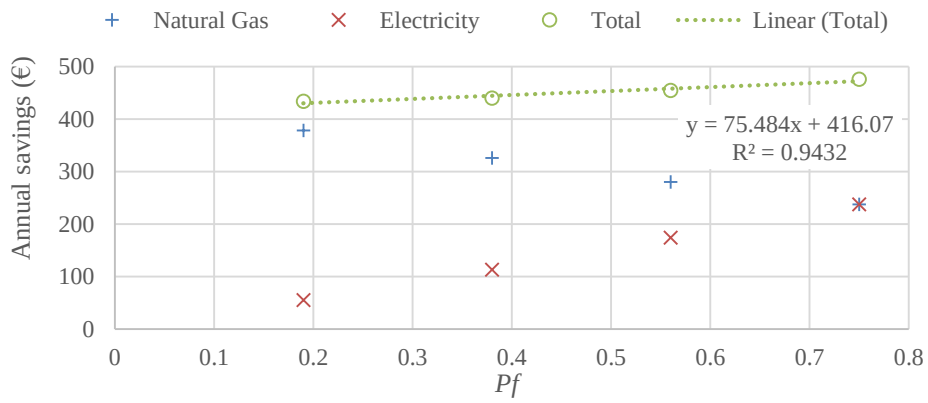

Figure 5.4 - Annual savings with the hybrid solar DHW system, for costs with natural gas and electricity, in Faro

It can be confirmed from the analysis of Figures 5.3 and 5.4 that the total savings increase with the packing factor, namely in Faro.

The same procedure is carried out for a different country, where the relation of the tariffs for electricity and natural gas is lower than for Portugal. In Bulgaria, the domestic tariff for natural gas and electrical power are 0.049 €/kWh and 0.083 €/kWh respectively. This country presents one of the lowest relative price for electricity, compared to natural gas. The results are listed in Table 5.6, and presented graphically in Figure 5.5.

Table 5.6 - Energetic and economic annual savings with the use of one hybrid collector, in Sofia, Bulgaria, for different values of Packing Factor

	P_f = 19%	P_f = 38%	P_f = 56%	P_f = 75%
Saved thermal energy (kWh/y)	2182	1860	1580	1328
Saved electricity (kWh/y)	164	333	508	691
Thermal energy savings (€/y)	91	77	66	55
Electricity savings (€/y)	14	28	42	57
Total annual savings (€/y)	104	105	108	113

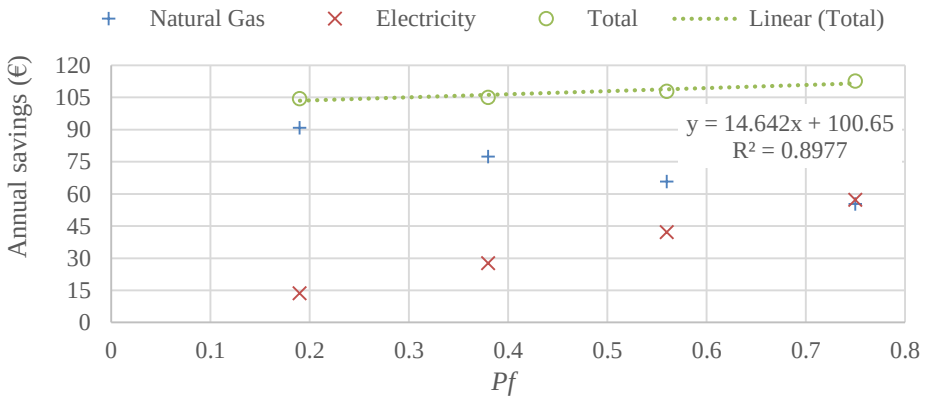

Figure 5.5 - Annual savings with the hybrid solar DHW system, for costs with natural gas and electricity, in Sofia, Bulgaria

It is observed from Figure 5.5 that, even in this scenario, the annual savings depend mainly from the packing factor, but in this case with a lower proportion.

It can be then concluded than the best configuration for a hybrid collector is the maximum area of the absorber covered with PV cells. A packing factor of 100% cannot be achieved, because there is a minimum space without PV cells that is needed to encapsulate the cells and integrate the electrical connections.

5.4 Environmental impact for different packing factors

The already referred study by Herrando *et al.* (2014) also included an estimation of the possible emissions savings achieved by the installation of a PV/T system, compared to the emissions associated with the use of conventional energy sources, based on the common current practices of buying the electricity from the grid, and using a boiler, heat pump or electrical heater to satisfy the hot water demand. With regards to electricity, the emission saving is due to the difference between the emissions associated with the purchase of all electricity from the grid and the emissions incurred after a PV/T unit is installed, while the hot water saving arises from the reduction in the required fuel for heating, from the conventional levels to the lower auxiliary heating levels needed by the PV/T system.

They concluded that the CO_2 emission savings due to PVT hot water production are more significant than the equivalent emission savings due to electricity production. Nevertheless, the total percentage of emission reductions is more sensitive to the electrical than the thermal emissions, due to the fact that the contribution of electricity generation towards the total emissions is higher than that associated with hot water production. Furthermore, the emission reductions due to hot water production decrease strongly as flow rate increases, due to the lower amount of net heat added to the tank, which means that more auxiliary heat is required. Therefore, low collector flow-rates can achieve a higher percentage of total emission savings. The emissions savings due to PVT electricity production increase as the covering factor *Pf* increases, while those due to hot water production decrease. Still, since the CO_2 emissions due to electricity production are significantly larger than those for hot water production, the total emission reductions follow the electrical trend, suggesting the use of high covering factors.

An analysis to the effect of the packing factor will be then presented, now in the perspective of the environmental impact. The savings on natural gas and electricity can be transposed to the corresponding avoided emissions of greenhouse gases. It was used emission factors defined in Despacho nº 17313/2008 (DR, 2008) that correspond to 56.1 kg CO_{2e}/GJ for natural gas and 0.47 kg CO_{2e}/kWh for electricity.

Table 5.7 - Annual savings on CO_2 emissions with the use of a hybrid DHW system, in Porto, for different values of *Pf*

	P_f = 19%	P_f = 38%	P_f = 56%	P_f = 75%
Saved Natural Gas CO_2 emissions (kg CO_{2e})	656	562	480	403
Saved electricity CO_2 emissions (kg CO_{2e})	102	208	318	433
Total saved emissions (kg CO_{2e})	758	770	798	837

Table 5.8 - Annual savings on CO_2 emissions with the use of a hybrid DHW system, in Faro, for different values of *Pf*

	P_f = 19%	P_f = 38%	P_f = 56%	P_f = 75%
Saved Natural Gas CO_2 emissions (kg CO_{2e})	823	709	609	517
Saved electricity CO_2 emissions (kg CO_{2e})	120	245	377	514
Total saved emissions (kg CO_{2e})	943	954	986	1031

Similarly to what happened with the annual savings, a higher packing factor also improves the environmental impact of the use of hybrid solar collectors in DHW systems. The type of the relation can be verified in Figure 5.6.

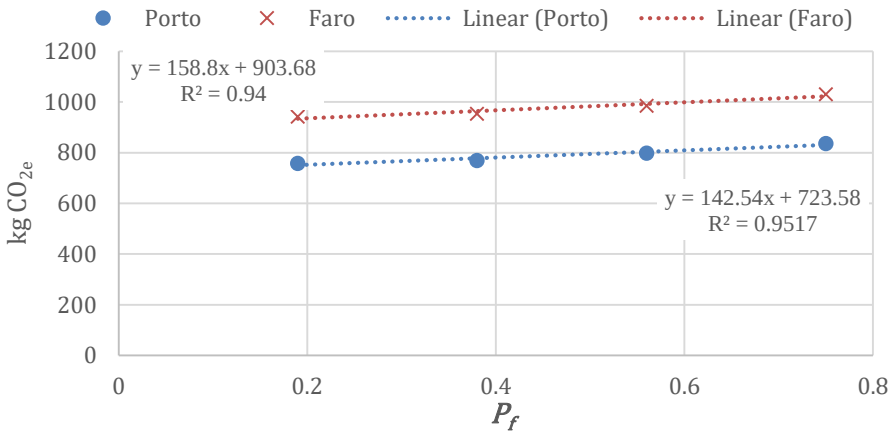

Figure 5.6. Annual saved emissions dependence on the packing factor for hybrid solar DHW system, in Porto and Faro

It can be confirmed in Figure 5.6 that the saved emissions during one year increase with the packing factor used in the hybrid solar collector, with a second order relation.

5.5 Conclusions

In this chapter a domestic hot water system with integrated hybrid solar collectors was modelled, using the TRNSYS software for dynamic simulation along one year. The thermal and electrical performance of the system was characterized, for different values of the packing factor of the hybrid collector, and considering the climatic data from Porto and

Faro. The results were assessed with respect to the energy and economic savings. The environmental benefits of the use of solar hybrid collectors was also evaluated, through the calculation of the CO_2 saved emissions, by comparison with the use of a traditional system, for equivalent energy outputs, using natural gas and electricity. The studies were all conducted focusing in the influence of the packing factor. It was concluded from the analysis the following main features:

- The total energy savings along one year decrease with the packing factor, with a linear proportion of 971 kWh/y for Porto 1207 kWh/y for Faro;
- The annual savings increase with the packing factor, due to the high cost of electricity, with a linear proportion of 66€ for Porto and 75€ for Faro. This corresponds to total savings (gas and electricity) up to 0.1265 €/kWh_{th} for Porto and 0.1556 €/kWh_{th} for Faro, regarding annual energy demand of the studied DHW system.
- The saved CO_2 emissions through the use of solar hybrid collectors in DHW systems increase with the packing factor, with a higher proportion for a system installed in Faro, 159 kg CO_{2e}, compared with Porto, with a coefficient of 143 kg CO_{2e}. This corresponds to total savings up to 0.2736 CO_{2e}/kWh_{th} for Porto and 0.3370 kg CO_{2e}/kWh_{th} for Faro, considering the annual energy demand of the studied.

This analysis leads to the general conclusion that a high packing factor is advantageous, according to the perspective of economic savings and environmental benefit. These findings can contribute to the diversification of the current range of commercial products available for solar energy conversion, which in Portugal are limited to photovoltaic-only and thermal-only panels. The ecological impact is well defined, and may supply grounding arguments for the certification entities, in a process of certification of a commercial PV/T collector. This advantage can also be integrated in a larger perspective of institutional measures to benefit the acquisition of “environment friendly” systems, recognizing the contribution of such a technology for the achievement of goals included in international measures for the climate change. Those incentives, combined with the monetary savings that were also quantified, may represent evidence for manufacturers and users for the assertion of PV/T collectors on the solar technology market. It is never too

much to reinforce the idea of the saved installation space and improved aesthetics, with the combined production of electricity and heat in the same equipment.

Chapter 6.

General conclusions and future work

This chapter summarizes the main contributions and findings from this thesis for the formulation of mathematical models of hybrid PV/T collectors. The topics for possible future work are also identified.

6.1 Summary of the work developed and main findings

The global purpose of this work was the characterization of the performance of water hybrid PV/T solar collectors, through experimental tests and a parametric analysis carried out using a developed mathematical model. It was of particular importance to understand the effect of the packing factor (*Pf*) on the collector performance, and to verify the best layout for the application of the PV modules.

The experimental tests were performed using a prototype with area of about 0.5 m^2, instrumented in order to measure the useful heat and power for different operational conditions of the water inlet temperature ($T_{f,IN}$), under registered environmental conditions (T_{amb}, G). It was followed a procedure defined by the standard for test methods of thermal systems (IPQ, 2007). The PV modules used consisted in 4x2 series arrangements of 5" c-Si cells. The cells, with nominal efficiency of about 18%, were encapsulated into EVA layers and laminated between two layers of 4mm thick glass. Three sets of tests were carried out in order to identify the effect of *Pf*, corresponding to the application of 1, 2 and 3 PV

modules over the absorber plate. Those configurations corresponded to *Pf* of 24%, 49% and 73%, respectively. The results for the thermal (η_{Th}), electrical (η_{El}) and combined efficiency (η_G) were presented as linear functions of the reduced temperature difference (T^*). Chauvenet criterion was applied to the results of η_{Th} to discard outliers from the final set of observations, previously validated according to stability conditions. In Table 6.1 are listed the regression analysis coefficients for η_{Th}, η_{El} and η_G obtained for the three configurations.

Table 6.1 – Regression analysis coefficients for η_{Th}, η_{El} and η_G obtained for configuration with 1, 2 and 3 PV modules applied

Pf	Intercept, $F'\eta_{Th,0}$ (%)	Slope, $F'U_L\eta_{Th}$ ($Wm^{-2}K^{-1}$)	Intercept, $F'\eta_{El,0}$ (%)	Slope, $F'U_L\eta_{El}$ ($Wm^{-2}K^{-1}$)	Intercept, $F'\eta_{G,0}$ (%)	Slope, $F'U_L\eta_G$ ($Wm^{-2}K^{-1}$)
24%	69	-5.30	2.6	-0.052	73	-5.84
49%	67	-6.26	5.4	-0.156	73	-6.41
73%	64	-6.40	7.6	-0.147	71	-6.54

The experimental results confirm some already known facts. The application of PV modules in a solar thermal collector reduces its thermal efficiency. Moreover, the increase in *Pf* intensifies that reduction, as can be easily found in the existing literature. However, the influence of *Pf* in the thermal losses ($F'U_L\eta_{Th}$) determined experimentally was still not referenced. Statistical techniques were applied to prove the existence of a correlation between *Pf* and the regression analysis coefficients for η_{Th}. It was found an almost linear reduction of 2% in η_{Th} per 24% *Pf* increase. The values for the thermal losses were found to increase with *Pf* from typical values for flat plate selective solar collectors of 4 W/(m^2K) to 5.3 W/(m^2K) with *Pf* = 24% and 6.26 W/(m^2K) for *Pf* = 49%. A higher emissivity of the PV cells, compared with the one of the absorber plate, results in higher losses that may explain that fact.

The increase of *Pf* obviously leads to a roughly linear increase in η_{El}, of about 2.5% per 24% of *Pf* increase. Nevertheless, the values of the electrical efficiency estimated based in the real PV area (η_{El}^*) were much lower than the nominal values of PV cells efficiency, as can be confirmed in Table 6.1. It was not identified a consistent relation between *Pf* and η_{El}^*. Specific comparison between the experimental results and referenced values found in literature was presented in subsections 3.3.1 and 3.3.3. References addressing to the influence of *Pf* in the electrical losses, reflected on the slope of η_{El}, are scarce, namely experimental studies.

The opposite effects of *Pf* in the thermal and electrical efficiencies does not allow to understand at the outset the *Pf* effect on the global efficiency. It was found a very small decrease of η_G for the *Pf* increase from 49% to 73%. However, already existing references state the opposite effect. Nevertheless, the differences are small. Once again, the experimental study of the *Pf* effect in the slope of η_G is a contribution to the global knowledge on the hybrid PV/T solar collectors.

The estimation of the uncertainty associated to the calculations of the thermal ($u_c(\eta_{Th})$) and electrical ($u_c(\eta_{El})$) efficiencies was exposed in section 3.3.3. It was found that the major contributor to the $u_c(\eta_{Th})$ and $u_c(\eta_{El})$ was the irradiance (G), due to the long period since the calibration of the pyranometer. The uncertainty associated to the electrical efficiency, of about 0.4%, can be neglected for the settlement of the uncertainty of the global efficiency. The uncertainty associated to the global efficiency is, thus, the uncertainty associated to the thermal efficiency ($u_c(\eta_{Th})$), that are about 7% (see table 3.8).

A comprehensive analysis on the effects of environmental (G, T_{amb}), operational ($T_{f,IN}$) and design parameters (*Pf*, layout "*In*" vs "*Out*") on the thermal (η_{Th}), electrical (η_{El}, η_{El}*) and combined (η_G) efficiencies of a PV/T-w collector was presented in chapter 4. This parametric study was carried out based on the results obtained through a developed mathematical model of a generic PV/T collector, implemented using EES software. The model was adapted to the particular geometry of the tested prototype, in order to be validated. The numerical and experimental results of η_{Th}, η_{El} and η_G were first compared through of a linear regression analysis. Statistical tests were applied to the slope values that have been determined, and its confidence intervals were estimated with 95% confidence level. Namely for the configurations with 1 and 2 PV modules applied, that interval included unity, or presented a maximum deviation of 0.002 (Table 4.2), meaning that a good degree of agreement between experimental and numerical results was achieved.

The analysis of the influence of PV cell layout, *Pf* and $T_{f,IN}$ was performed with ambient temperature of 20ºC, and total irradiance of 1000 W/m^2. The separated effects of some of the referred parameters were already known: an increase in $T_{f,IN}$ leads to the decrease in the efficiencies, *Pf* favours η_{El} but causes a decrease of η_{Th} and η_G, and the "Inlet" layout favours η_{El} and η_{El}*. Reporting to Figure 4.20, the linear decrease of η_{Th} and η_G with *Pf* was 17.1% and 7%, respectively. The analysis focused mainly in the unknown effects, and in the combined effects of conflicting parameters.

It was proved with the parametrical study that applying the PV modules on the inlet side of the collector is the best option, both regarding for η_{Th} and η_G, but with low significance. Simulations were carried out for different values of *Pf* (25%, 35%, 50% and 75%), considering the two layouts: PV modules applied at the inlet ("*In*"), and at the outlet ("*Out*"). It was proved that the influence of the layout was more pronounced for balanced values of *Pf* (Figure 4.19). The combined effect of $T_{f,IN}$ was also included, considering inlet fluid temperatures of 20ºC, 40ºC and 60ºC. The impact of the layout adopted was slightly more pronounced for the combined efficiency results, with a maximum difference of 3.1% for *Pf*=25% and $T_{f,IN}$ = 60ºC (Table 4.6). This is understandable, since the configuration with *Pf* = 25% is the most "unbalanced", with extreme minimum and maximum values for cells average temperature, respectively for "*in*" and "*out*" configurations. Reporting to Figures 4.21 and 4.22, the decrease of η_{El} and η_{El}* with *Pf* is in the order of 2.6% and 0.04% per 25% increase in *Pf*, so, basically, *Pf* has no effect in η_{El}*. It was found a linear decrease in η_{El}* with $T_{f,IN}$ of about 41%/(Km^2/W), while, for η_{El} it ranged from 10%/(Km^2/W) for *Pf* = 25% to 41%/(Km^2/W), for *Pf* = 100%.

The effect of the ambient temperature (T_{amb}) and solar irradiance (G) in the increase of η_{Th} is well known from literature and practice. Its combined influence was analysed, considering values for G from 400 to 1000 W/m^2, and ambient temperature of 10°C, 20°C and 30°C. A maximum value of 71.3% was found for η_G, with G = 1000 W/m^2, T_{amb} = 30ºC and *Pf* = 25%. It was found that the effect of G reduces with T_{amb}, both for results of η_{Th} and η_G. Similarly, it was found that G inhibits the effect of T_{amb} on η_G. The combined effect of $T_{f,IN}$ was also included, considering temperatures ranging from 25ºC to 60ºC. Despite its effect is opposite to the one of G, it was verified that it enhances the increase of η_G with G. The combined effects of G, T_{amb} and *Pf* were also addressed. It was found that the *Pf* enhances the increase of the combined efficiency with G, namely for a low value of T_{amb} (10ºC).

The performance of a DHW system integrating PV/T hybrid collectors for a typical 4 person household is carried out in chapter 5, taking into account energy, economic and environmental perspectives. A dynamic simulation was developed using TRNSYS, considering two distinct climates in Portugal: Porto and Faro. The impact of *Pf* was assessed, through its impact in the annual energy, economic and CO_2 emissions savings through the use of the PV/T collector.

It was concluded that the annual energy savings decreased with *Pf*, which was expected, since the former conclusions indicated that the electric output obtained with more PV cells area did not make up for the heat lost with its application. However, when the annual energy savings were converted in economic savings, through the attribution of electricity and natural gas prices in Portugal, it was verified that the electricity saved with *Pf* increase pays off the savings decrease in natural gas. Through a perspective of CO_2 emissions saved, it was also proved that maximize *Pf* benefits the environmental performance of a PV/T system. Thus, PV/T collectors with maximum *Pf* are advantageous for the users.

As a global conclusion, the use of hybrid PV/T collectors are favourable according to an economical perspective of annual savings. However, it was not proved an improved global energetic performance, when compared with thermal-only collectors, in those absolute terms. The value of the electric output, in particular situations when it is need, may contribute to relativize that disadvantage. Other collateral grounds, like compactness of the system and aesthetics of the building, may also be valid for the option for a PV/T collector. The environmental benefits are strong, and are maximized with maximum values of *Pf*.

6.2 Future work

Throughout the present work, several relevant findings were identified, in the context of achieving the main objectives purposed. The presented work focused on different aspects of the performance evaluation of hybrid solar collectors, some of which may be further developed.

It was found that the increase of the area of the solar collector with PV cells applied has a negative effect on the energetic performance of the system. In order to complement this study, an analogous analysis can be developed, based in the exergy performance of the PV/T collector. The impact of *Pf* should be also focused.

The economic assessment of the performance of the hybrid collector just took into account the savings through the energy that could be annually retained. This study could be complemented with a life cycle cost analysis, with the inclusion of the initial and operational cost of the system and economic scenarios.

The relevance of the use of hybrid collectors could be also more perceived, when its performance is assessed when integrated in examples of real buildings, with real cases of energetic demands. Two different interesting situations could be its integration in zero-net energy buildings, or in isolated buildings with no electric grid.

Those complementary studies would contribute to a global perception of the benefits, and disadvantages, of the application of PV/T collectors.

Bibliography

Affolter, Pascal, Wolfgang Eisenmann, Huber Fechner, Mathias Rommel, Anton Schaap, Henrik Sorensen, Yiannis Tripanagnostopoulos, and Herbert Zondag. 2006. PVT Roadmap - a European Guide for the development and market introduction of a PV-Thermal technology. Energy Resource Centre of the Netherlands.

Agrawal, B., and G. N. Tiwari. 2010. "Optimizing the energy and exergy of building integrated photovoltaic thermal (BIPVT) systems under cold climatic conditions." Review of 171th ref on Riffat and sAFFA (2011). *Applied Energy* 87 (2):417-426. doi: DOI 10.1016/j.apenergy.2009.06.011.

Agua Quente Solar. 2015a. "Certified solar thermal collectors - Cicero Hellas SA, model Calpak 20 VT." Accessed 23/07/2015. http://www.aguaquentesolar.com/_fich/20/CALPAK_20VT.pdf.

Agua Quente Solar. 2015b. "Certified solar thermal collectors - Jacques Giordano Industries, model C8/12 S.U." Accessed 23/07/2015. http://www.aguaquentesolar.com/_fich/20/PSK_017-2008.pdf.

Agua Quente Solar. 2015c. "Certified solar thermal collectors - Richworld Renewables – Sistemas de Energias Renováveis, Lda, model B200." Accessed 23/07/2015. http://www.aguaquentesolar.com/_fich/20/PSK_077-2009_Bongas.pdf.

Agua Quente Solar. 2015d. "Certified solar thermal collectors - Solarfocus GmbH, model CPC S1." Accessed 23/07/2015. http://www.aguaquentesolar.com/_fich/20/011-7S095_F.pdf.

Agua Quente Solar. 2015e. "Certified solar thermal collectors - Sunda Solartechnik GmbH, model SEIDO 1." Accessed 23/07/2015. http://www.aguaquentesolar.com/_fich/20/011-7S127_R.pdf.

Água Quente Solar. 2004. Guia para instaladores de colectores solares. edited by Direcção Geral Energia e Geologia.

Água Quente Solar. 2015. "Colectores solares térmicos certificados." Accessed 23/07/72015. http://www.aguaquentesolar.com/observatorio/equipamentos/colectores.asp.

Also Media Ltd. 2013. "Pilkington Optiwhite™ Literature." Nippon Sheet Glass Co., Ltd., Pilkington Group Limited Accessed 23/04/2013. http://www.pilkington.com/products/bp/bybenefit/solarenergy/optiwhitese/literature.htm.

Ammar, Majed Ben, Maher Chaabene, and Zied Chtourou. 2013. "Artificial Neural Network based control for PV/T panel to track optimum thermal and electrical power." *Energy Conversion and Management* 65 (0):372-380. doi: http://dx.doi.org/10.1016/j.enconman.2012.08.003.

Anderson, T. N., M. Duke, G. L. Morrison, and J. K. Carson. 2009. "Performance of a building integrated photovoltaic/thermal (BIPVT) solar collector." Review of 175th ref on riffat and Saffa (2011). *Solar Energy* 83 (4):445-455. doi: DOI 10.1016/j.solener.2008.08.013.

ANSYS FLUENT.

APA, (Agência Portuguesa do Ambiente). 2014. Portuguese national inventory report on greenhouse gases, 1990 - 2012.

APREN. 2015a. "Potência: VARIAÇÃO ANUAL DE POTÊNCIA LIGADA À REDE PÚBLICA DA PRE RENOVÁVEL EM PORTUGAL CONTINENTAL." Accessed 23/03/2015. http://apren.pt/pt/dados-tecnicos-3/dados-nacionais-2/potencia-2/3-6/variacao-anual-de-potencia-ligada-a-rede-publica-da-pre-renovavel-em-portugal-continental/.

APREN, (Associação Portuguesa das Energias Renováveis). 2015b. "EVOLUÇÃO DO PESO DA ELECTRICIDADE DE ORIGEM RENOVÁVEL EM PORTUGAL ENTRE 1999 E 2014 (COM CORRECÇÃO DE HIDRAULICIDADE)." Accessed 7/07/2015. http://apren.pt/pt/dados-tecnicos-3/dados-nacionais-2/producao-2/a-producao-de-electricidade-em-portugal-2/1-6/evolucao-do-peso-da-electricidade-de-origem-renovavel-em-portugal-entre-1999-e-2014-com-correccao-de-hidraulicidade/.

APREN, (Associação Portuguesa das Energias Renováveis). 2015c. "A produção de electricidade em Portugal: Peso das fontes de produção de electricidade em Portugal em 2014 (c/ correcção de hidraulicidade)." Accessed 23/03/2015. http://www.apren.pt/pt/dados-tecnicos-3/dados-nacionais-2/producao-2/a-producao-de-electricidade-em-portugal-2/1-2/peso-das-fontes-de-producao-de-electricidade-em-portugal-em-2013-c/-correccao-de-hidraulicidade/.

APREN, (Associação Portuguesa das Energias Renováveis). 2015d. "Production of electricity in Portugal - Evolution between 1999 and 2013." Accessed 07/07/2015. http://www.apren.pt/pt/dados-tecnicos-3/dados-nacionais-2/producao-2/a-producao-de-electricidade-em-portugal-2/1-1/evolucao-da-producao-de-electricidade-em-portugal-entre-1999-e-2013-c/correccao-de-hidraulicidade/.

ArchiExpo. 2015. "Products-Renewable energies-Sun rain-Evacuated tubular solar thermal collector / with frame-CPC " Accessed 04/08/2015. http://www.archiexpo.com/prod/sun-rain/product-108627-1270689.html.

Armstrong, S., and W. G. Hurley. 2010. "A thermal model for photovoltaic panels under varying atmospheric conditions." *Applied Thermal Engineering* 30 (11–12):1488-1495. doi: http://dx.doi.org/10.1016/j.applthermaleng.2010.03.012.

Aste, Niccolò, Claudio Del Pero, and Fabrizio Leonforte. 2012. "Optimization of Solar Thermal Fraction in PVT Systems." *Energy Procedia* 30 (0):8-18. doi: http://dx.doi.org/10.1016/j.egypro.2012.11.003.

Aste, Niccolò, Claudio del Pero, and Fabrizio Leonforte. 2014. "Water flat plate PV–thermal collectors: A review." *Solar Energy* 102 (0):98-115. doi: http://dx.doi.org/10.1016/j.solener.2014.01.025.

Axaopoulos, Petros J., and Emmanouil D. Fylladitakis. 2013. "Performance and economic evaluation of a hybrid photovoltaic/thermal solar system for residential applications." *Energy and Buildings* 65 (0):488-496. doi: http://dx.doi.org/10.1016/j.enbuild.2013.06.027.

Bai, Y., T. T. Chow, C. Menezo, P. Dupeyrat, and Publishing Hindawi. 2012. "Analysis of a Hybrid PV/Thermal Solar-Assisted Heat Pump System for Sports Center Water Heating Application." *International Journal of Photoenergy*.

Bejan, Adrian. 1993. *Heat transfer*. New York [etc.]: John Wiley & Sons.

Bergene, T., and O. M. Lovvik. 1995. "Model calculations on a flat-plate solar heat collector with integrated solar cells." Review of 61th ref on Riffat and Cuce (2011). *Solar Energy* 55 (6):453-462.

Bhargava, A. K., H. P. Garg, and R. K. Agarwal. 1991. "Study of a Hybrid Solar-System Solar Air Heater Combined with Solar-Cells." *Energy conversion and management* 31 (5):471-479.

Bhattarai, S., J. H. Oh, S. H. Euh, G. K. Kafle, and D. H. Kim. 2012. "Simulation and model validation of sheet and tube type photovoltaic thermal solar system and conventional solar collecting system in transient states." *Solar Energy Materials and Solar Cells* 103:184-193. doi: DOI 10.1016/j.solmat.2012.04.017.

Boer, K. W., and G. Tamm. 2003. "Solar conversion under consideration of energy and entropy." Review of 15th ref on Riffat and Cuce (2011). *Solar Energy* 74 (6):525-528. doi: 10.1016/s0038-092x(03)00198-1.

Brinkworth, B. J., B. M. Cross, R. H. Marshall, and H. X. Yang. 1997. "Thermal regulation of photovoltaic cladding." *Solar Energy* 61 (3):169-178.

Brogren, M., and B. Karlsson. 2001. "LOW-CONCENTRATING WATER-COOLED PV-THERMAL HYBRID SYSTEMS FOR HIGH LATITUDES." 17th European Photovoltaic Solar Energy Conference and Exhibition, Munich.

Brogren, Maria, Mats Rönnelid, and Björn Karlsson. 2000. PV-thermal hybrid low-concentrating CPC module.

Buildings Performance Institute Europe. 2011. Europe's buildings under the microscope: A country-by-country review of the energy performance of buildings.

Calise, Francesco, Massimo Dentice d'Accadia, and Laura Vanoli. 2012. "Design and dynamic simulation of a novel solar trigeneration system based on hybrid photovoltaic/thermal collectors (PVT)." *Energy conversion and management* 60 (0):214-225. doi: 10.1016/j.enconman.2012.01.025.

Calise, Francesco, Massimo Dentice d'Accadia, and Antonio Piacentino. 2014. "A novel solar trigeneration system integrating PVT (photovoltaic/thermal collectors) and SW (seawater) desalination: Dynamic simulation and economic assessment." *Energy* 67 (0):129-148. doi: http://dx.doi.org/10.1016/j.energy.2013.12.060.

Candelise, Chiara, Mark Winskel, and Robert J. K. Gross. 2013. "The dynamics of solar PV costs and prices as a challenge for technology forecasting." *Renewable and Sustainable Energy Reviews* 26:96-107. doi: http://dx.doi.org/10.1016/j.rser.2013.05.012.

Chapin, D. M., C. S. Fuller, and G. L. Pearson. 1954. "A new silicon p-n junction photocell for converting solar radiation into electrical power [3]." *Journal of Applied Physics* 25 (5):676-677. doi: 10.1063/1.1721711.

Charalambous, P. G., S. A. Kalogirou, G. G. Maidment, and K. Yiakoumetti. 2011. "Optimization of the photovoltaic thermal (PV/T) collector absorber." Review of 214th ref on Riffat and Saffa (2011). *Solar Energy* 85 (5):871-880. doi: DOI 10.1016/j.solener.2011.02.003.

Charalambous, P. G., G. G. Maidment, S. A. Kalogirou, and K. Yiakoumetti. 2007. "Photovoltaic thermal (PV/T) collectors: A review." *Applied Thermal Engineering* 27 (2-3):275-286. doi: DOI 10.1016/j.applthermaleng.2006.06.007.

Chen, Hongbing, and Saffa Riffat. 2011. "Development of photovoltaic thermal technology in recent years: a review." *The international journal of low carbon technologies* 6 (1):1-13.

Chow, T. T. 2003. "Performance analysis of photovoltaic-thermal collector by explicit dynamic model." Review of 74th ref on Riffat and Cuce (2011). *Solar Energy* 75 (2):143-152. doi: DOI 10.1016/j.solener.2003.07.001.

Chow, T. T. 2009. "Annual performance of building-integrated photovoltaic/water-heating system for warm climate application." Review of 95th ref on Riffat and Cuce (2011). *Applied Energy* 86 (5):689-696.

Chow, T. T. 2010. "A review on photovoltaic/thermal hybrid solar technology." Review of 91th ref on Riffat and Cuce (2011). *Applied Energy* 87 (2):365-379. doi: DOI 10.1016/j.apenergy.2009.06.037.

Chow, T. T., K. F. Fong, G. Pei, J. Ji, and M. He. 2010. "Potential use of photovoltaic-integrated solar heat pump system in Hong Kong." *Applied Thermal Engineering* 30 (8–9):1066-1072. doi: http://dx.doi.org/10.1016/j.applthermaleng.2010.01.013.

Chow, T. T., W. He, A. L. S. Chan, K. F. Fong, Z. Lin, and J. Ji. 2008. "Computer modeling and experimental validation of a building-integrated photovoltaic and water heating system." Review of 172th ref on Riffat and Saffa (2011). *Applied Thermal Engineering* 28 (11-12):1356-1364. doi: DOI 10.1016/j.applthermaleng.2007.10.007.

Chow, T. T., W. He, and J. Ji. 2006. "Hybrid photovoltaic-thermosyphon water heating system for residential application." Review of 80th ref on Riffat and Cuce (2011). *Solar Energy* 80 (3):298-306. doi: DOI 10.1016/j.solener.2005.02.003.

Chow, T. T., W. He, J. Ji, and A. L. S. Chan. 2007. "Performance evaluation of photovoltaic-thermosyphon system for subtropical climate application." *Solar Energy* 81 (1):123-130. doi: DOI 10.1016/j.solener.2006.05.005.

Chow, T. T., G. Pei, K. F. Fong, Z. Lin, A. L. S. Chan, and J. Ji. 2009. "Energy and exergy analysis of photovoltaic–thermal collector with and without glass cover." *Applied Energy* 86 (3):310-316. doi: 10.1016/j.apenergy.2008.04.016.

Clarke, J. A., J. W. Hand, C. M. Johnstone, N. Kelly, and P. A. Strachan. 1996. "Photovoltaic-integrated building facades." *Renewable Energy* 8 (1-4):475-479.

Coventry, J. S., and K. Lovegrove. 2003. "Development of an approach to compare the 'value' of electrical and thermal output from a domestic Pv/thermal system." Review of 218th ref on Riffat and Saffa (2011). *Solar Energy* 75:63-72.

Cox, C. H., and P. Raghuraman. 1985. "Design Considerations for Flat-Plate-Photovoltaic Thermal Collectors." *Solar Energy* 35 (3):227-241.

Cristofari, C. 2012. "Innovative patented PV/TH solar collector: Optimization and performance evaluation." *Energy Procedia* 14:235-240.

Cristofari, C., G. Notton, and J. L. Canaletti. 2009. "Thermal behavior of a copolymer PV/Th solar system in low flow rate conditions." *Solar Energy* 83 (8):1123-1138. doi: DOI 10.1016/j.solener.2009.01.008.

Cristofari, C., G. Notton, P. Poggi, and A. Louche. 2002. "Modelling and performance of a copolymer solar water heating collector." *Solar Energy* 72 (2):99-112. doi: 10.1016/s0038-092x(01)00092-5.

Daghigh, Ronak. 2011. "Predicting the performance of amorphous and crystalline silicon based photovoltaic solar thermal collectors." Review of 98th ref on Riffat and Cuce (2011). *Energy conversion and management* 52 (3):1741-1747.

Daghigh, Ronak, Adnan Ibrahim, Goh Li Jin, Mohd Hafidz Ruslan, and Kamaruzzaman Sopian. 2011. "Predicting the performance of amorphous and crystalline silicon based photovoltaic solar thermal collectors." *Energy conversion and management* 52 (3):1741-1747. doi: http://dx.doi.org/10.1016/j.enconman.2010.10.039.

Direcção Geral da Energia e Geologia. 2015. Renováveis: estatísticas rápidas - nº 122 - dezembro de 2014.

DR. 2006. Decreto-Lei n.º 80/2006.

DR. 2008. Despacho nº 17313/2008. In *2ª Série*.

DR. 2013. Decreto Lei 118/2013.

Dubey, S., G. S. Sandhu, and G. N. Tiwari. 2009a. "Analytical expression for electrical efficiency of PV/T hybrid air collector." Review of 144th ref on riffat and saffa (2011). *Applied Energy* 86 (5):697-705. doi: DOI 10.1016/j.apenergy.2008.09.003.

Dubey, S., S. C. Solanki, and A. Tiwari. 2009b. "Energy and exergy analysis of PV/T air collectors connected in series." *Energy and Buildings* 41 (8):863-870. doi: DOI 10.1016/j.enbuild.2009.03.010.

Dubey, S., and G. N. Tiwari. 2008. "Thermal modeling of a combined system of photovoltaic thermal (PV/T) solar water heater." Review of 89th ref on Riffat and Cuce (2011). *Solar Energy* 82 (7):602-612. doi: DOI 10.1016/j.solener.2008.02.005.

Dubey, S., and G. N. Tiwari. 2009. "Analysis of PV/T flat plate water collectors connected in series." Review of 92th ref on Riffat and Cuce (2011). *Solar Energy* 83 (9):1485-1498. doi: DOI 10.1016/j.solener.2009.04.002.

Dubey, Swapnil, Jatin Narotam Sarvaiya, and Bharath Seshadri. 2013. "Temperature Dependent Photovoltaic (PV) Efficiency and Its Effect on PV Production in the World – A Review." *Energy Procedia* 33 (0):311-321. doi: http://dx.doi.org/10.1016/j.egypro.2013.05.072.

Duffie, John A. 1991. *Solar engineering of thermal processes*. Edited by William A. Beckman. Vol. 2nd ed 0009. New York [etc.]: John Wiley & Sons.

Dupeyrat, P., C. Ménézo, and S. Fortuin. 2014. "Study of the thermal and electrical performances of PVT solar hot water system." *Energy and Buildings* 68, Part C (0):751-755. doi: http://dx.doi.org/10.1016/j.enbuild.2012.09.032.

Dupeyrat, Patrick, Christophe Ménézo, Matthias Rommel, and Hans-Martin Henning. 2011a. "Efficient single glazed flat plate photovoltaic–thermal hybrid collector for domestic hot water system." *Solar Energy* 85 (7):1457-1468. doi: 10.1016/j.solener.2011.04.002.

Dupeyrat, Patrick, Christophe Ménézo, Harry Wirth, and Matthias Rommel. 2011b. "Improvement of PV module optical properties for PV-thermal hybrid collector application." *Solar Energy Materials and Solar Cells* 95 (8):2028-2036. doi: http://dx.doi.org/10.1016/j.solmat.2011.04.036.

EC, (European Comission). 2015. Renewable energy progress report

Eicker, Ursula, and Antoine Dalibard. 2011. "Photovoltaic–thermal collectors for night radiative cooling of buildings." *Solar Energy* 85 (7):1322-1335. doi: 10.1016/j.solener.2011.03.015.

Eisenmann, W., K. Vajen, and H. Ackermann. 2004. "On the correlations between collector efficiency factor and material content of parallel flow flat-plate solar collectors." *Solar Energy* 76 (4):381-387. doi: http://dx.doi.org/10.1016/j.solener.2003.10.005.

Enerdata. 2014. "Global Energy Statistical Yearbook 2014." Accessed 25/03/2015. https://yearbook.enerdata.net.

EPIA, (European Photovoltaic Industry Association). 2014. Global Market Outlook for Photovoltaics 2014-2018. edited by (European Photovoltaic Industry Association) EPIA.

Erdil, E., M. Ilkan, and F. Egelioglu. 2008. "An experimental study on energy generation with a photovoltaic (PV) - solar thermal hybrid system." Review of 183th ref on Riffat and Saffa (2011). *Energy* 33 (8):1241-1245. doi: DOI 10.1016/j.energy.2008.03.005.

EREC. 2011. Mapping Renewable Energy Pathways towards 2020 - EU ROADMAP.

ESTIF. 2014. Solar Thermal Markets in Europe - Trends and Market Statistics 2013. edited by European Solar Thermal Industrial Federation.

ESTIF. 2015. Solar Thermal Markets in Europe - Trends and Market Statistics 2014.

European Comission - DG Climate Action. 2015. "The 2020 climate and energy package." Accessed 05/07/2015. http://ec.europa.eu/clima/policies/strategies/2020/index_en.htm.

European Forum for Renewable Energy Sources. 2011. POLICY CONCLUSIONS AND RECOMMENDATIONS from the National Renewable Energy Action Plans. REPAP2020 - Renewable Energy Policy Action Paving the Way towards 2020.

European Parliament. 2010. DIRECTIVE 2010/31/EU on the energy performance of buildings (recast)

eurostat. 2015a. "Electricity and natural gas price statistics." Accessed 07/05/2015. http://ec.europa.eu/eurostat/statistics-explained/index.php/Electricity_and_natural_gas_price_statistics.

Eurostat. 2015b. "Energy from renewable sources." Accessed 07/07/2015. http://ec.europa.eu/eurostat/statistics-explained/index.php/Energy_from_renewable_sources#Share_of_energy_from_renewable_sources:_heating_and_cooling.

Evola, G., and L. Marletta. 2014. "Exergy and thermoeconomic optimization of a water-cooled glazed hybrid photovoltaic/thermal (PVT) collector." *Solar Energy* 107 (0):12-25. doi: http://dx.doi.org/10.1016/j.solener.2014.05.041.

EES 2014.

Ferdous, J. 2012. "Performance improvement of SHWS by increasing thermal efficiency using insulation materials and optimum position of solar collectors." *Proceedings of the 2012 2nd International Conference on the Developments in Renewable Energy Technology (ICDRET 2012)* ISSU (PAGE):6 .

Ferreira, Isabel. 1999. Determinação da curva característica de um módulo solar (Guião de trabalho prático).

Fixapart, Nedis -. 2015. "Products: Tools: Thermal paste: Nedis Fixapart." Accessed 14/12/2015. http://webshop.nedis.es/es-es/678111/wpt-25gram.

Florides, G. A., S. A. Kalogirou, S. A. Tassou, and L. C. Wrobel. 2002. "Modelling and simulation of an absorption solar cooling system for Cyprus." *Solar Energy* 72 (1):43-51. doi: http://dx.doi.org/10.1016/S0038-092X(01)00081-0.

Florschuetz, L. W. 1976. *EXTENSION OF THE HOTTEL-WHILLIER-BLISS MODEL TO THE ANALYSIS OF COMBINED PHOTOVOLTAIC/THERMAL FLAT PLATE COLLECTORS*.

Fraisse, G., C. Menezo, and K. Johannes. 2007. "Energy performance of water hybrid PV/T collectors applied to combisystems of Direct Solar Floor type." *Solar Energy* 81 (11):1426-1438. doi: DOI 10.1016/j.solener.2006.11.017.

Frankl, P., M. Gamberale, and F. Bttisti. 2000. "Life cycle assessment of a pv cogenerative system: comparison with a solar thermal collector and a PV system." 16th European Photovoltaic Solar Energy Conference, Glasgow.

Fujisawa, T., and T. Tani. 1997. "Annual exergy evaluation on photovoltaic-thermal hybrid collector." Review of 65th ref on Riffat and Cuce (2011). *Solar Energy Materials and Solar Cells* 47 (1-4):135-148.

Gao, Jianqiang. 2010. "Study on the Temperature Variation of the Water-cooled Photovoltaic Solar Template." *Proceedings 2010 International Conference on Intelligent System Design and Engineering Application (ISDEA 2010)*:502.

Garg, H. P., and R. S. Adhikari. 1997. "Conventional hybrid photovoltaic/thermal (PV/T) air heating collectors: Steady-state simulation." Review of 116th ref on Riffat and Cuce (2011). *Renewable Energy* 11 (3):363-385.

Garg, H. P., and R. S. Adhikari. 1999. "Performance analysis of a hybrid photovoltaic/thermal (PV/T) collector with integrated CPC troughs." *International Journal of Energy Research* 23 (15):1295-1304.

Garg, H. P., and R. K. Agarwal. 1995. "Some Aspects of a Pv/T Collector Forced Circulation Flat-Plate Solar Water-Heater with Solar-Cells." *Energy conversion and management* 36 (2):87-99.

Garg, H. P., R. K. Agarwal, and A. K. Bhargava. 1991. "The Effect of Plane Booster Reflectors on the Performance of a Solar Air Heater with Solar-Cells Suitable for a Solar Dryer." *Energy conversion and management* 32 (6):543-554.

Gordon, J. 2001. *Solar Energy-the State of the Art: Ises Position Papers*. Edited by International Solar Energy Society: James & James Science Publishers.

Grupo About Media. 2015. "Renováveis crescem na electricidade mas diminuem no aquecimento e arrefecimento." Accessed 07/07/2015. http://www.ambienteonline.pt/canal/detalhe/renovaveis-crescem-na-electricidade-mas-diminuem-no-aquecimento-e-arrefecimento.

Guardian Industries Corp. "UltraWhite Low-Iron Glass." Guardian Industries Corp. Accessed 23/04/2013. https://www.guardian.com/GuardianGlass/glassproducts/UltraWhite/index.htm.

Guiavarch, A., and B. Peuportier. 2006. "Photovoltaic collectors efficiency according to their integration in buildings." Review of 137th ref on riffat and Saffa (2011). *Solar Energy* 80 (1):65-77. doi: DOI 10.1016/j.solener.2005.07.004.

Guimarães, Rui Manuel Campos. 2009. *Estatística*. Edited by José António Sarsfield Pereira Cabral. 2009 ed. Porto:: Associação de Estudantes da Faculdade de Engenharia da Universidade do Porto.

He, W., T. T. Chow, J. Ji, J. P. Lu, G. Pei, and L. S. Chan. 2006. "Hybrid photovoltaic and thermal solar-collector designed for natural circulation of water." Review of 81th ref on Riffat and Cuce (2011). *Applied Energy* 83 (3):199-210. doi: DOI 10.1016/j.apenergy.2005.02.007.

Hegazy, A. A. 2000. "Comparative study of the performances of four photovoltaic/thermal solar air collectors." Review of 127th ref on Riffat and Saffa. *Energy conversion and management* 41 (8):861-881.

Hegazy, Adel A. 1999. "Optimum channel geometry for solar air heaters of conventional design and constant flow operation." *Energy conversion and management* 40 (7):757-774. doi: 10.1016/s0196-8904(98)00107-1.

Hendrie, S.D. 1982. Photovoltaic/thermal collector development program. Final report. In *Other Information: Portions of document are illegible*.

Hendrie, Susan D. 1979. "EVALUATION OF COMBINED PHOTOVOLTAIC/THERMAL COLLECTORS." *Electric Power Research Institute (Report) EPRI EA* ISSU (PAGE):1865-1869.

Hermann, Michael. 2011. Project BIONICOL: Development of a bionic solar collector with aluminium roll-bond absorber. Fraunhofer Institute for Solar Energy Systems ISE.

Herrando, María, Christos N. Markides, and Klaus Hellgardt. 2014. "A UK-based assessment of hybrid PV and solar-thermal systems for domestic heating and power: System performance." *Applied Energy* 122 (0):288-309. doi: http://dx.doi.org/10.1016/j.apenergy.2014.01.061.

Holman, J. P. 1989. *Heat transfer*. Singapore: McGraw-Hill.

Honsberg, Christiana, and Stuart Bowden. "Solar cell operation - Other Effects - Light intensity." Accessed 25 Fev 2015. http://www.pveducation.org/pvcdrom/solar-cell-operation/effect-of-light-intensity.

Honsberg, Christiana, and Stuart Bowden. "Solar cell operation - Solar cell parameters - Fill factor." Accessed 25 Fev 2015. http://www.pveducation.org/pvcdrom/solar-cell-operation/fill-factor.

Honsberg, Christiana, and Stuart Bowden. "Solar cell operation - Solar cell parameters - Open circuit voltage." Accessed 25 Fev 2015. http://www.pveducation.org/pvcdrom/solar-cell-operation/open-circuit-voltage.

Huang, B. J., T. H. Lin, W. C. Hung, and F. S. Sun. 2001. "Performance evaluation of solar photovoltaic/thermal systems." Review of 68th ref on Riffat and Cuce (2011). *Solar Energy* 70 (5):443-448.

Hussain, F. 2013. "Design development and performance evaluation of photovoltaic/thermal (PV/T) air base solar collector." *Renewable and Sustainable Energy Reviews* 25:431-441.

Ibrahim, A., K. Sopian, M. Y. Othman, M. A. AlGhoul, and A. Zaharim. 2008. "Simulation of different configuration of hybrid Photovoltaic Thermal Solar Collector (PVTS) Designs." *Advances in Applied Mathematics, Systems, Communications and Computers*:44-49

275.

IEA, (International Energy Agency). 2007. IEA solar heating and cooling programme.

IEA, (International Energy Agency). 2010. Technology Roadmap: Solar photovoltaic energy.

IEA, (International Energy Agency). 2011. Solar Energy Perspectives. IEA.

IEA, (International Energy Agency). 2013. Transition to Sustainable Buildings: Strategies and Opportunities to 2050.

IEA, (International Energy Agency). 2015. "FAQs: Energy efficiency." Accessed 25/03/2015. http://www.iea.org/aboutus/faqs/energyefficiency/.

IPMA. 2015. "Climate normals." IPMA Accessed 11/12/2015. https://www.ipma.pt/en/oclima/normais.clima/.

IPQ. 2007. Instalações solares térmicas e seus componentes colectores solares NP EN 12975-2: 2007 Parte 2 métodos de ensaio. Lisboa: IPQ.

ISE, © Fraunhofer. 2015. "BIONICOL - DEVELOPMENT OF A BIONIC SOLAR COLLECTOR WITH ALUMINIUM ROLL-BOND ABSORBER." Accessed 1/04/2015. http://www.bionicol.eu.

Ito, S., N. Miura, J. Q. Wang, and M. Nishikawa. 1997. "Heat pump using a solar collector with photovoltaic modules on the surface." *Journal of Solar Energy Engineering-Transactions of the Asme* 119 (2):147-151.

Ito, S., N. Miura, and K. Wang. 1999. "Performance of a heat pump using direct expansion solar collectors." Review of 190th ref on Riffat and Saffa (2011). *Solar Energy* 65 (3):189-196.

Jack, Steffen, Nills Katenbrink, and Felix Schubert. 2011. "Evaluation Methods for Heat Pipes in Solar Thermal Collectors - Test equipment and first results." ISES Solar World Congress.

JCGM, Joint Committee for Guides in Metrology. 2008. Evaluation of measurement data — Guide to the expression of uncertainty in measurement.

Ji, J., J. P. Lu, T. T. Chow, W. He, and G. Pei. 2007. "A sensitivity study of a hybrid photovoltaic/thermal water-heating system with natural circulation." Review of 84th ref on Riffat and Cuce (2011). *Applied Energy* 84 (2):222-237. doi: DOI 10.1016/j.apenergy.2006.04.009.

Ji, Jie. 2006. "Effect of fluid flow and packing factor on energy performance of a wall-mounted hybrid photovoltaic/water-heating collector system." Review of 199th ref on Riffat and Saffa (2011). *Energy & Buildings* 38 (12):1380-1387.

João, Ana M. R., and Armando C. Oliveira. 2015. "Modelling and analysis of photovoltaic/thermal collectors – influence of PV cell location and area." *International Journal of Ambient Energy* 36 (2):76-86. doi: 10.1080/01430750.2013.823109.

Johnston, D. 2010. "Functional requirements for component films in a solar thin-film photovoltaic/thermal panel." *Solar Energy* 84 (3):384-389. doi: DOI 10.1016/j.solener.2009.12.001.

Joshi, A. S., and A. Tiwari. 2007. "Energy and exergy efficiencies of a hybrid photovoltaic-thermal (PV/T) air collector." Review of 140th ref on Riffat and Saffa (2011). *Renewable Energy* 32 (13):2223-2241. doi: DOI 10.1016/j.renene.2006.11.013.

Kalogirou, S. A. 2001. "Use of TRNSYS for modelling and simulation of a hybrid pv–thermal solar system for Cyprus." Review of 69th ref on Riffat and Cuce (2011). *Renewable Energy* 23:247-260.

Kalogirou, S. A., and C. Papamarcou. 2000. "Modelling of a thermosyphon solar water heating system and simple model validation." *Renewable Energy* 21 (3-4):471-493.

Kalogirou, S. A., and Y. Tripanagnostopoulos. 2006. "Hybrid PV/T solar systems for domestic hot water and electricity production." Review of 83th ref on Riffat and Cuce (2011). *Energy conversion and management* 47 (18-19):3368-3382. doi: DOI 10.1016/j.enconman.2006.01.012.

Kalogirou, S. A., and Y. Tripanagnostopoulos. 2007. "Industrial application of PV/T solar energy systems." *Applied Thermal Engineering* 27 (8-9):1259-1270. doi: DOI 10.1016/j.applthermaleng.2006.11.003.

Kalogirou, Soteris A. 2004. "Solar thermal collectors and applications." *Progress in Energy and Combustion Science* 30 (3):231-295. doi: http://dx.doi.org/10.1016/j.pecs.2004.02.001.

Kalogirou, Soteris A. 2009. *Solar energy engineering processes and systems*. California: Academic Press.

Kamel, Raghad S., Alan S. Fung, and Peter R. H. Dash. 2015. "Solar systems and their integration with heat pumps: A review." *Energy and Buildings* 87 (0):395-412. doi: http://dx.doi.org/10.1016/j.enbuild.2014.11.030.

Kern Jr, E. C., and M. C. Russell. 1978. "COMBINED PHOTOVOLTAIC AND THERMAL HYBRID COLLECTOR SYSTEMS." *Conference Record of the IEEE Photovoltaic Specialists Conference*:1153.

Khandelwal, S., K. S. Reddy, and S. Srinivasa Murthy. 2007. "Performance of contact and non-contact type hybrid photovoltaic-thermal (PV-T) collectors." *International Journal of Low Carbon Technologies* 2 (4):359-733.

Kim, Jin-Hee. 2012. "The experimental performance of an unglazed PV-thermal collector with a fully wetted absorber." *1ST INTERNATIONAL CONFERENCE ON SOLAR HEATING AND COOLING FOR BUILDINGS AND INDUSTRY (SHC 2012)* 30:144-151.

Kumar, Anil, Prashant Baredar, and Uzma Qureshi. 2015. "Historical and recent development of photovoltaic thermal (PVT) technologies." *Renewable and Sustainable Energy Reviews* 42 (0):1428-1436. doi: http://dx.doi.org/10.1016/j.rser.2014.11.044.

Kumar, R., and M. A. Rosen. 2011a. "A critical review of photovoltaic-thermal solar collectors for air heating." Review of 185th ref on Riffat and saffa (2011). *Applied Energy* 88 (11):3603-3614. doi: DOI 10.1016/j.apenergy.2011.04.044.

Kumar, R., and M. A. Rosen. 2011b. "Performance evaluation of a double pass PV/T solar air heater with and without fins." Review of 151th ref on Riffat and saffa (2011). *Applied Thermal Engineering* 31 (8-9):1402-1410. doi: DOI 10.1016/j.applthermaleng.2010.12.037.

Kumar, Shiv, and G. N. Tiwari. 2009. "Life cycle cost analysis of single slope hybrid (PV/T) active solar still." *Applied Energy* 86 (10):1995-2004. doi: http://dx.doi.org/10.1016/j.apenergy.2009.03.005.

Lalovic, B., Z. Kiss, and H. Weakliem. 1986. "A Hybrid Amorphous-Silicon Photovoltaic and Thermal Solar Collector." Review of Bergene, T. and Lovvik, O.M. (1995). *Solar Cells* 19 (2):131-138.

Loferski, J.J., J. Beall, C. Case, R. Dobbins, G. Doodlescack, J. Krikorian, B. Roessler, and T. Russell. 1982. "Design and construction of a hybrid photovoltaic (3KWp) -thermal solar energy system for a residential/commercial building." 16. IEEE Photovoltaics Specialists Conference, San Diego, CA, USA.

Madhukeshwara, N., and E. S. Prakash. 2012. "An investigation on the performance characteristics of solar flat plate collector with different selective surface coatings." *International Journal of Energy and Environment* 3 (1):99-108.

Matuska, Tomas. 2014. "Performance and Economic Analysis of Hybrid PVT Collectors in Solar DHW System." *Energy Procedia* 48 (0):150-156. doi: http://dx.doi.org/10.1016/j.egypro.2014.02.019.

MINISTÉRIO DO AMBIENTE, ORDENAMENTO DO TERRITÓRIO E ENERGIA. 2014. Decreto-Lei n.º 153/2014. Diário da República.

Mishra, R. K., and G. N. Tiwari. 2013. "Energy matrices analyses of hybrid photovoltaic thermal (HPVT) water collector with different PV technology." *Solar Energy* 91 (0):161-173. doi: http://dx.doi.org/10.1016/j.solener.2013.02.002.

Mittelman, G., A. Kribus, O. Mouchtar, and A. Dayan. 2009. "Water desalination with concentrating photovoltaic/thermal (CPVT) systems." *Solar Energy* 83 (8):1322-1334. doi: DOI 10.1016/j.solener.2009.04.003.

Mittelman, Gur, Abraham Kribus, and Abraham Dayan. 2007. "Solar cooling with concentrating photovoltaic/thermal (CPVT) systems." *Energy Conversion and Management* 48 (9):2481-2490. doi: http://dx.doi.org/10.1016/j.enconman.2007.04.004.

Moradi, Kamran, M. Ali Ebadian, and Cheng-Xian Lin. 2013. "A review of PV/T technologies: Effects of control parameters." *International Journal of Heat and Mass Transfer* 64 (0):483-500. doi: http://dx.doi.org/10.1016/j.ijheatmasstransfer.2013.04.044.

Morita, Y., T. Fujisawa, and T. Tani. 2000. "Moment performance of photovoltaic/thermal hybrid panel (numerical analysis and exergetic evaluation)." Review of 213th ref on Riffat and Saffa (2011). *Electrical Engineering in Japan* 133 (2):43-51.

Muresan, C., C. Menezo, R. Bennacer, and R. Vaillon. 2006. "Numerical simulation of a vertical solar collector integrated in a building frame: Radiation and turbulent natural convection coupling." *Heat Transfer Engineering* 27 (2):29-42. doi: Doi 10.1080/01457630500397658.

Nagano, K., T. Mochida, K. Shimakura, K. Murashita, and S. Takeda. 2003. "Development of thermal-photovoltaic hybrid exterior wallboards incorporating PV cells in and their winter performances." Review of 163th ref on riffat and saffa (2011). *Solar Energy Materials and Solar Cells* 77 (3):265-282. doi: Pii S0927-0248(02)00348-3.

Nayak, Sujata, and G. N. Tiwari. 2008. "Energy and exergy analysis of photovoltaic/thermal integrated with a solar greenhouse." *Energy and Buildings* 40 (11):2015-2021. doi: http://dx.doi.org/10.1016/j.enbuild.2008.05.007.

NREL. 2013. "NREL Spurred the Success of Multijunction Solar Cells " Accessed 05/08/2015. http://www.nrel.gov/docs/fy13osti/59142.pdf.

NREL. 2015a. "Best research-cells efficiency." Accessed 05/08/2015. http://www.nrel.gov/ncpv/images/efficiency_chart.jpg.

NREL. 2015b. "Solar Spectra: Standard Air Mass Zero." Accessed 24/07/205. http://rredc.nrel.gov/solar/spectra/am0/ASTM2000.html.

Nualboonrueng, Thipjak, Pongpith Tuenpusa, Yuki Ueda, Atsushi Akisawa, and Blackwell Wiley. 2013. "The performance of PV-t systems for residential application in Bangkok." *Progress in Photovoltaics* 21 (5):1204-1213.

Onyx Solar. 2015. "Onyx Solar." Accessed 20/07/2015. http://www.onyxsolar.com/pt/index.html.

Othman, M. Y. H., H. Ruslan, K. Sopian, and G. L. Jin. 2009. "Performance Study of Photovoltaic-Thermal (PV/T) Solar Collector with del-Grooved Absorber Plate." *Sains Malaysiana* 38 (4):537-541.

Othman, M. Y. H., B. Yatim, K. Sopian, and M. N. Abu Bakara. 2005. "Performance analysis of a double-pass photovoltaic/thermal (PV/T) solar collector with CPC and fins." *Renewable Energy* 30 (13):2005-2017. doi: DOI 10.1016/j.renene.2004.10.007.

Othman, Mohd Yusof, Baharudin Yatim, Kamaruzzaman Sopian, and Mohd Nazari Abu Bakar. 2007. "Performance studies on a finned double-pass photovoltaic-thermal (PV/T) solar collector." *Desalination* 209 (1–3):43-49. doi: 10.1016/j.desal.2007.04.007.

Parque de Ciência e Tecnologia da Universidade do Porto. 2015. "Empresas - Associação Rede Competência em Polímeros." Accessed 10/08/2015. http://uptec.up.pt/empresa/associacao-rede-competencia-em-polimeros.

Pieper, M., and P. Klein. 2011. "A simple and accurate numerical network flow model for bionic micro heat exchangers." *Heat and Mass Transfer* 47 (5):491-503. doi: 10.1007/s00231-010-0739-7.

Portal das Energias Renováveis. 2015. "Solar Térmico em Portugal." Accessed 23/03/2015. http://www.energiasrenovaveis.com/DetalheConceitos.asp?ID_conteudo=47&ID_area=8&ID_sub_area=27.

Posnanky, M., S Gnos, and S. Coonen. 1994. "The importance of hybrid pv-building integration." First World Conference on Photovoltaic Energy Conversion, Hawaii, USA.

Posnanky, M., H. Hochreutener, and S Gnos. 1992. "Building integrated photovoltaic systems: examples of realized PV-roof and PV-facade power plants with specially conceived PV-modules for building integration." 11th European Photovoltaic Solar Energy Conference, Montreux, Switzerland.

Poulek, V., D. S. Strebkov, I. S. Persic, and M. Libra. 2012. "Towards 50 years lifetime of PV panels laminated with silicone gel technology." *Solar Energy* 86 (10):3103-3108. doi: http://dx.doi.org/10.1016/j.solener.2012.07.013.

Prakash, Jai. 1994. "Transient analysis of a photovoltaic-thermal solar collector for co-generation of electricity and hot air/water." Review of referenced. *Energy Conversion and Management* 35 (11):967-972. doi: 10.1016/0196-8904(94)90027-2.

Quaschning, Volker 2003. "The Sun as an Energy Resource." http://www.volker-quaschning.de Accessed 26/02/2015. http://www.volker-quaschning.de/articles/fundamentals1/index_e.php.

Raghuraman, P. 1981. "Analytical predictions of liquid and air photovoltaic/thermal, flat-plate collector performance." *Journal of solar energy engineering* 103 (4):291-8.

RenOn Energie. 2014. "Variants of hibrid collectors." Accessed 21/07/2015. http://ren-on.com/Solarkollektoren.html.

Ricaud, A., and P. Roubeau. 1994. "Capthel, a 66% efficient hybrid solar module and the Ecothel co-generation solar system." Photovoltaic Energy Conversion, 1994., Conference Record of the Twenty Fourth. IEEE Photovoltaic Specialists Conference - 1994, 1994 IEEE First World Conference on, 5-9 Dec 1994.

Riffat, S. B., and E. Cuce. 2011. "A review on hybrid photovoltaic/thermal collectors and systems." *Int. J. Low-Carbon Tech.* 6 (3):212-241.

Rohsenow, W. M. 1961. *Heat, mass and momentum transfer*. Edited by H. Y. Choi. New Jersey:: Prentice Hall.

Saidov, M. S. 1995. "Temperature characteristics of silicon solar cells." *Applied Solar Energy (English translation of Geliotekhnika)* 31 (6):84-88.

Sandberg, M., and B. Moshfegh. 1998. "Ventilated-solar roof air flow and heat transfer investigation." *Renewable Energy* 15 (1-4):287-292.

Sandberg, M., and B. Moshfegh. 2002. "Buoyancy-induced air flow in photovoltaic facades: Effect of geometry of the air gap and location of solar cell modules." *Building and Environment* 37 (3):211-218. doi: http://dx.doi.org/10.1016/S0360-1323(01)00025-7.

Sandnes, B., and J. Rekstad. 2002. "A photovoltaic/thermal (PV/T) collector with a polymer absorber plate. Experimental study and analytical model." Review of 72th ref on Riffat and Cuce (2011). *Solar Energy* 72 (1):63-73.

Sarhaddi, F., S. Farahat, H. Ajam, and A. Behzadmehr. 2010. "Exergetic performance assessment of a solar photovoltaic thermal (PV/T) air collector." *Energy and Buildings* 42 (11):2184-2199. doi: 10.1016/j.enbuild.2010.07.011.

Selvakumar, N., and Harish C. Barshilia. 2012. "Review of physical vapor deposited (PVD) spectrally selective coatings for mid- and high-temperature solar thermal applications." *Solar Energy Materials and Solar Cells* 98 (0):1-23. doi: http://dx.doi.org/10.1016/j.solmat.2011.10.028.

Sharp. 2013. "Sharp Develops Concentrator Solar Cell with World's Highest Conversion Efficiency of 44.4%." Accessed 05/08/2015. http://sharp-world.com/corporate/news/130614.html.

Siddiqui, M. Usama , A. F. M. Arif, Leah Kelley, and Steven Dubowsky. 2012. "Three-dimensional thermal modeling of a photovoltaic module under varying conditions." *Solar Energy* 86 (9):2620-2631. doi: http://dx.doi.org/10.1016/j.solener.2012.05.034.

Singh, Gajendra. 2011. "Design, fabrication and performance evaluation of a hybrid photovoltaic thermal (PVT) double slope active solar still." *Desalination* 277 (1-3):399-406.

Skoplaki, E., and J. A. Palyvos. 2009a. "On the temperature dependence of photovoltaic module electrical performance: A review of efficiency/power correlations." *Solar Energy* 83 (5):614-624. doi: DOI 10.1016/j.solener.2008.10.008.

Skoplaki, E., and J. A. Palyvos. 2009b. "Operating temperature of photovoltaic modules: A survey of pertinent correlations." *Renewable Energy* 34 (1):23-29. doi: DOI 10.1016/j.renene.2008.04.009.

Smith, J.G. 1986. "Comparison of transient models for flat-plates and trough concentrators." *Journal Name: J. Sol. Energy Eng.; (United States); Journal Volume: 108:4*:Medium: X; Size: Pages: 341-343.

Sobhnamayan, F., F. Sarhaddi, M. A. Alavi, S. Farahat, and J. Yazdanpanahi. 2014. "Optimization of a solar photovoltaic thermal (PV/T) water collector based on exergy concept." *Renewable Energy* 68 (0):356-365. doi: http://dx.doi.org/10.1016/j.renene.2014.01.048.

SolarBuzz. 2015. "Multicrystalline Silicon Modules to Dominate Solar PV Industry in 2014, According to NPD Solarbuzz " Accessed 05/08/2015. http://www.solarbuzz.com/news/recent-findings/multicrystalline-silicon-modules-dominate-solar-pv-industry-2014.

Sonneveld, P. J., G. L. A. M. Swinkels, G. P. A. Bot, Y. Tuzel, G. B. Oztekin, M. K. Meric, and Soc Horticultural Int. 2009. "Design of a Solar Greenhouse with Energy Delivery by the Conversion of Near Infrared Radiation - Part 1 Optics and PV-cells." *Acta horticulturae* 807:47-53.

Sonneveld, P. J., G. L. A. M. Swinkels, J. Campen, B. A. J. van Tuijl, H. J. J. Janssen, and G. P. A. Bot. 2010. "Performance results of a solar greenhouse combining electrical and thermal energy production." *Biosystems Engineering* 106 (1):48-57. doi: http://dx.doi.org/10.1016/j.biosystemseng.2010.02.003.

Sopian, K., M. A. Alghoul, Ebrahim M. Alfegi, M. Y. Sulaiman, and E. A. Musa. 2009. "Evaluation of thermal efficiency of double-pass solar collector with porous–nonporous media." *Renewable Energy* 34 (3):640-645. doi: http://dx.doi.org/10.1016/j.renene.2008.05.027.

Sopian, K., H. T. Liu, S. Kakac, and T. N. Veziroglu. 2000. "Performance of a double pass photovoltaic thermal solar collector suitable for solar drying systems." *Energy conversion and management* 41 (4):353-365.

Sopian, K., K. S. Yigit, H. T. Liu, S. Kakac, and T. N. Veziroglu. 1996. "Performance analysis of photovoltaic thermal air heaters." Review of 115th ref on Riffat and Cuce (2011). *Energy conversion and management* 37 (11):1657-1670.

Sunda Solar. 2015. "Seido2 series Direct Flow Vacuum Tube Solar Collector." Accessed 25/07/2015. http://www.sundasolar.com/product_seido2%20series%20collector.html.

Sustainable Business.com. 2014. "Solar Prices Keep Dropping, NREL Achieves 46% Efficiency for Concentrating Solar Cells." Accessed 05/08/2015. http://www.sustainablebusiness.com/index.cfm/go/news.display/id/26060.

Teo, H. G., P. S. Lee, and M. N. A. Hawlader. 2012. "An active cooling system for photovoltaic modules." *Applied Energy* 90 (1):309-315. doi: http://dx.doi.org/10.1016/j.apenergy.2011.01.017.

Thacker, Ben H., Scott W. Doebling, Francois M. Hemez, Mark C. Anderson, Jason E. Pepin, and Edward A. Rodriguez. 2004. Concepts of Model Verification and Validation. edited by Charmian Schaller: Los Alamos National Laboratory.

Tiwari, A., and M. S. Sodha. 2007. "Parametric study of various configurations of hybrid PV/thermal air collector: Experimental validation of theoretical model." Review of 181th ref on Riffat and Saffa (2011). *Solar Energy Materials and Solar Cells* 91 (1):17-28. doi: DOI 10.1016/j.solmat.2006.06.061.

Tiwari, G. N., R. K. Mishra, and S. C. Solanki. 2011. "Photovoltaic modules and their applications: A review on thermal modelling." *Applied Energy* 88 (7):2287-2304. doi: DOI 10.1016/j.apenergy.2011.01.005.

Tonui, J. K., and Y. Tripanagnostopoulos. 2007a. "Air-cooled PV/T solar collectors with low cost performance improvements." Review of 138th ref on Riffat and Saffa (2011). *Solar Energy* 81 (4):498-511. doi: DOI 10.1016/j.solener.2006.08.002.

Tonui, J. K., and Y. Tripanagnostopoulos. 2007b. "Improved PV/T solar collectors with heat extraction by forced or natural air circulation." *Renewable Energy* 32 (4):623-637. doi: DOI 10.1016/j.renene.2006.03.006.

Tonui, J. K., and Y. Tripanagnostopoulos. 2008. "Performance improvement of PV/T solar collectors with natural air flow operation." *Solar Energy* 82 (1):1-12. doi: 10.1016/j.solener.2007.06.004.

Treberspurg, Martin, and Mariam Djalili. 2011. New technical solutions for energy efficient buildings - State of the Art Report - Photovoltaic/Thermal Systems (PV/T). edited by Sustainable Construction and Innovation through Procurement.

Tripanagnostopoulos, Y. 2007. "Aspects and improvements of hybrid photovoltaic/thermal solar energy systems." Review of 219th ref on Riffat and Saffa (2011). *Solar Energy* 81 (9):1117-1131. doi: DOI 10.1016/j.solener.2007.04.002.

Tripanagnostopoulos, Y. 2010. "Design and Performance of a Hybrid PV/T Solar Water Heater." *AIP Conference Proceedings* 1203 (1):1019-1024.

Tripanagnostopoulos, Y., T. Nousia, M. Souliotis, and P. Yianoulis. 2002. "Hybrid photovoltaic/thermal solar systems." Review of 19th ref on Riffat and Cuce (2011). *Solar Energy* 72 (3):217-234. doi: Pii S0038-092x(01)00096-2.

Tripanagnostopoulos, Y., M. Souliotis, R. Battisti, and A. Corrado. 2005. "Energy, cost and LCA results of PV and hybrid PV/T solar systems." *Progress in photovoltaics* 13 (3):235-250. doi: Doi 10.1002/Ipi.590.

Tripanagnostopoulos, Y., P. Yianoulis, and D. Patrikios. 1996. "Hybrid PV-TC solar systems." *Renewable Energy* 8 (1–4):505-508. doi: 10.1016/0960-1481(96)88908-7.

TRNSYS (Transient System Simulation Tool) 2006.

Tselepis, S., and Y. Tripanagnostopoulos. 2002. "Economic analysis of hybrid photovoltaic/thermal solar systems and comparison with standard PV modules." PV in Europe-From PV Technology to Energy Solutions, Rome.

Tyagi, V. V., Nurul A. A. Rahim, N. A. Rahim, and Jeyraj A. L. Selvaraj. 2013. "Progress in solar PV technology: Research and achievement." *Renewable and Sustainable Energy Reviews* 20:443-461. doi: http://dx.doi.org/10.1016/j.rser.2012.09.028.

UN Framework Convention on Climate Change. 2014. "Kyoto Protocol." Accessed 04/07/2015. http://unfccc.int/kyoto_protocol/items/3145.php.

Van Helden, W. G. J., R. J. Ch Van Zolingen, and H. A. Zondag. 2004. "PV Thermal systems: PV panels supplying renewable electricity and heat." *Progress in photovoltaics: Research and applications* 12 (6):415.

Vats, K., V. Tomar, and G. N. Tiwari. 2012. "Effect of packing factor on the performance of a building integrated semitransparent photovoltaic thermal (BISPVT) system with air duct." *Energy and Buildings* 53:159-165. doi: 10.1016/j.enbuild.2012.07.004.

Vera, J. Tamayo, T. Laukkanen, and K. Sirén. 2014. "Performance evaluation and multi-objective optimization of hybrid photovoltaic–thermal collectors." *Solar Energy* 102 (0):223-233. doi: http://dx.doi.org/10.1016/j.solener.2014.01.014.

Watmuff, J. H., W. W. S. Charters, and D. Proctor. 1977. "Solar and wind induced external coefficients - Solar collectors." *Cooperation Mediterraneenne pour l'Energie Solaire, Revue Internationale d'Heliotechnique* 2nd quarter:56.

Wolf, M. 1976. "Performance Analyses of Combined Heating and Photovoltaic Power-Systems for Residences." Review of 16tf ref on Riffat and Cuce (2011). *Energy Conversion* 16 (1-2):79-90.

Wu, Shuang-Ying, Qiao-Ling Zhang, Lan Xiao, and Feng-Hua Guo. 2011. "A heat pipe photovoltaic/thermal (PV/T) hybrid system and its performance evaluation." *Energy and Buildings* 43 (12):3558-3567. doi: 10.1016/j.enbuild.2011.09.017.

Wysocki, J. J., and P. Rappaport. 1960. "Effect of Temperature on Photovoltaic Solar Energy Conversion." *Journal of Applied Physics* 31 (3):571-578.

Yamawaki, T., S. Mizukami, T. Masui, and H. Takahashi. 2001. "Experimental investigation on generated power of amorphous PV module for roof azimuth." *Solar Energy Materials and Solar Cells* 67 (1-4):369-377.

Young, Hugh D. 1996. *Statistical Treatment of Experimental Data: An Introduction to Statistical Methods*: Waveland Pr Inc; Reprint edition (Aug. 1996).

Zakharchenko, R., L. Licea-Jimenez, S. A. Perez-Garcia, P. Vorobiev, U. Dehesa-Carrasco, J. F. Perez-Robles, J. Gonzalez-Hernandez, and Y. Vorobiev. 2004. "Photovoltaic solar panel for a hybrid PV/thermal system." Review of 82th ref on Riffat and Cuce (2011). *Solar Energy Materials and Solar Cells* 82 (1-2):253-261. doi: DOI 10.1016/j.solmat.2004.01.022.

Zhang, X. X., X. D. Zhao, S. Smith, J. H. Xu, and X. T. Yu. 2012. "Review of R&D progress and practical application of the solar photovoltaic/thermal (PV/T) technologies." *Renewable & Sustainable Energy Reviews* 16 (1):599-617. doi: DOI 10.1016/j.rser.2011.08.026.

Zondag, H. A. 2008. "Flat-plate PV-Thermal collectors and systems: A review." Review of 14th ref on Riffat and Cuce (2011). *Renewable & Sustainable Energy Reviews* 12 (4):891-959. doi: DOI 10.1016/j.rser.2005.12.012.

Zondag, H. A., D. W. De Vries, W. G. J. Van Helden, R. J. C. Van Zolingen, and A. A. Van Steenhoven. 2002. "The thermal and electrical yield of a PV-thermal collector." *Solar Energy* 72 (2):113-128.

Zondag, H. A., D. W. de Vries, W. G. J. van Helden, R. J. C. van Zolingen, and A. A. van Steenhoven. 2003. "The yield of different combined PV-thermal collector designs." *Solar Energy* 74 (3):253-269. doi: Doi 10.1016/S0038-092x(03)00121-X.

Appendix A

Description of the elements used in the TRNSYS model

A1 – Load profile - Type 14b

i. Parameters

25 points besides the initial point

Table A1

	Value of time(h)	Water Draw (kg/h)
0	0	0
1	6	0
2	6	5
3	7	5
4	7	30
5	8	30
6	8	25
7	9	25
8	9	5
9	10	5
10	10	0
11	17	0
12	17	5
13	18	5
14	18	25
15	19	25
16	19	30
17	20	30
18	20	20
19	21	20
20	21	10
21	22	10
22	22	5
23	23	5
24	23	0
25	24	0

A2 – Pump - Type 114

i. Parameters

Table A2-i

Rated flow rate (kg/h)	Rated power (W)	Motor heat loss fraction
380	124	0

ii. Inputs

Table A2-ii

Overall pump efficiency	Motor efficiency
0.5	0.9

A3 – Differential controller with hysteresis for temperature - Type 2b

i. Parameters

Table A3-i

Number of oscillations	High limit cut-out (ºC)
5	95

ii. Inputs

Table A3-ii

Upper input temperature Th (ºC)	Lower input temperature Tl (ºC)	Monitoring temperature Tin (ºC)	Input control function	Upper dead band DT(ºC)	Lower dead band DT(ºC)
20	10	20	0	4	2

A4 – PV/T collector – Photovoltaic panels -Type 50a

i. Parameters

Table A4-i

Area (m^2)	Collector fin efficiency factor	Collector plate absorptance	Collector loss coefficient	Cover transmittance	Temperature coefficient of solar cell efficiency	Reference temperature for cell efficiency	**Packing factor**
5.28	Table 5.1	0.93	6.8646	0.85	0.0045	25	Table 5.1

ii. Inputs

Cell efficiency: 0.18

A5 – HVAC – Auxiliary heaters - Type 6

i. Parameters

Table A5-i

Maximum heating rate (kW)	Overall loss coefficient for heater during operation	Efficiency
24	0	0.85

ii. Inputs

iii. Table A5-i

Control function	Set point temperature (ºC)	Temperature of surroundings (ºC)
1	60	20

A6 – Thermal storage – Stratified storage tank - Fixed inlets – Uniform losses - Type 4a

i. Parameters

Six nodes, distant 0.3 m between each node.

Table A6-i

Tank volume (m^3)	Tank loss coefficient (W/m^2K)	Monitoring temperature Tin (ºC)	Auxiliary heater mode	Node containing heating element 1	Node containing thermostat 1	Setpoint temperature for element 1
0.295	0.68	20	1	1	1	8

Deadband for heating element 1 (ºC)	Maximum heating rate of element 1 (kW)	Node containing heating element 2	Deadband for heating element 2	Setpoint temperature for element 2
5	0	1	1	55

Deadband for heating element 2 (ºC)	Maximum heating rate of element 2 (kW)	Node containing heating element 2	Deadband for heating element 2	Setpoint temperature for element 1
5	0	1	1	55

ii. Inputs

Table A6-ii

Hot side temperature (ºC)	Cold side temperature (ºC)	Environmental temperature (ºC)	Control signal for element 1	Control signal for element 1
45	15	20	0	0